Structure, Function, and Inhibition of Peptidoglycan *O*-Acetyltransferase A from *Staphylococcus aureus*

By

Carys S. Jones

A Thesis

presented to

The University of Guelph

In partial fulfilment of requirements
for the degree of

Doctor of Philosophy

in

Molecular and Cellular Biology

Guelph, Ontario, Canada

ABSTRACT

STRUCTURE, FUNCTION, AND INHIBITION OF PEPTIDOGLYCAN *O*-ACETYLTRANSFERASE A FROM *STAPHYLOCOCCUS AUREUS*

Carys S. Jones
University of Guelph, 2020

Advisor:
Dr. Anthony J. Clarke

Peptidoglycan (PG) is an essential cell wall component of most bacteria and serves to resist turgor pressure and protect the cell. Many bacteria modify their PG layer post-biosynthetically, which can have implications on pathogenicity. O-Acetylation of PG is an important modification utilized by both Gram-positive and Gram-negative bacteria to regulate autolysins and provide resistance to host-immune attack by lysozyme. This modification commonly occurs in several notable pathogens, including *Staphylococcus aureus*. In Gram-positive bacteria, PG O-acetylation is accomplished by a single dual domain enzyme, *O*-acetyltransferase A (OatA). As a recognized virulence factor, OatA is of interest in the development of novel strategies to overcome antimicrobial resistance. In this study, *S. aureus* OatA was subjected to a large high-throughput screen to identify and characterize inhibitors of the enzyme. To improve our understanding of the PG O-acetylation system as a whole, the structures and functions of both domains of *S. aureus* OatA were also investigated. The topology of the N-terminal transmembrane domain was determined, and putative functional residues were investigated with *in vivo* and *in vitro* mutagenesis studies. A model for its mechanism and interaction with the C-terminal domain is proposed. Furthermore, the crystal structure of the C-terminal domain of *S. aureus* OatA is presented alongside an analysis of its catalytic mechanism.

Acknowledgements

My sincerest gratitude to Dr. Anthony Clarke for his mentorship, guidance, and patience in helping me achieve my scientific goals. I am also grateful to my advisory committee Drs. Cezar Khursigara and Joel Weadge for their support and advice over the course of my degree. A big thank you to all the members of the Clarke Lab, past and present, in particular Dr. David Sychantha, Ashley Brott, and Chris Vandenende for all their helpful dicussions and advice. Thank you as well to the undergrads who worked on this project: Alicia Eng, Bryan Fraser, Katie Jany, and Laura Thompson.

Table of Contents

List of Figures

List of Tables

List of Abbreviations

Amp	Ampicillin
Ape1	*O*-acetyl peptidoglycan esterase
ATP	Adenosine tri-phosphate
BCIP	5-bromo-4-chloro-3-indolyl phosphate
CH	Cytoplasmic helix
CoA	Coenzyme A
Cm	Chloramphenicol
DDM	dodecylmaltoside
DMSO	dimethylsulfoxide
DTDP	4',4'-dithiodipyridine
DTT	dithiothreitol
GlcNAc	*N*-acetylglucosamine
GT	Glycosyltransferase
HPAEC	High-performance anion exchange chromatography
HTS	High throughput screen
IMAC	Immobilised metal-ion affinity chromatography
Kan	Kanamycin
LB	Luria-Bertani
LC-MS	Liquid chromatography mass spectrometry
LT	Lytic transglycosylase
LTA	Lipoteichoic acid
MBOAT	Membrane-bound *O*-acyltransferase
MIC	Minimal inhibitory concentration
MRSA	Methicillin-resistant *Staphylococcus aureus*
MTSES	2-sulfonatoethyl methanethiosulphonate
MTSET	2-(Trimethylammonium)ethyl methane thiosulfonate
MurNAc	*N*-acetylmuramic acid
Ni-NTA	Nicket nitriloacetic acid
OatA	*O*-acetyltransferase A
ONPG	ortho-nitrophenyl-β-galactoside
PAD	Pulse-amperometric detection
PAINS	Pan-assay interference compounds
PatA/B	Peptidoglycan *O*-acetyltransferase A/B
PBP	Penicillin binding protein
PEG	Polyethylene glycol
PEGmal	Polyethylene glycol-maleimide
PG	Peptidoglycan
*p*NP	para-nitrophenol
*p*NP-Ac	*para*-nitrophenyl acetate
*p*NPP	*para*-nitrophenyl-phosphate
Q-TOF	Quadrupole-time-of-flight
Red-Gal	6-chloro-3-indolyl-β-D-galactopyranoside
*Sa*OatA$_C$	*S. aureus* OatA C-terminal domain
*Sa*OatA$_N$	*S. aureus* OatA N-terminal domain

SDS-PAGE	sodium dodecyl sulphate-polyacrylamide gel electrophoresis
SEC	Size-exclusion chromatography
SUMO	Small ubiquitin-like modifier
TMS	Transmembrane segment
TP	Transpeptidase
TSB	Tryptic soy broth
UDP	Uridine diphosphate
VRSA	Vancomycin-resistant *Staphylococcus aureus*
WTA	Wall teichoic acid
4MU-Ac	4-methylumbelliferyl acetate
4MU	4-methylumbelliferone

Chapter 1. Introduction

1.1 Bacterial cell envelope

The bacterial cell envelope is a critical component of bacteria and performs the complex task of protecting the cells from a great diversity of threats whilst simultaneously allowing for the passage of essential nutrients, waste, and other molecules (Silhavy et al., 2010). Most bacteria can be classified as either Gram-negative or Gram-positive due to fundamental differences in this cell envelope. The Gram-negative cell envelope consists of three principle layers: a cytoplasmic (inner) membrane, a thin peptidoglycan (PG) layer, and an outer membrane (Figure 1.1A). In contrast, the Gram-positive cell envelope has only two principle layers: a cytoplasmic membrane, and a thick PG layer. In addition to the standard cell wall components, some Gram-positive and Gram-negative bacteria may also have additional structures such as capsules or S-layer proteins.

The cytoplasmic membrane in both Gram-negative and Gram-positive bacteria is a fluid phospholipid bilayer (Silhavy et al., 2010). It is differentially permeable, allowing for the passive diffusion of molecules such as water and oxygen, but is impermeable to electrolytes and protons, and contains protein transporters for a variety of molecules. The cytoplasmic membrane is home to the electron transport chain and also plays crucial roles in protein translocation, motility, chemotaxis, and lipid synthesis.

The outer membrane, unique to Gram-negative bacteria, is an asymmetric lipid bilayer with phospholipids comprising the inner leaflet, and glycolipids, mainly lipopolysaccharide (LPS), comprising the outer leaflet (Kamio and Nikaido, 1976; Raetz and Whitfield, 2002). The outer membrane serves as a protective barrier and is essential for the survival of Gram-negative bacteria. The outer membrane proteins are mainly β-barrel proteins, including porins, which allow for the passive diffusion of small molecules across the outer membrane, and lipoproteins. One important lipoprotein is Braun's lipoprotein, which is imbedded in the inner leaflet of the outer membrane and covalently attaches to the underlying PG layer, effectively tethering the outer membrane to the cell. The region between the inner and outer membrane of Gram-negative bacteria is known as the periplasm, a viscous aqueous compartment that is densely packed with enzymes and proteins involved in a variety of processes (Mullineaux et al., 2006).

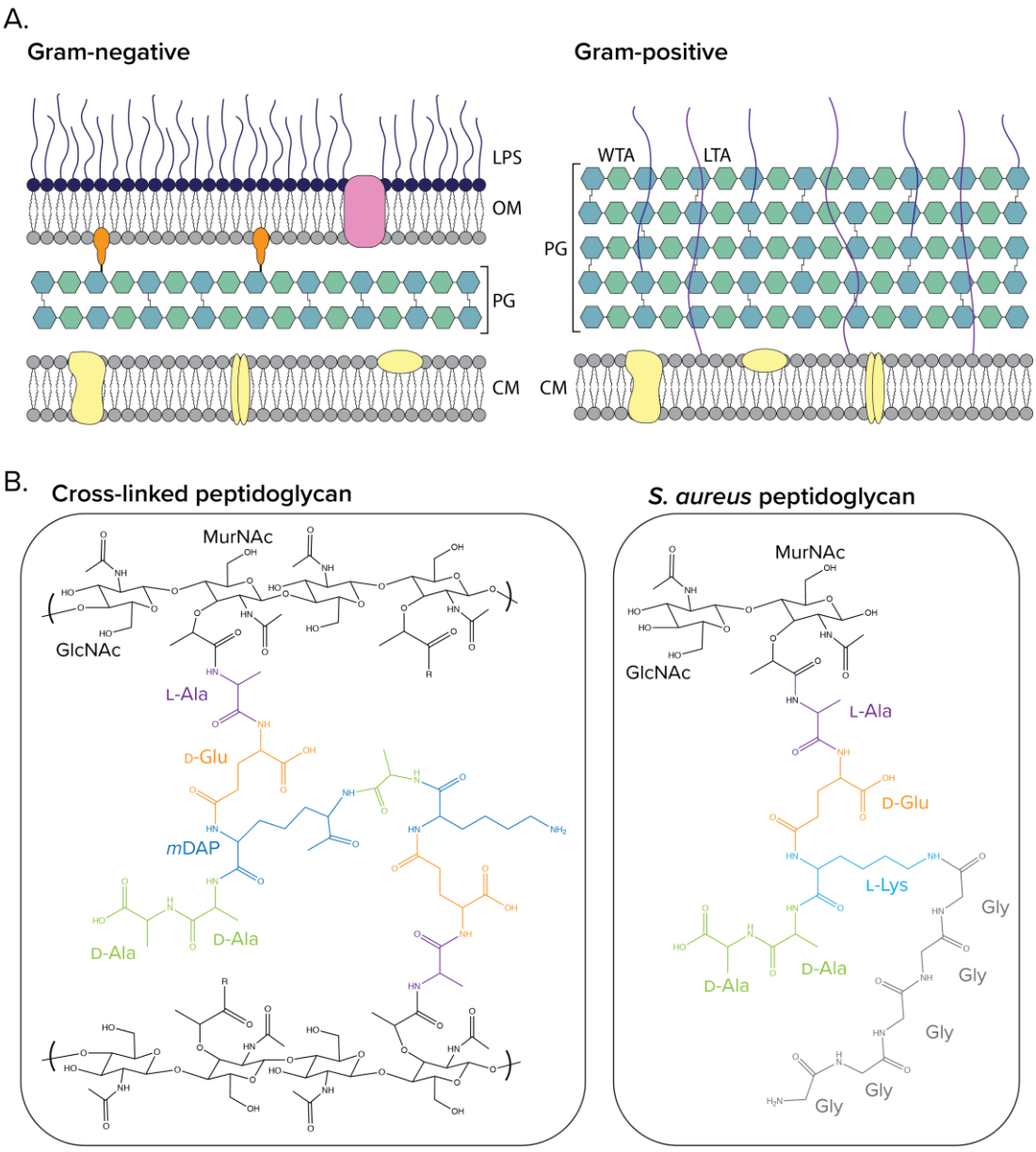

Figure 1.1 Bacterial cell envelope. A. The organization of the major structural components of the cell envelope of Gram-negative bacteria (left) and Gram-positive bacteria (right). B. PG consists of β-1,4-linked GlcNAc and MurNAc residues cross-linked by short peptide stems attached to MurNAc residues (left). *Staphylococcus aureus* possess a pentaglycine interpeptide bridge attached to L-Lys involved in cross-linking (right). LPS, lipopolysaccharide; OM, outer membrane; PG, peptidoglycan; CM, cytoplasmic membrane; WTA, wall teichoic acid; LTA, lipoteichoic acid.

Although Gram-positive bacteria do not have an outer membrane, they do possess additional and unique cell wall polysaccharides (Weidenmaier and Peschel, 2008). These

include wall teichoic acids (WTA), lipoteichoic acids (LTA), secondary cell wall polysaccharides, and mycobacterial arabinogalactan. Teichoic acids are long anionic polymers and can be divided into two classes: wall teichoic acids, which are covalently linked to PG (Brown et al., 2013), and lipoteichoic acids, which are attached to the phospholipid head groups of the outer leaflet of the cytoplasmic membrane (Reichmann and Gründling, 2011). Teichoic acids provide a continuum of negative charge that extends beyond the PG layer and although not essential, the absence of teichoic acids can cause morphological and growth defects. Teichoic acids are known to play a role in cation homeostasis (Marquis et al., 1976), heat stress (Hoover and Gray, 1977), resistance to antimicrobial cationic peptides (Peschel et al., 1999), and resistance to glycopeptides and autolytic enzymes (Peschel et al., 2000). Secondary cell wall polysaccharides are almost exclusively found in the *Bacilliaceae* family and are covalently attached to PG (Schäffer and Messner, 2005). Their main role is to anchor surface layer proteins to the cell wall. Despite the many cell wall polysaccharides, due to the lack of outer membrane, Gram-positive bacteria were initially thought not to possess a periplasm. Cryo-electron microscopy, however, revealed the existence of a low density zone between the cytoplasmic membrane and the PG layer, which is being proposed as a periplasmic space (Matias and Beveridge, 2005, 2006).

The PG layer of Gram-negative and Gram-positive bacteria is similar in terms of chemical composition, however, it differs greatly in thickness. In Gram-positive bacteria, the PG sacculus is external to the cytoplasmic membrane and consists of several layers and is around 30 nm thick (Matias and Beveridge, 2005). In contrast, PG in Gram-negative bacteria is found in a thin layer in the periplasm, sandwiched between the cytoplasmic (inner) and outer membranes and is only a few nm thick (Yao et al., 1999). PG will be the focus of this introduction.

1.1.1 Peptidoglycan

PG is an essential component of bacterial cell walls, contributing to both cell shape and protection (Turner et al., 2014; Vollmer et al., 2008a). The rigid, single macromolecule (sacculus) surrounds the cytoplasmic membrane and enables the cell to resist the turgor pressure resulting from the difference in osmolality between the cytoplasm and the external environment (Dover et al., 2015). Although over 50 chemotypes of PG are known, the

basic structure PG is conserved among bacteria (Schleifer and Kandler, 1972). PG is composed of long glycan strands consisting of repeating units of β-1,4-linked *N*-acetylglucosamine (GlcNAc) and *N*-acetylmuramic acid (MurNAc). Glycan chains can vary in length and are cross-linked by short peptides covalently attached to MurNAc residues to create one large polymer surrounding the cell (Figure 1.1B). The core peptide stem is a pentapeptide that alternates L- and D- amino acids. The first position is almost always L-Ala and the second position D-Glu. Some bacteria, such as *S. aureus*, amidate the D-Glu post-biosynthetically producing *iso*-D-Gln (Münch et al., 2012). The greatest variation is found at position 3, which is generally a diamino – *meso*-diaminopimelic acid (*m*DAP) in most Gram-negatives and L-Lys in most Gram-positives. The terminal residues are D-Ala- D-Ala. Whilst the 4th position is almost exclusively D-Ala, both D-Lac and D-Ser have been encountered at position 5, most notably in organism with natural or acquired resistance to vancomycin (Bugg et al., 1991; Reynolds et al., 1994). Cross-linking between stem peptides of adjacent glycan strands can occur either directly, as in most Gram-negatives, or indirectly via an interpeptide bridge, as in most Gram-positives (Schleifer and Kandler, 1972). The most common cross-linking occurs between the 3rd amino acid of one peptide stem and the 4th amino acid of the other. Cross-linking can also occur between the 2nd and 4th amino acid of two peptide stems but this is mainly isolated to coryneform bacteria (Vollmer et al., 2008a). The degree of cross-linking of PG can also vary by species and environment. For example, *Escherichia coli* tends to have a degree of cross-linking around 31-61% (Vollmer and Seligman, 2010), whereas *Staphylococcus aureus* has a much higher degree of cross-linking ranging from 70-80% (Snowden and Perkins, 1990). Furthermore, the growth state of bacteria can affect the cross-link type and stem peptide composition, as demonstrated by a study of the PG composition from planktonic and biofilm state *Pseudomonas aeruginosa* (Anderson et al., 2020).

1.2 Peptidoglycan biosynthesis

PG biosynthesis occurs in greater than 10 basic steps on either side of the cytoplasmic membrane and employs a large complement of enzymes (Figure 1.2A). The biosynthetic pathway for PG is the target for one of the most clinically successful group of antibiotics (β-lactams) and as such has been extensively studied. Despite occasional

differences in the bacterial stem peptide, the biosynthesis of PG is generally the same for most bacterial species.

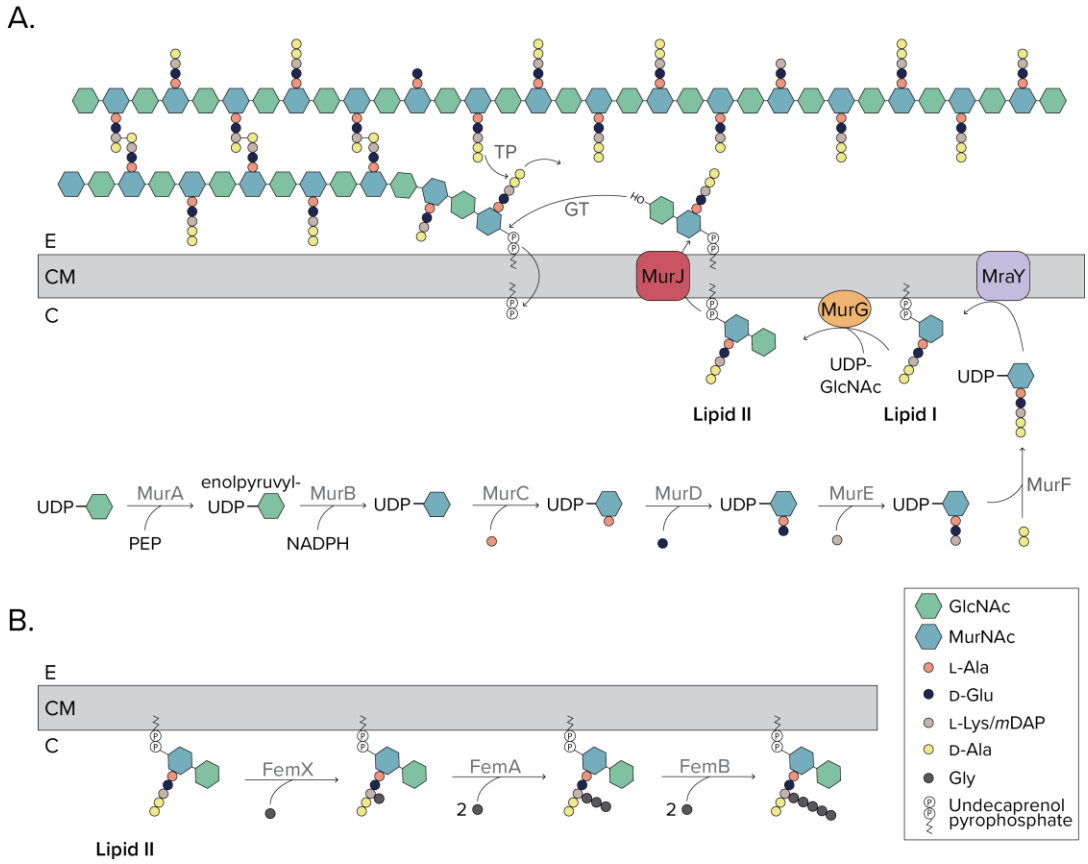

Figure 1.2 Peptidoglycan biosynthesis. A. The biosynthesis of PG begins with the cytoplasmic synthesis of the nucleotide sugars UDP-GlcNAc and UDP-MurNAc. A series of Mur ligases attach the peptide stem to UDP-MurNAc. MurNAc-pentapeptide is transferred onto undecaprenol-pyrophosphate in the inner leaflet of the cytoplasmic membrane, forming Lipid I, and the addition of GlcNAc forms Lipid II. Lipid II is then flipped to the outer leaflet of the cytoplasmic membrane where glycosyltransferase and transpeptidases incorporate the PG subunits into the pre-existing sacculus. B. The pentaglycine bridge in *S. aureus* in synthesized in the cytoplasm by the Fem enzymes, which sequentially add glycines to L-Lys on Lipid II. UDP, uridine diphosphate; GT, glycosyltransferase; TP, transpeptidase; E, external; CM, cytoplasmic membrane; C, cytoplasm.

1.2.1 Precursor formation

The first stage of PG synthesis involves the production of the precursor molecule uridine diphosphate (UDP)-GlcNAc. UDP-GlcNAc is an important precursor molecule in the cell and its synthesis pathway is shared by many cellular processes. UDP-GlcNAc is synthesised from fructose-6-phosphate in a series of four reactions. Initially, fructose-6-

phosphate (F-6-P) is converted to glucosamine-6-phosphate (GlcN-6-P) by a fructose-6-phosphate amidotransferase, GlmS (Badet et al., 1987). GlcN-6-P can also be produced from recycled *N*-acetylglucosamine-6-phosphate by NagA (Peri et al., 1990). A phosphoglucosamine mutase, GlmM, catalyses the isomerisation of GlcN-6-P to GlcN-1-P (Mengin-Lecreulx and Van Heijenoort, 1996) and lastly, the bifunctional enzyme GlmU functions as a GlcN-1-P uridyltransferase, performing the final two steps (Mengin-Lecreulx and Van Heijenoort, 1994). GlmU catalyzes the formation of *N*-acetylglucosamine-1-phosphate (GlcNAc-1-P) from GlcN-1-P first, followed by the addition of UTP to GlcNAc-1-P forming UDP-GlcNAc (Mengin-Lecreulx and Heijenoort, 1993; Mengin-Lecreulx and Van Heijenoort, 1994). UDP-GlcNAc then goes on to subsequent steps in the PG biosynthetic pathway, as well as other cellular processes.

The second sugar precursor, UDP-MurNAc, is synthesized from UDP-GlcNAc in a series of two reactions that represent the first committed steps of PG biosynthesis. The first step involves the transfer of the enolpyruvyl moiety from phosphoenolpyruvate to UDP-GlcNAc (Marquardt et al., 1992). This reaction, catalyzed by MurA, results in the production of enolpyruvyl UDP-GlcNAc (Marquardt et al., 1992). Whilst Gram-negative bacteria have only one copy of MurA, formerly known as MurZ, Gram-positive bacteria have two copies of MurA that can substitute for each other (Du et al., 2000). In the next step, MurB catalyzes the NADPH-dependent reaction converting enolpyruvyl UDP-GlcNAc to UDP-MurNAc (Pucci et al., 1992).

1.2.2 Peptide stem formation

The following stage of PG biosynthesis entails a series of enzymatic reactions to form the pentapeptide sidechain. The Mur ligases, Mur C-F, are ATP-dependent amino acid ligases that catalyse the sequential addition of amino acids onto UDP-MurNAc. MurC catalyzes the addition of L-Ala (Liger et al., 1995), followed by MurD, which catalyzes the additional of D-Glu (Pratviel-Sosa et al., 1991). MurE catalyzes the addition of the third amino acid in the stem peptide, *m*DAP in the case of many Gram-negatives, or L-Lys in the case of many Gram-positives (Michaud et al., 1990). Whilst the MurE enzymes that catalyze these different additions are structurally very similar, they differ in the identity of one critical residue. MurE enzymes that catalyze the addition of *m*DAP possess a critical Arg residue at position 416 (Gordon et al., 2001). In contrast, MurE enzymes that catalyze

the addition of L-Lys possess an Ala or Asn at this position instead (Gordon et al., 2001). This amino acid change appears to be the main structural reason for *m*DAP/L-Lys discrimination by MurE enzymes of different bacterial species. The last step involves the addition of a D-Ala-D-Ala dipeptide to the stem peptide by MurF (Duncan et al., 1990). The D-Ala-D-Ala dipeptide is formed by the action of a D-Ala:D-Ala ligase, Ddl, that catalyzes the ligation of two D-Ala residues (Ito and Strominger, 1973; Neuhaus, 1962). Ddl and MurF have complementary specificities for the amino acid at each position, known as a "double-sieving" mechanism, which prevents incorporation of the wrong amino acids into the terminal positions of the stem peptide (Neuhaus and Struve, 1965).

Upon completion of the stem peptide, the MurNAc-pentapeptide is transferred from UDP in the cytoplasm to an undecaprenyl phosphate carrier imbedded in the inner leaflet of the cytoplasmic membrane (Ikeda et al., 1991). This transfer is catalyzed by the integral membrane protein MraY and results in the formation of the precursor known as lipid I (Ikeda et al., 1991). Following this, MurG catalyzes the transfer of GlcNAc from a UDP-GlcNAc precursor onto lipid I, generating lipid II (Mengin-Lecreulx et al., 1991).

1.2.3 Lipid II translocation

The subsequent step of PG biosynthesis involves translocating lipid II from the inner leaflet of the cytoplasmic membrane to the outer leaflet of the cytoplasmic membrane. After the discovery that lipid II translocation was not spontaneous (van Dam et al., 2007), the search for a dedicated lipid II flippase led to the emergence of two potential candidates: FtsW and MurJ. For over a decade, contradictory evidence supported the claims for each candidate lipid II flippase, with the identity of the true flippase ultimately emerging as MurJ (Kuk et al., 2017; Taguchi et al., 2019).

The argument for FtsW stemmed from the finding that the polytopic membrane protein was part of the shape, elongation, division, and sporulation (SEDS) family of proteins, of which at least one member appeared to be present in all bacteria that produce PG (Lara and Ayala, 2002). The *ftsW* gene is located in a division and cell wall biosynthetic gene cluster in close proximity to the genes encoding PBP3 and MurG, consistent with a role in PG biosynthesis. Furthermore, FtsW was found to localize to the septum and interact with PBP3 during cell division (Wang et al., 1998). Using a Förster resonance energy transfer-based *in vitro* assay and bacterial membrane vesicles, Mohammadi *et al.*

(Mohammadi et al., 2011) demonstrated that overexpression of FtsW promoted lipid II translocation, whereas FtsW depletion reduced translocation. In addition, the authors were able to show lipid II flipping in proteoliposomes using a fluorescence-based assay (Mohammadi et al., 2011). However, in the same assay, FtsW was seen to flip phospholipids, suggesting promiscuity in substrate recognition (Mohammadi et al., 2014). Furthermore, despite the *in vitro* evidence suggesting FtsW as the lipid II flippase, there was no *in vivo* evidence to corroborate the findings. Another member of the SEDS family of proteins, RodA, was then discovered to act as a glycosyltransferase in the elongasome, the protein complex involved in cell elongation and growth, and this led to the hypothesis that FtsW serves a similar role in the divisome, the protein complex involved in cell division (Cho et al., 2017). Recently, Taguchi *et al*., demonstrated PG polymerase activity by FtsW orthologs from *Streptococcus thermophilus* and *Staphylococcus aureus* (Taguchi et al., 2019). They found that this activity was only present in the presence of a class B penicillin-binding protein (Taguchi et al., 2019). This evidence has led to the conclusion that FtsW is not, in fact, the lipid II flippase, and instead plays an essential role as a glycosyltransferase in the polymerization of PG at the division site. This leaves MurJ as the favoured candidate for the lipid II flippase.

MurJ is 14 transmembrane helix protein part of the multidrug/oligosaccharidyl-lipid/polysaccharide (MOP) transporter superfamily (Butler et al., 2013; Kuk et al., 2017). MurJ is essential in *E. coli* and cells depleted of MurJ accumulate PG precursors and lyse (Inoue et al., 2008). Attempts to demonstrate lipid II flippase activity using the *in vitro* assays described for FtsW were unsuccessful (Mohammadi et al., 2011), however, an assay was developed to monitor the lipid II flipping activity of MurJ *in vivo* (Sham et al., 2014). A single-Cys MurJ variant was expressed in *E. coli* and rendered non-functional by the addition of the thiol-specific reagent 2-sulfonatoethyl methanethiosulphonate (MTSES) (Sham et al., 2014). ColM, a protein toxin that localizes to the periplasm and cleaves lipid II, was used to differentiate radiolabelled lipid II that had been translocated to the periplasm from cytoplasmic lipid II (Sham et al., 2014). When MurJ was inactivated by MTSES, lipid II was protected from ColM cleavage, suggesting that lipid II was not flipped (Sham et al., 2014). As further evidence, MurJ was demonstrated to have high affinity binding to lipid II in a native mass spectrometry experiment (Bolla et al., 2018). Additionally, Monteiro *et*

al. (2018) found that MurJ is recruited to the septum by the DivIB/DivIC/FtsL complex, thereby driving PG incorporation at the division site (Monteiro et al., 2018). The crystal structure of MurJ from *Thermosipho africanus* was first published in 2017, exhibiting a solvent exposed cavity (Kuk et al., 2017). In subsequent work, MurJ 3-dimensional crystal structures were solved in open and closed conformations, consistent with an alternating access model for the transport of lipid II (Kuk et al., 2019).

In *Bacillus subtilis*, a MurJ homologue (YtgP) was identified as the potential lipid II flippase, however it is non-essential for viability in rich media (Meeske et al., 2015). Using a genetic screen for synthetic lethality in a Δ*ytgP* background, Amj was identified as a putative lipid II flippase (Meeske et al., 2015). Amj has no detectable sequence similarity to MOP exporters or ABC transporters and it is not widely conserved, however, it can substitute for MurJ in *E. coli*, suggesting lipid II flippase activity (Meeske et al., 2015). Additionally, the transcription of *amj* is upregulated by cell wall stress and in the absence of YtgP in *B. subtilis* (Meeske et al., 2015). This raises the idea of redundancy of lipid II transporters and whether there is indeed only one dedicated lipid II flippase in bacteria.

1.2.4 Transglycosylation and transpeptidation

An understanding of the final stages of PG biosynthesis first arose with the discovery of the mode of action of penicillin by Park and Strominger (Park and Strominger, 1957), and the use of penicillin as an investigative tool thereafter. The incorporation of translocated lipid II precursors into the PG sacculus requires the concerted activity of various PG synthases. Glycosyltransferases (GTs) catalyze the formation of a β-1,4-GlcNAc-MurNAc linkage between lipid II monomers and the existing sacculus with the loss of undecaprenyl-pyrophosphate (Terrak et al., 1999). Transpeptidases (TPs) are acyl-serine transferases that cross-link the peptide stems in a two-step mechanism. The first step involves the attack of the active-site serine from the TP on the terminal D-Ala-D-Ala peptide bond of the donating stem peptide forming an acyl-enzyme intermediate with the loss of the terminal D-Ala (McDonough et al., 2002). The acyl intermediate is resolved by attack from the amino group of the accepting stem peptide resulting in the formation of a new peptide bond and the cross-linking of PG strands (McDonough et al., 2002). Transpeptidation works in conjunction with other peptide "trimming" and hydrolyzing

PBPs to control the level of cross-linking in the PG sacculus (Ghosh et al., 2008). Transpeptidation has only been seen to occur on glycan-polymerized substrate, and thus glycan polymerization appears to precede peptide cross-linking (Born et al., 2006; Terrak et al., 1999).

PG polymerization is mediated by PG synthases known as penicillin binding proteins (PBPs), which can be divided into several classes (Sauvage et al., 2008). High-molecular-mass PBPs are multimodular, membrane-anchored PBPs, divided into class A and class B. Class A PBPs are bifunctional enzymes with a GT domain and a TP domain. Class B PBPs are monofunctional TPs with an additional domain associated with binding (Typas et al., 2012). Class C PBPs are not actually PG synthases. Although they possess catalytic similarities to TPases, class C PBPs are soluble endopeptidases and carboxypeptidases involved in PG hydrolysis.

The historical view of PG synthesis was that the bifunctional class A PBPs mediated both glycan polymerization and transpeptidation. Although some bacteria possess monofunctional enzymes with glycosyltransferase domains similar to those found in the class A PBPs, the role of these enzymes was unknown for a long time. Recent research, however, has challenged the view that class A PBPs are primarily responsible for glycan polymerization. Whilst class A PBPs are indispensable for growth in many organisms (Hoskins et al., 1999; Yousif et al., 2009), certain Gram-positive bacteria, such as *B. subtilis* and *Enterococcus faecium*, do not require class A PBPs for growth and continue producing PG in their absence (McPherson and Popham, 2003; Rice et al., 2009). A study published in 2017 by Cho *et al.* showed that within the cell elongation complex of *E. coli*, RodA, a SEDS family protein, was responsible for the observed glycosyltransferase activity (Cho et al., 2017). Class A PBPs, in contrast, appeared to mediate cytoskeleton-independent synthesis (Cho et al., 2017). Similarly, as described previously, FtsW was recently found to be a PG polymerase that acts alongside its cognate class B PBP to produce PG at the septum during cell division (Taguchi et al., 2019). In *S. aureus*, the RodA-PBP3 pair played an important role in sidewall PG synthesis to maintain the correct coccus shape, whereas the FtsW-PBP1 pair worked in the divisome complex at midcell (Reichmann et al., 2019). This challenges the previous model for PG synthesis and provides a significant role for SEDS family proteins and class B PBP pairs in PG biosynthesis.

1.2.5 Interpeptide bridge formation

In many Gram-positive bacteria, peptide stem cross-linking occurs indirectly, via an interpeptide bridge (Schleifer and Kandler, 1972). This bridge allows for highly flexible cross-linking in the cell wall. The interpeptide bridge can range in length from one to seven amino acids and several variations in composition exist among bacteria as do numerous branching enzymes responsible for their synthesis (Vollmer et al., 2008a). *Streptococcus pneumoniae*, for example, produces an L-Ser-L-Ala interpeptide bridge (Garcia-Bustos et al., 1987) while *S. aureus* produces a pentaglycine bridge (Ghuysen et al., 1965). In both cases, absence of the interpeptide bridges results in increased β-lactam resistance, although the interpeptide bridge is only essential in *S. aureus* (Fiser et al., 2003; Strandén et al., 1997). The interpeptide bridge is generally added to the lipid II precursor in the cytoplasm, however in some bacteria the interpeptide bridge is added to the UDP-MurNAc-pentapeptide precursor (lipid I) (Fiser et al., 2003; Strandén et al., 1997). The pentaglycine bridge of *S. aureus* is synthesized sequentially by FemABX, a family of non-ribosomal peptidyltransferases (Figure 1.2B). FemX catalyzes the addition of the first glycine to L-Lys, the third amino acid of the stem peptide (Rohrer et al., 1999), followed by FemA which catalyzes the addition of the second and third glycines and FemB which adds the fourth and fifth (Strandén et al., 1997).

1.3 Peptidoglycan degradation and recycling

PG is a highly dynamic macromolecule and this allows for growth and division of the cell as well as insertion and removal of large appendages such as flagella or pili. The process involves the concerted activity of a battery of endogenous enzymes that cleave the glycan backbone and peptide cross-links working alongside biosynthetic enzymes and PG recycling enzymes (Figure 1.3). Many, but not all, of these lytic enzymes are referred to as autolysins because, if left unchecked, they would result in complete degradation of the cell wall and cell lysis would ensue (reviewed in (Vollmer et al., 2008b)).

1.3.1 Cleavage of the glycan backbone

Enzymes involved in cleaving the glycan backbone of PG are recognized as autolysins. Therefore, given that PG is the main shape-determining structure and provides stability to the cell, these autolysins must be under tight control in order to prevent rampant activity. There are three main classes of enzymes that cleave the glycan backbone:

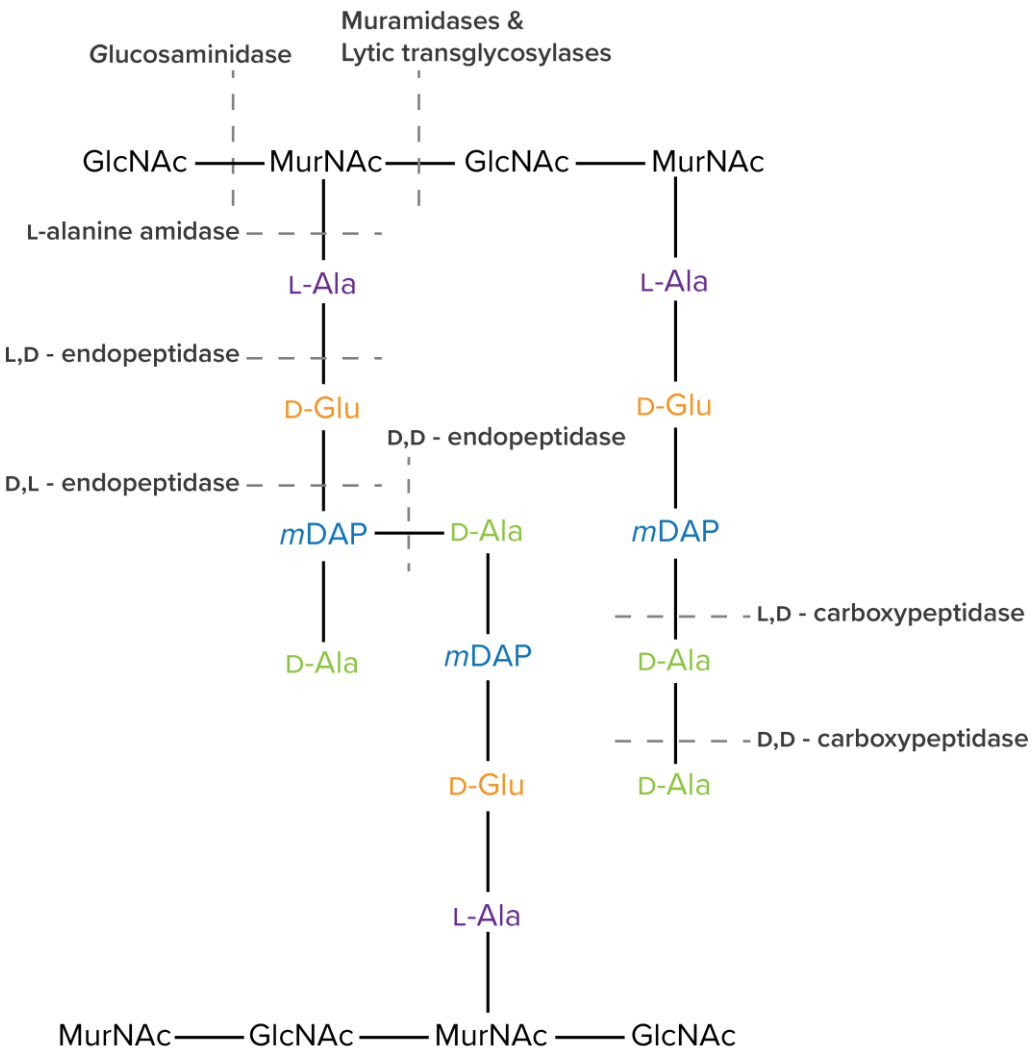

Figure 1.3 Substrate specificity of autolytic enzymes. Bacteria possess a battery of enzymes to cleave PG at every available linkage for growth, division, and other purposes. Glucosaminidases and muramidases/lytic transglycosylases cleave the β-1,4-glycosidic bonds between GlcNAc and MurNAc residues, and MurNAc and GlcNAc residues, respectively. Amidases cleave the bond between the stem peptide and MurNAc residues, whereas endopeptidases and carboxypeptidases with different specificities cleave the bonds within the stem peptides and cross-linkages.

N-acetylglucosaminidases, *N*-acetylmuramidases and lytic transglycosylases (LTs). *N*-Acetylglucosaminidases (EC 3.2.1.92) are hydrolases that cleave the glycosidic bond between GlcNAc and MurNAc of PG and are found almost exclusively in Gram-positive bacteria. The only known *N*-acetylglucosaminidase produced by a Gram-negative bacterium is FlgJ from *Salmonella enterica* that is involved in flagella insertion (Herlihey et al., 2014).

Both *N*-acetylmuramidases (EC 3.2.1.17, lysozyme) and LTs (EC 4.2.2.n1/n2) cleave the β-1,4-glycosidic linkage between MurNAc and GlcNAc. LTs, unlike lysozymes, are not hydrolases; they instead cleave the MurNAc-GlcNAc linkage with the concomitant formation of 1,6-anhydro-*N*-acetylmuramic acid (anhMurNAc) (Höltje et al., 1975). There are six known families of LTs and significant redundancy is seen within a species (Herlihey and Clarke, 2017). Lysozymes cleave the same bond as LTs, however they are hydrolases. Lysozymes are generally found across vertebrates, invertebrates, phages, and fungi and serve several different roles (Vollmer et al., 2008b). Bacterial lysozymes are rare and do not seem to be involved in PG metabolism; hence, they are not considered to be autolysins. Instead, they are secreted by some bacteria as weapons against competing bacteria (Dong et al., 2013; Russell et al., 2011). Lysozyme from mammals, on the other hand, plays an important role in the host defence against bacterial pathogens and provides a significant challenge for invading bacteria to overcome. Lysozymes, like LTs, bind PG and form hydrogen bonds between amino acids in the active site cleft of the enzyme and the *N*-acetyl and C-6 hydroxyl groups of three successive GlcNAc and MurNAc residues (Phillips, 1967). Thus, many bacteria modify their PG as both a means to both control LT activity and inhibit lysozyme.

1.3.2 Cleavage of the peptide stem

The stem peptide of PG can be cleaved at every available bond by a battery of specialized enzymes (reviewed in (Vollmer et al., 2008b). *N*-Acetylmuramyl-L-alanine amidases hydrolyze the bond between MurNAc and the peptide stem. Amidases constitute the major autolysins in several Gram-positive bacteria, including *S. aureus* AtlA (Oshida et al., 1995) and *S. pneumoniae* LytA (Sanchez-Puelles et al., 1986). Carboxypeptidases and endopeptidases are enzymes that hydrolyze the amide bonds between amino acids in the stem peptide. Carboxypeptidases remove C-terminal amino acids (and hence are not autolytic), whereas endopeptidases cleave within the peptide, including cross-links. Although some D,D-endopeptidases belong to class C PBPs and are thus sensitive to β-lactam antibiotics, there are other unrelated D,D-endopeptidases that are not inhibited by β-lactam antibiotics (Keck and Schwarz, 1979; Keck et al., 1990).

1.3.3 Role of PG lytic enzymes

A wide range of PG lytic enzymes can be found in different operons and expressed

under different conditions within a bacterium and play a wide variety of roles. In many cases, the catalytic module is attached to a binding module that is responsible for localizing the enzyme appropriately. The latter can either be carbohydrate-binding modules or direct-repeat domains (Baba and Schneewind, 1998; Biswas et al., 2006; Fernández-Tornero et al., 2001; Joris et al., 1992; Steen et al., 2005). The most evident role of the lytic enzymes is in the control of cell wall growth. The so-called "trimming" of stem peptides by DD-carboxypeptidases from pentapeptides to tetrapeptides controls the level of cross-linking within the sacculus, as tetrapeptides can only serve as cross-linking acceptors, not donors (Ghosh et al., 2008). Bacteria deplete of carboxypeptidases often have abnormal cell shapes and thickened cell walls (Korsak et al., 2005; Nelson and Young, 2001; Schuster et al., 1990). PG lytic enzymes have been postulated to belong to multi-enzyme complexes for PG synthesis that include PG synthases (Höltje, 1996, 1998). The balance of the lytic enzymes to synthases allows for the proper expansion of the PG sacculus, whereby old material can be cleaved to allow for the insertion of new material. In Gram-positive bacteria, the PG sacculus is thought to grow in an inside to outside mode with autolysins acting on the outermost layers of the PG sacculus, releasing degraded cell wall components into the environment (Archibald, 1976; Koch and Doyle, 1985). Autolysins are also key players in the separation of daughter cells during cell division. Several autolysins may be involved, including amidases, LTs, and endopeptidases. Bacteria lacking autolysins involved in cell division show aberrant phenotypes. In *E. coli*, strains deficient in one or more amidase form chains of unseparated cells (Heidrich et al., 2001). Furthermore, multiple deletion strains of *E. coli* lacking a combination of amidases, LTs and endopeptidases display deficiency in septum cleavage (Heidrich et al., 2002). *S. pneumoniae* forms long chains of attached cells when it lacks *lytB*, a major amidase (Sanchez-Puelles et al., 1986). The *atl* gene in *S. aureus* encodes a bifunctional PG hydrolase that is processed into an amidase and glucosaminidase, and in an *atl* null mutant, *S. aureus* forms large clusters of non-separated cells (Takahashi et al., 2002).

PG lytic enzymes also play important roles in sporulation and germination. Different PG lytic enzymes play differing roles throughout the entire process, starting with hydrolysis of the septum in the initial stages of spore formation. This requires the action of SpoIID and SpoIIP, PG endopeptidases that degrade the septum and allow for prespore

engulfment (Abanes-De Mello et al., 2002; Chastanet and Losick, 2007). Endospores have two PG layers which differ in structure (reviewed in (Popham, 2002)). The inner PG layer is known as the primordial (or germ) cell wall and becomes the cell wall in the new vegetative cell after germination. The outer layer is the spore-specific cortex which has a unique PG structure. Around 50% of the MurNAc residues comprising the disaccharide subunits within the cortical PG, approximately every other one, are replaced with muramic acid δ-lactam, an aminosugar that is only found in bacterial endospores (Atrih et al., 1996; Warth and Strominger, 1969, 1972). This modification requires the concerted action of a sporulation-specific amidase, CwlD (Gilmore et al., 2004), to remove the stem peptide, and PdaA, which deacetylates MurNAc to allow formation of the lactam ring (Fukushima et al., 2002). Furthermore, approximately a quarter of the MurNAc residues only have a single L-Ala sidechain, formed by the action of the endopeptidase LytH (Atrih et al., 1996; Horsburgh et al., 2003; Warth and Strominger, 1972). The final stage of sporulation, the release of the endospore into the environment, also requires the action of two PG hydrolases, LytC, the major vegetative amidase, and CwlC, a late-stage sporulation-specific amidase (Smith and Foster, 1995). When the spore receives signals to initiate germination, the spore cortex must be degraded. The germination specific lytic enzymes only act on PG with the δ-lactam structure, and this prevents the germ cell wall from being degraded as the cortex PG is being degraded (Popham et al., 1996).

Not all bacteria can sporulate, however, as many as 60 bacterial species are known to be able to enter a viable-but-nonculturable (VBNC) state wherein the cells do not divide but still maintain low levels of metabolic activity (reviewed in (Oliver, 2005)). Resuscitation-promotion factors (Rpf) are involved in stimulating resuscitation and division of the dormant cells (Mukamolova et al., 1998). Interestingly, Rpf proteins have weak amino acid sequence and structural similarity to lysozymes and LTs (Cohen-Gonsaud et al., 2005) and indeed Rpf from *Micrococcus luteus* has been found to act as a PG lytic enzyme (Mukamolova et al., 2006). Whilst it is not known exactly how PG lytic enzymes would stimulate resuscitation, the current thought is that they are either important for the first round of cell division post-dormancy, or the PG fragments they release act as signalling molecules important for initiating regrowth of the dormant cells (reviewed in (Keep et al., 2006)).

Although the pores in PG can allow passage of proteins up to 100 kDa in size (Vázquez-Laslop et al., 2001), MDa-scale trans-envelope structures such as secretion systems, flagella, or pili cannot pass through the PG layer unassisted. Genes encoding PG lytic enzymes are often found in the gene clusters for these complexes and such enzymes act to create holes in the PG to accommodate the large structures (reviewed in (Koraimann, 2003)). An example of this is FlgJ, a glucosaminidase found in the operon for flagella synthesis in *S. enterica* (Herlihey et al., 2014).

PG lytic enzymes also appear to be important for biofilm formation. In *S. epidermidis* and *Streptococcus mutans*, strains lacking their major autolysins, AtlE and AtlA, respectively, are unable to form biofilms (Heilmann et al., 1997; Shibata et al., 2005). The current opinion is that these hydrolases alter the surface charge of the bacteria or expose cellular adhesins, a necessary precursor for biofilm formation.

PG lytic enzymes play several other more obscure roles. These include predatory roles as exo-enzymes released by some species of myxobacteria and actinomycetes (Brönneke and Fiedler, 1994; Daft et al., 1985). PG hydrolases are also involved in a process known as allolysis, whereby competent cells of *S. pneumoniae* can trigger lysis of their co-culture non-competent counterparts (Steinmoen et al., 2003). This requires the action of a bacteriocin, CibAB expressed by competent cells alongside its immunity factor, CibC, and two autolysins, LytA and LytC (Guiral et al., 2005). As non-competent cells are not expressing the immunity factor they are susceptible to the bacteriocin, which activates the autolysins, causing cell lysis (Guiral et al., 2005).

Most bacteria produce numerous PG synthases and PG lytic enzymes. Although several of these play specific roles, as described previously, there is still an apparent redundancy amongst these classes of enzymes. *E. coli*, for example, has more than 50 enzymes for PG synthesis and degradation, of which more than 20 are PG hydrolases (Pazos et al., 2017). A large barrier to the study of PG lytic enzymes is the apparent non-essential nature of most of the enzymes. Single and even multiple knockouts are viable (Denome et al., 1999), and although some PG hydrolases have specialized functions, as described, partial compensation by paralogues is common. The major redundancy is seen among periplasmic enzymes, which may allow bacteria to grow in a wide range of growth conditions (Pazos et al., 2017). The cytoplasm is a well-buffered compartment with more

constant conditions, protected by the cytoplasmic membrane from the changing environmental conditions the bacterium might encounter. In contrast, the properties of the periplasm, such as osmolality, pH, and ionic strength, vary with changes to the cell's environment. Sets of enzymes may have different optimal conditions for activity, and thus, in combination, there will always be a set of enzymes active in all periplasmic growth conditions. For example, PBP6b is one of several D,D-carboxypeptidases found in *E. coli* that did not seem to play an important role under standard growth conditions, whereas PBP5 comprises the major D,D-carboxypeptidase. Under acidic conditions, however, PBP6b was responsible for the majority of the observed D,D-carboxypeptidase activity (Peters et al., 2016b). Under growth at pH 7.5, PBP6b is almost undetectable, however, growth at pH 5.0 induces gene expression of PBP6b (Peters et al., 2016b). Furthermore, the enzyme displays much greater activity at acidic pH compared to neutral pH (Peters et al., 2016b). This favours a model wherein PG synthesis and degradation are mediated by dynamic multi-enzyme complexes with an enzyme composition that varies depending on the environmental conditions of growth.

1.3.4 PG recycling

PG recycling is an efficient way for bacteria to conserve resources by reusing components of PG that are released by autolytic enzymes. The first PG recycling pathway was discovered in *E. coli* by Goodell in 1985 when it was estimated that as much as 50% of the PG is recycled in one growth cycle (Goodell, 1985). As Gram-positive bacteria do not possess an outer membrane barrier, it was initially assumed that Gram-positive PG was not recycled. However, cryo-electron microscopy has revealed the existence of a pseudo-"periplasmic space" in *S. aureus* and *Bacillus subtilis* (Matias and Beveridge, 2005, 2006) that may be capable of retaining released PG fragments and indeed, PG recycling pathways are found in both Gram-positive and Gram-negative bacteria.

There are two main PG recycling pathways, one termed the catabolic recycling pathway, which is dependent on the presence of the etherase MurQ, and the other termed the anabolic recycling pathway (reviewed in (Mayer et al., 2019)). In both cases, GlcNAc-AnhydroMurNAc-peptides released by PG hydrolases are imported into the cytoplasm by a dedicated permease, AmpG (Jacobs et al., 1994). These muropeptides are then broken down into tripeptides, GlcNAc, and AnhMurNAc by 3 distinct enzymes, the L,D-

carboxypeptidase LdcA (Templin et al., 1999), the *N*-acetylglucosaminidase NagZ (Cheng et al., 2000), and the AnhMurNAc-L-alanine amidase AmpD (Jacobs et al., 1995). In the catabolic recycling pathway found in *E. coli* and many other Gram-negative bacteria, the tripeptides can enter the PG biosynthesis pathway directly through the action of Mpl (Mengin-Lecreulx et al., 1996). Mpl attaches tripeptides to UDP-MurNAc, bypassing MurC, MurD, and MurE. GlcNAc is converted to GlcNAc-6-phosphate by NagK (Uehara and Park, 2004), where it then enters the catabolic pathway of GlcNAc to be converted to UDP-GlcNAc for PG biosynthesis or other functions. AnhydroMurNAc is phosphorylated to MurNAc-6-phosphate by AnmK (Uehara et al., 2005), which is acted upon by the crucial etherase, MurQ, converting MurNAc-6-phosphate to GlcNAc-6-phosphate (Jaeger et al., 2005; Uehara et al., 2006), converging with the GlcNAc recycling pathway. In contrast, the anabolic recycling pathway lacks MurQ and thus MurNAc cannot be recycled via GlcNAc-6-phosphate. Instead researchers found that MurNAc-6-phosphate is converted directly to MurNAc by MupP (Borisova et al., 2017; Fumeaux and Bernhardt, 2017), and then phosphorylated to MurNAc-α-1-phosphate by AmgK (Gisin et al., 2013). The anomeric kinase AmgK has a broad substrate specificity and is also able to phosphorylate GlcNAc to GlcNAc- α-1-phosphate, bypassing several steps in the GlcNAc catabolic pathway (Gisin et al., 2013). MurU converts MurNAc-α-1-phosphate to UDP-MurNAc, which then enters the PG biosynthesis pathway directly (Gisin et al., 2013; Renner-Schneck et al., 2015).

The anabolic pathway was first identified in *Pseudomonas* species but functional orthologs were identified in *Neisseria meningitidis* and *Caulobacter crescentus* (Borisova et al., 2014; Gisin et al., 2013). Some bacteria can possess both the catabolic and anabolic pathways described above, such as *Tannerella forsythia.* Interestingly, *T. forsythia* is a MurNAc auxotroph and lacks GlmS and GlmU, the enzymes that synthesize UDP-GlcNAc, and MurA and MurB, the enzymes required to synthesize UDP-MurNAc from UDP-GlcNAc (Ruscitto et al., 2016; Wyss, 1989). Thus, *T. forsythia* obtains its required MurNAc and GlcNAc from scavenging and recycling from its environment using both the MurQ etherase and the anabolic recycling pathway (Hottmann et al., 2018; Ruscitto et al., 2016). Gram-positive bacteria do not have an anabolic PG recycling pathway and instead possess one or more MurQ orthologs and utilize a variation of the catabolic pathway

(Borisova et al., 2016). For example, *S. aureus* has one MurQ ortholog and recovers MurNAc through this pathway (Borisova et al., 2016). The main products of the major autolysin of *S. aureus*, Atl, are MurNAc-GlcNAc dipeptides, which are imported into the cell and simultaneously phosphorylated *via* the MurP transporter (Kluj et al., 2018). MupG cleaves the phosphorylated disaccharide into GlcNAc and MurNAc-6-phosphate, which is then converted to GlcNAc-6-phophate by MurQ (Kluj et al., 2018). It is interesting to speculate on the fate of modified MurNAc and GlcNAc residues in these recycling pathways and whether such modifications preclude recycling of these sugars or whether specialized enzymes are required.

Whilst recycling peptides and amino sugars has an evident advantage to bacteria, PG recycling is also linked to cell wall signalling in Gram-negatives and induction of the antibiotic resistance gene *ampC*, which codes for a β-lactamase (Jacobs et al., 1994). These bacteria sense the relative amounts of the PG precursor, UDP-MurNAc-pentapeptide and the degradation product anhydroMurNAc-peptapeptide. As β-lactam antibiotics block PG crosslinking, the amount of degradation product increases relative to the precursor, leading to the induction of *ampC* expression by transcriptional regulator AmpR (Jacobs et al., 1994).

1.4 Peptidoglycan modifications

The fundamental structure of PG is highly conserved, however, PG composition can vary within and among bacterial species due predominantly to post-biosynthetic modifications. Although some of these modifications involve the peptide stem, the focus of this section is modifications to the glycan backbone. These modifications generally occur at the C-2 amine or C-6 hydroxyl of either GlcNAc or MurNAc residues. Some examples include N-glycolylation of MurNAc (Raymond et al., 2005), N-deacetylation of GlcNAc or MurNAc (Zipperle et al., 1984), and O-acetylation of MurNAc (Clarke and Dupont, 1992) or GlcNAc (Bernard et al., 2011) (Figure 1.4). Furthermore, covalent attachment of teichoic acids, arabinogalactans, and capsular polysaccharides occurs on the C-6 hydroxyl of MurNAc (Moynihan et al., 2014). These modifications can serve to protect the bacteria from external factors as well as its own autolysins and additionally may modulate the host-bacterial interaction. PG O-acetylation will be the focus of this research and is discussed in depth later on.

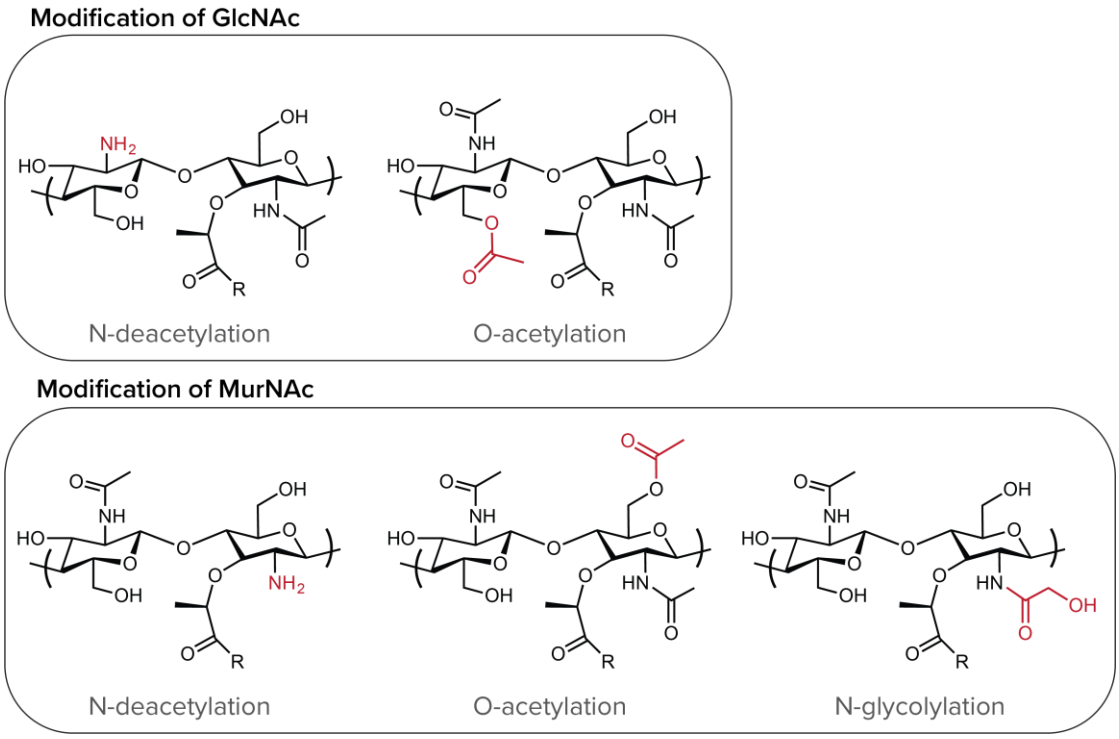

Figure 1.4 Glycan chain modifications. The glycan backbone of PG can be modified on both GlcNAc and MurNAc residues, including N-deacetylation of the C2 position and O-acetylation of the C6 hydroxyl. N-glycolylation can also occur at the C2 position of MurNAc residues, most commonly in mycobacteria.

1.4.1 Peptidoglycan N-glycolylation

N-Glycolylation of MurNAc occurs principally in mycobacteria such as *Mycobacterium tuberculosis* and *Mycobacterium smegmatis* and other closely related genera such as *Nocardia* (Azuma et al., 1970). The gene responsible for the modification to the C-2 amine of MurNAc is *namH*, a UDP-*N*-acetylmuramic acid hydroxylase identified in 2005 by Raymond *et al*. (Raymond et al., 2005). Deletion of this gene renders the organism more susceptible to lysozyme and β-lactam antibiotics, implicating N-glycolylation of MurNAc in resistance towards these antibacterials (Raymond et al., 2005). Raymond and colleagues proposed that the glycolylation of MurNAc stabilizes the cell wall via hydrogen bonding and therefore loss of this modification decrease cell wall stability, rendering it more susceptible to β-lactams and lysozyme (Raymond et al., 2005). Moreover, further research discovered that *N*-glycolyl-muramyl dipeptides were a more potent stimulus for NOD2a and cytokine production than *N*-acetylmuramyl dipeptides, and this is a significant contributing factor to the substantial immunogenicity of mycobacterial

cell walls (Coulombe et al., 2009).

1.4.2 Peptidoglycan N-deacetylation

N-Deacetylation is a common modification found almost exclusively in Gram-positive bacteria. Indeed, *Helicobacter pylori* is the only Gram-negative bacterium known to N-deacetylate its PG (Wang et al., 2009). Either MurNAc or GlcNAc can be N-deacetylated, with the degree of N-deacetylation ranging from ~25-50% for MurNAc and ~15-90% for GlcNAc in *Bacillus* species (Zipperle et al., 1984). This modification is accomplished by an *N*-acetyl-D-glucosamine amidohydrolase (deacetylase) (Vollmer and Tomasz, 2000). Such an enzyme was reported in bacteria in 1957 (Roseman, 1957) and the gene responsible, *pgdA*, was more recently identified in *Streptococcus pneumoniae* in 2000 (Vollmer and Tomasz, 2000). Homologous genes have since been discovered in other bacteria including *Listeria monocytogenes* (Boneca et al., 2007), *Enterococcus faecalis* (Hébert et al., 2007), and *H. pylori* (Wang et al., 2009). These enzymes often have broad substrate specificity, deacetylating not only PG but also glycol chitin, chitooligosaccharides, and artificial substrates (Balomenou et al., 2013). N-Deacetylated GlcNAc plays an important role in lysozyme resistance by precluding binding of the enzyme (Hayashi et al., 1973). Additionally, phenotypic studies on *N*-acetylglycosamine deacetylases from *Bacillus anthracis* revealed that they might also play roles in cell shape and neutral polysaccharide attachment to the cell wall (Balomenou et al., 2013). N-Deacetylated MurNAc, on the other hand, does not contribute to lysozyme resistance as the *N*-acetyl moiety is not involved in lysozyme binding (Phillips, 1967). Whether N-deacetylated MurNAc plays a physiological role in PG metabolism has yet to be established.

1.5 Peptidoglycan O-acetylation

PG O-acetylation occurs at the C-6 hydroxyl of MurNAc residues in both Gram-positive and Gram-negative bacteria (reviewed in (Moynihan et al., 2014)). Though more rare, it can also occur at GlcNAc residues, notably in lactobacilli (Bernard et al., 2011). Initially described in 1958 (Brumfitt, 1959), this modification is now known to occur in a large number of bacteria. A complete list of bacteria with experimentally determined O-acetylated PG is given in Table 1. Although it appears that PG O-acetylation is a very common modification, neither *E. coli* nor *Pseudomonas aeruginosa*, both notable

pathogens, have O-acetylated PG (Clarke, 1993a). In bacteria that O-acetylate their PG, the degree of O-acetylated MurNAc residues can range from 20-70% depending on the organism, environmental conditions and age of the culture (Clarke, 1993a; Johannsen et al., 1983; Swim et al., 1983). For example, one study found that PG O-acetylation levels increased 10-40% for *E. faecalis* as the culture entered stationary phase, and a further 10-16% as cells entered the viable but nonculturable state (Pfeffer et al., 2006). It is not yet known if O-acetylated moieties are dispersed throughout the PG sacculus or localised to particular regions (Moynihan et al., 2014).

Table 1.1 List of bacterial species known to produce O-acetylated PG.

Gram-positive bacteria	Gram-negative bacteria
Bacillus anthracis	*Acinetobacter lwoffi*
Bacillus cereus	*Acinetobacter anitratus*
Bacillus megaterium	*Bacteroides fragilis*
Bacillus subtilis	*Bacteroides thetaiotaomicron*
Enterococcus durans	*Bradyrhizobium japonicum*
Enterococcus faecium	*Campylobacter jejuni*
Enterococcus faecalis	*Chromobacterium violaceum*
Enterococcus hirae	*Morganella morganii*
Lactobacillus acidophilus	*Neisseria gonorrhoeae*
Lactobacillus casei	*Neisseria lactamica*
Lactobacillus fermentum	*Neisseria meningitides*
Lactobacillus plantarum (MurNAc & GlcNAc)	*Neisseria perflava*
Lactobacillus sakei (GlcNAc)	*Photorhabdus luminescens*
Lactococcus lactis	*Proteus mirabilis*
Listeria monocytogenes	*Proteus myxofaciens*
Macroccous caselyticus	*Proteus penneri*
Micrococcus luteus	*Proteus vulgaris*
Ruminococcus flavefaciens	*Providencia alcalifaciens*
Staphylococcus aureus	*Providencia heimachae*
Staphylococcus epidermidis	*Providencia rettgeri*
Staphylococcus haemolyticus	*Providencia stuartii*
Staphylococcus hyicus	*Pseudomonas alcaligenes*
Staphylococcus lugdunensis	*Synchocystis sp.*
Staphylococcus saccharolyticus	
Staphylococcus saprophyticus	
Streptococcus pneumoniae	
Weissella paramesenteroides (GlcNAc)	

1.5.1 Physiological role

PG O-acetylation plays an important role in PG turnover by controlling the activity of LTs. As noted above, LTs cleave between MurNAc and GlcNAc residues with the concomitant formation of an anhydroMurNAc residue, which requires a free C-6 hydroxyl on MurNAc. Thus, the presence of an *O*-acetyl group on the C-6 hydroxyl of MurNAc residues precludes the activity of LTs (Blackburn and Clarke, 2002). In this way, O-acetylation serves to control the activity of these autolysins. In order for LTs to be functional and for PG turnover to occur, the *O*-acetyl groups would need to be removed which, in Gram-negative bacteria, is performed by an *O*-acetyl PG esterase (Weadge and Clarke, 2006).

As previously mentioned, the housekeeping function of LTs appears to be minimal in Gram-positive bacteria, nor do they have *O*-acetyl PG esterases. It appears that these bacteria instead possess a broad collection of autolysins active on both non-O-acetylated, and O-acetylated PG (Pfeffer et al., 2006; Strating and Clarke, 2001). PG O-acetylation was found, however, to have a slight inhibitory effect on the autolytic activities of *N*-acetylglucosaminidase and *N*-acetylmuramidase from Gram-positive *E. faecalis,* thus contributing to control of PG turnover (Emirian et al., 2009). Additionally, research by Bernard *et al*. (2012) on the PG *O*-acetyltransferase, OatA, from *Lactocbacillus plantarum* revealed a secondary role for the enzyme in the spatio-temporal control of the cell cycle and septation (Bernard et al., 2012). The principle role for PG O-acetylation in Gram-positive bacteria, however, seems to be in the defence of external threats.

1.5.2 Pathobiological role

The main pathobiological role of PG O-acetylation is the inhibition of lysozyme. Lysozymes are muramidases that hydrolyze the glycosidice linkage between the MurNAc and GlcNAc residues of PG, causing bacterial cells to lyse (Phillips, 1967). These extensively-studied enzymes are found across invertebrates and vertebrates, as well as fungi and phages, and serve many roles (Vollmer et al., 2008b). In mammals, lysozyme plays a crucial role in the host defence against invading bacterial pathogens. The C-6 hydroxyl of MurNAc is important in the coordination of PG into the substrate-binding cleft of lysozyme (Phillips, 1967) and an *O*-acetyl group sterically hinders such interactions, thereby rendering the organism resistant to lysozyme (Brumfitt, 1959; Pushkaran et al.,

2015). This modification thus provides a significant advantage to invading bacteria, helping them resist the host immune system and aiding in colonization.

The contribution of PG O-acetylation to lysozyme resistance has several important implications in virulence and disease progression. Due to the host immune system's inability to hydrolyse O-acetylated PG, high molecular weight O-acetylated PG fragments persist in the body, even once the bacteria have been eliminated (Fleming et al., 1986). These fragments have been shown to have significant arthropathic properties and result in inflammation and rheumatoid arthritis in *Neisseria gonorrhoeae* infections (Fleming et al., 1986). Furthermore, for a similar reason, *S. aureus* strains that cannot O-acetylate its PG cause significantly less joint destruction and overall reduced septic arthritic disease progression in a mouse model compared to *S. aureus* that can O-acetylate its PG (Baranwal et al., 2017). In *L. monocytogenes*, in addition to providing resistance to lysozyme, O-acetylated PG was found to be important for growth in macrophages, conferring resistance to bacteriocins and β-lactam antibiotics, and limiting the innate immune response (Aubry et al., 2011). The ability of PG O-acetylation to modulate the immune system is of particular interest as it has recently been shown that during *S. aureus* infection, O-acetylation of PG limits the T-helper cell priming required to develop an effective protective response to systemic infection (Sanchez et al., 2017). For these reasons, PG O-acetylation is considered important for virulence in numerous pathogens including *S. aureus* (Baranwal et al., 2017; Bera et al., 2005; Sanchez et al., 2017), *S. pneumoniae* (Crisostomo et al., 2006), *L. monocytogenes* (Aubry et al., 2011), *N. meningitidis* (Veyrier et al., 2013), *N. gonorrhoeae* (Blundell et al., 1980; Fleming et al., 1986), *H. pylori* (Wang et al., 2012), and *E. faecalis* (Hébert et al., 2007).

1.5.3 Peptidoglycan O-acetylation pathways

O-Acetylation of PG is a post-biosynthetic modification that likely occurs after the incorporation of lipid II precursors into the existing sacculus (Gmeiner and Kroll, 1981; Gmeiner and Sarnow, 1987; Lear and Perkins, 1986; Snowden et al., 1989). The source of acetate must therefore be transferred from the cytoplasm to the cell wall *via* the cytoplasmic membrane. Two distinct enzymatic systems have been identified that are proposed to be involved in PG O-acetylation, one in Gram-positive bacteria (Bera et al., 2005) and one in Gram-negative bacteria (Weadge et al., 2005) (Figure 1.5). O-Acetylation and O-

deacetylation of PG in Gram-negative bacteria occur *via* a three-protein system that was first identified in *N. gonorrhoeae* (Weadge et al., 2005) (Figure 1.5A). The gene cluster, named *oap* (**O**-**a**cetylation of **P**G), was identified based on sequence homology to *P. aeruginosa* AlgI, an integral membrane protein involved in the O-acetylation of alginate. Further investigation into the *oap* gene cluster has led to the formation of a working model involving three proteins (Moynihan and Clarke, 2010). In this model, PG *O*-acetyltransferase A (PatA), a putative integral membrane protein, transfers acetyl groups from an unknown donor across the cytoplasmic membrane and passes them, either directly or indirectly, to PG *O*-acetyltransferase B (PatB), a soluble periplasmic protein. PatB then transfers the acetyl groups onto MurNAc residues. Lastly, *O*-acetylPG esterase (Ape1) hydrolyzes *O*-acetyl groups from PG (Weadge and Clarke, 2006).

In Gram-positive bacteria the process of O-acetylation utilises a somewhat different system (Figure 1.5B). This system is comprised of a single dual domain protein, *O*-acetyltransferase A (OatA), that adopts the functions of both PatA and PatB. To date, no *O*-acetylPG esterase has been identified in a Gram-positive bacterium. OatA was first discovered in *S. aureus* (Bera et al., 2005) and orthologues were subsequently identified in numerous Staphylococcal species (Bera et al., 2006), as well as other Gram-positive bacteria, including *S. pneumoniae* (Crisostomo et al., 2006), *Lactococcus lactis* (Veiga et al., 2007), and *Listeria monocytogenes* (Aubry et al., 2011). The N-terminal region of OatA is predicted to a transmembrane domain and, like PatA, this domain is thought to shuttle the acetyl groups across the cytoplasmic membrane to pass to the C-terminal soluble domain for their transfer onto MurNAc residues (Moynihan and Clarke, 2011).

A paralog of OatA, named OatB, was identified in *Bacillus anthracis* by Laaberki *et al*. in 2010 and it was demonstrated to contribute to levels of PG *O*-acetylation, although there was no obvious phenotype observed with an *oatB* deletion mutant (Laaberki et al., 2010). The following year, Bernard *et al*. reported the identification of another *O*-acetyltransferase in *Lactobacillus plantarum*, *Lactobacillus sakei*, and *Weissella paramesenteroides*, also named OatB, and this enzyme was confirmed experimentally to O-acetylate GlcNAc (Bernard et al., 2011).

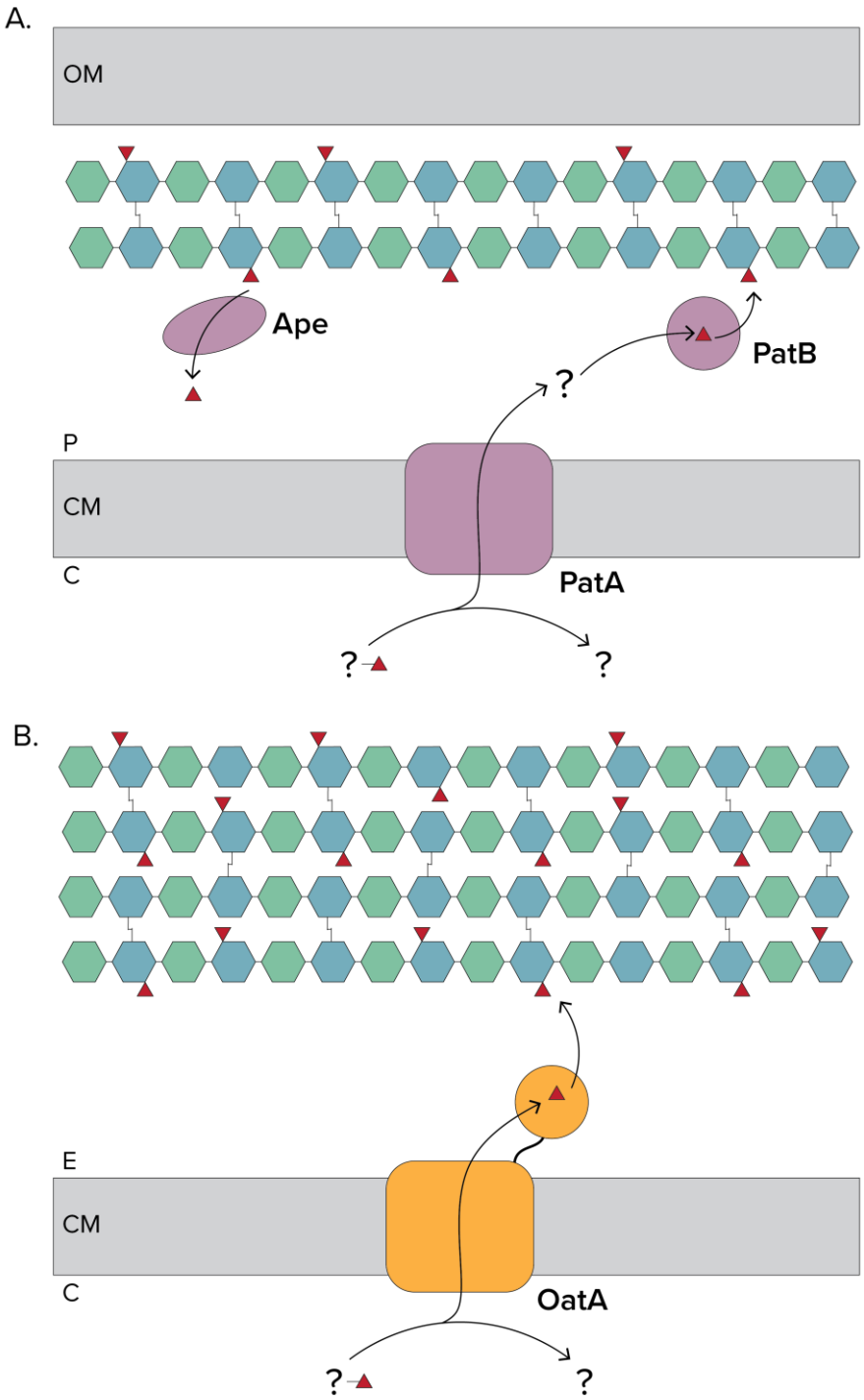

Figure 1.5 PG O-acetylation pathways. A. PG O-acetylation in Gram-negative bacteria involves three enzymes found in the *oap* cluster. PatA is an integral membrane protein that is predicted to shuttle acetyl groups across the cytoplasmic membrane to PatB, which transfers acetyl groups onto PG. The *O*-acetylesterase, Ape, acts to remove acetyl groups from PG. B. In Gram-positive bacteria, PG O-acetylation involves a single bimodular enzyme, OatA, with an integral membrane domain that is predicted to function analogously to PatA and transfer acetyl groups across the cytoplasmic membrane to the C-terminal domain for their transfer onto PG. No *O*-acetylesterase has been identified thus far in Gram-positive bacteria. E, external; P, periplasm; CM, cytoplasmic membrane; C, cytoplasm.

1.5.4 Regulation of peptidoglycan O-acetylation

There is very little known about the regulation of PG O-acetylation at either the genetic or enzymatic level (Moynihan and Clarke, 2011). *In-silico* analysis suggested that the *oap* gene cluster in *N. gonorrhoeae* is transcribed from a shared promoter and this was later confirmed in *N. meningitidis*, though no inducing molecule or regulator has been identified (Veyrier et al., 2013). Given that O-acetylation has been implicated in chain-length regulation of PG and control of autolysins in Gram-negatives, regulation of the *O*-acetyltransferases and *O*-acetylPG esterases would, presumably, be important. Overexpression of OatA in the Gram-positive bacterium *L. lactis* results in severe cell morphological defects, giving credence to the idea of a regulatory system (Veiga et al., 2007). In *L. lactis*, a novel regulator, SpxB, was found to increase *oatA* expression in response to the CesSR two-component system that senses cell-wall damage (Veiga et al., 2007). Thus far, however, similar systems have not been found or investigated in other organisms.

Additionally, there may also be a degree of control at the post-translational level with the association of PG *O*-acetyltransferases with murosomes or PG replicases (Moynihan and Clarke, 2011). Well before the discovery of PatA and B, it was observed that inactivation of PBP2 by penicillin in *N. gonorrhoeae* resulted in a decrease in the level of O-acetylation (Dougherty, 1985). This implies, in the very least, a relationship between a PG *O*-acetyltransferases and PBPs, though this has not been investigated further.

1.6 *O*-acetyltransferase A

O-Acetyltransferase A (OatA) from *S. aureus* was the first enzyme identified to be involved in PG O-acetylation (Bera et al., 2005). The N-terminal region of OatA is a member of the acyltransferase 3 family of enzymes and an *in silico* analysis predicted 11 transmembrane helices. As stated above, this domain was predicted to shuttle the acetyl group across the cytoplasmic membrane (Moynihan and Clarke, 2011). The C-terminal domain is extracytoplasmic and predicted to function in the attachment of *O*-acetyl groups to PG (Moynihan and Clarke, 2011). Whether the N-terminal domain passes the acetyl group to the C-terminal domain directly or indirectly is still unknown. Indeed, it is still unclear whether the two domains remain attached. *S. aureus* OatA possesses a non-canonical signal peptidase site between the two domains, and the C -terminal domain alone

was detected in spent culture media (Schallenberger et al., 2012). Upon discovery of OatA in *S. aureus*, Bera *et al.* predicted that a lysine-rich region in the C-terminal domain contained the catalytic activity (Bera et al., 2005). Further *in silico* analysis, however, revealed that OatA was a member of the SGNH/GDSL hydrolase/esterase family along with PatB and Ape1 (Moynihan and Clarke, 2011, 2014a; Weadge and Clarke, 2007). Despite low sequence identity between PatB and OatA, and among these enzymes from different organisms, there is biochemical and structural evidence to suggest these features are conserved for *S. pneumoniae* OatA (Sychantha et al., 2017), *N. gonorrhoeae* PatB (Moynihan and Clarke, 2014b) (Brott and Clarke, unpublished), and *N. meningitidis* Ape1 (Williams et al., 2014).

1.6.1 SGNH/GDSL hydrolase family

SGNH/GDSL hydrolases share little overall sequence identity, however, they are characterised by four invariant residues: Ser, Gly, Asn, and His in four consensus sequence blocks (I, II, III, V; block IV was originally described but has since been discounted) (Akoh et al., 2004). The typical catalytic triad consists of a Ser from Block I and His and Asp residues from Block III. The oxyanion hole of SGNH hydrolases is typically formed by the backbone NH of the catalytic Ser in Block I, the backbone NH of Gly from Block II, and the side chain amide of Asn in Block III (Akoh et al., 2004). Enzymes in this family include esterases and acyl transferases, though the features resulting in these differing functions is not known. Some researchers propose that subtle differences in the active site of acyl transferases favour binding of an amine or alcohol acceptor and disfavour water binding (Rauwerdink and Kazlauskas, 2015). For example, a hydrophobic active site that favours the binding of a more hydrophobic acceptor over water and/or hindering the appropriate approach of a water acceptor (Sychantha et al., 2017), and hydrogen bonds and ion-pair interactions to bind and orient the preferred acceptor (Lejon et al., 2008). Additionally, subtle changes to the oxyanion hole may lower the reactivity with water. In esterases, a water molecule coordinated in the active site may act as a base to increase the nucleophilicity of an attacking water, whereas a slight change in the orientation of the oxyanion hole residues in a transferase may displace such a bridging water (Jiang et al., 2011).

SGNH hydrolase family enzymes with Ser-His-Asp catalytic triads function *via* the

ping-pong bi-bi reaction mechanism, and this is the mechanism by which OatA is predicted to function (Figure 1.6) (Moynihan and Clarke, 2014b). In this proposed mechanism, the carboxyl group of the catalytic Asp forms a salt bridge with a nitrogen atom in the imidazole ring of His, rendering the His more nucleophilic and enabling His to deprotonate Ser. This renders Ser nucleophilic, allowing it to attack the carbonyl carbon of the acetyl donor, generating a tetrahedral transition state. Residues at the active centre of the enzyme form an oxyanion hole that stabilizes the transition state, which then collapses into a covalently-bound acetyl-enzyme intermediate. The acetyl donor is released upon acquisition of the proton from the serine hydroxyl from His. The glycan accepter, in the case of OatA a MurNAc residue of the PG backbone, can then bind the active site cleft. Through acid/base catalysis, His abstracts a proton from the C-6 hydroxyl of MurNAc, rendering the carbon atom nucleophilic and resulting in its attack on the carbonyl centre of the acetyl-Ser intermediate. This leads to the formation of a second tetrahedral transition state, collapse of which results in the release of the O-acetylated product and free enzyme.

1.6.2 Acyltransferase 3 family

Whilst PatA is part of the membrane-bound *O*-acyltransferase (MBOAT) family of enzymes, with a characteristic putative catalytic His, the N-terminal domain of OatA is a member of the acyltransferase 3 family. The acyltransferase 3 family of enzymes is a poorly studied group with no defining characteristics, other than several transmembrane helices and a role in acyl transfer. Acyltransferase 3 family enzyme are involved in a variety of functions including O-antigen O-acetylation. Investigation into enzymes involved in these processes has revealed some potentially conserved features.

Although the majority of the enzymes in the acyltransferase 3 family are monofunctional, representative enzymes with one or more accessory domains are also found, including proteins with SGNH hydrolase domains. An *O*-acetyltransferase involved in *O*-acetylation of O-antigen in some *Salmonella typhimurium* serotypes, OafA, was genetically characterized over 2 decades ago (Slauch et al., 1996) and found to possess an N-terminal acyltransferase 3 domain and a C-terminal stretch of 250 amino acids that is not predicted to be in the membrane. Similarly, Oac from *P. aeruginosa* serotype O20 is also involved in O-antigen acetylation and possesses an N-terminal acyltransferase 3 domain and a C-terminal periplasmic domain of 287 amino acids (Newton et al., 2001). A

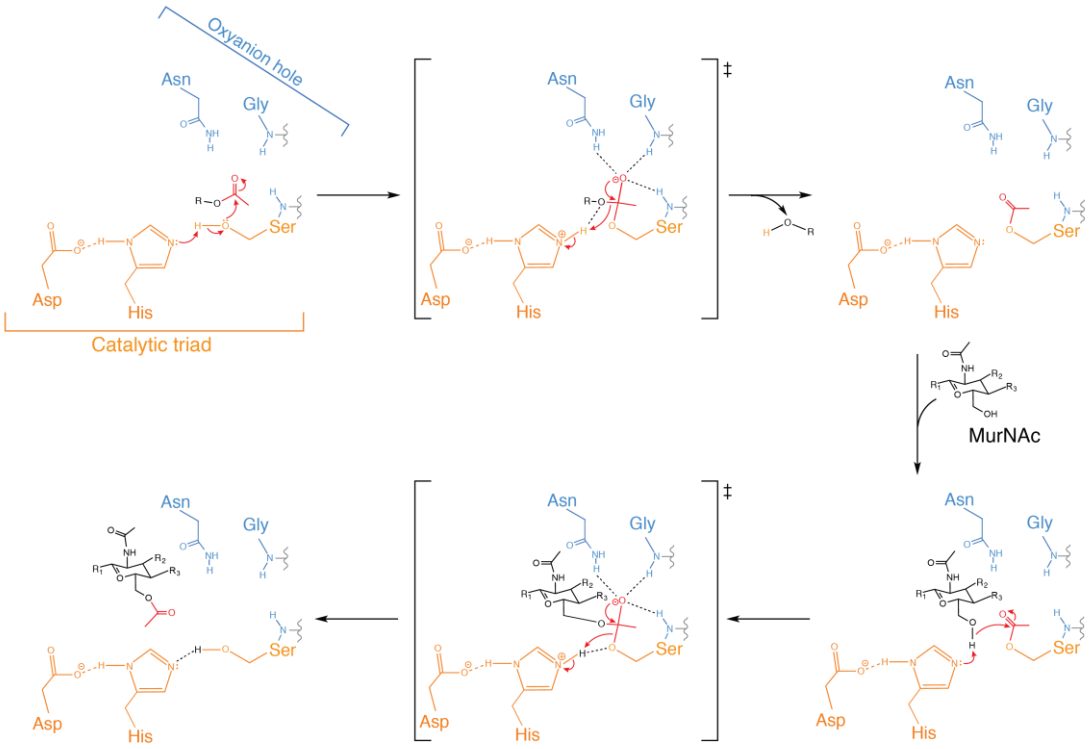

Figure 1.6 SGNH hydrolase reaction mechanism. SGNH hydrolase family enzymes are predicted to catalyze reactions using the ping-pong bi-bi reaction mechanism. An acetyl donor enters the active site, where Ser, rendered nucleophilic by the H-bonding network of the Asp and His catalytic triad residues, attacks the carbonyl carbon of the acetyl donor. A tetrahedral transition state forms, which is stabilized by residues forming the oxyanion hole, typically the backbone amides of a Gly residue and the catalytic Ser, and the sidechain amid of an Asn. The transition state collapses into a covalently-bound acetyl-Ser intermediate and the acetyl donor is released. The glycan accepter, a MurNAc residue of the PG backbone (in the case of OatA), binds the active site and the accepting carbon atom is rendered nucleophilic by the catalytic His, resulting in an attack on the carbonyl centre of the acetyl-Ser intermediate. This leads to the formation of a second tetrahedral transition state, collapse of which results in the release of the O-acetylated product and free enzyme.

homologous enzyme in *Haemophilus influenzae* was also found, but was not characterized beyond the genetic level (Fox et al., 2005). At the time, the authors could not identify anything homologous to the C-terminal domain in the database, even though it appeared to be essential for function. A recent search of numerous databases, however, revealed that the C-terminal domain has homology to the SGNH hydrolase family of enzymes, like OatA, and the characteristic G-x-S-x and D-x-x-H motifs were identified in the sequences.

A putative conserved motif of V-x-x-F-F-x-I/V/L-S-G-F/W/Y was identified in

several O-antigen *O*-acetyltransferases (Lück et al., 2001; Thanweer et al., 2008). These acetyltransferases lack additional domains. However, such a motif was also found in *S. aureus* OatA and homologues and thus may be relevant to function regardless of domain architecture. In some strains of *Legionella pneumophila*, the O-antigen is O-acetylated by an enzyme known as Lag-1 (Lück et al., 2001). A non-functional isogenic mutant of Lag-1 was identified with a single point mutation that resulted in a change from a serine residue to a leucine residue. This replacement was in the highly conserved motif (V-x-x-F-F-x-I/V/L-S-G-F/W/Y), leading to the hypothesis that this is a catalytic motif. The same conserved motif was identified in OacA, an *O*-acetyltransferase involved in the O-acetylation of the C-2 hydroxyl of Rha II of O-antigen in *Shigella flexneri* (Thanweer et al., 2008). Futhermore, topology mapping with the dual reporter PhoA-LacZα, Oac was found to have 10 α-helical membrane-spanning regions with both N- and C-termini located in the cytoplasm. Further study of the conserved motifs in transmembrane spanning helices and hydrophilic loops confirmed several residues important for proper protein assembly and catalysis, including a catalytic arginine (Thanweer and Verma, 2012). The work, however, was based on phenotypic observations alone and investigation into specific roles or mechanisms is still lacking.

Lastly, O-acetylation of Enterobacterial Common Antigen (ECA) in *E. coli* is accomplished by WecH, a 331-amino acid protein with 10 predicted transmembrane helices (Kajimura et al., 2006). O-Acetylation occurs at the C-6 hydroxyl of GlcNAc residues in both water-soluble cyclic ECA and phosphoglyceride-lined linear ECA, however very little is known about this enzyme beyond that. Interestingly, WecH can compensate for PatA to allow for PG O-acetylation in *E. coli* by recombinantly expressed *N. gonorrhoeae* PatB (Moynihan and Clarke, 2010).

1.6.3 Recent research

Initial inferences as to the function and role of OatA were based on studies of the soluble enzyme PatB from *N. gonorrhoeae*. Biochemical evidence confirmed the localisation of PatB to the periplasm, and its activity and substrate specificity as an acetyltransferase (Moynihan and Clarke, 2010, 2014a). Furthermore, this research also demonstrated the dependence of PatB on a functional acetate translocator, hypothetically PatA (Moynihan and Clarke, 2010). PatB was confirmed to function *via* a ping-pong bi-bi

reaction mechanism utilizing a Ser-His-Asp catalytic triad (Moynihan and Clarke, 2014b).

The first in-depth study on any OatA was executed on OatA (originally designated Adr) from *S. pneumoniae* (Sychantha et al., 2017). The X-ray crystal structure of this enzyme was solved, revealing an α/β-fold characteristic of SGNH hydrolase enzymes. In addition, like PatB, the reaction was confirmed to occur *via* a ping-pong bi-bi mechanism involving a Ser-His-Asp catalytic triad (Sychantha and Clarke, 2018; Sychantha et al., 2017). The active site of the enzyme had some marked differences when compared to other SGNH hydrolase enzymes, particularly in the residues forming the oxyanion hole (Sychantha et al., 2017). Whilst the exact mechanism by which OatA acts as a transferase remains unclear, Sychantha *et al*. (2017) proposed that a conserved Val/Ile adjacent to the oxyanion hole Arg may stabilize carbohydrate acceptors in *S. pneumoniae* OatA and related OatA enzymes. As this position is often occupied by a polar residue in OatA homologues from other genera, it remains to be determined how these OatA enzymes might favour transferase activity.

The substrate specificity of *S. pneumoniae* OatA was also investigated and compared to that of *S. aureus* OatA using artificial muroglycans (Sychantha et al., 2017). Interestingly, *S. pneumoniae* OatA was shown to have a specificity for MurNAc with a tetrapeptide stem, whereas *S. aureus* OatA had a specificity for MurNAc with a pentapeptide stem. Neither utilized MurNAc with a tripeptide stem. This differs from the finding that PatB from *N. gonorrhoeae* has a substrate specificity for muropeptides with tri- and tetrapeptide stems (Moynihan and Clarke, 2014a) and suggests that the PG *O*-acetyltransferases from different bacteria may act at different sites and/or stages of PG assembly.

1.7 Hypothesis and thesis objectives

S. aureus is an opportunistic pathogen, and although humans can carry *S. aureus* asymptomatically, this bacterium is a leading cause of bacteremia, infective endocarditis, and toxic shock syndrome and it ranks as the second most common cause of nosocomial bloodstream infections (Pittet and Wenzel, 1995; Tong et al., 2015). Methicillin-resistant *S. aureus* (MRSA) has become increasingly prevalent, and *S. aureus* resistant to vancomycin (VRSA), the primary antibiotic used to treat MRSA, was identified in 2002 (Centers for Disease Control and Prevention, 2002). Due to their increasing prevalence and

mortality, MRSA and VRSA are on the Centres for Disease Control and Prevention (CDC) serious threats list and have been identified by the World Health Organization as high priority pathogens for the research and development of new antibiotics (Centers for Disease Control and Prevention, 2013; The World Health Organization, 2017). Given the rapid rise of antimicrobial resistance, many researchers are pursuing alternative approaches to combat multi-drug resistant infections. One example is searching for ways to disarm bacteria with non-traditional therapeutic agents (Rex et al., 2019). By targeting virulence factors that significantly contribute to the ability of a bacterium to colonize a host or cause infection, it will be possible to prevent infection without otherwise affecting survivability of the bacterium. The current thought is that drugs targeting virulence factors may suffer less from the development of resistance (Rex et al., 2019). The role of PG O-acetylation in lysozyme resistance has been well established, but it is not otherwise essential to growth, replication or viability, and therefore the enzymes involved are promising candidate targets for the development of novel anti-virulence drugs. The purpose of this research was to gain a greater understanding of PG O-acetylation in Gram-positive bacteria using *S. aureus* as a model organism in an effort to guide the development of novel antimicrobials.

A pilot screen of *S. aureus* OatA of approximately 4000 compounds was conducted prior to this study (Kell, 2015), however the inhibitors identified in this screen were not particularly potent or fully characterized. The first stage in the development of a novel antimicrobial is the identification of a lead compound, which requires the screening of potentially thousands of compounds. To facilitate this, the first objective of this thesis was to complete a large-scale high-throughput screen for inhibitors of the C-terminal SGNH hydrolase domain from *S. aureus* OatA (*Sa*OatA$_C$) and characterize lead compounds. This work sought to investigate the hypothesis that inhibitors of *Sa*OatA$_C$ will sensitize *S. aureus* to lysozyme.

Designing and optimizing inhibitors for OatA can be aided by a thorough understanding of the PG O-acetylation system gained through structural and biochemical studies. Whilst the GDSL/SGNH hydrolase domain of *S. pneumoniae* OatA (Sychantha and Clarke, 2018; Sychantha et al., 2017) and *N. gonorrhoeae* PatB (Moynihan and Clarke, 2010, 2014b, 2014a) have been well characterized, the cognate transmembrane domains have not been studied at all. I hypothesize that the N-terminal domain of OatA is a

transmembrane protein that serves to transfer acetyl groups from the cytoplasm to the C-terminal domain of OatA. To addresss this hypothesis, the topology of the N-terminal acyltransferase 3 domain of *S. aureus* OatA (*Sa*OatA$_N$) was determined and putative functional residues were characterized with mutagenesis studies. In addition, the interaction between the N- and C-terminal domains was investigated.

Lastly, although *S. aureus* OatA is predicted to function similarly to *S. pneumoniae* OatA, data on their different substrate specificities suggests they may not function in identical ways (Sychantha et al., 2017). I hypothesize that the structure and mechanism of the C-terminal domain of *S. aureus* OatA will differ from that of *S. pneumoniae* OatA. To explore this idea, the crystal structure of *Sa*OatA$_C$ was solved and the catalytic mechanism was investigated with structure guided mutagenesis studies.

Chapter 2. Materials and methods

2.1 Bacterial strains and growth conditions

Cultures of bacteria (Table 2.1) were grown at 37ºC with aeration in Luria-Bertani broth (LB) (Difco) or Tryptic Soy Broth (TSB) (Difco), as indicated. Media were supplemented with appropriate antibiotics (*E. coli*: 100 µg/mL ampicillin, 50 µg/mL kanamycin; *S. aureus*: 10 µg/mL chloramphenicol) when required.

Table 2.1 Strain List

Strain name	Description	Reference
E. coli DH5α	Cloning host (F^- *endA1 glnV44 thi-1 recA1 relA1 gyrA96 deoR nupG purB20* φ80d*lacZ* ΔM15 Δ(*lacZYA-argF*)U169, hsdR17($r_K^- m_K^+$), λ^-)	Invitrogen
E. coli BL21 (DE3)	Overexpression host (F^- *ompT gal dcm lon hsdS*$_B$($r_B^- m_B^-$) λ(DE3 [*lacI lacUV5-T7p07 ind1 sam7 nin5*]) [*malB*$^+$]$_{K\text{-}12}$(λ^S))	Invitrogen
E. coli C43 (DE3)	Overexpression host derived from *E. coli* BL21 that contains uncharacterized genetic mutations that confer tolerance to toxic proteins (F^- *ompT gal dcm hsdS*$_B$(r_B^- m_B^-) (DE3)	(Miroux and Walker, 1996)
S. aureus RN4220	Intermediate cloning host; restriction-deficient mutant of strain NCTC8325-4 that accepts foreign DNA (*sau1*$^-$ *hsdR*$^-$)	(Kreiswirth et al., 1983; Nair et al., 2011)
S. aureus USA300	Community-associated methicillin resistant *S. aureus* strain	(Christianson et al., 2007)
S. aureus USA300 Δ*oatA*	*S. aureus* USA300 with a deletion of base pairs 440-1523 in the *oatA* gene (SAUSA300_2504)	This study
S. aureus USA300 Δ*tarO*	*S. aureus* USA300 with the *tarO* gene replaced with a spectinomycin cassette	(Farha et al., 2013)
Bacillus cereus 10987	Non-lethal dairy isolate of *B. cereus*	(Rasko et al., 2004)

2.2 Cloning methods

Plasmids generated and/or used in this study are listed in Table 2.2. Custom DNA oligonucleotide primers (Table 2.3) were obtained from Integrated DNA Technologies. Chromosomal DNA was obtained using the PureLink Genomic DNA Mini Kit (Invitrogen)

Table 2.2 Plasmid List

Plasmid name	Description	Reference or source
pDSAC71	pET-sumo derivative containing *S. aureus* SA113 OatA (445-601); Kan^r	Dr. David Sychantha
pACCJ2	pET-21b derivative containing *S. aureus* ATCC6538 OatA (1-603); Amp^r	This study
pALC2073	*E. coli-S. aureus* shuttle vector with tetracycline inducible promotor; Amp^r in *E. coli*, Cm^r in *S. aureus*	(Bateman et al., 2001)
pACCJ3	pALC2073 derivative containing *S. aureus* ATCC6538 OatA (1-603) cloned with an N-terminal Shine-Dalgarno sequence and a C-terminal His_{10}-tag; Amp^r in *E. coli*, Cm^r in *S. aureus*	This study
pKOR1	Plasmid vector for knocking out genes in *S. aureus* containing a lambda recombination cassette, antisense *secY* expression cassette, tetracycline inducible promoter, and a temperature sensitive origin of replication for *S. aureus*; Amp^r in *E. coli*, Cm^r in *S. aureus*	(Bae and Schneewind, 2006)
pACCJ4	pALC2073 derivative containing *S. pneumoniae* R6 OatA (1-604) cloned with an N-terminal Shine-Dalgarno sequence and a C-terminal His_{10}-tag; Amp^r in *E. coli*, Cm^r in *S. aureus*	This study
pACCJ5	pALC2073 derivative containing a chimera OatA consisting of the N-terminal domain of *S. aureus* ATCC6538 OatA (1-401) and the C-terminal domain of *S. pneumoniae* R6 OatA (395-604) cloned with an N-terminal Shine-Dalgarno sequence and a C-terminal His_{10}-tag; Amp^r in *E. coli*, Cm^r in *S. aureus*	This study
pACCJ6	pALC2073 derivative containing a chimera OatA consisting of the N-terminal domain of *S. pneumoniae* R6 OatA (1-394) and the C-terminal domain of *S. aureus* ATCC6538 OatA (402-603) cloned with an N-terminal Shine-Dalgarno sequence and a C-terminal His_{10}-tag; Amp^r in *E. coli*, Cm^r in *S. aureus*	This study
pPLE01	Empty *E. coli* vector for LacZα-PhoA fusion protein tagging; Amp^r	(Islam et al., 2010)
pACCJ8	pPLE01 derivative containing *S. aureus* ATCC6538 OatA (1-603) with a A401E mutation and the *PstI* site in the gene eliminated by silent site-directed mutagenesis; Amp^r	This study

and the PureLink Quick Plasmid Miniprep kit (Invitrogen) was used to isolate plasmid DNA from overnight cultures. PCR-amplification was performed using KAPA HiFi

Polymerase (Sigma Aldrich). Restriction enzymes (NEB), *Dpn1* (Thermo Scientific), and T4 DNA Ligase (Thermo Scientific) were used according to manufacturer's instructions. DNA sequencing was performed in the Genomics Facility of the Advanced Analysis Center at the University of Guelph. Plasmids were transformed into chemically competent *E. coli* strains by heat-shock. Briefly, Competent cells (100 µL) were incubated on ice with ~50 ng plasmid for 30 min. The cells were heat-shocked for 3 min at 37 ºC and then mixed with 500 µL LB broth and allowed to recover for 1 hr at 37ºC before plating on LB agar with appropriate antibiotic. Plasmids to be placed in *S. aureus* USA300 were first transformed into electrocompetent *S. aureus* RN4220 by electroporation for modification and then isolated and transformed into the appropriate strain of electrocompetent *S. aureus* USA300. Electrocompetent *S. aureus* cells (60 µL) were incubated on ice with 50-100 ng of plasmid for 30 min. Cells were transferred into an electroporation cuvettes and electroporated (2.5 kV). TSB (940 µL) was added and the cells were allowed to recover for 1-3 hr at 30 ºC or 37 ºC before plating onto Tryptic Soy Agar (TSA) with appropriate antibiotic.

Table 2.3 Primer List

Primer Name	**Primer Sequence (5′ – 3′)[1]**	**Resultant plasmid name**
01saOatAFull	GATC*GCTAGC*ATGGATACAAAAGACTTTAAACGTT	pACCJ2
02saOatAFull	CGTA*CTCGAG*TTTCTTATTTGTAGCATGTGTTTCC	
01saOatA KK141&142	ATTGGTAATGTCTTTACT**GC**G**GCA**ATACCAAATGCACAAATT	pDSAC71 KK464&465AA
02saOatA KK141&142	AATTTGTGCATTTGGTAT**TGCCGC**AGTAAAGACATTACCAAT	
01saOatA KK172&173	CAATATAAAGACTATGCT**GCAGCA**GGTCAAAAAGTTGTAGTA	pDSAC71 KK495&496AA
02saOatA KK172&173	TACTACAACTTTTTGACC**TGCTGC**AGCATAGTCTTTATATTG	
01saOatA EK228&229	TTAATTTATGAGGCAGCT**GCAGCG**CGCTCTAATGTACATCTA	pDSAC71 EK551&552AA
02saOatA EK228&229	TAGATGTACATTAGAGCG**CGCTGC**AGCTGCCTCATAAATTAA	
01saOatAFull C96A	GCAGTGTTATTTTTAATC**GCT**GTCGTGCTTACGTTCACA	pACCJ3 C96A

02saOatAFull C96A	TGTGAACGTAAGCACGAC**AGC**GATTAA AAATAACACTGC	
01saOatAFull C220A	CAAACTTTATTGCTTGGT**GC<u>T</u>**ATATTAG CATTTATTTGG	pACCJ3 C220A
02saOatAFull C220A	CCAAATAAATGCTAATAT**AGC**ACCAAG CAATAAAGTTTG	
OatA attB1 upstream F	*GGGGACAAGTTTGTACAAAAAAGCAGGCT* TTCGATGCAATAATAATTGATATGAC	pKOR1-Δ*oatA*
OatA sacII upstream R	GGACCT*CCGCGG*CACAGATTAAAAATA ACACTGCC	
OatA sacII downstream F	GGACCT*CCGCGG*TTGGTAATGTCTTTAC TAAGAAAATAC	
OatA attB2 downstream R	*GGGGACCACTTTGTACAAGAAAGCTGGGT* AATTAAATATCCTCCCAATAATCAAAAC	
Upstream amplicon F	GATAATCTATGTTATGTAGTAAAATCGA C	
Downstream amplicon R	ATCATTTTTGATAATAAATATCAGAAGT AATG	
FLSaOatA SacI-SD-F	GATC*GAGCTC*GGGAGGTTTTAAACATGG ATACAAAAGACTTTAAACGTT	pACCJ3
FLSaOatA EcoRI-R	GATC*GAATTC*TCAGTGGTGGTGGTGG	pACCJ3/ pACCJ4
FLSaOatA S14C F	CGTTTAGAAAAAATGTAT**T<u>G</u>C**CCGCGA TACTTACCTGGA	pACCJ3 S14C
FLSaOatA S14C R	TCCAGGTAAGTATCGCGG**G<u>C</u>A**ATACAT TTTTTCTAAACG	
FLSaOatA G403C F	GGACAGTTTGATGCACTT**<u>T</u>GC**AAACAA CATGAAGCCGAG	pACCJ3 G403C
FLSaOatA G403C R	CTCGGCTTCATGTTGTTT**GC<u>A</u>**AAGTGCA TCAAACTGTCC	
FLSaOatA L42C F	CACTTGAATGCACAATGG**T<u>GT</u>**AGTGGG GGCTTTTTAGGA	pACCJ3 L42C
FLSaOatA L42C R	TCCTAAAAAGCCCCCACT**<u>AC</u>A**CCATTGT GCATTCAAGTG	
FLSaOatA I121C F	CGAGATGCTATTGCAGCT**<u>TGT</u>**TTCTATG TTTCAAACTGG	pACCJ3 I121C
FLSaOatA I121C R	CCAGTTTGAAACATAGAA**<u>ACA</u>**AGCTGC AATAGCATCTCG	
FLSaOatA V205C F	ACTGGAGATAATTCACGT**<u>TGT</u>**TATTTTG GGACAGATACA	pACCJ3 V205C
FLSaOatA V205C R	TGTATCTGTCCCAAAATA**<u>ACA</u>**ACGTGAA TTATCTCCAGT	
FLSaOatA Q264C F	GACTTTGTTCTTTATAGTTGGAGAC**<u>TGT</u>** GATCAATGG	pACCJ3 Q264C
FLSaOatA Q264C R	CTCCATTATAGATCCATTGATC**<u>ACA</u>**GTC TCCAAC	

FLSaOatA A401E F	CTCAGTGGACAGTTTGAT**GAA**CTTGGCA AACAACATGAA	pACCJ3 A401E
FLSaOatA A401E R	TTCATGTTGTTTGCCAAG**TTC**ATCAAAC TGTCCACTGAG	
FLSaOatA A401L F	CTCAGTGGACAGTTTGAT**CTA**CTTGGCA AACAACATGAA	pACCJ3 A401L
FLSaOatA A401L R	TTCATGTTGTTTGCCAAG**TAG**ATCAAAC TGTCCACTGAG	
FLSaOatA R25A F	CCTGGATTAGATGGATTG**GCG**GCATTC GCAGTTATAGGA	pACCJ2 R25A/ pACCJ3 R25A
FLSaOatA R25A R	TCCTATAACTGCGAATGC**CGC**CAATCCA TCTAATCCAGG	
FLSaOatA H36A F	ATAGGAATCATTATTTAT**GCC**TTGAATG CACAATGGTTA	pACCJ3 H36A
FLSaOatA H36A R	TAACCATTGTGCATTCAA**GGC**ATAAAT AATGATTCCTAT	
FLSaOatA V49A F	AGTGGGGGCTTTTTAGGA**GCA**GATACA TTCTTCGTTATT	pACCJ3 V49A
FLSaOatA V49A R	AATAACGAAGAATGTATC**TGC**TCCTAA AAAGCCCCCACT	
FLSaOatA F52A F	TTTTTAGGAGTAGATACA**GCC**TTCGTTA TTTCAGGTTAT	pACCJ3 F52A
FLSaOatA F52A R	ATAACCTGAAATAACGAA**GGC**TGTATC TACTCCTAAAAA	
FLSaOatA S56A F	GATACATTCTTCGTTATT**G**CAGGTTATT TAATAACAAGT	pACCJ3 S56A
FLSaOatA S56A R	ACTTGTTATTAAATAACCTG**C**AATAACG AAGAATGTATC	
SaOatAc D457A F	GGTGACTCGGTCATGGTG**GCT**ATTGGTA ATGTCTTTACT	pDSAC71 D457A/ pACCJ3 D457A
SaOatAc D457A R	AGTAAAGACATTACCAATA**GC**CACCAT GACCGAGTCACC	
SaOatAc D457N F	GGTGACTCGGTCATGGTG**AAT**ATTGGTA ATGTCTTTACT	pDSAC71 D457N/ pACCJ3 D457N
SaOatAc D457N R	AGTAAAGACATTACCAATA**TT**CACCAT GACCGAGTCACC	
SaOatA S453A F	CTATTAATTGGTGAC**GCG**GTCATGGTGG ATATT	pDSAC71 S453A
SaOatA S453A R	AATATCCACCATGAC**CGC**GTCACCAATT AATAG	
SaOatA D575A F	GAATACTTTGCATAT**GCC**GGTATTCACT TAGAA	pDSAC71 D575A/ pACCJ3 D575A
SaOatA D575A R	TTCTAAGTGAATACC**GGC**ATATGCAAA GTATTC	
SaOatA H577A F	GCATATGACGGTATT**GCC**TTAGAATATG CAGGT	pDSAC71 H578A/

SaOatA H577A R	ACCTGCATATTCTAA**GGC**AATACCGTCA TATGC	pACCJ3 H578A
FLSaOatA R83A F	GAGTTTTGGAAGCGA**GCA**TTGAAACGA CTCATT	pACCJ3 R83A
FLSaOatA R83A R	AATGAGTCGTTTCAA**TGC**TCGCTTCCAA AACTC	
FLSaOatA S453A-2 F	AAGTCATCACCACTATTAATTGGTGAC**G CG**GTCATGGTG	pACCJ3 S453A/ pACCJ2 S453A
FLSaOatA S453A-2 R	AGTAAAGACATTACCAATATCCACCATG AC**CGC**GTCACCAAT	
FLSaOatA R86A-2 F	GAGTTTTGGAAGCGACGATTGAAA**GCA** CTCATTCCG	pACCJ2 R86A/ pACCJ3 R86A
FLSaOatA R86A-2 R	GACACAGATTAAAAATAACACTGCCGG AATGAG**TGC**TTTCAATCG	
FLSaOatA Y136A-2 F	TGGTGGTACATTTCACAGAATGTAGAT**G CT**TTTAACCAA	pACCJ2 Y136A/ pACCJ3 Y136A
FLSaOatA Y136A-2 R	GTTTGAGTGGTTCAATAGCAAATTGGTT AAA**AGC**ATCTACATT	
FLSaOatA Y206A-2 F	TTCATCACTGGAGATAATTCACGTGTG**G CT**TTTGGGACA	pACCJ2 Y206A/ pACCJ3 Y206A
FLSaOatA Y206A-2 R	CAGTCGTGTATCTGTCCCAAAA**AGC**CACA CGTGA	
SaN401-SpC395 F	TGTGCTCAGTGGACAGTTTGATGCATTT GAGACAGACTTGACTGTCAATGGCTT	pACCJ5
SaN401-SpC395 R	AAGCCATTGACAGTCAAGTCTGTCTCAA ATGCATCAAACTGTCCACTGAGCACA	
SpN394-SaC402 F	TTGGCACCACAAGTGGGAGCGCTTGGC AAACAACATGAAGCCGAGAAGAA	pACCJ6
SpN394-SaC402 R	TTCTTCTCGGCTTCATGTTGTTTGCCAAG CGCTCCCACTTGTGGTGCCAA	
FLSpOatA SacI-SD F	GATC*GAGCTC*GGGAGGTTTTAAACATGC GCATTAAATGGTTTTCCTTGATTAGGAT TAT	pACCJ4
FLSaOatA N126A IVA F	ATTGCAGCTATATTCTATGTTTCA**GCC**T GGTGGTAC	pACCJ3 N126A
FLSaOatA N126A IVA R	TGAAACATAGAATATAGCTGCAATAGC ATCTCGTTTCATTTGTA	
FLSaOatA E154A IVA F	CATTTATGGTCTTTAGCCATT**GCA**GAAC AATTTTACTTG	pACCJ3 E154AA
FLSaOatA E154A IVA R	AATGGCTAAAGACCATAAATGTTTGAGT GGTT	
SaOatA N507A F	GTAGTAGAGCTTGGTACA**GCT**GGGGCA TTT	pDSAC71 N507A/ pACCJ3 N507A
SaOatA N507A R	TGATCTTTCGTAAATGCCCC**AGC**TGTAC CAAG	

SaOatA V475G F	GCACAAATTGATGGTAAA**GGT**GGACGGCAA	pDSAC71 V475A/ pACCJ3 V475A
SaOatA V475G R	CAACGAGTTGCCGTCC**ACC**TTTACCATC	
SaOatA R477A F	ATTGATGGTAAAGTTGGA**GCG**CAACTCGTT	pDSAC71 R477A/ pACCJ3 R477A
SaOatA R477A R	GCATCAACGAGTTG**CGC**TCCAACTTT	
FLSaOatA S310A F	CCTTTACTAATTATAGGTAAACGA**GCA**TATAGCTTATACTTATGGCA	pACCJ3 S310A
FLSaOatA S310A R	TCGTTTACCTATAATTAGTAAAGGTTTCATACTTAAAAATTTAGCAAATAAAC	
FLSaOatA Y311A F	CCTTTACTAATTATAGGTAAACGATCA**GCT**AGCTTATACTTATGG	pACCJ2 Y311A/ pACCJ3 Y311A
FLSaOatA Y311A R	TGATCGTTTACCTATAATTAGTAAAGGTTTCATACTTAAAAATTTAGCA	
FLSaOatA Y314A F	ATAGGTAAACGATCATATAGCTTA**GCC**TTATGGCATTATCC	pACCJ3 Y314A
FLSaOatA Y314A R	TAAGCTATATGATCGTTTACCTATAATTAGTAAAGGTTTCATACTTAAAAATTTAGC	
FLSaOatA H317A F	CGATCATATAGCTTATACTTATGG**GCT**TATCCTATCATTGTTTTTG	pACCJ3 H317A
FLSaOatA H317A R	CCATAAGTATAAGCTATATGATCGTTTACCTATAATTAGTAAAGGTTTCATACT	
FLSaOatA E357A F	TGAAATTTCGTATCGCTTTATT**GCA**ACACCTATACGT	pACCJ2 E357A/ pACCJ3 E357A
FLSaOatA E357A R	AATAAAGCGATACGAAATTTCAGCCATTAACGCTG	
FLSaOatA F79A F	CAAAAAATCGATTTGCTAGAG**GCT**TGGAAGCG	pACCJ3 F79A
FLSaOatA F79A R	CTCTAGCAAATCGATTTTTTGCGTCCGATAATACTCAC	
FLSaOatA PstI mut F	GATTGGTATAAAGCTTCTGCCGGTCATCCGG	pACCJ8
FLSaOatA PstI mut R	CAAAGTATTCCGGATGACCGGCAGAAGCTTT	
FLSaOatA SacI F	GATC*GAGCTC*ATGGATACAAAAGACTTTAAACGTT	pACCJ8
FLSaOatA XbaI R	GAT*CTCTAGA*TTTCTTATTTGTAGCATGTGTTTCCATCG	
FLSaOatA Y35A F	TTCGCAGTTATAGGAATCATTATT**GCT**CACTTGAATGC	pACCJ3 Y35A
FLSaOatA Y35A R	AATAATGATTCCTATAACTGCGAATGCCCTCAATC	

FLSaOatA W149A F	CTATTGAACCACTCAAACATTTA**GCG**TC TTTAGCC	pACCJ3 W149A
FLSaOatA W149A R	TAAATGTTTGAGTGGTTCAATAGCAAAT TGGTTAAAATAATCT	
FLSaOatA Y158A F	CTTTAGCCATTGAAGAACAATTT**GCC**TT GCTTTTC	pACCJ3 Y158A
FLSaOatA Y158A R	AAATTGTTCTTCAATGGCTAAAGACCAT AAATGTTTGAG	
FLSaOatA Y269A F	GAGACCAAGATCAATGGATC**GCT**AATG GAGGATTTTA	pACCJ3 Y269A
FLSaOatA Y269A R	GATCCATTGATCTTGGTCTCCAACTATA AAGAACAAAG	
FLSaOatA H289A F	TCATTATTGCAATTGCGGTA**GCT**CCTTC TAG	pACCJ3 H289A
FLSaOatA H289A R	TACCGCAATTGCAATAATGAATAAAGTT GCAAATGA	
FLSaOatA S352A F	AGCGTTAATGGCTGAAATT**GCG**TATCG CT	pACCJ3 S352A
FLSaOatA S352A R	AATTTCAGCCATTAACGCTGTTAACAAA ATTTCTATAATATAAACGTATACCGG	
FLSaOatA 1-R380 XbaI R	GATC*TCTAGA*TCTAGCAAATTGCCCCTTC TTTTTAG	pACCJ8 1-R380
FLSaOatA 1-F365 XbaI R	GATC*TCTAGA*AAATCCTTTTTTACGTATA GGTGTTTCAATAAAGC	pACCJ8 1-F365
FLSaOatA 1-L231 XbaI R	GATC*TCTAGA*CAAAGCAAACGGAGGCCA AATAAATG	pACCJ8 1-L231
FLSaOatA 1-I305 XbaI R	GATC*TCTAGA*AATTAGTAAAGGTTTCAT ACTTAAAAATTTAGCAAATAAACT	pACCJ8 1-I305
FLSaOatA 1-R171 XbaI R	GATC*TCTAGA*TCTATGTAATAAGAACGT GATAACCAATGGGAA	pACCJ8 1-R171
FLSaOatA 1-R83 XbaI R	GATC*TCTAGA*TCGTCGCTTCCAAAACTCT AGCA	pACCJ8 1-R83
FLSaOatA 1-V253 XbaI R	GATC*TCTAGA*AACCGCAAAACCAGATAT CCCTATAATATCTAATG	pACCJ8 1-V253
FLSaOatA 1-A120 XbaI R	GATC*TCTAGA*AGCTGCAATAGCATCTCG TTTCATTTG	pACCJ8 1-A120
FLSaOatA 1-L281 XbaI R	GATC*TCTAGA*TAAAGTTGCAAATGATAT AATGTAAAATCCTCCATTATAGATCC	pACCJ8 1-L281
FLSaOatA 1-Q332 XbaI R	GATC*TCTAGA*TTGTCCTTGTACGTAATAA CTGTTCACAAAAAC	pACCJ8 1-Q332
FLSaOatA 1-P144 XbaI R	GATC*TCTAGA*TGGTTCAATAGCAAATTG GTTAAAATAATCTACATTCTG	pACCJ8 1-P144
FLSaOatA 1-L168 XbaI R	GATC*TCTAGA*TAAGAACGTGATAACCAA TGGGAAAAGCA	pACCJ8 1-L168
FLSaOatA 1-Y68 XbaI R	GATC*TCTAGA*ATACTCACTTATCAACAA ACTTGTTATTAAATAACCTGAAATAAC	pACCJ8 1-Y68

FLSaOatA 1-L344 XbaI R	GATC*TCTAGA*TAACAAAATTTCTATAATATAAACGTATACCGGTATTTGTCCT	pACCJ8 1-L344
FLSaOatA 1-A367 XbaI R	GATC*TCTAGA*AGCTTTAAATCCTTTTTTACGTATAGGTGTTTCAAT	pACCJ8 1-A367
FLSaOatA 1-L386 XbaI R	GATC*TCTAGA*TAGGATAACTAACACTGTTCTAGCAAATTGCC	pACCJ8 1-L386
FLSaOatA 1-Q40 XbaI R	GATC*TCTAGA*TTGTGCATTCAAGTGATAAATAATGATTCCTATAACTG	pACCJ8 1-Q40
FLSaOatA 1-I65 XbaI R	GATC*TCTAGA*TATCAACAAACTTGTTATTAAATAACCTGAAATAACGAAGA	pACCJ8 1-I65
FLSaOatA 1-L76 XbaI R	GATC*TCTAGA*CAAATCGATTTTTTGCGTCCGATAATACT	pACCJ8 1-L76
FLSaOatA 1-L87 XbaI R	GATC*TCTAGA*GAGTCGTTTCAATCGTCGCTTC	pACCJ8 1-L87
FLSaOatA 1-I130 XbaI R	GATC*TCTAGA*AATGTACCACCAGTTTGAAACATAGAATATAGC	pACCJ8 1-I130
FLSaOatA 1-Q139 XbaI R	GATC*TCTAGA*TTGGTTAAAATAATCTACATTCTGTGAAATGTACCAC	pACCJ8 1-Q139
FLSaOatA 1-P162 XbaI R	GATC*TCTAGA*TGGGAAAAGCAAGTAAAATTGTTCTTCAATG	pACCJ8 1-P162
FLSaOatA 1-I183 XbaI R	GATC*TCTAGA*AATAAATAGCGTTTGAATAATATTTCTCGGTTTAAATCTATGT	pACCJ8 1-I183
FLSaOatA 1-L189 XbaI R	GATC*TCTAGA*TAAAGAAATCAACGATACAATAAATAGCGTTTGAATAATATTTCT	pACCJ8 1-L189
FLSaOatA 1-R212 XbaI R	GATC*TCTAGA*TCGTGTATCTGTCCCAAAATACACAC	pACCJ8 1-R212
FLSaOatA 1-G247 XbaI R	GATC*TCTAGA*CCCTATAATATCTAATGATACGACAATCTTTTTAGAAATATCTT	pACCJ8 1-G247
FLSaOatA 1-Q264 XbaI R	GATC*TCTAGA*TTGGTCTCCAACTATAAAGAACAAAGTCATTAGA	pACCJ8 1-Q264
FLSaOatA 1-I275 XbaI R	GATC*TCTAGA*AATGTAAAATCCTCCATTATAGATCCATTGATCTTGG	pACCJ8 1-I275
FLSaOatA 1-A287 XbaI R	GATC*TCTAGA*CGCAATTGCAATAATGAATAAAGTTGCA	pACCJ8 1-A287
FLSaOatA 1-S326 XbaI R	GATC*TCTAGA*ACTGTTCACAAAAACAATGATAGGATAATGCC	pACCJ8 1-S326
FLSaOatA 1-Y338 XbaI R	GATC*TCTAGA*ATAAACGTATACCGGTATTTGTCCTTGTACG	pACCJ8 1-Y338
FLSaOatA 1-I356 XbaI R	GATC*TCTAGA*AATAAAGCGATACGAAATTTCAGCCATTAACG	pACCJ8 1-I356
FLSaOatA 1-K373 XbaI R	GATC*TCTAGA*TTTAGGTAAAAATGCAAAAGCTTTAAATCCTTTTTTACG	pACCJ8 1-K373
FLSaOatA 1-L395 XbaI R	GATC*TCTAGA*GAGCACAACGATAGACGGAA	pACCJ8 1-L395
FLSaOatA Y136F F	TGGTGGTACATTTCACAGAATGTAGAT**T** **TT**TTTAACCAA	pACCJ3 Y136F

FLSaOatA Y136F R	GTTTGAGTGGTTCAATAGCAAATTGGTTAAAA**A**<u>**A**</u>**A**ATCTACATT	
FLSaOatA Y136S F	TGGTGGTACATTTCACAGAATGTAGAT<u>**A**</u><u>**GT**</u>TTTAACCAA	pACCJ3 Y136S
FLSaOatA Y136S R	GTTTGAGTGGTTCAATAGCAAATTGGTTAAAA<u>**ACT**</u>ATCTACATT	
FLSaOatA R25K F	TGGATTAGATGGATTG<u>**A**</u><u>**AG**</u>GCATTCGCA	pACCJ2 R25K/ pACCJ3 R25K
FLSaOatA R25K R	GATTCCTATAACTGCGAATGC<u>**CTT**</u>CAATCCATC	
FLSaOatA R86K F	AAGCGACGATTGAAA<u>**AAA**</u>CTCATTCCG	pACCJ2 R86K/ pACCJ3 R86K
FLSaOatA R86K R	ACTGCCGGAATGAG<u>**TTT**</u>TTTCAATCG	
FLSaOatA Y206F F	CTGGAGATAATTCACGTGTG<u>**TTT**</u>TTTGGGACA	pACCJ2 Y206F/ pACCJ3 Y206F
FLSaOatA Y206F R	CGTGTATCTGTCCCAAA<u>**AAA**</u>CACACGTGA	
FLSaOatA Y206S F	CTGGAGATAATTCACGTGTG<u>**TCT**</u>TTTGGGACA	pACCJ2 Y206F/ pACCJ3 Y206F
FLSaOatA Y206S R	CGTGTATCTGTCCCAAA<u>**AGA**</u>CACACGTGA	
FLSaOatA Y311F F	TTTAAGTATGAAACCTTTACTAATTATAGGTAAACGATCA<u>**TTT**</u>AGCTTATAC	pACCJ3 Y311F
FLSaOatA Y311F R	AATGATAGGATAATGCCATAAGTATAAGCT<u>**AAA**</u>TGATCGTTT	
FLSaOatA Y311S F	TTTAAGTATGAAACCTTTACTAATTATAGGTAAACGATCA<u>**TCT**</u>AGCTTATAC	pACCJ3 Y311S
FLSaOatA Y311S R	AATGATAGGATAATGCCATAAGTATAAGCT<u>**AGA**</u>TGATCGTTT	
FLSaOatA E357D F	GCTGAAATTTCGTATCGCTTTATT<u>**GAC**</u>ACACCTATA	pACCJ3 E357D
FLSaOatA E357D R	CTTTAAATCCTTTTTTACGTATAGGTG<u>**TC**</u>AATAAAGCG	
FLSaOatA E357Q F	GGCTGAAATTTCGTATCGCTTTATT<u>**CAA**</u>ACACCTATA	pACCJ3 E357Q
FLSaOatA E357Q R	GACTTTAAATCCTTTTTTACGTATAGGTGT<u>**TTG**</u>AATAAAGCG	
FLSaOatA E154D F	CTCAAACATTTATGGTCTTTAGCCATT<u>**GAC**</u>GAACAATTT	pACCJ3 E154D
FLSaOatA E154D R	GGGAAAAGCAAGTAAAATTGTTC<u>**GTC**</u>AATGGCTAA	
FLSaOatA E154Q F	CTCAAACATTTATGGTCTTTAGCCATT<u>**CAA**</u>GAACAATTT	pACCJ3 E154Q
FLSaOatA E154Q R	GGGAAAAGCAAGTAAAATTGTTC<u>**TTG**</u>AATGGCTAA	

FLSaOatA 1-S42 XbaI R	GATC*TCTAGA*TAACCATTGTGCATTCAA GTGATAAATAATGATTCC	pACCJ8 1-S42
FLSaOatA 1-Y136 XbaI R	GATC*TCTAGA*ATAATCTACATTCTGTGA AATGTACCACCAGTTT	pACCJ8 1-Y136
FLSaOatA 1-F182 XbaI R	GATC*TCTAGA*AAATAGCGTTTGAATAAT ATTTCTCGGTTTAAATCTATGTAATAAG	pACCJ8 1-F182
FLSaOatA 1-R204 XbaI R	GATC*TCTAGA*ACGTGAATTATCTCCAGT GATGAAATGAATC	pACCJ8 1-R204
FLSaOatA 1-L257 XbaI R	GATCT*CTAGA*CAAAGTCATTAGAACCGC AAAACCAGATATC	pACCJ8 1-L257
FLSaOatA H36A-2 F	TTCGCAGTTATAGGAATCATTATTTAT**G<u>C</u>C**TTGAATGCA	pACCJ2 H36A
FLSaOatA H36A-2 R	CCCACTTAACCATTGTGCATTCAA**GG<u>C</u>**A TAAATAAT	
FLSaOatA E154A-2 F	CTCAAACATTTATGGTCTTTAGCCATT**G <u>C</u>A**GAACAATTT	pACCJ2 E154A
FLSaOatA E154A-2 R	GGGAAAAGCAAGTAAAATTGTTC**T<u>G</u>C**A ATGGCTAA	
FLSaOatA Y311A-2 F	TTTAAGTATGAAACCTTTACTAATTATA GGTAAACGATCA**<u>GC</u>T**AGCTTATAC	pACCJ2 Y311A
FLSaOatA Y311A-2 R	AATGATAGGATAATGCCATAAGTATAA GCT**A<u>GC</u>**TGATCGTTT	
FLSaOatA E357A-2 F	GCTGAAATTTCGTATCGCTTTATT**G<u>C</u>A**A CACCTATA	pACCJ2 E357A
FLSaOatA E357A-2 R	CTTTAAATCCTTTTTTACGTATAGGTGT**T <u>G</u>C**AATAAAGCG	
FLSaOatA F137G F	GGTGGTACATTTCACAGAATGTAGATTA T**<u>GG</u>T**AACCAATTT	pACCJ2 F137G /pACCJ3 F137G
FLSaOatA F137G R	TGTTTGAGTGGTTCAATAGCAAATTGGT T**A<u>CC</u>**ATAATCTAC	
FLSaOatA F207G F	GGAGATAATTCACGTGTGTAT**<u>GG</u>T**GGG ACAGAT	pACCJ2 F207G /pACCJ3 F207G
FLSaOatA F207G R	AGTCGTGTATCTGTCCC**A<u>CC</u>**ATACACAC G	

1. Restriction endonuclease sites are italicized. Codons being mutated are in bold, with the changed nucleic acids underlined.

2.2.1 Cloning of C-terminal and full-length *S. aureus* OatA and full-length *S. pneumoniae* OatA

The gene fragment encoding residues 445-601 of OatA from *S. aureus* SA113 (*Sa*OatA$_C$) was ligated into pET-SUMO such that the construct had an N-terminal His$_6$-SUMO tag under the control of a lactose-inducible promoter (pDSAC71). The gene encoding full length *S. aureus* OatA (residues 1-603) (*Sa*OatA) was amplified from *S.*

aureus ATCC 6538 genomic DNA using primers 01SaOatAFull and 02SaOatAFull carrying *Nhe*1 and *Xho*1 restriction sites, respectively. The resultant PCR product was digested and ligated into a modified pET-28A such that the construct had an N-terminal His_{10} tag and was under the control of a *lac* promoter (pACCJ2). The *Sa*OatA gene with its encoded His_{10} tag was amplified from pACCJ2 using primers FL*Sa*OatA SacI-SD-F, carrying a *Sac*I restriction site and Shine-Dalgarno sequence, and FL*Sa*OatA EcoRI-R, carrying an *Eco*RI restriction site. The resultant PCR product was digested and ligated into pALC2073 (Bateman et al., 2001), such that the construct had an N-terminal His_{10} tag and was under the control of a tetracycline-inducible promoter (pACCJ3). The gene encoding full length *S. pneumoniae* OatA (residues 1-604) (*Sp*OatA) was amplified from pDSAC993 using primers FL*Sp*OatA SacI-SD F, carrying a *Sac*I restriction site and Shine-Dalgarno sequence, and FL*Sa*OatA EcoRI-R, carrying an *Eco*RI restriction site. The resultant PCR product was digested and ligated into pALC2073 (Bateman et al., 2001), such that the construct had an N-terminal His_{10} tag and was under the control of a tetracycline-inducible promoter (pACCJ4).

2.2.2 Cloning of C-terminal *S. aureus* OatA and full-length *S. aureus* OatA variants

The generation of *Sa*$OatA_C$ and *Sa*OatA possessing single site-specific amino acid replacements was achieved by site-directed mutagenesis. PCR products incorporating the desired mutations were obtained using KAPA HiFi polymerase with pDSAC71, pACCJ2, or pACCJ3 as template and the appropriate primers listed in Table 2.3. Following PCR amplification, the reaction was incubated with *Dpn1* (Thermo Scientific) for 1 hr at 37 ºC, followed by transformation into *E. coli* DH5α. The sequences of all resultant plasmids were verified before use.

2.2.3 Cloning of *S. aureus* and *S. pneumoniae* chimeric OatA

Overlap extension PCR was used to clone two constructs of chimeric OatA: pACCJ5 (*Sa*$OatA_N$-*Sp*$OatA_C$) encoding residues 1-401 of *S. aureus* OatA joined to residues 395-604 of *S. pneumoniae* OatA; and pACCJ6 (*Sp*$OatA_N$-*Sa*$OatA_C$) encoding residues 1-394 of *S. pneumoniae* OatA joined to residues 402-603 of *S. aureus* OatA. First, each respective domain was amplified by PCR using the following primers: *Sa*$OatA_N$ – FL*Sa*OatA SacI-SD F and SaN401-SpC395 F, Sp$OatA_C$ – SaN401-SpC395 F and

FL*Sa*OatA EcoRI R, $SpOatA_N$ – FLSpOatA SacI-SD F and SpN394-SaC402 R, and $SaOatA_C$ - SpN394-SaC402 F and FL*Sa*OatA EcoRI R. The primers incorporate a region homologous to the gene to which the PCR product will be joined. Next, an overlap PCR was performed by combining the PCR products of the amplification of $SaOatA_N$ with $SpOatA_C$ and $SpOatA_N$ with $SaOatA_C$. The PCR products served as both template and primers due to their overlapping homologous regions. The PCR reactions were separated by agarose gel electrophoresis and the correct sized band was extracted from the gel and purified. The purified PCR products were digested with *Sac*I and *Eco*RI and cloned into digested pALC2073 (Bateman et al., 2001). Sequencing of plasmids was done to ensure correct ligation and gene stitching occurred.

2.2.4 Generation of an *oatA* knockout in *S. aureus* USA300

Deletion mutagenesis of nucleotides 440 - 1523 of *oatA* in *S. aureus* USA300 (SAUSA300_2504) was accomplished using the pKOR1 knockout plasmid and protocol (Bae and Schneewind, 2006). DNA fragments for 800 bp upstream and downstream of the aforementioned *oatA* nucleotides were amplified by PCR from chromosomal DNA of *S. aureus* USA300 using primers OatA-attB1-upstream-F and OatA-sacII-upstream-R for the upstream fragment and OatA-sacII-downstream-F and OatA-attb2-downstream-R for the downstream fragment. The PCR products were digested with *sac*II, mixed together, and ligated using T4 DNA ligase. The ligation product was amplified by PCR using primers OatA-attB1-upstream-F and OatA-attb2-downstream-R, followed by recombination with pKOR1 using the BP Clonase II kit (Invitrogen) according to manufacturer's instructions. The recombination reaction was transformed into chemically competent *E. coli* DH5α. The resultant plasmid (pKOR1-Δ*oatA*) was extracted from *E. coli* DH5α and transformed into *S. aureus* RN4220 to modify the DNA, and subsequently transformed into *S. aureus* USA300. Allelic replacement of *oatA* was accomplished in a two-step process: integration of the plasmid into the chromosome through homologous recombination at the sites flanking the *oatA* gene resulting in loss of *oatA*, followed by plasmid excision. Integration of the plasmid was accomplished by growing the culture at 42 ºC, a non-permissible temperature for the self-replication of the plasmid. In order to excise the plasmid, the cells were grown in the presence of anhydrotetracycline to induce antisense *secY* RNA expression and force plasmid resolution.

2.3 Protein Methods

2.3.1 Overproduction and Purification of *Sa*OatA$_C$

E. coli BL21 (DE3) was transformed with pDSAC71 or pDSAC71 carrying the desired mutation. Luria-Burtani broth was inoculated with 1/100 volumes of 18 hr cultures of *E. coli* BL21 (DE3) carrying pDSAC71 and grown at 37 ºC with shaking until an OD_{600} of 0.6 was reached (*i.e.*, mid-exponential phase), at which point 1mM IPTG was added. The culture continued to grow at 37 ºC for an additional 4 h, after which the cells were harvested by centrifugation (JA 10, 8600 × *g*, 4 ºC, 15 min), and frozen at -20 ºC until required. Cell pellets (from 1-2 L) were thawed on ice and resuspended in 25 mL lysis buffer (50 mM sodium phosphate, pH 7.5, 200 mM NaCl, 20 µg/mL DNase, 20 µg/mL RNase, 50 µg/mL hen egg-white lysozyme (BioBasics), and cOmplete EDTA-free protease inhibitor cocktail (Roche)). The cells were disrupted by sonication on ice (15 min, pulse 10:20 sec, 50% amplitude) and unbroken cells were collected by centrifugation (JA 25.5, 12 000 × *g*, 4 ºC, 20 min). The soluble lysate was then incubated with cOmplete His-Tag purification resin (Roche; 0.5 mL per 1 L culture) pre-equilibrated with wash buffer (50 mM sodium phosphate, pH 7.5, 200 mM NaCl). After 1 hr at 4 ºC with nutation, the cell lysate and resin slurry was loaded into a gravity-flow column and the cell lysate containing all unbound proteins was allowed to pass through. The resin was washed with 75 mL of wash buffer before elution of *Sa*OatA$_C$ from the resin with 10 mL of elution buffer (50 mM sodium phosphate, pH 7.5, 200 mM NaCl, 400 mM imidazole). Approximately 1.2 mg of purified SUMO protease was added to the IMAC elution fraction to cleave the His_6-SUMO tag. This protein mixture was then dialyzed against 50 mM sodium phosphate pH 6.5, 150 mM NaCl at ambient temperature for 2 hr with one buffer change. The dialyzed fraction was then incubated for 1 hr with nutation at 4 ºC with fresh cOmplete His-Tag purification resin (Roche; 0.5 mL per 1 L culture) pre-equilibrated with dialysis buffer to bind the His_6-SUMO tag. The solution containing untagged *Sa*OatA$_C$ was allowed to pass through the column and it was collected. The *Sa*OatA$_C$ fraction was concentrated using an Amicon Ultra-15 centrifugal filter (10 kDa MWCO; Millipore (Canada) Ltd., Etobicoke, ON) at 4,000 × *g* at 4 ºC. After concentration, the protein was filtered using a syringe-driven filter (0.22 µm; Milipore), and loaded onto a HiLoad Superdex 75PG column (GE Healthcare), pre-equilibrated with gel filtration buffer (50 mM sodium phosphate pH 6.5, 150 mM

NaCl). Gel filtration buffer consisting of 50 mM Tris pH 7.5, 150 mM NaCl was substituted when the protein was being purified for the purpose of crystallography. Protein elution was achieved using an isocratic flow of gel filtration buffer at a flow-rate of 1 mL/min.

The overproduction and purification of *Sa*OatA$_C$ possessing site-specific single amino acid replacements were performed as described above using fresh IMAC resin each time to prevent cross-contamination. The stability of each purified protein was assessed by SYPRO Orange Thermal Shift assay as a means to infer proper folding (Huynh and Partch, 2015). Briefly, *Sa*OatA$_C$ and variants were diluted to 5 µM in 50 mM sodium phosphate pH 7.0 and mixed with 2X SYPRO Orange (Thermo Fisher Scientific, Mississauga, ON) in 50 µL reactions. The melting temperature (Tm) of each protein was determined using a StepOnePlus Real-Time PCR machine using a temperature gradient of 4 ºC to 95 ºC over 60 min. Data was analyzed using the StepOnePlus software.

2.3.2 Overproduction and Purification of full-length *Sa*OatA

E. coli C43 was transformed with pACCJ2, or pACCJ2 carrying the desired mutation. Luria-Burtani broth was inoculated 1/100 with overnight culture of *E. coli* C43 carrying pACCJ2 and grown at 37 ºC with shaking until an OD_{600} of 0.6 was reached, at which point 0.5 mM IPTG was added. The culture continued to grow at 37 ºC for an additional 4 hr, after which the cells were harvested by centrifugation (JA 10, 8600 × *g*, 4 ºC, 15 min), and frozen at -20 ºC until required. Cell pellets (1-2 L) were thawed on ice and resuspended in 25 mL lysis buffer (50 mM sodium phosphate, pH 6.5, 200 mM NaCl, 10% (v/v) glycerol, 20 µg/mL DNase, 20 µg/mL RNase, 50 µg/mL hen egg-white lysozyme (BioBasics), and cOmplete EDTA-free protease inhibitor cocktail (Roche)). The cells were disrupted by sonication on ice (15 min, pulse 10:20 s, 50% amplitude) and unbroken cells were collected by centrifugation (JA 25.5, 12 000 × *g*, 4 ºC, 20 min). The membrane fraction was isolated from the soluble lysate by ultracentrifugation (Ti 45, 142 000 × *g*, 4 ºC, 1 h). The membrane pellet was resuspended in wash buffer (50 mM sodium phosphate, pH 7.5, 200 mM NaCl, 10% (v/v) glycerol) with 2 % (w/v) dodecyl maltoside (DDM). The membrane fraction was incubated at room temperature for 1 hr with nutation followed by incubation at 4 ºC with nutation overnight. The insoluble fraction was pelleted by ultracentrifugation (MLA-80, 210 000 × *g*, 4 ºC, 1 h). The soluble fraction was then incubated with Talon Cobalt resin (Takara; 0.5 mL per 1 L culture) pre-equilibrated with

wash buffer containing 0.1% (w/v) DDM. After 1 hr at 4 ºC with nutation, the cell lysate and resin slurry was loaded onto a gravity-flow column and the cell lysate containing all unbound proteins was allowed to pass through. The resin was washed with 50 mL of wash buffer with 0.1% (w/v) DDM, followed by 25 mL of wash buffer containing 0.1% (w/v) DDM and 10 mM imidazole. Elution of *Sa*OatA from the resin was accomplished with 15 mL of elution buffer (50 mM sodium phosphate, pH 6.5, 200 mM NaCl, 10% (v/v) glycerol, 0.1% (w/v) DDM, 250 mM imidazole). The *Sa*OatA elution fraction was then dialyzed against 50 mM sodium phosphate pH 6.5, 250 mM NaCl, 10% (v/v) glycerol at ambient temperature for 2 hr with one buffer change. *Sa*OatA was concentrated using an Amicon Ultra-15 centrifugal filter (30 kDa MWCO; Millipore (Canada) Ltd., Etobicoke, ON) (TX-400, 4,000 × *g* at 4 ºC).

The overproduction and purification of *Sa*OatA possessing site-specific single amino acid replacements were performed as described above using fresh IMAC resin each time to prevent cross-contamination.

2.3.3 SDS-PAGE analysis

SDS-PAGE analysis was performed using the method of Laemmli (Laemmli, 1970) and the Bio-Rad mini-PROTEIN system. Gels were cast with a 0.75 mm thickness with 4% acrylamide in the stacking, and 15% or 10% acrylamide in the resolving gel for $SaOatA_C$ and full-length *Sa*OatA, respectively. All samples were prepared in 3x SDS-PAGE sample buffer (0.2M Tris pH 6.8, 20% (v/v) glycerol, 10% (w/v) SDS, 1% (w/v) bromophenol blue) and heated for 10 min at 95 ºC for *Sa*$OatA_C$ samples, or 30 min at 45 ºC for full-length *Sa*OatA samples. Electrophoresis was conducted at 170V in running buffer (190 mM glycine, 25 mM Tris, 0.1% (w/v) SDS) for approximately 1 hr. Following electrophoresis, gels were either transferred for western immunoblotting or stained with 0.1% (w/v) Coomassie Brilliant Blue for 30 min. To obtain a desired contrast following Coomassie staining, gels were detained with a solution of 40% (v/v) methanol and 1% (v/v) acetic acid. Either the PageRuler pre-stained protein ladder (Thermo Fisher) or the Bluelf protein ladder (FroggaBio) were used as protein standards to estimate protein sizes following SDS-PAGE.

2.3.4 Western blotting

For western immunoblot analysis, proteins were transferred to nitrocellulose

membranes (GE Healthcare) for *Sa*OatA$_C$ or PVDF (GE Healthcare) presoaked in methanol for full-length *Sa*OatA. The membranes were blocked with 3% (w/v) bovine serum albumin for a minimum of 1 hr. Commercial murine monoclonal anti-His primary antibodies (Santa Cruz Biotechnologies, diluted 1:1000 in blocking buffer) were incubated with the membrane for a minimum of 1 hr. Commercial goat anti-mouse alkaline phosphatase conjugate secondary antibodies (Biorad, diluted 1:2000 in blocking buffer) were incubated with the membrane for 1 hr. Membranes were washed between incubations with TBS (10mM Tris pH 7.5, 150 mM NaCl) and TTBS (20mM Tris pH 7.5, 150 mM NaCl, 0.05% (v/v) Tween-20, 20% (v/v) Triton). The detection reagent used was 5-bromo-4-chloro-3-indoyl phosphate and nitroblue tetrazolium (Thermo Scientific). Western blots were imaged using the Biorad ChemiDoc imaging system and Image Lab software (Biorad).

2.3.5 Localization of full-length *Sa*OatA by western blot

TSB was inoculated 1/100 with overnight culture of *S. aureus* USA300 Δ*oatA* carrying the pACCJ3 with desired mutation, and chloramphenicol (10 µg/mL). The culture was grown at 37 ºC overnight with shaking. The following day, 15 mL of culture normalized to an OD_{600} of 10 was harvested by centrifugation (TX-400, 4,000 × *g* at 4 ºC, 15 min). The cell pellet was resuspended in 250 µL of lysis buffer (50 mM HEPES pH 6.8, 50 mM NaCl, 160 µg/mL lysostaphin, 20 µg/mL DNase, 20 µg/mL RNase, and cOmplete EDTA-free protease inhibitor cocktail (Roche)) and incubated for 1 hr at 37 ºC with nutation. The cells were disrupted by sonication on ice (10 min, pulse 5:5 s, 45% amplitude) and unbroken cells were collected by centrifugation (21 000 × *g*, 5 min). The membrane fraction was isolated from the soluble lysate by air-driven ultracentrifugation using a Beckman Airfuge (A-95, 178 000 × *g*, 30 min). The membrane pellet was resuspended in 50 µL HEPES buffer (50 mM HEPES pH 6.8, 50 mM NaCl). The samples were analyzed by anti-His western blotting on PVDF membrane.

2.3.6 Protein Quantification

Protein concentrations were determined using a bicinchoninic acid (BCA) assay (Pierce, Thermo Fisher Scientific) with bovine serum albumin (BSA) as the standard (0-1 mg/mL). Briefly, 25 µL of each BSA standard (diluted in the protein sample buffer) and protein sample were loaded into a 96-well microtitre plate (Corning) in triplicate. To each

well, 200 µL of working reagent (50:1 BCA:cupric sulphate) was added, and the plate was incubated at 37 ºC for 30 min. Subsequently, the absorbance at 595 nm was measured on Synergy microplate reader (Biotek) and a standard curve was generated using the BSA standards and used to interpolate the protein sample concentrations. Following quantification by BCA assay the first time, an extinction coefficient of 0.5622 Abs•mg^{-1}•mL at 280 nm was determined for *Sa*OatA$_C$ by creating a standard curve of *Sa*OatA$_C$ in water in a 200 µL volume in a Costar UV-transparent 96-well plate and Synergy plate reader. This extinction coefficient was used to determine the protein concentration under these conditions in all subsequent purifications of *Sa*OatA$_C$.

2.4 *In vitro* enzyme assays

2.4.1 Steady-State Kinetics of *Sa*OatA$_C$ with *p*NP-Ac and 4MU-Ac

The specific activity of *Sa*OatA$_C$ acting as an esterase was determined as previously described (Sychantha et al., 2017). Briefly, 5 µM *Sa*OatA$_C$ was incubated in 50 mM sodium phosphate pH 6.5 with either 5 mM *p*-nitrophenyl-acetate (*p*NP-Ac) or 0.1 mM 4-methylumbelliferyl acetate (4MU-Ac) as surrogate acetyl donors. Product release was monitored spectrophotometrically using a Synergy plate reader, measuring absorbance at 410 nm for reactions with *p*NP-Ac and measuring fluorescence using an excitation wavelength of 325 nm and an emission wavelength of 450 nm for reactions with 4MU-Ac. Control reactions were performed using gel filtration buffer in place of *Sa*OatA$_C$ to account for spontaneous substrate hydrolysis. The rate of background hydrolysis was subtracted from the rate of reactions with enzyme to determine a rate of esterase activity. Each reaction was performed in triplicate.

The pH dependence of *Sa*OatA$_C$ activity was determined by substituting the sodium phosphate buffer in the reaction described above with a 50 mM tripartite buffer consisting of one-third sodium citrate, one-third sodium phosphate, and one-third sodium borate. Using either NaOH or HCl, the pH of the buffer was altered to produce a range of pHs from pH 4 to pH 10. The pH dependence of the reactions with both *p*NP-Ac and 4MU-Ac was determined.

Michaelis-Menten steady-state kinetic parameters for *Sa*OatA$_C$ were established by determining esterase rates as described above for a range of concentrations from 0.1 – 5 mM for *p*NP-Ac and 0.02 – 0.5 mM for 4MU-Ac. The initial velocity of each reaction was

plotted against substrate concentration and the kinetic parameters were determined by non-linear regression analysis using GraphPad Prism 6 software for Mac, GraphPad Software, La Jolla California USA, www.graphpad.com.

2.4.2 High-Throughput Screening for Inhibitors

High-throughput screening for inhibitors of *Sa*OatA$_C$ was performed at the SPARC BioCentre (Hospital for Sick Children, Toronto, ON). *Sa*OatA$_C$ was screened against the GlycoNET ChemBridge and Enamine compound collection in singlicate for the primary screen. Forty-five µL of reaction buffer (50 mM sodium phosphate buffer, pH 7) was dispensed to columns 1 and 2 (no enzyme positive control wells) of barcoded NUNC plates using the MultiDrop Combi fitted with standard cassette (Thermo Fisher Scientific). *Sa*OatA$_C$ was diluted in reaction buffer to 0.78 µM and 45 µL was dispensed into columns 3-24 as described above. Compounds were added to columns 3-22 of each assay plate using the Echo 550 (Labcyte) to a final concentration of 20 µM. Similarly, DMSO was added to columns 1, 2, 23, and 24. The plate containing SaOatA$_C$ and compounds was incubated for approximately 10 min at ambient temperature before addition of 2 µL of 4MU-Ac for a final concentration of 0.2 mM using the MultiDrop Combi fitted with the small cassette. The plate was then incubated for 40 min at ambient temperature. After incubation, the fluorescence signal was read by a SynergyNeo microplate reader (BioTek, 390 nm excitation, 420 nm emission). Data analysis was performed using CDD Vault software, using columns 1 and 2 (no enzyme, DMSO) as positive controls, representing 100% inhibition, and columns 23 and 24 (enzyme, DMSO) as negative controls, representing 0% inhibition for each plate. With a selection criterion of z-score $\leq$ - 4.05 and inhibition $\geq$ 20%, 631 compounds were identified as potential hits from the GlycoNET ChemBridge and Enamine collections.

The secondary screen was performed similarly, wherein *Sa*OatA$_C$ was tested in triplicate against the 631 hits identified from the primary screen as well as against the 329 hits identified in a *Neisseria gonorrhoeae* PatB screen.

2.4.3 Dose Response

Dose response curves were performed at the SPARC BioCentre (Hospital for Sick Children, Toronto, ON) on 21 compounds selected from the secondary screen. Each compound was tested as described above in triplicate at 8 concentrations: 0 µM, 0.5 µM,

1.6 µM, 4.8 µM, 10.1 µM, 20.2 µM, 40.3 µM, 80.2 µM, and 129.3 µM. IC50 values were determined using the using CDD Vault software (Burlingame, CA., www.collaborativedrug.com).

2.4.4 Determination of fluorescence quenching

To determine whether or not a compound quenched the fluorescence of 4-methylumbelliferone (4MU), the fluorescence of 4MU was measured in the presence of varying concentrations of compound. Three concentrations of compound increasing by a factor of 10 (when possible) were mixed 50 mM sodium phosphate pH 7 with 4MU at a final concentration of 70 µM. Fluorescence was measured using a Synergy plate reader and an excitation wavelength of 390 nm and an emission wavelength of 420 nm.

2.4.5 Dose response of inhibitors in house

Dose response curves for promising compounds were performed in-house using *p*NP-Ac. Each compound was tested at eight different concentrations up to the maximum solubility in a 1:2 dilution series, in triplicate. In a 100 µL reaction volume, 1.5 µM *Sa*OatA$_C$ was incubated in 50 mM sodium phosphate pH 7 with 3 µL of compound dissolved in DMSO at desired concentration. Enzyme and compound were incubated for 10 min at ambient temperature followed by the addition of 2 µL *p*NP-Ac (dissolved in DMSO) for a final concentration of 1.1 mM. Product release was monitored spectrophotometrically at 37 ºC using a Synergy plate reader, measuring absorbance at 410 nm. A no-enzyme control reaction was performed in triplicate for each concentration of compound to account for spontaneous substrate hydrolysis and any contribution by the compound to absorbance at 410 nm. This control rate was subtracted from the rates of reactions with enzyme and compound to determine a rate of esterase activity. The initial velocity of each reaction was then plotted against compound concentration and, if possible, an IC_{50} value was calculated by Graph Pad prism 6 software for Mac, GraphPad Software, La Jolla California USA, www.graphpad.com.

Dose response curves with 4MU-Ac for select compounds were also reproduced in house. The reactions were performed as above, substituting 2 µL 4MU-Ac (dissolved in DMSO) for a final concentration of 0.1 mM. Product release was monitored spectrophotometrically using a Synergy plate reader, simultaneously measuring fluorescence using an excitation wavelength of 325 nm and an emission wavelength of 450

nm, and absorbance at 355 nm. The data were analyzed as previously described.

2.4.6 Trapping acetyl-*Sa*OatA$_C$ intermediate

Direct observation of the covalent acetyl-*Sa*OatA$_C$ intermediate was achieved by real-time analysis of a reaction by liquid chromatography-mass spectrometry (LC-MS) as previously described (Sychantha and Clarke, 2018) with minor modifications. The reaction mixture consisted of 5 µM *Sa*OatA$_C$ in 50 mM sodium phosphate pH 6.5 with 1 mM *p*NP-Ac as acetyl donor, and was incubated for 15 minutes in an MS-grade sample vial. A control reaction without *p*NP-Ac was also performed. The site of O-acetylation was identified by a tryptic digest of an acetone-quenched reaction mixture of *Sa*OatA$_C$ with *p*NP-Ac, as previously described (Sychantha and Clarke, 2018). In this case, the reaction mixture consisted of 5 µM *Sa*OatA$_C$ in 50 mM sodium phosphate pH 6.5 with 1 mM *p*NP-Ac, incubated for 30 min in an MS-grade sample vial. A control reaction without *p*NP-Ac was also performed. All samples and experiments were run as previously described (Sychantha and Clarke, 2018). Data analyses were performed using MassHunter Qualitative Analysis version B.06.00 (Agilent).

2.4.7 Steady State Kinetics of full-length *Sa*OatA

The specific activity of full-length *Sa*OatA acting as an esterase was determined using a modified aldrithiol assay (Grassetti and Murray, 1967). Briefly, 5 µM *Sa*OatA was incubated in 50 mM sodium phosphate pH 7.0 with 0.1 mM acetyl-CoA and 0.2 mM 4,4′-dithiodipyridine (DTDP; dissolved in DMSO). Released CoASH reacts with DTDP producing 4-thiopyridone, which was monitored spectrophotometrically using a Synergy plate reader measuring absorbance at 324 nm. Two control reactions were performed: to account for spontaneous substrate hydrolysis, a reaction with acetyl-CoA and DTDP was performed using dialysis buffer in place of *Sa*OatA; and to account for background thiol reactions, a reaction was performed with DTDP and *Sa*OatA in the absence of acetyl-CoA. The rates of control reactions were subtracted from the rate of the reaction with enzyme and substrate to determine a rate of esterase activity. Each reaction was performed in triplicate.

Michaelis-Menten steady-state kinetic parameters for *Sa*OatA were established by determining esterase rates as described above for a range of concentrations from 0.0125 - 300 µM acetyl-CoA. For Michaelis-Menten kinetics, 0.4 mM DTDP was used in each

reaction. The initial velocity of each control-corrected reaction was plotted against substrate concentration and the kinetic parameters were determined by non-linear regression analysis using GraphPad Prism 6 software for Mac, GraphPad Software, La Jolla California USA, www.graphpad.com.

2.4.8 Transferase assay

A modified mass spectrometry-based transferase assay (Sychantha et al., 2017) was used to detect the ability of OatA to acetylate pseudo-acceptors. For assays using muroglycans as pseudo-acceptors, enzyme (5µM) in 50 mM sodium phosphate buffer, pH 6.5 was incubated with 1 mM acetyl-CoA and 10 µg/mL muroglycans with pentapeptide stems (Sychantha et al., 2017) at 37 ºC with gentle nutation. After 18 hr incubation, 100 µg/mL mutanolysin was added to the reaction and incubated for a further 24 hr to digest the muroglycans into disaccharides. For assays using pentaacetyl-chitopentaose as a pseudo-acceptor, enzyme (5µM) in 50 mM sodium phosphate buffer, pH 6.5 was incubated with 1 mM acetyl-CoA and 2 mM pentaacetyl-chitopentaose (Megazyme) overnight at 37 ºC with gentle nutation. In both cases, after incubation, the reactions were centrifuged (21 000 × *g*, 5 min) to remove insoluble components and the soluble fractions were frozen at -20 ºC until analysis. The reactions were analyzed by LC-MS/MS using an Agilent 1200 HPLC system interfaced with an Agilent UHD 6520 Q-TOF mass spectrometer. Data analysis was performed using MassHunter Qualitative Analysis version B.06.00 (Agilent).

2.4.9 *O*-Acetyl-Tyr assay

The specific activity of *Sa*OatA$_C$ acting as an esterase towards *O*-acetyl-Tyr containing peptides was determined by monitoring the increase in absorbance at 278 nm.

2.4.9.1 Preparation of *O*-acetylated Tyr-containing peptides

N-Acetyl-Tyr-ethyl ester was purchased from SigmaAldrich and the peptides Asp-Tyr-Phe-amide, Val-Tyr-Phe-amide, Val-Tyr-Phe-Gly-amide, Glu-Asn-Val-Asp-Tyr-Phe-Asn-Glu-amine and Arg-Val-Tyr-Phe-Gly-Thr-Asp-amide were prepared by Biomatik Corp. (Cambridge, ON). Peptides were acetylated at both the N-terminus and tyrosine hydroxyl with acetic anhydride by Dr. Anthony J. Clarke. Each peptide in 0.8 – 1.0 mL of 50 mM sodium phosphate buffer, pH 7.4 containing 50% (v/v) DMSO was treated with approximately 30-fold molar excess of re-distilled acetic anhydride at ambient temperature. The absorbance at 278 nm was monitored and when no further decrease was

detected (typically 10-15 min) (Figure 2.1), reaction mixtures were injected onto a 10 x 250 mm semi-preparative Gemini (C18; 5 micron) HPLC column, pre-equilibrated with 2% (v/v) acetonitrile in 0.1% (v/v) TFA. Elution of reaction products was achieved by applying a linear gradient to 65% acetonitrile in 0.1% (v/v)TFA over 33 min at 3 mL/min with monitoring the absorbance at both 215 nm and 278 nm. Fractions were collected manually, and samples were withdrawn for MS analysis (Figure 2.2); the remainder was freeze-dried and stored at -20 °C until required.

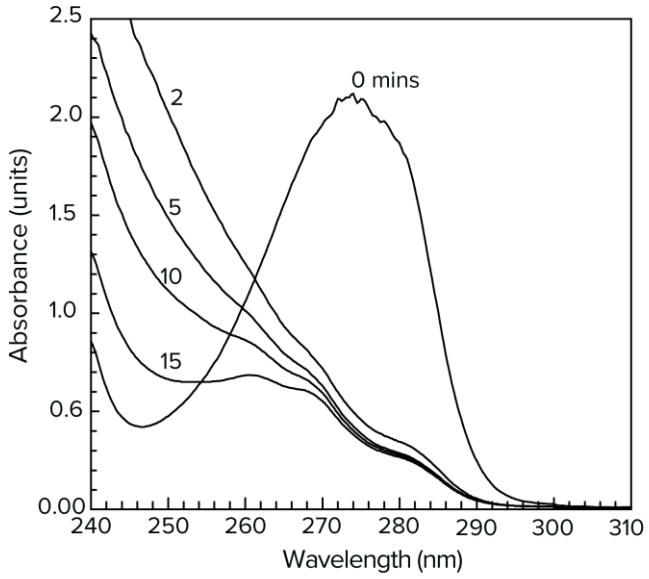

Figure 2.1 Acetylation of Tyr-containing peptides. Representative UV absorbance scans of a sample of Tyr treated with a 30-fold molar excess of acetic anhydride at pH 7.4 for the times indicated.

2.4.9.2 Reactions of *O*-acetyl-Tyr-containing peptides with *Sa*OatA$_C$

To account for spontaneous hydrolysis of the acetyl group, the absorbance of peptides in 44.3% (v/v) DMSO and 50 mM sodium phosphate pH 6.5 in a 700 µL volume was monitored at 278 nm in 1-mL UV-transparent cuvettes. Five µM *Sa*OatA$_C$ was added and the reaction was monitored at 278 nm. When applicable, the rate of spontaneous hydrolysis was subtracted from the rate of the reaction with enzyme to determine a rate of esterase activity. Michaelis-Menten steady-state kinetic parameters for *Sa*OatA$_C$ towards select *O*-acetyl-Tyr substrates were established by determining esterase rates as described above for a range of concentrations of acetyl donors. The initial velocity of each control-corrected reaction was plotted against substrate concentration and the kinetic parameters

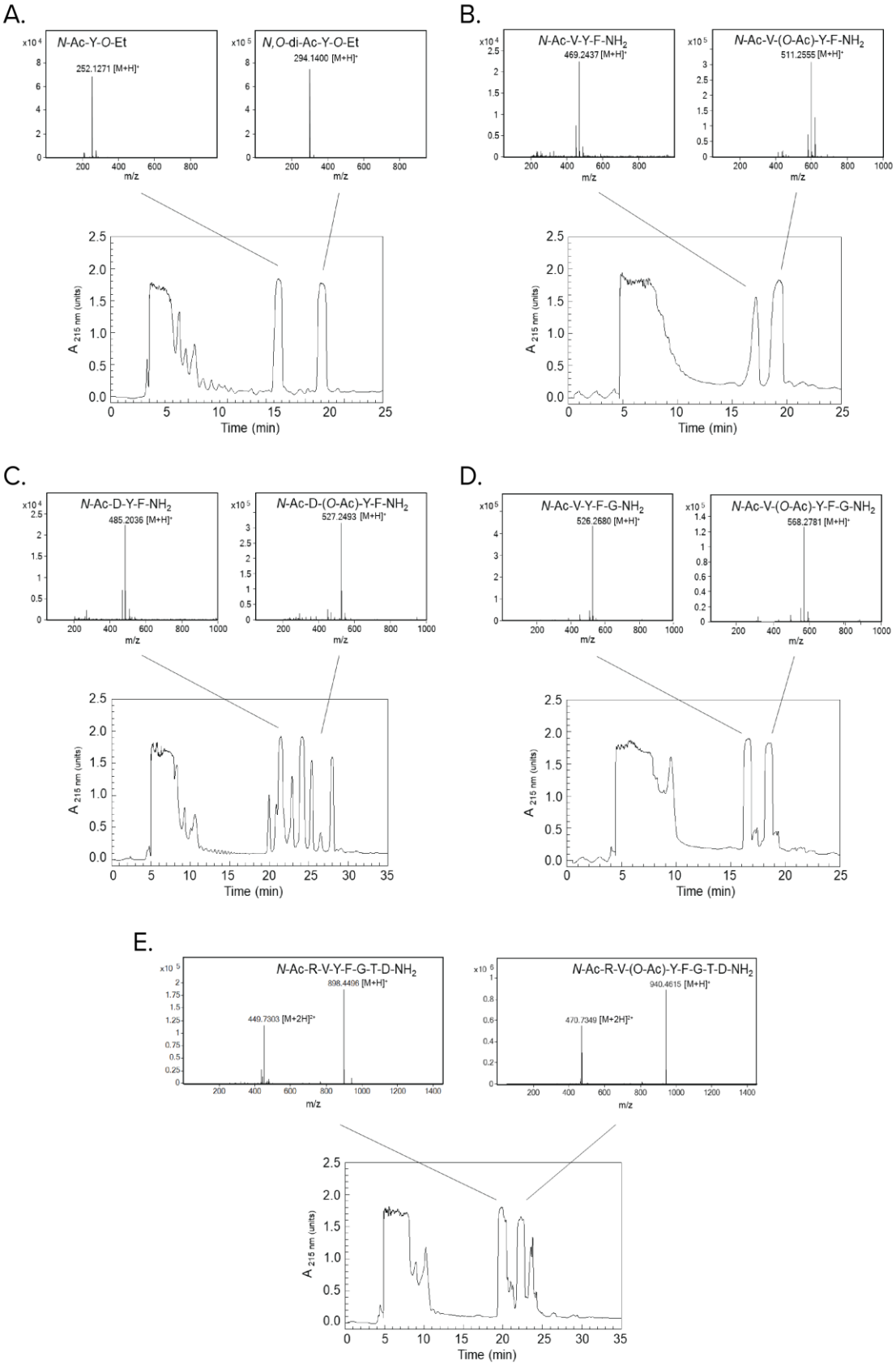
A.
N-Ac-Y-O-Et
252.1271 [M+H]+
N,O-di-Ac-Y-O-Et
294.1400 [M+H]+
m/z
A 215 nm (units)
Time (min)
B.
N-Ac-V-Y-F-NH2
469.2437 [M+H]+
N-Ac-V-(O-Ac)-Y-F-NH2
511.2555 [M+H]+
m/z
A 215 nm (units)
Time (min)
C.
N-Ac-D-Y-F-NH2
485.2036 [M+H]+
N-Ac-D-(O-Ac)-Y-F-NH2
527.2493 [M+H]+
m/z
A 215 nm (units)
Time (min)
D.
N-Ac-V-Y-F-G-NH2
526.2680 [M+H]+
N-Ac-V-(O-Ac)-Y-F-G-NH2
568.2781 [M+H]+
m/z
A 215 nm (units)
Time (min)
E.
N-Ac-R-V-Y-F-G-T-D-NH2
898.4496 [M+H]+
449.7303 [M+2H]2+
N-Ac-R-V-(O-Ac)-Y-F-G-T-D-NH2
940.4615 [M+H]+
470.7349 [M+2H]2+
m/z
A 215 nm (units)
Time (min)

Figure 2.2. Separation and analysis of acetylated Tyr-containing peptides. Bottom panels: Peptides (A, Tyr-ethyl ester; B, Asp-Tyr-Phe-amide; C, Val-Tyr-Phe-amide; D, Val-Tyr-Phe-Gly-amide; E, Arg-Val-Tyr-Phe-Gly-Thr-Asp-amide) in 0.8 – 1.0 ml of 50 mM sodium phosphate buffer, pH 7.4 containing 50% (v/v) DMSO were treated with approx. 30-fold molar excess of acetic anhydride. Following incubation for 10-15 mins at ambient temperature, reaction mixtures injected onto a 10 x 250 mm semi-preparative Gemini HPLC column, pre-equilibrated with 2% (v/v) acetonitrile in 0.1% (v/v) TFA. Elution was achieved by application of a linear gradient to 65% (v/v) acetonitrile in 0.1% (v/v) TFA over 33 min at 3 ml/min. Top panels: MS analysis of indicated fractions.

were determined by non-linear regression analysis using GraphPad Prism 6 software software for Mac, GraphPad Software, La Jolla California USA, www.graphpad.com. One-way ANOVA followed by Tukey's multiple comparison's test was performed using GraphPad Prism 6.

2.4.9.3 Determination of *O*-Acetyl-Tyr concentrations

The spectrophotometric method of Riordan and Vallee (Riordan and Vallee, 1972) based on the difference in absorbance at 278 nm (A_{278}) between O-acetylated and un-O-acetylated Tyr was used to determine the final concentration of *O*-acetyl-Tyr in peptide samples. Following determination of the initial A_{278}, an appropriate volume of a stock 10 M $NH_2OH{\cdot}HCl$ in 1M Tris·HCl buffer, pH 7.5 was added to samples to provide a 1 M final concentration of NH_2OH as catalyst for ester hydrolysis. Reaction mixtures were incubated until no further increase in absorbance at 278 nm was detected (typically 2 h) (Figure 2.3). A final absorbance reading was taken, and the concentration of *O*-acetyl-Tyr was calculated from the difference in absorbance at 278 nm using equation 1 and the previously determined molar extinction coefficient of 1160 for the conversion of *O*-acetyl-Tyr to Tyr at 278 nm (Riordan and Vallee, 1972),

$$C = \Delta A_{278} \text{ units} / 1160 \text{ units}{\cdot}M^{-1} \qquad (1)$$

where C is the molarity of the peptide and ΔA_{278} is the difference in absorbance before and after Tyr de-O-acetylation.

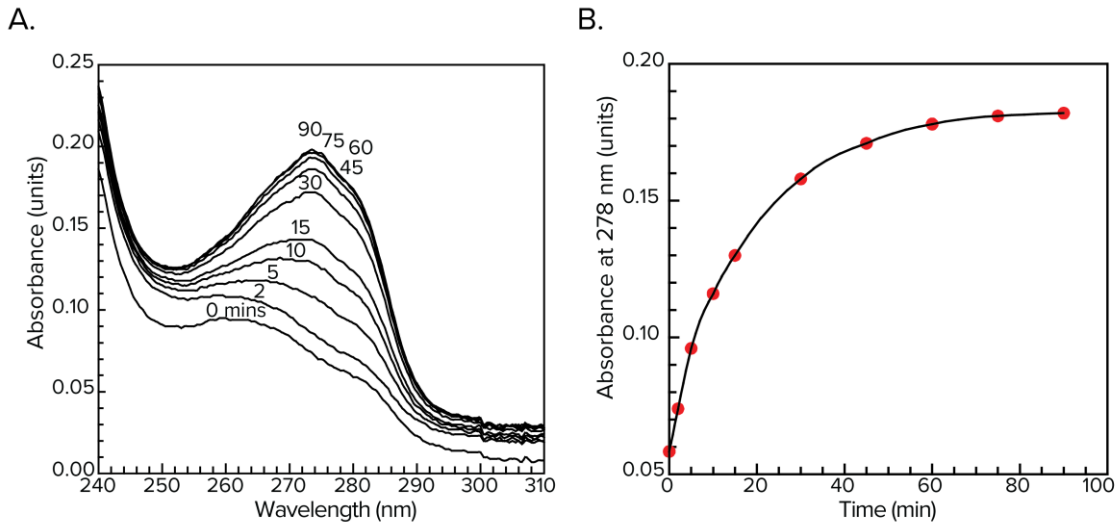

Figure 2.3. Determination of *O*-acetyl-Tyr concentration. A representative peptide containing O-acetylated Tyr was incubated with 1 M $NH_2OH{\cdot}HCl$ in 0.1 M Tris·HCl buffer, pH 7.5 to hydrolyze the acetyl groups. A. UV absorbance scans were taken throughout incubation, showing an increase in absorbance as the acetyl groups are released. B. Absorbance readings at 278 nm were plotted against time, showing that ester hydrolysis by NH_2OH is complete at 90 min.

2.5 Structure determination of *Sa*OatA$_C$

2.5.1 Crystallization

*Sa*OatA$_C$ surface entropy variants (section 2.2.2) were concentrated to 30 mg/mL using an Amicon Ultra-15 centrifugal filter (10 kDa MWCO; Millipore (Canada) Ltd., Etobicoke, ON) (4,000 × *g*, 4 ºC). Commercial Midwest Center for Structural Genomics (MCSG) Crystallization Suite sparse matrix crystallization screens 1 to 4 (Microlytic North America Inc., Burlington, MA) were prepared at room temperature with (E551A/K552A)- and (K495A/K496A)-*Sa*OatA$_C$. Crystallization screening by sitting drop vapour diffusion was setup using a Gryphon robot (Art Robbins Instruments, Sunnyvale, CA) with 1 µL protein drops (30 mg/mL) and a protein to reservoir ratio of 1:1 for afinal drop volume of 2 µL. Crystal trays were stored at 22 ºC. Optimization of crystal conditions was performed to produce crystals of (E551A/K552A)-*Sa*OatA$_C$ in 0.008 M zinc acetate, 20% (v/v) PEG 3350, and crystals of (K495A/K496A)-*Sa*OatA$_C$ in 27% (v/v) PEG 6000, 0.015 M sodium citrate.

2.5.2 X-ray diffraction data collection and structure determination

Crystals were cryoprotected for 30 s in reservoir solution supplemented with 60% (v/v) ethylene glycol prior to vitrification in liquid nitrogen. Zinc single-wavelength anomalous diffraction (Zn-SAD) data for (E551A/K552A)-*Sa*OatA$_C$ were collected on beam line 08B1-1 at the Canadian Synchrotron Light Source (Saskatoon, SK). Native data for (K495A/K496A)-*Sa*OatA$_C$ were collected on beam line 17-ID2 at the National Synchrotron Light Source II (Upton, NY). The data were indexed and scaled using HKL2000 (Otwinowski and Minor, 1997). Three zinc sites were located in the (E551A/K552A)-*Sa*OatA$_C$ Zn-SAD data using HKL2MAP (Pape and Schneider, 2004), and density modified phases were calculated using SOLVE/RESOLVE (Terwilliger, 2003). The resulting electron density map was of good quality and allowed for PHENIX AutoBuild (Terwilliger et al., 2007) to build 100% of the protein. Manual model building was done in COOT (Emsley and Cowtan, 2004), alternated with refinement using PHENIX.REFINE (Adams et al., 2011). The structure of native (K495A/K496A)-*Sa*OatA$_C$ was determined by molecular replacement using PHENIX AutoMR (Adams et al., 2011) with the Zn incorporated derivative as the search model. Manual model building and refinement was carried out as described previously. All molecular models were generated using Pymol (The PyMOL Molecular Graphics System, Version 1.2r3pre, Schrödinger, LLC).

2.6 Topology mapping of full-length *Sa*OatA

2.6.1 Substituted cysteine accessibility method

LB (50 mL) was inoculated 1/100 with an overnight culture of *S. aureus* USA300 Δ*oatA* carrying pACCJ3 with desired mutation and chloramphenicol (10 µg/mL). The culture was grown at 37ºC to OD_{600} = 5 and protein expression was induced with 40 ng/mL anhydrotetracycline. The culture was then incubated overnight at 15ºC. Two 15 mL samples of culture were harvested by centrifugation (TX-400, 4000 × *g*, 4 ºC, 15 min). The cell pellets were washed with 1 mL of HEPES buffer (50 mM HEPES pH 6.8, 50 mM NaCl) and transferred to a microfuge tube. For extracytoplasmic labelling in whole cells, an aliquot of cells was resuspended in 800 µL HEPES buffer with 5 mM methoxypolyethylene glycol maleimide (PEGmal). The sample was incubated for 1 hr at room temperature with nutation. The reaction was quenched with 45 mM dithiothreitol

(DTT) for 10 min at room temperature after which the cells were collected by centrifugation (21 000 × *g*, 2 min) and washed two times with 1 mL of HEPES buffer. For extracytoplasmic blocking in whole cells, an aliquot of cells was resuspended in 4 mL HEPES buffer with 2 mM 2-(Trimethylammonium)ethyl methane thiosulfonate (MTSET). The sample was incubated for 30 min at room temperature with nutation. The cells were pelleted by centrifugation (21 000 × *g*, 2 min) and washed three times with 1 mL of HEPES buffer. Cell pellets were frozen at -20 ºC at this stage if needed. For both labelled and blocked samples, the cell pellets were thawed and resuspended in 250 µL of HEPES buffer with 0.14 mg/mL lysostaphin (Sigma), 10 µg/mL DNase, 10 µg/mL RNase and cOmplete EDTA-free protease inhibitor cocktail (Roche). The samples were incubated for 1 hr at 37 ºC and then the cells were disrupted by sonication on ice (10 min, pulse 5:5 sec, 45% amplitude). Unbroken cells were collected by centrifugation (21 000 × *g*, 5 min). The membrane fraction was isolated from the soluble lysate by air-driven ultracentrifugation using a Beckman Airfuge (A-95, 178 000 × *g*, 30 min). The membrane pellet was resuspended in 480 µL HEPES buffer and frozen at -20 ºC if needed. For labelling of the isolated membranes, the membrane fraction was thawed and 25 mM PEGmal was added. The sample was incubated for 15 min at room temperature with nutation. The membranes were permeabilized with 3 cycles of freeze-thaw on dry ice and then incubated for a further 45 min at room temperature with nutation. The aliquot was quenched with 45 mM DTT for 10 min at room temperature. The membrane fraction was isolated again by air-driven ultracentrifugation using a Beckman Airfuge (A-95, 178 000 × *g*, 30 min). The membrane fractions were then resuspended in 50 µL HEPES buffer. In all experiments, unblocked and unlabelled control samples were included. The samples were analyzed by anti-His western blotting on PVDF membrane. The above protocol was followed for most SCAM experiments with changes to reagent concentrations when noted.

2.6.2 Construction of full-length *Sa*OatA PhoA-LacZ*α* truncation fusions

The gene encoding full-length *Sa*OatA (residues 1-603) was amplified from pACCJ2 using primers FLSaOatA SacI F and FLSaOatA XbaI R, carrying *Sac*I and *Xba*I sites, respectively. The resultant PCR product was digested with *Sac*I and *Xba*I and ligated into pPLEO1 (Islam et al., 2010) upstream of *phoA-lacZα*. Site-directed mutagenesis was performed on the resulting plasmid to remove a *pst*I site in the *oatA* gene by silent mutation

using primers FL*Sa*OatA PstI mut F and FLSaOatA PstI mut R, generating plasmids pACCJ8. Random exonuclease III-generated truncation fusion libraries were created as previously described by Alexeyev and Winkler (Alexeyev and Winkler, 1999), using the *Pst*I and *Xba*I sites in the plasmid. Targeted truncation fusions were created in the same manner as the full-length construct by cloning *oatA* with various 3′ truncations sites into pPLEO1 using specific reverse primers listed in Table 2.3.

2.6.3 Colour scoring and enzyme quantification

The *Sa*OatA truncation plasmid library was transformed into *E. coli* DH5α as an α-complementing host strain and plated on dual indicator plates containing 1.5% (w/v) agar, 1% (w/v) tryptone, 0.5% (w/v) yeast extract, 0.5% (w/v) NaCl, 80 mM K_2HPO_4, 80 mg/mL 5-bromo-4-chloro-3-indolyl phosphate disodium salt (BCIP, Sigma), 100 mg/mL 6-chloro-3-indolyl-β-D-galactopyranoside (Red-Gal, Sigma), 1 mM IPTG, and 100 µg/mL ampicillin as previously described (Alexeyev and Winkler, 1999). The β-galactosidase and alkaline phosphatase assays were performed as previously described (Manoil and Alan, 1991) with adaptation to 96-well plate format. For the β-galactosidase assay, subcultures from overnight inoculations were grown to mid-exponential phase in LB broth (Difco) supplemented with 100 µg/mL ampicillin and 1 mM IPTG in a 200 µL volume in a 96-well microtitre plate at 37 ºC with shaking. 100 µL was removed to a new 96-well microtitre plate and cells were permeabilized with 0.0045% (w/v) SDS and 0.045% (v/v) chloroform in Z buffer (60 mM $Na_{2H}PO_4$, 40 mM NaH_2PO_4, 10 mM KCl, 1 mM $MgSO_4$, 5 mM β-mercaptoethanol, pH 7.0) for 5 min at 30 ºC. Volumes (120 µL) of lysed cells were removed to a new 96-well microtitre plate, and 25 µL of ortho-nitrophenyl-β-galactoside (ONPG; 4 mg/mL in Z-buffer) was added. The reactions were incubated for 90 min at 30 ºC, followed by the addition of 55 µL of 1M Na_2CO_3 to stop the reaction. The absorbance at 420 nm and 550 nm was throughout the reaction. The alkaline phosphatase assay was performed similarly, however, once the cells reached mid-exponential phase, they were washed once with Wash buffer (10 mM Tris-HCl, 10 mM $MgSO_4$, pH 8.0) and resuspended in PM1 buffer (1 M Tris-HCl, 0.1 mM $ZnCl_2$, 1 mM iodoacetamide, pH 8.0). The cells were lysed in PM1 buffer with SDS and chloroform at 37 ºC followed by chilling at 4 ºC for 5 min. The substrate used was *p*-nitrophenyl-phosphate (*p*NPP, 0.21% (w/v) in 1M Tris-HCl, pH 8.0) and the reaction was incubated at 37 ºC followed by the addition of

cold 100 mM EDTA, pH 8.0, 200 mM KH_2PO_4 to stop the reaction. Each truncation was assayed in triplicate. The data for the alkaline phosphatase (AP) and β-galactosidase (BG) assays was normalized using equation 2:

$$\text{Miller Units} = 1000 \times \frac{(\text{A420}_{90\text{min}} - \text{A420}_{0\text{ min}})}{(\text{Time (min) x vol (mL) x OD}_{600})} \qquad (2)$$

To determine the location of each truncation site, equation 3 was used:

$$\text{NAR} = \left(\left(\frac{\text{AP}}{\text{AP}_{\text{highest}}}\right) \div \left(\frac{\text{BG}}{\text{BG}_{\text{highest}}}\right)\right) \qquad (3)$$

where value greater than 2 indicated a periplasmic location, a value between 0.1 and 2 indicated transmembrane, and a value below 0.1 indication a cytoplasmic location.

2.7 *In vivo* assays

2.7.1 Functional complementation assay of OatA variants in *S. aureus*

S. aureus USA300 Δ*oatA* was transformed with pACCJ3 carrying the desired mutation. Minimal inhibitory concentration assays were performed with lysozyme in the presence of tunicamycin (0.4 µg/mL) in 200 µL volumes in a 96-well microtitre plate. A 20 hr overnight culture of *S. aureus* USA300 Δ*oatA* pACCJ3 was diluted 1/10,000 in sterile TSB with 0.4 µg/mL tunicamycin (in DMSO) such that the final concentration of DMSO was a constant 1% (v/v). Filter-sterilized hen-egg white lysozyme (BioBasics) dissolved in water was added at concentrations ranging from 0.25 mg/mL to 4 mg/mL to each well. Each plate was covered with a Breathe-Easy sealing membrane (Millipore Sigma) and incubated in a Synergy plate reader at 37 ºC with double-orbital shaking for 20 hr, monitoring OD_{600} every 20 min.

2.7.2 Minimal inhibitory concentration assays with *S. aureus* and *B. cereus* 10987

To determine the minimal inhibitory concentrations (MIC) of inhibitors identified through HTS against *S. aureus* strains, growth curves were performed in the presence of compound and lysozyme in 200 µL volumes in a 96-well microtitre plate. A 20 hr overnight culture of either *S. aureus* USA300, *S. aureus* USA300 Δ*tarO*, or *S. aureus* USA300 Δ*oatA* was diluted 1/10,000 in sterile TSB and compound (dissolved in DMSO) was added such that the final DMSO percentage was 1% (v/v). If it was used, filter-sterilized hen-egg white

lysozyme (dissolved in water) was added at varying concentrations to each well. Each plate was covered with a Breathe-Easy sealing membrane (Millipore Sigma) and incubated in a Synergy plate reader at 37 ºC with double-orbital shaking for 20 hr, monitoring OD_{600} every 20 min.

Determination of the MIC of each compound against *B. cereus* 10987 was done as described for *S. aureus* above, however, the overnight culture was diluted 1/100.

2.8 Peptidoglycan isolation and analysis

2.8.1 Peptidoglycan isolation

PG was isolated as based on the method of Hoyle and Beveridge described previously (Hoyle and Beveridge, 1984). *S. aureus* cultures were grown to mid-exponential phase and pelleted by centrifugation (JA 10, 8600 × *g*, 4 ºC). Cell pellets were resuspended in a minimal volume of cold phosphate buffer (50 mM sodium phosphate, pH 6.0). The cell suspension was then added to an equal volume of boiling 8% (w/v) sodium dodecyl sulphate (SDS) in 50 mM sodium phosphate, pH 6.0. The suspension was boiled for 1 hr under reflux and then cooled to room temperature. The insoluble PG was sedimented by centrifugation (JA 10, 8600 × *g*, 25 ºC) and washed repeatedly with room temperature phosphate buffer until no more SDS remained, as judged by assaying for residual SDS using stains-all (Rusconi et al., 2001). The PG pellet was then resuspended in a small volume of phosphate buffer and the cell walls were broken by sonication on ice (10 min, 30:30, 50% amplitude). The broken cell suspension was treated with 5 µg/mL RNase, 5 µg/mL DNase, 10 mM $MgCl_2$, and 0.02% (w/v) sodium azide for 1 hr at 37 ºC with nutation. Following this, 100 µg/mL of pronase was added and the suspension was incubated at 37 ºC overnight. Subsequently, the PG was sedimented and resuspended in phosphate buffer containing 2% (w/v) SDS. The PG suspension was then boiled for 30 min. After cooling to room temperature, the PG was sedimented by centrifugation (21,100 × *g*, 2 min, room temperature), and washed repeatedly with room temperature water to remove SDS. The PG was subsequently frozen and lyophilized.

2.8.2 Quantification of muramic acid and *O*-linked acetate

Lyophilized PG was resuspended to 10 mg/mL in water and the same suspension was analyzed for muramic acid and acetate content. Muramic acid content of PG was quantified as previously described (Clarke, 1993b). PG was hydrolyzed into its constituent

sugars and amino acids by incubating with 6 M HCl at 95 ºC for 1 hr *in vacuo*. The acid was removed by evaporation in a heated vacuum chamber. The hydrolyzed PG samples were resuspended in water and separated and analyzed for muramic acid content by high-pH anion-exchange chromatography (HPAEC) on a PA20 CarboPAc analytical column (3 x 150 mm) with pulsed-amperometric detection. For O-linked acetate quantification, 10 mg/mL suspension of PG was treated with 100 mM NaOH for 3 hr at 37 ºC to hydrolyze all *O*-acetyl groups. Quantification of acetate was accomplished by a coupled enzyme assay using the K-ACETRM kit (Megazyme) (Pfeffer et al., 2006). The percentage PG O-acetylation was determined as the relative amount of acetate released after base-treatment to the amount of muramic acid in the PG sample. All analyses were done in triplicate.

Chapter 3. Inhibition of the C-terminal domain of *S. aureus* OatA

Parts of this chapter were published in *Antibiotics* in a modified form (Brott et al., 2019).

3.1 Statement of contributions

Dr. Anthony J. Clarke and I conceived the study. I performed all experiments. High throughput screening was performed by Dr. Leanne Wybenga-Groot at the SPARC BioCentre, Hospital for Sick Children. Compounds from PatB screen were identified by Ashley S. Brott. Technical assistance was provided by Katie Jany. A.J.C. and I analyzed and interpreted the data.

3.2 Overview

The purpose of this study was to identify novel inhibitors of *S. aureus* OatA. A pilot screen of nearly 4,000 compounds was completed previously to validate OatA as a target (Kell, 2015). For this study, a large-scale screen of small molecules was performed with the C-terminal SGNH hydrolase domain of *S. aureus* OatA, and lead compounds were characterized. Identification of inhibitors of *S. aureus* OatA will provide a basis for the development of novel anti-virulence drugs to combat multi-drug resistant infections. Furthermore, they can serve as tools to investigate the structure-function of the enzyme.

3.3 Results

3.3.1 Production, purification, and stability of *Sa*OatA$_C$ constructs

A soluble construct of *Sa*OatA$_C$ consisting of residues 435-603 (*Sa*OatA$_{\Delta 435}$) was used in previous studies to characterize PG *O*-acetyltransferase activity *in vivo* (Sychantha et al., 2017). A pilot screen for inhibitors was completed using this construct wherein the protein was stable for the duration of the experiments (Kell, 2015), however, over extended periods of time at 4ºC, *Sa*OatA$_{\Delta 435}$ experienced partial degradation, based on observations from SDS-PAGE gels (Figure 3.1A). The individual degradation products were subject to a trypsin digest and the resulting peptides were separated by LC-MS/MS. A stable core was observed corresponding to a loss of 10 amino acids from the N-terminus of *Sa*OatA$_{\Delta 435}$. To improve short-term and long-term stability, a construct of *Sa*OatA$_C$ consisting of residues 445-601 (*Sa*OatA$_{\Delta 445}$) was engineered with a N-terminal SUMO-tag. *Sa*OatA$_{\Delta 445}$ was overproduced in large quantities and purified by a combination of immobilized metal-ion affinity and size-exclusion chromatography to apparent

homogeneity, as judged by SDS-PAGE analysis (Figure 3.1B). Yields of *Sa*OatA$_{\Delta 445}$ averaged 4 mg per litre culture. *Sa*OatA$_{\Delta 445}$ is henceforth denoted as *Sa*OatA$_C$.

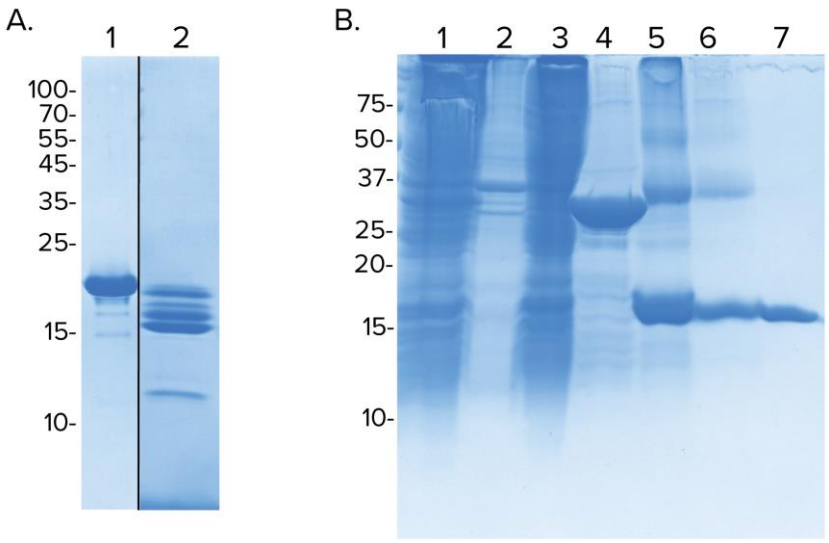

Figure 3.1 SDS-PAGE analysis of *Sa*OatA$_{\Delta 435}$ and the purification of *Sa*OatA$_{\Delta 445}$. A. SDS-PAGE analysis of *Sa*OatA$_{\Delta 435}$ immediately after purification (lane 1) and 2 weeks after purification with storage at 4ºC (lane 2). B. His$_6$-SUMO-tagged *Sa*OatA$_{\Delta 445}$ was purified by immobilized metal-ion affinity and size-exclusion chromatography, with removal of the His$_6$-SUMO-tag by SUMO protease. Lanes: 1, clarified soluble lysate; 2, insoluble lysate; 3, flow through after incubation with Ni^{2+} affinity (IMAC) resin; 4, 1st IMAC elution fraction; 5, Sample following SUMO protease digestion; 6, flow through after incubation of digested sample with Ni^{2+} affinity (IMAC) resin; 7, pooled size exclusion chromatography fractions. Molecular weight markers are given in kDa.

3.3.2 Kinetic parameters of *Sa*OatA$_C$

The steady state kinetic parameters were determined for the *Sa*OatA$_C$-catalyzed hydrolysis of both the fluorometric substrate 4-methylumbelliferyl-acetate (4MU-Ac) and the colorimetric substrate *p*-nitrophenyl-acetate (*p*NP-Ac) (Figure 3.2A-C). The values for *p*NP-Ac were similar to those reported previously for the earlier construct of recombinant *Sa*OatA$_C$ (*Sa*OatA$_{\Delta 435}$) (K_M of 1.15 mM ± 0.070, k_{cat} of 0.060 s^{-1} ± 0.00078) (Sychantha et al., 2017). Substrate inhibition was observed for the reaction of *Sa*OatA$_C$ with 4MU-Ac, with a K_i of 0.32 mM. Interestingly, coumarin-derived small molecules were identified as weak inhibitors of *Sa*OatA$_{\Delta 435}$ in the pilot screen (Brott et al., 2019). As 4MU-Ac shares a coumarin-core, it is not surprising that at high concentrations, this substrate causes inhibition of *Sa*OatA$_C$. The pH-activity optimum of *Sa*OatA$_C$ was found to be 8.5 and 8.0 with *p*NP-Ac and 4MU-Ac, respectively (Figure 3.2D-E). This differs from the pH

optimum of 7.0 reported previously (Sychantha et al., 2017). The reason for this difference remains unknown, however, the HTS assay described below was conducted at pH 7.0 to minimize spontaneous hydrolysis of the ester-linked substrate, which occurs more rapidly at alkaline pH.

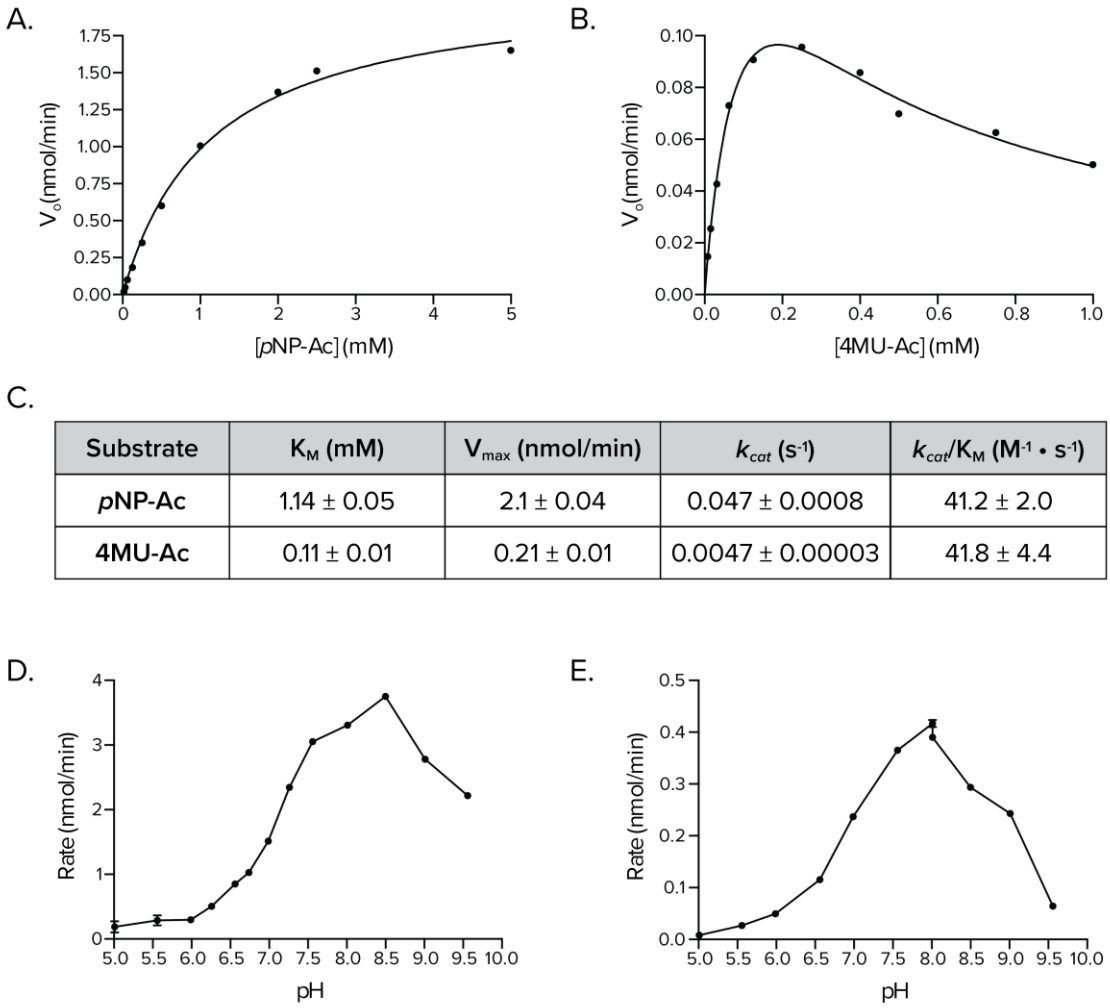

C.

Substrate	K_M (mM)	V_{max} (nmol/min)	k_{cat} (s^{-1})	k_{cat}/K_M ($M^{-1} \cdot s^{-1}$)
***p*NP-Ac**	1.14 ± 0.05	2.1 ± 0.04	0.047 ± 0.0008	41.2 ± 2.0
4MU-Ac	0.11 ± 0.01	0.21 ± 0.01	0.0047 ± 0.00003	41.8 ± 4.4

Figure 3.2 Kinetic analysis of *Sa*OatA$_C$ acting as an *O*-acetylesterase. The steady state parameters were determined for *Sa*OatA$_C$ (5µM) in 50 mM sodium phosphate pH 6.5 using 0.005-5 mM *p*NP-Ac (A) or 0.02-1 mM 4MU-Ac (B) as substrates. C. The Michaelis-Menten steady state parameters were determined for the experiments presented in panels A and B. The dependence of *Sa*OatA$_C$ esterase activity on pH was determined by incubating *Sa*OatA$_C$ (5 or 10 µM) with 1mM *p*NP-Ac (D) or 0.2 mM 4MU-Ac (E) in 50 mM tripartite buffer consisting of equal parts sodium citrate, sodium borate, and sodium phosphate, at the pH indicated. Data were analyzed in GraphPad Prism. Error bars and '±' denote standard deviation (n=3).

3.3.3 Large scale high throughput screen for inhibitors of *Sa*OatA$_C$

The pilot screen of *Sa*OatA$_{\Delta 435}$ was performed previously at McMaster University with 3921 compounds from the Bioactive Subset of the Canadian Compound Collection (Brott et al., 2019). The Bioactives library consists of small molecules that have previously exhibited biological activity against various enzymes and organisms. Given the success of the pilot screen (Brott et al., 2019), a larger scale HTS was performed at the SPARC BioCentre against drug-like collections of small molecules (Sick Kids Hospital, Toronto). As many of the compounds in HTS collections are naturally yellow when dissolved in aqueous solution, the fluorogenic substrate 4MU-Ac was used for screening, instead of the chromogenic substrate *p*NP-Ac, to avoid possible interference by coloured compounds. Furthermore, proteins can induce non-enzymatic hydrolysis of *p*-nitrophenyl acyl esters (Østdal and Andersen, 1996), and this was suspected to be occurring in the reaction with *Sa*OatA$_C$ alongside enzymatic hydrolysis (data not shown). Given the substrate inhibition observed with 4MU-Ac and *Sa*OatA$_C$, and to favour the discovery of competitive inhibitors, the large scale HTS was performed with the concentration of 4MU-Ac at the K_M value of 0.1 mM. This assay was optimized for use with the tipless Dual VaLet^{TM} (Vertical Array Loader) HTS system at the Drug Discovery Facility at the SPARC BioCentre by determining Z′ values for the end-point assay with varying incubation times, volumes, and concentrations of enzyme. The Z′ is a statistical parameter or "screening window coefficient", that reflects the assay signal dynamic range and the data variation of high and low controls (Zhang et al., 1999). A Z′ value of ≥ 0.5 indicates the existence of a well-defined hit-window in the assay that will allow for accurate differentiation between "hits" and background. The maximum value of 1.0 represents an assay with a large dynamic range and no data variation. In this instance, the high and low controls were fully active enzyme and no enzyme controls, respectively. Optimal conditions for *Sa*OatA$_C$ involved incubation of 0.75 µM enzyme with 0.1 mM 4MU-Ac in a total volume of 47.1 µL for 42 min at 22 ºC, which gave a Z′ value of 0.85 (Figure 3.3).

All compounds from the GlycoNET collection (66,065 compounds) were tested in singlicate for inhibition of *Sa*OatA$_C$ at the SPARC Biocentre (Sick Kids Hospital, Toronto). The GlycoNET compound collect consists of compounds selected from the ChemBridge and Enamine small molecule collections, with no structural overlap with

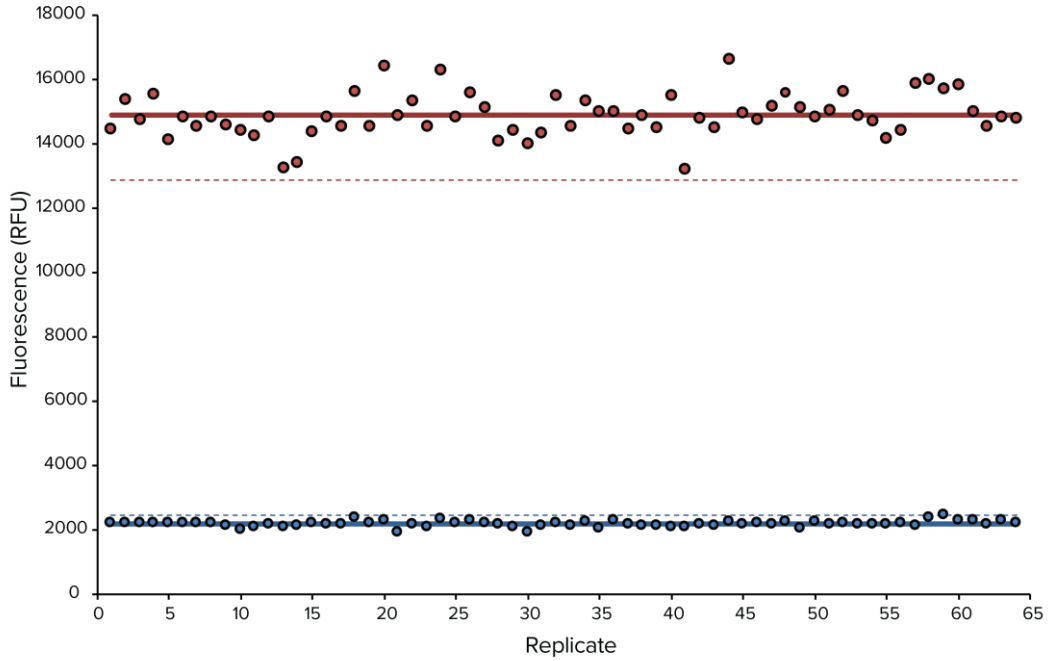

Figure 3.3 Z′ graph for the large scale HTS with *Sa*OatA$_C$. A reaction of 0.1 mM 4MU-Ac in 50 mM sodium phosphate pH 7.0 in a volume of 47.1 µL was incubated for 42 min at 22 ºC in the presence (red) or absence (blue) of 0.75 µM *Sa*OatA$_C$ and gave a Z' value of 0.85. The solid line represents the average for the respective controls and the dotted line represents 3 standard deviations above or below the low and high controls, respectively.

existing SPARC Biocentre screens. In addition, pan-assay interference compounds (PAINS) were excluded to increase the likelihood of identifying true hits. Primary screen "hits" were defined as compounds causing ≥ 20% inhibition with a z-score of ≤ -3 compared to in-plate controls. In total, 4944 hits were identified, giving an unusually high hit rate of 7.5%. In order to reduce the number of initial hits, the data sets were re-evaluated using a percent inhibition of ≥ 20% and a z-score of ≤ -4.05, giving 631 hit compounds. In parallel, *N. gonorrhoeae* PatB was tested against the remaining 68,928 different compounds available at the SPARC BioCentre from the Maybridge HitFinder, ChemBridge DIVERset and GlycoNET ChemBridge Collections, with a total of 329 hits using the same hit criteria (Brott et al., 2019). Between *Sa*OatA$_C$ and *N. gonorrhoeae* PatB, all the drug-like compound collections available at the SPARC Biocentre were screened to maximize the potential for inhibitor discovery.

In order to maximize the potential inhibitors identified from the two large-scale

screens, hits identified from the HTS of *N. gonorrhoeae* PatB were cross-screened against *Sa*OatA$_C$. For hit validation, 960 compounds were selected from the combined list of initial hits from the two primary screens and tested each compound against *Sa*OatA$_C$ in triplicate using 4MU-Ac as substrate. Authentic hits were considered to be those compounds for which all three replicates gave a percent inhibition of ≥ 20% and a z-score of ≤ -4.05. From this screen, 67 compounds were identified as potential inhibitors of *Sa*OatA$_C$. These compounds were examined for reactive functional groups and similarity to pan assay interference compounds (PAINS) (Baell and Holloway, 2010) and such compounds were removed from further consideration. The remaining 21 compounds were subjected to secondary dose response screening.

3.3.4 Dose response screening of potential OatA inhibitors with 4MU-Ac

To further evaluate the inhibitory potential of the 21 compounds, each compound was subject to an 8-point dose response assay with 4MU-Ac and *Sa*OatA$_C$ at the SPARC BioCentre to determine an IC$_{50}$ value (Appendix 1). For six compounds, the IC$_{50}$ value could not be determined in the range of concentrations tested in the dose response assay and as such these compounds were not considered further. The remaining 15 compounds were evaluated for their potential to be chemically modified, a downstream step in the optimization of inhibitor leads. In considering both the IC$_{50}$ values and the amenability of each compound to medicinal chemistry, five compounds were selected for further investigation, HSC-0018420, HSC-0094998, HSC-0059363, HSC-0114311, and HSC-0037577 (Figure 3.4). Two of these compounds were also identified in the *N. gonorrhoeae* PatB screen. Compound HSC-0128287 was included in the follow-up tests as well because, although it was only identified in the *N. gonorrhoeae* PatB screen, it displayed considerate antibacterial activity against *N. gonorrhoeae*. These six compounds were subject to a series of in-lab experiments to assess their potential as *Sa*OatA inhibitors, including dose response curves with *p*NP-Ac, fluorescence quenching tests, and minimal inhibitory concentration (MIC) assays with *S. aureus* and *B. cereus*.

3.3.5 Antibacterial activity of inhibitors

Before evaluating the compounds biochemically, each compound was subject to a MIC assay with *S. aureus* USA300 Δ*tarO* in the presence of lysozyme. TarO is an enzyme involved in the biosynthesis of wall teichoic acid (WTA) in *S. aureus*. WTAs are attached

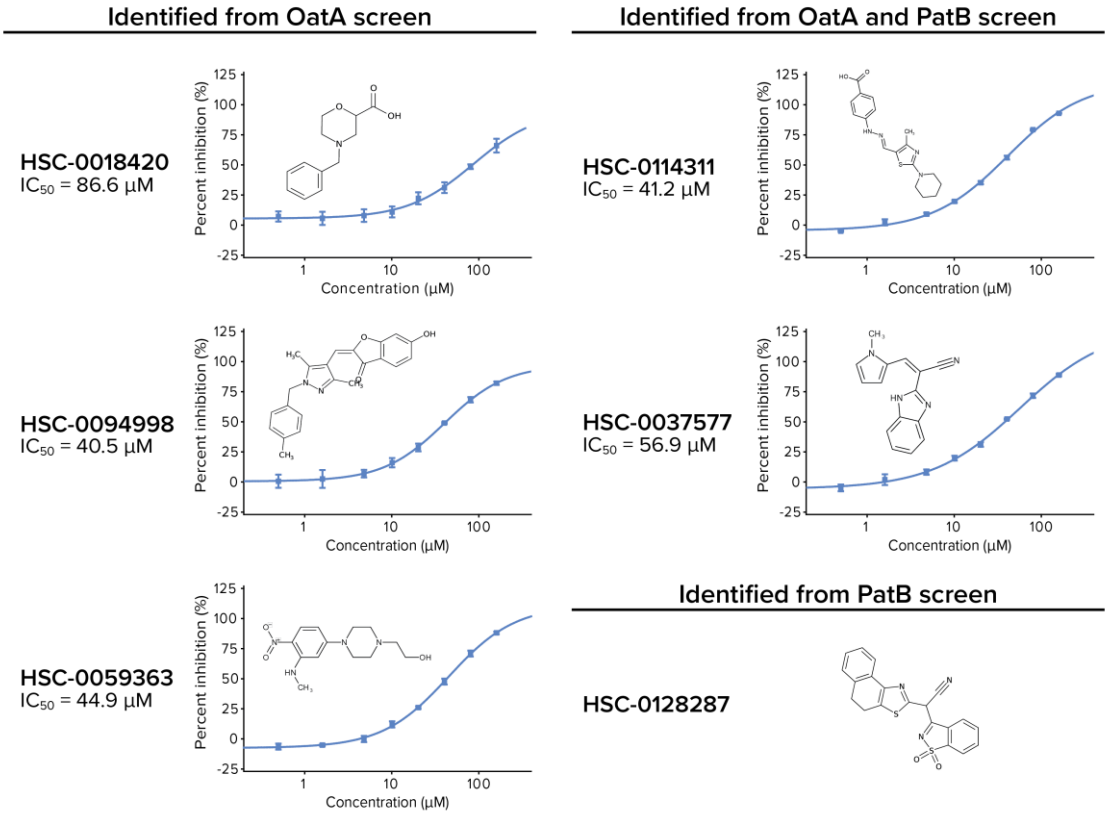

Figure 3.4 Chemical structures and dose-response assays for the six chosen inhibitor leads. Promising compounds were subject to 8-point dose response assays with *Sa*OatA$_C$ (0.75 µM) and 4MU-Ac (0.1 mM) at the SPARC BioCentre to determine IC_{50} values. Error bars denote standard deviation (n=3).

at the C-6 hydroxyl of MurNAc residues of PG, and as such, contribute to lysozyme resistance like PG O-acetylation. Elimination of WTAs in a Δ*tarO* strain does not significantly decrease lysozyme resistance the way that elimination of PG O-acetylation in a Δ*oatA* strain does, however, a double knockout of TarO and OatA is significantly more lysozyme sensitive than a single OatA knockout (Bera et al., 2007). Furthermore, the levels of PG O-acetylation do not increase to compensate for the lack of WTA (Bera et al., 2007). As elimination of PG *O*-acetylation only affects the survival of *S. aureus* in the presence of lysozyme, testing the effect of potential inhibitors of OatA had to be done with lysozyme and, in theory, a Δ*tarO* strain should be more sensitive to an inhibitor of OatA in the presence of lysozyme than a wild-type strain. This assay allows not only for the effect of each compound to be determined, but also the specificity of the compound towards OatA,

as a compound with general toxic effects would affect growth in the absence of lysozyme, whereas one specific for OatA would only affect growth in the presence of lysozyme.

Each compound was tested to its maximum solubility in a multi-point MIC assay with *S. aureus* USA300 Δ*tarO* in the absence and presence of 1 and 4 mg/mL lysozyme (Figure 3.5). Compound HSC-0018420 had no effect on growth in either the presence or absence of lysozyme. For compounds HSC-0094998, HSC-0059363, and HSC-0037577, a slight or drastic lag in growth was observed, however, the final optical density was increased or unchanged. Interestingly, the lag in growth observed for a given concentration of compound HSC-0094998 was exacerbated with the addition of lysozyme, however, cells with compound were still in exponential phase at the end of the 20 hr growth period and there appeared to be some compound precipitation. An MIC value of 1.2 mM was obtained for compound HSC-0114311, however, this compound killed *S. aureus* in both the presence and absence of lysozyme indicating the compound was not targeting OatA specifically. Similarly, compound HSC-0128287 gave a remarkably low MIC value of 72.5 nM, however, it too was seemingly non-specific.

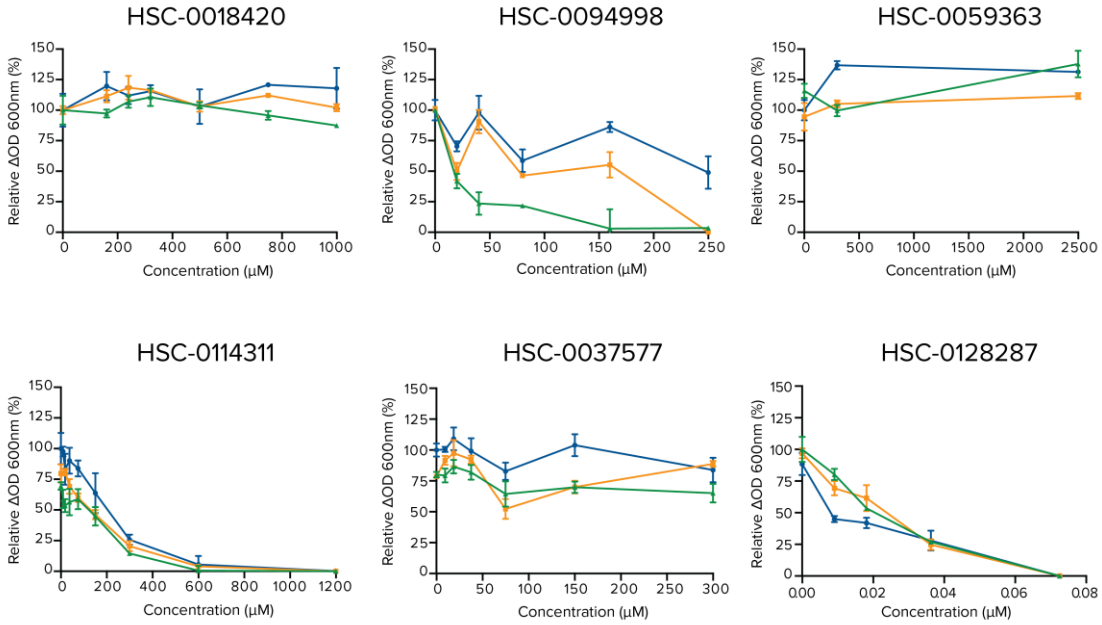

Figure 3.5 MIC assays of *S. aureus* USA300 Δ*tarO* with inhibitors in the presence and absence of lysozyme. MIC assays were performed for each compound at the concentrations indicated with *S. aureus* USA300 Δ*tarO* in the presence of 1 mg/mL (orange), 4 mg/mL (green) or absence (blue) of lysozyme. The relative OD (%) was calculated by subtracting OD (600 nm) at 16 hr from OD (600 nm) at 0 hr and normalizing to the no compound control. Error bars denote standard deviation (n=3).

OatA is not an essential gene and therefore its absence is not detrimental to *S. aureus* except in the presence of lysozyme. In theory, however, inhibition of OatA could have a different effect than the complete absence of the protein as inhibition may interfere with compensatory mechanisms, normal pathway function, or cause a build-up of intermediates. For example, a compensatory enzyme or alternate pathway, if indeed one exists, might not be activated as long as the cell senses OatA expression, regardless of whether OatA is active. Furthermore, all previous work on the role of OatA involved completely knocking out the gene, however, these inhibitors were discovered in an assay of only the C-terminal domain of the enzyme. It is therefore unknown how the cells will behave with an inactive C-terminal domain of OatA but an active N-terminal domain and this arrangement might in fact be lethal or cause growth defects. To test this, the growth of wild-type (WT) *S. aureus* USA300 was compared to the growth of *S. aureus* USA300 Δ*oatA* in the presence of two different concentrations of each compound. In theory, if the growth changes were, at least in part, a result of inhibition of OatA, the compound would not affect the growth of the *S. aureus* USA300 Δ*oatA* strain. For every compound but one, the growth of both strains in the presence of the same concentration of compound was virtually identical and followed the same trend as seen with *S. aureus* USA300 Δ*tarO* (Figure 3.6). The exception to this was HSC-0018420 which produced a lag in growth for both the wild-type and Δ*oatA* strains of *S. aureus* but not the Δ*tarO* strain. No changes were observed in the cellular morphology. This raises an interesting question as to whether this compound is affecting TarO or wall teichoic acid synthesis, however this idea was not pursued further.

MICs were also determined for each compound with *B. cereus* 10987. This strain had been previously confirmed to lack PG *O*-acetylation (Sychantha et al., 2018) and thus it served as a Gram-positive control for non-*O*-acetylating bacteria. The results seen with *B. cereus* 10987 were very similar to those seen with *S. aureus* USA300 Δ*tarO* for each compound, with the exception of HSC-0114311 (Figure 3.7). The MIC of HSC-0114311 for *S. aureus* USA300 Δ*tarO* in the absence and presence of lysozyme was 1.2 mM whereas

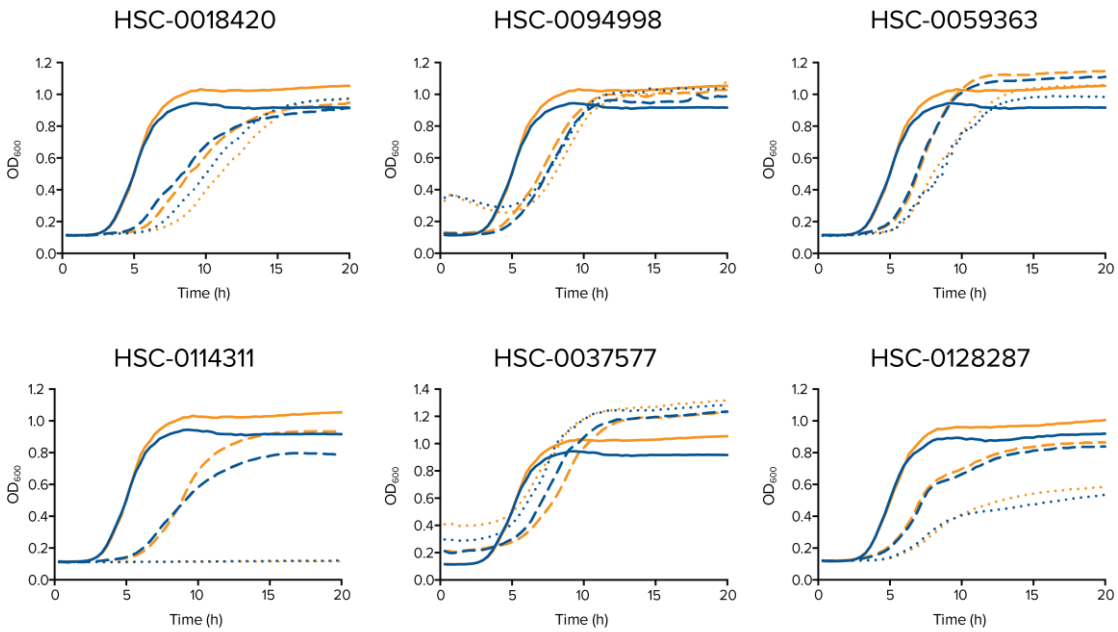

Figure 3.6 Effect of inhibitors on the growth of *S. aureus* USA300 (WT) and *S. aureus* USA300 Δ*oatA*. The growth of *S. aureus* USA300 WT was compared to the growth of *S. aureus* USA300 Δ*oatA* in the presence of two different concentrations of each inhibitor compound over 20 hr at 37 ºC. Blue lines represent *S. aureus* USA300 WT and orange lines represent *S. aureus* USA300 Δ*oatA*. Dashed and dotted lines represent low and high concentrations of compound, respectively, which were as follows for each compound: HSC-0018420, 150 µM and 1 mM; HSC-0094998, 80 µM and 250 µM; HSC-0059363, 150 µM and 1.5 mM; HSC-0114311, 150 µM and 1.5 mM; HSC-0037577, 150 µM and 300 µM; HSC-0128287, 9.06 nM and 36.3 mM.

the MIC with *B. cereus* 10987 was 0.3 mM. This indicates that *B. cereus* is more sensitive to compound HSC-0114311 than *S. aureus*, however the reason for this remains unknown.

3.3.6 Fluorescence quenching

Given that the inhibitors were identified using a fluorescence-based assay, it is possible that the decrease of fluorescent signal was due to fluorescence quenching by the compounds and not a result of decreased 4MU-Ac turnover due to inhibited *Sa*OatA$_C$. To test the fluorescence quenching properties of the compounds, an assay was performed where a fixed concentration of 4MU was titrated with increasing concentrations of compound. Compounds that reduced 4MU fluorescence in a concentration dependent manner were deemed to be quenchers. All compounds except HSC-0018420 were found to be fluorescence quenchers (Figure 3.8).

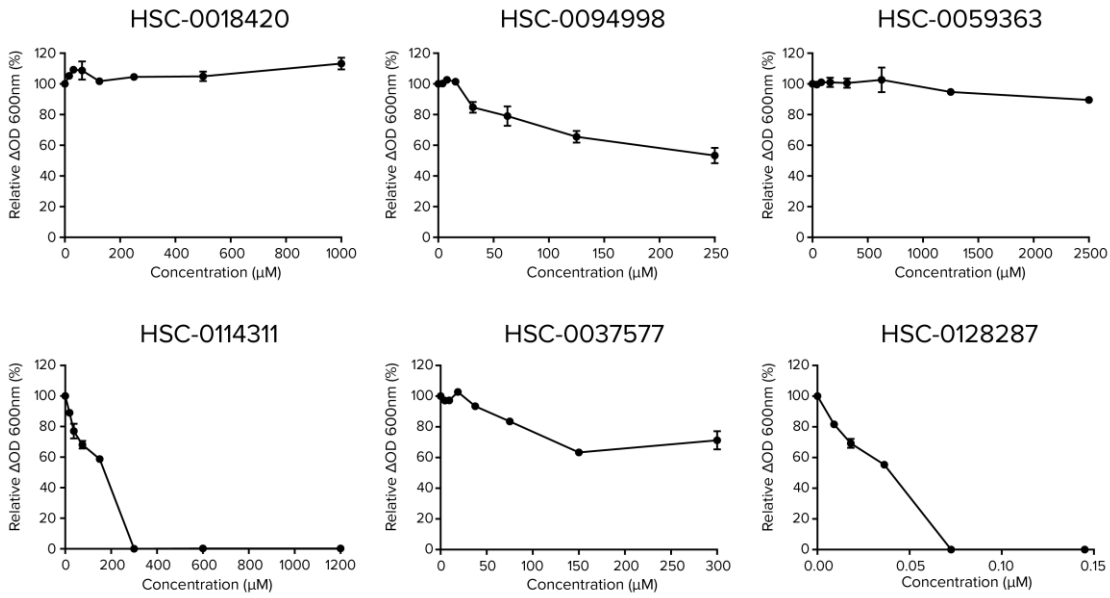

Figure 3.7 MIC assays of *B. cereus* 10987 with inhibitors. MIC assays were performed for each compound with *B. cereus* 10987. The relative OD (%) was calculated by subtracting OD (600 nm) at 16 hr from OD (600 nm) at 0 hr and normalizing to the no compound control. Error bars denote standard deviation (n=3).

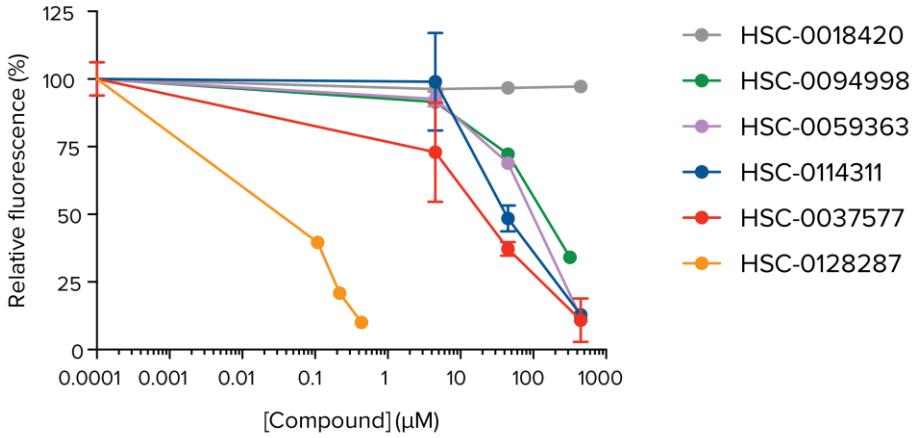

Figure 3.8 Fluorescence quenching experiment for inhibitors with 4MU. A fixed concentration of 4MU (70 μM) was titrated with increasing concentrations of compound and the fluorescence output measured. Error bars denote standard deviation (n=3).

3.3.7 Dose response screening of potential OatA inhibitors in-house

Although five of the six compounds were found to be fluorescence quenchers, it is still possible that they inhibit OatA as well. To test this, each compound was subjected to a dose response assay with the colorimetric substrate, *p*NP-Ac. As some of the compounds were yellow and absorbed in the same range as *p*-nitrophenol, proper controls were run to

account for the contribution of increasing compound concentration to the absorbance at 410 nm. IC_{50} values could be determined for compounds HSC-0018420 and HSC-0059363 only, with values of 10.3 mM and 312 µM, respectively (Figure 3.9A). As the dose response assay with *p*NP-Ac was performed with 1.5 µM *Sa*OatA$_C$, double the concentration than used for the dose response assay with 4MU-Ac, it was not possible to directly compare the IC_{50} values for the two assays. However, compound HSC-0018420 gave an IC_{50} value of 86.6 µM with 4MU-Ac, almost double the value of 44.9 µM obtained for HSC-0059363, whereas the IC_{50} value for HSC-0018420 with *p*NP-Ac was 33 times higher than the value for HSC-0059363. Compound HSC-0018420 was not a fluorescence quencher and therefore it is not surprising that it inhibited *Sa*OatA$_C$ in a *p*NP-Ac assay, however, the value obtained suggests that it is not as strong of an inhibitor as previously thought. Whilst HSC-0059363 was found to quench fluorescence, it still appears to be capable of inhibiting *Sa*OatA$_C$, although its inhibitory potential may have been overestimated due to the contribution of quenching to the final fluorescence values.

For two of the remaining four compounds, the maximum solubility limit was reached before 50% inhibition was achieved and as such obtaining an IC_{50} value for these compounds with *p*NP-Ac was not possible (Figure 3.9A). For the remaining two, HSC-0114311 and HSC-0128287, the absorbance in the assay increased above the limit of the detector before 50% inhibition was achieved (Figure 3.9A). For these two compounds, the dose response assay was attempted with 4MU-Ac and 1.5 µM enzyme, monitoring fluorescence, as well as absorbance at 355 nm. A noticeable decrease in fluorescence was observed with increasing concentration of each compound, however, the same trend was not seen with absorbance (Figure 3.9B). These results were therefore inconclusive and it was not possible to confirm these compounds as inhibitors using these assays. These results imply, however, that the IC_{50} values obtained with 4MU-Ac for these compounds were a result of fluorescence quenching and not strictly inhibition of *Sa*OatA$_C$.

3.3.8 Differential scanning fluorometry

Of the six selected compounds, only two demonstrated measurable inhibition *in vitro*: HSC-0018420 and HSC-0059363. Differential scanning fluorometry was used to further understand the interaction between *Sa*OatA$_C$ and these potential inhibitors. This assay, also known as a thermal shift assay, measures the melting point of a protein through

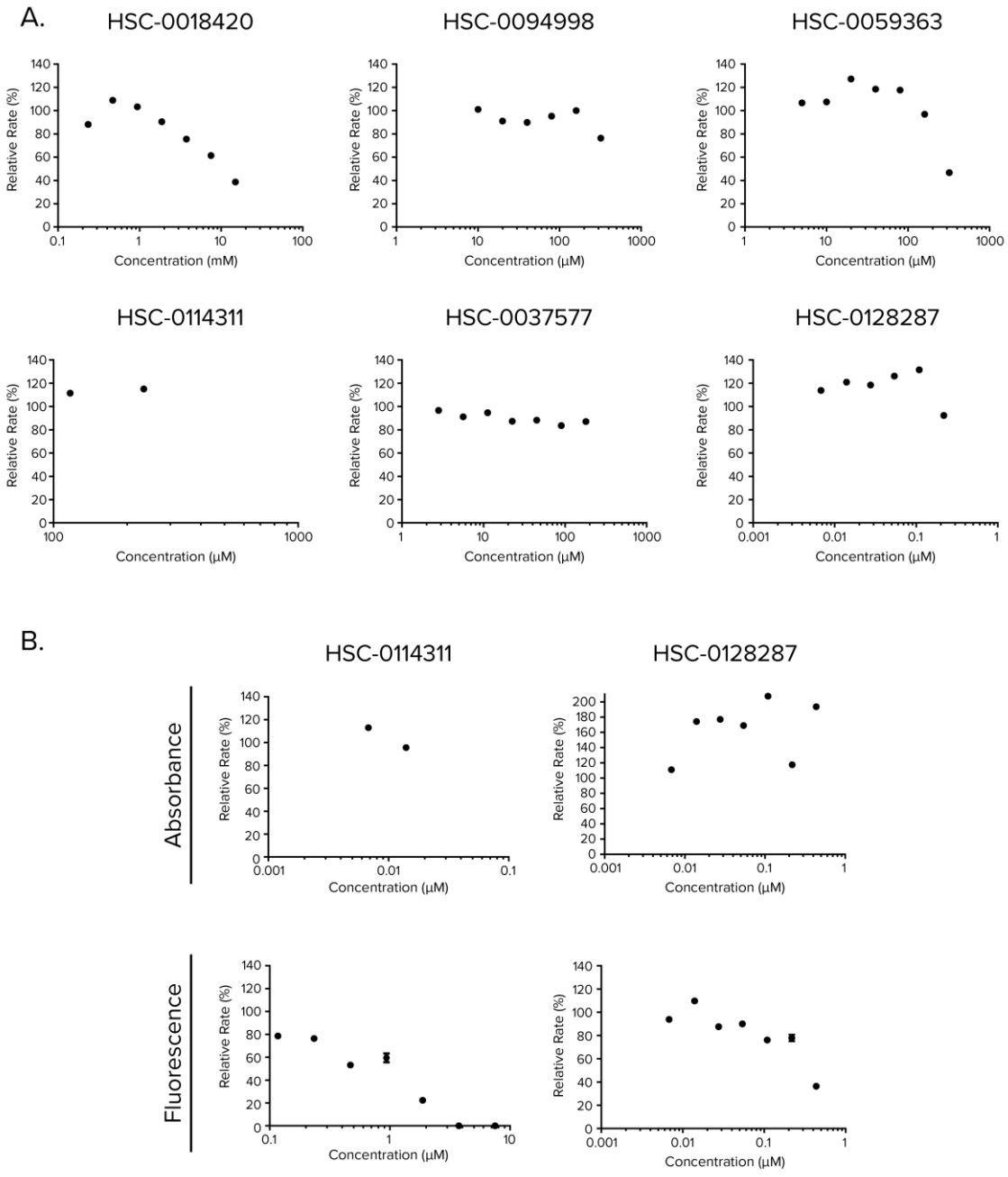

Figure 3.9 Dose response assays for inhibitors with *p*NP-Ac and 4MU-Ac. A. Dose response assays for each compound with *Sa*OatA$_C$ (1.5 μM) and *p*NP-Ac (1.1 mM). B. Dose response assays for each compound with *Sa*OatA$_C$ (1.5 μM) and 4MU-Ac (0.1 mM). Reactions were monitored measuring both fluorescence emission and absorbance simultaneously. Relative rates (%) represent the rate of reaction with compound relative to the rate of reaction without compound. Error bars denote standard deviation (n=3).

use of a dye, in this case SYPRO Orange, that fluoresces when bound to the hydrophobic groups of a protein. The protein of interest is slowly heated and unfolds, exposing its hydrophobic core, thereby increasing SYPRO Orange fluorescence. The midpoint of the unfolding transition is known as the melting temperature, or T_m. Ligands, such as inhibitors, that interact with a protein will generally stabilize a folded protein, resulting in an upward "shift" in the melting temperature (Kranz and Schalk-Hihi, 2011). This technique has been used to screen a fragment library for potential inhibitors (Pantoliano et al., 2001), as well as to compare binding affinities of lead compounds (Mahendrarajah et al., 2011). The average T_m of *Sa*OatA$_C$ is 57.2 ºC in the presence of 5% (v/v) DMSO. In the presence of 7.5 mM HSC-0018420 in 5% (v/v) DMSO, the T_m increased to 61.1 ºC. This implies binding of the compound to the enzyme likely stabilizes the enzyme slightly. Unfortunately, compound HSC-0059363, in addition to quenching 4MU fluorescence, also quenches fluorescence of SYPRO Orange. It was therefore not possible to determine a melting temperature of *Sa*OatA$_C$ in the presence of this potential inhibitor as addition of the compound abolished the SYPRO Orange signal.

3.4 Discussion

In the pilot HTS of *Sa*OatA$_C$, a group of inhibitors with a common coumarin core were identified (Brott et al., 2019; Kell, 2015). Whilst these compounds did not have ideal IC_{50} values with *p*NP-Ac, these findings did suggest a structural specificity of the enzyme, especially given that the substrate 4MU-Ac also has a coumarin core. The selected hits identified in the large scale HTS, however, varied considerably, with less evident chemical similarities. Within the 67 reconfirmed hits, six compounds were identified with varied inhibition levels that shared a similar 1-(4-nitrophenyl)piperazine core. Interestingly, 4(*p*)-nitrophenyl-Ac is an effective acetate donor for *Sa*OatA$_C$, suggesting that *Sa*OatA$_C$ has a binding site that can accommodate, or even select for, this chemical feature. Since nitro groups are notorious for quenching fluorescence, this common 1-(4-nitrophenyl)piperazine structural feature was initially disregarded. Nonetheless, one of these compounds, HSC-0059363, was selected for dose response and follow-up. As expected, HSC-0059363 quenches fluorescence (Figure 3.8), however, unlike the other compounds that quenched 4MU fluorescence, HSC-0059363 gave an IC_{50} value of 312.5 µM with *p*NP-Ac (Figure 3.9). It may therefore be worth revisiting the other

compounds with a 1-(4-nitrophenyl)piperazine core to assess their inhibitory potential. Chemical modifications or additions to the core structure may give rise to inhibitors with different potency and selectivity.

The putative active site of *Sa*OatA$_C$ is very shallow and, unlike lysozyme, lacks a deep binding cleft. *Sa*OatA$_C$, as well as two other *O*-acetyltransferases, *S. pneumoniae* OatA$_C$ and *N. gonorrhoeae* PatB, display increasing transfer efficiency with increasing degrees of polymerization of artificial glycan acceptors (Moynihan and Clarke, 2014a; Sychantha et al., 2017). Furthermore, these enzymes show specificity for the muramoyl peptide length (Moynihan and Clarke, 2014a; Sychantha et al., 2017). Both *S. aureus* and *S. pneumoniae* OatA$_C$ are unable to transfer acetyl groups to disaccharides of GlcNAc or disaccharides of GlcNAc-MurNAc. This experimental evidence strongly suggests that PG *O*-acetyltransferases contain multiple binding subsites, as is seen with lysozyme and other carbohydrate-binding enzymes (Song et al., 1994). This finding has numerous implications for inhibitor screening and discovery. The two artificial acetyl donors employed in the high throughput screen and follow-up may indeed bind to different subsites of the *Sa*OatA$_C$ active site, which may explain the significant difference in IC_{50} values obtained with the 4MU-Ac and *p*NP-Ac assays. In the absence of co-crystal structures with either substrate it is not possible to reliably predict how the substrates bind. Furthermore, all three of the aforementioned *O*-acetyltransferases display different substrate specificities and tolerances. This can be an advantage in designing a compound that specifically inhibits one *O*-acetyltransferase and not closely related enzymes, however, it may mean cross-sharing HTS hits, as was done here, is not judicious. Rescreening the second half of the compound library may unveil new inhibitors that were not identified when *N. gonorrhoeae* PatB was screened against these compounds.

A significant problem with this screen was regarding false positives: the misidentification of fluorescence quenching compounds as inhibitors. A fluorescence-based assay was chosen as it was deemed to be preferable over an absorbance-based assay, which would suffer from interference with any compound that absorbed at a similar wavelength. As many of the compounds in large compound libraries are coloured, this was seen to be a large potential problem. In reality, the fluorescence-based assay suffered significantly from interference by fluorescence quenching compounds. Whilst in theory it

would be possible to account for absorbance interference in an absorbance-based assay by running appropriate controls, this would effectively double the number of reactions run, doubling both cost and resources for a single HTS. In future, the more advisable approach might be to run the initial primary screen with the 4MU-Ac fluorescent assay but run the second confirmation screen of top hits with the *p*NP-Ac assay. This would, in theory, eliminate any false positives due to fluorescence quenching from further consideration right up front as they would not demonstrate inhibition with the *p*NP-Ac.

In this screen for inhibitors of *Sa*OatA$_C$, a notable challenge was the translation of inhibitors between *in vitro* and *in vivo* assays. Issues of fluorescence quenching aside, both compounds that were found to inhibit *Sa*OatA$_C$ *in vitro* (HSC-0059363 and HSC-0018420; Figure 3.8) in the *p*NP-Ac assay had limited effect on the growth of *S. aureus in vivo* (Figure 3.5). Some of the other compounds resulted in *S. aureus* cell death despite not inhibiting *Sa*OatA$_C$ *in vitro*. Furthermore, all of the compounds had similar growth effects for the WT and Δ*oatA* strains of *S. aureus* USA300 (Figure 3.6). The growth effects of HSC-0094998 towards *S. aureus* Δ*tarO* were exacerbated with the addition of lysozyme (Figure 3.5), however, given that HSC-0094998 quenches fluorescence, there is no evidence that this compound actually does inhibit OatA. HSC-0094998 caused a lag in growth even in the absence of lysozyme which implies a mechanism of non-specific killing – the addition of lysozyme may simply have aided in clearance of the cells. There has been thought for some time that bacteria that *O*-acetylate their PG may have a compensatory *O*-acetyltransferase that can acetylate PG in the absence of the primary PatA/PatB or OatA system, particularly for Gram-negative bacteria where PG *O*-acetylation controls autolysins. One could therefore speculate that, in theory, the growth defects caused by inhibitors for *S. aureus* USA300 Δ*oatA* could be a result of the compounds inhibiting a homologous and compensatory *O*-acetyltransferase, and not simply a result of general toxic effects. However, given that the compounds caused the same growth defects in *B. cereus* 10987, a bacterium that does not O-acetylate its PG, this theory is most likely not valid. This does not, however, rule out that the compounds might be broadly inhibiting SGNH hydrolases involved in other tasks.

PG *O*-acetyltransferases remain interesting targets for anti-virulence drug discovery. Although the chosen compounds from this study did not prove to be fruitful

leads, two of the compounds were able to inhibit the enzyme, validating *Sa*OatA$_C$ as a target for inhibition. Adaptation of the screening and follow-up approach may increase the chances of finding novel inhibitors to combat antimicrobial resistance.

Chapter 4. Topology and function of the N-terminal domain of *S. aureus* OatA

4.1 Statement of contributions

Dr. Anthony J. Clarke and I conceived the study. I performed all the experiments and A.J.C. prepared the acetylated peptide substrates. Mass-spectrometry and DNA sequencing was performed by the Advanced Analysis Centre at the University of Guelph. Dr. Nicola F. Galley produced the homopolymeric muroglycan substrate. Technical assistance was provided by Alica Eng, Bryan Fraser, Katie Jany, and Laura Thompson. A.J.C. and I analyzed and interpreted the data.

4.2 Overview

The purpose of this study was to investigate the structure and function of the N-terminal domain of *S. aureus* OatA (*Sa*OatA$_N$). Although the *Sa*OatA$_N$ is considered analogous to PatA in the Gram-negative PG O-acetylation system, PatA is a member of the membrane-bound *O*-acyltransferase (MBOAT) family of proteins, whereas *Sa*OatA$_N$ is a member of the acyltransferase 3 family (Moynihan and Clarke, 2011). Whilst the SGNH hydrolase domain of PG *O*-acetyltransferase systems was previously well characterized in both *S. pneumoniae* (Sychantha and Clarke, 2018; Sychantha et al., 2017) and *N. gonorrhoeae* (Moynihan and Clarke, 2014b, 2014a), the integral membrane domains have not been studied experimentally. Indeed, the acyltransferase 3 family is altogether a very poorly studied family of enzymes, with limited structural and biochemical information available. In this study, the topology of *Sa*OatA$_N$ was determined by PhoA-LacZα reporter fusions. In addition, putative functional residues were investigated using both *in vivo* and *in vitro* assays. Finally, a model is presented for the mechanism of *Sa*OatA$_N$ and its interaction with *Sa*OatA$_C$. A complete understanding of the process of PG O-acetylation will be valuable in guiding the development of novel therapeutics to target drug-resistant bacteria. Moreover, knowledge gained here may have widespread applicability to the understanding of related *O*-acetyltransferases, which modify diverse polysaccharide structures in all domains of life.

4.3 Results

4.3.1 Topology mapping using the substituted cysteine accessibility method

Initially, the substituted cysteine accessibility method (SCAM) was attempted to determine the topology of full-length *Sa*OatA. This technique was chosen as it allows the topology to be determined on a non-truncated functional protein. In SCAM, a Cys-free construct of the protein of interest is generated, and single cysteines are introduced into the protein in a region of interest one by one and assessed for retention of function (Bogdanov et al., 2005). The cytosolic or extracellular localisation of the cysteine is then evaluated using a combination of thiol-specific detectable reagents, and thiol-specific blocking reagents (Figure 4.1). *S. aureus* was chosen as the expression host in an effort to maintain the natural environment during topology mapping. In order to prevent interference from native OatA, a marker-less deletion of base pairs 440-1523 of *oatA* was made in *S. aureus* USA300 using the pKOR1 knockout plasmid (Bae and Schneewind, 2006), generating *S. aureus* USA300 Δ*oatA*. PEGmal, a 5 kDa thiol reactive reagent, was chosen to label Cys residues in single-Cys OatA variants due to the ease of detection in a homogenous protein mixture. PEGmal is membrane impermeant and irreversibly binds to accessible Cys residues resulting in a 5 kDa increases in the molecular weight of a labelled protein, observable by western blotting (Furlong et al., 2015).

His_{10}-tagged Cys-free *Sa*OatA ((C96A/C220A)-*Sa*OatA; *Sa*$OatA_{\Delta Cys}$) and single-Cys *Sa*OatA variants in the ΔCys background were cloned and expressed in *S. aureus* USA300 Δ*oatA*. Whole cells expressing *Sa*$OatA_{\Delta Cys}$ and (S14C)-*Sa*$OatA_{\Delta Cys}$ were labelled with 5 mM PEGmal or blocked with 2 mM MTSET after which the cells were lysed and the membranes were isolated. The membranes from the blocked aliquot were further permeabilized and labelled with 5 mM PEGmal. Results showed that *Sa*$OatA_{\Delta Cys}$ was not labelled in either aliquote, whereas (S14C)-*Sa*$OatA_{\Delta Cys}$ was labelled in the isolated membrane aliquot only (Figure 4.2A). This initial experiment proved promising: *Sa*$OatA_{\Delta Cys}$ could not be labelled by PEGmal whereas (S14C)-*Sa*$OatA_{\Delta Cys}$, a predicted cytoplasmic residue, could only be labelled when the cells were permeabilized, giving PEGmal access to the cytoplasmic facing residues. In order to assess whether extracytoplasmic cysteines could be labelled by PEGmal, whole cells of *S. aureus* USA300 Δ*oatA* expressing (G403C)-*Sa*$OatA_{\Delta Cys}$ and (I121C)-*Sa*$OatA_{\Delta Cys}$ were treated with

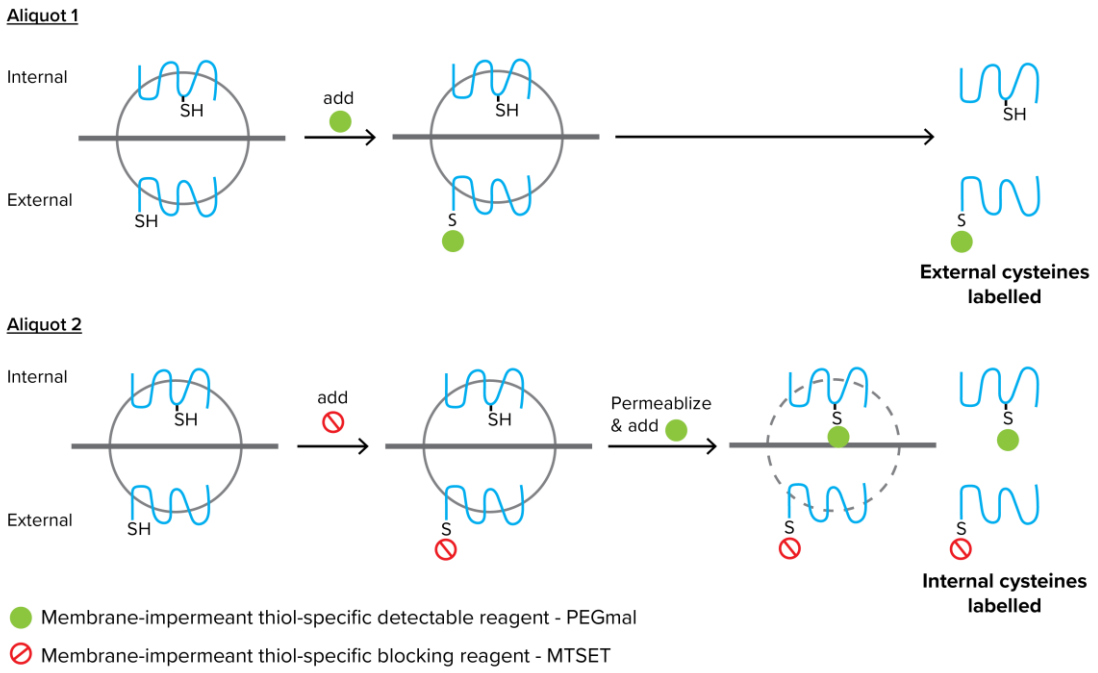

Figure 4.1 Experimental schematic of the substituted cysteine accessibility method (SCAM). Samples of culture expressing a single cysteine variant membrane protein are divided into aliquots and treated separately. To label external-facing cysteines, intact cells are treated with a membrane-impermeant thiol-specific detectable reagent, in this case PEGmal (5kDa). The protein is then isolated and detected by Western blotting. To label internal, or cytoplasmic-facing cysteines, intact cells are treated with a membrane-impermeant thiol-specific blocking reagent, in this case MTSET, to prevent all external-facing cysteines from being labelled in subsequent steps. The membranes are then isolated, permeabilized, and treated with PEGmal to label all cysteines that were not blocked in the previous step, namely internal cysteines.

PEGmal and analyzed by western blot. According to *in silico* predictions, these residues were both extracytoplasmic. Moreover, G403C is predicted to be in the linker region between the N- and C-terminal domains, which makes it more likely to be extracytoplasmic. However, despite several attempts, including changing the growth phase of the cells and concentration of PEGmal, labelling was not seen in either of these variants in whole cells (Figure 4.2A).

To investigate whether the issue was due to localization of the cysteine or accessibility, a series of blocking experiments were performed with various single-Cys variants. Whole cells of *S. aureus* USA300 Δ*oatA* expressing (G403C)-*Sa*OatA$_{\Delta Cys}$, (S14C)-*Sa*OatA$_{\Delta Cys}$, and (Q264C)-*Sa*OatA$_{\Delta Cys}$ were treated with 2mM MTSET, a

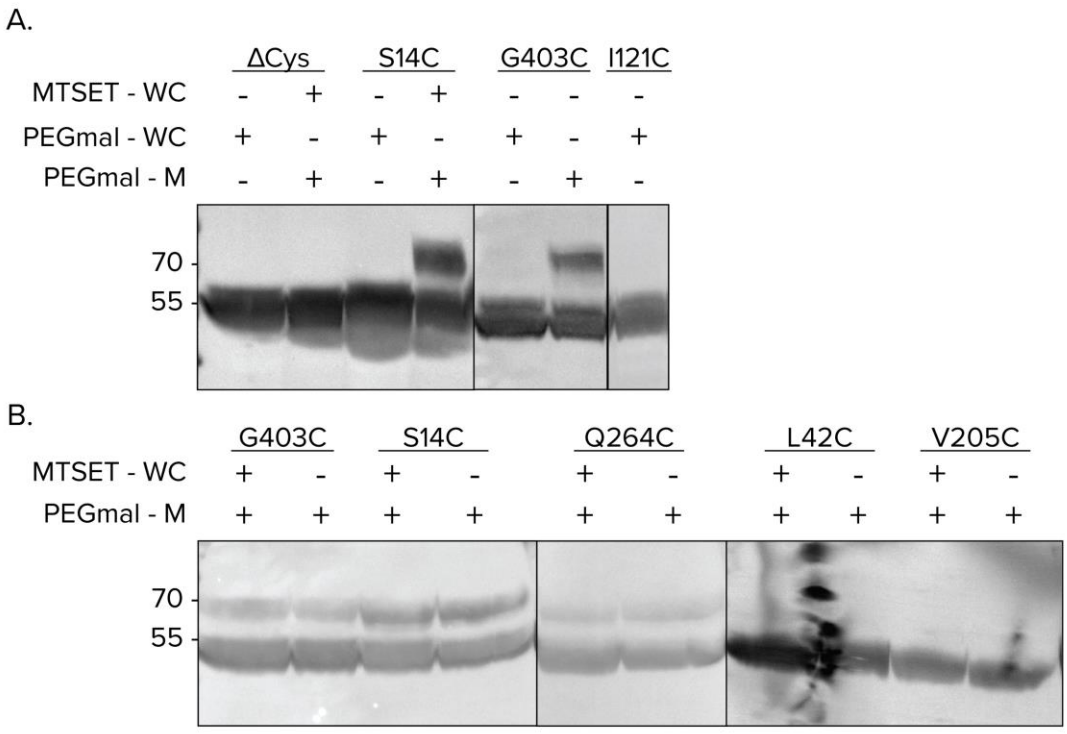

Figure 4.2 Substituted cysteine accessibility method (SCAM) mapping trials for *Sa*OatA. A. *S. aureus* USA300 Δ*oatA* carrying single-Cys variants of *Sa*OatA$_{\Delta Cys}$ were grown to mid-exponential phase and induced with 40 ng/mL anhydrotetracycline overnight at 15ºC. Cells were harvested and the whole cells (WC) were either treated with PEGmal, MTSET, or neither. After washing, the cells were lysed and the membranes were harvested by ultracentrifugation. The membranes (M) were then permeabilized and treated with PEGmal or nothing. Samples were analyzed by anti-His western blot. The upper band indicates PEGmal-labelled *Sa*OatA. B. The experiments were performed as in A, with one aliquot of each variant being treating with MTSET as whole cells, and both aliquots treated with PEGmal after membrane isolation and permeabilization. Molecular weight markers are given in kDa.

membrane impermeable thiol-blocking reagent. The membranes were then isolated, permeabilized and treated with 5mM PEGmal. In parallel, as a labelling control, an aliquot of each cell culture was not blocked with MTSET before treatment with PEGmal. Extracytoplasmic cysteines residues would theoretically be blocked by MTSET during treatment of whole cells and therefore would not be labelled by PEGmal in the subsequent step, however they would be labelled in the control sample. In all cases, PEGmal labelling occurred even after MTSET blocking (Figure 4.2B). A similar experiment was done for whole cells expressing (L42C)-*Sa*OatA$_{\Delta Cys}$ and (V205C)-*Sa*OatA$_{\Delta Cys}$, however 4 mM MTSET was used. In this experiment, labelling was not seen at all, even in the sample that

was not blocked, suggesting these residues might be buried in the membrane (Figure 4.2B). Given that 6 residues were tested for PEGmal labelling and blocking, it seems unlikely that blocking did not occur because the residues were all transmembrane or cytoplasmic. Furthermore, although PEGmal is a large molecule and may have difficulties accessing the cysteine residues through the PG layer, MTSET is small and should not suffer from the same problem. Based on these results, we hypothesized that the cysteine residues were inaccessible to MTSET and PEGmal due to interactions with the C-terminal domain of *Sa*OatA or other proteins, thereby preventing exposure to the labelling chemicals. As a result, this topology mapping strategy was abandoned.

4.3.2 Topology determination of *Sa*OatA using the PhoA-LacZα method

Due to the lack of success with SCAM, the PhoA-LacZα method was used to determine the topology of *Sa*OatA (Alexeyev and Winkler, 1999). This method relies on truncated gene constructs of the protein of interest fused to *phoA-lacZα* and expressed in *E. coli*. The localization of the terminal residue in the truncated construct is determined based on the differential activities of PhoA and LacZ in the different cellular compartmens. PhoA is only active when it dimerizes in the periplasm whereas LacZ is only active when the α-fragment fused to the protein of interest interacts with the ω-fragment expressed by the host *E. coli* in the cytoplasm. Random 3′ gene truncation libraries of *oatA* from *S. aureus* ATCC 6538 fused to *phoA-lacZα* were generated and sequenced as described in section 2.6.2. Targeted truncations were cloned for regions of the protein lacking sufficient coverage in the random truncation library. The subcellular localization of each truncation site was determined by colony colour formation on dual-indicator agar plates and β-galactosidase (BG) and alkaline phosphatase (AP) assays. A few truncations displayed no colour on the dual-indicator agar plates and these truncations were discluded as it was assumed the truncated protein was not sufficiently expressed. The dual-indicator agar plates contained Red-Gal, a substrate for BG, the product of which is red, and BCIP, a substrate for AP, the product of which is blue. Each truncated fusion protein was expressed in *E. coli* and the cells were lysed and assayed for BG activity using ONPG and AP activity using pNPP. Altered Miller Units (see section 2.6.3) were calculated for the normalized rate of reaction of each truncation with ONPG and pNPP. The normalized activity ratio (NAR) was then calculated as the percentage relative AP activity relative to the percentage

relative BG activity. In theory, cytoplasmic truncation sites would have a significantly higher reaction rate with ONPG than pNPP and periplasmic truncation sites would have a significantly higher reaction rate with pNPP than ONPG. Truncations at residues normally localized within the membrane display a "frustrated" topology wherein a certain proportion display the fusion protein in the periplasm and a certain proportion in the cytoplasm. These truncations therefore display moderate activity with both ONPG and pNPP. Based on the data for all 53 truncations, the NAR cut-off was set at <0.1 for a cytoplasmic location, and >2.5 for a periplasmic location. Results for all truncations are given in Table 4.1. A truncation site was localized to the cytoplasm when the colony produced a red colour on dual indicator agar plates and had a NAR of <0.1. Conversely, the truncation site was localized to periplasm when the colony produced a blue colour on dual indicator agar plates and and had a NAR of >2.5. When colonies produced a purple colour on dual indicator agar plates and had a NAR of 0.1-2.5, the truncation site was presumed to be transmembrane.

The results determined by PhoA-LacZα fusion tagging were mapped onto the existing *in silico* topology prediction (Figure 4.3). The topology prediction was a consensus model of the predictions given by the softwares listed in Figure 4.4B. generated from the TM prediction softwares listed in Figure 4.4B Whilst the data is relatively consistent with the *in silico* prediction for the first three transmembrane segments (TMS), the data deviates significantly for the rest. In order to develop a model that more accurately reflected the experimental evidence, the PhoA-LacZα fusion tagging data was evaluated alongside *in silico* predictions. Other considerations included general rules for transmembrane proteins. Approximately 15-30 amino acids are needed for α-helical TMS to cross the membrane - an average of 25 residues was found in a comprehensive analysis of the structures of 235 prokaryotic, eukaryotic, and viral integral membrane proteins (Saidijam et al., 2018). Furthermore, successive positive amino acids are not usually found in a TMS. For large regions of the protein found experimentally to be localized to the same compartment, JPred, a helix prediction software (Drozdetskiy et al., 2015), was used to predict where helices would be likely to form. The overall result was a new topology model for *Sa*OatA with ten transmembrane segments (TMS), 4 extra-cytoplasmic loops, and 4 cytoplasmic loops (Figure 4.4A). The C-terminal and N-terminal ends of TMS 5 both were localized to the

Table 4.1 Normalized AP and BG activities for OatA truncation fusions to PhoA-LacZ*α*

Residue[1]	AP[2]	BG[2]	%AP[3]	%BG[3]	NAR (%AP/%BG)	Colony colour[4]	Localization[5]
Q40	183.9	268.1	36.2	157.1	0.23	Purple	TM
S43	114.7	34.3	22.6	20.1	1.12	Purple	TM
G45	220.0	70.5	43.3	41.3	1.05	Purple	TM
S56	69.9	11.6	13.8	6.8	2.03	Purple	TM
I65	-2.6	6.2	-0.5	3.6	<0.01	Red	C
Y68	1.7	26.3	0.3	15.4	0.02	Red	C
R83	-3.1	155.1	-0.6	90.9	<0.01	Red	C
L87	-1.9	5.4	-0.4	3.2	<0.01	Red	C
C96	35.7	14.1	7.0	8.2	0.85	Purple	TM
P107	507.9	16.2	100.0	9.5	10.50	Blue	P
L109	302.7	15.0	59.6	8.8	6.77	Blue	P
A120	90.3	19.0	17.8	11.1	1.60	Purple	TM
I130	-1.5	53.2	-0.3	31.2	<0.01	Red	C
Q139	37.7	54.3	7.4	31.8	0.23	Purple	TM
P144	77.7	56.6	15.3	33.2	0.46	Purple	TM
Q156	100.4	27.4	19.8	16.1	1.23	Purple	TM
P162	2.0	10.1	0.4	5.9	0.06	Purple	TM
L168	-2.3	11.3	-0.5	6.6	<0.01	Red	C
N176	-3.9	57.4	-0.8	33.6	<0.01	Red	C
F182	-5.1	111.2	-1.0	65.2	<0.01	Red	C
I195	219.7	46.5	43.3	27.3	1.59	Purple	TM
N202	359.5	100.2	70.8	58.7	1.20	Purple	TM
R204	34.5	22.3	6.8	13.1	0.52	Purple	TM
T209	216.7	5.6	42.7	3.3	13.08	Blue	P

R212	19.1	11.1	3.8	6.5	0.58	Purple	TM
L218	290.3	61.1	57.2	35.8	1.60	Purple	TM
L231	254.5	55.5	50.1	32.6	1.54	Purple	TM
K233	47.6	10.2	9.4	6.0	1.56	Purple	TM
K238	187.9	26.8	37.0	15.7	2.36	Purple	TM
V241	272.1	170.6	53.6	100.0	0.54	Purple	TM
G247	57.4	51.5	11.3	30.2	0.37	Purple	TM
V253	8.9	12.7	1.7	7.5	0.23	Purple	TM
L257	168.0	33.0	33.1	19.4	1.71	Purple	TM
I260	342.9	21.5	67.5	12.6	5.36	Blue	P
Q264	177.1	8.0	34.9	4.7	7.46	Blue	P
I275	52.2	4.4	10.3	2.6	4.01	Blue	P
L281	4.9	30.0	1.0	17.6	0.06	Red	C
A287	-3.9	25.3	-0.8	14.9	<0.01	Red	C
F294	-5.1	21.8	-1.0	12.8	<0.01	Red	C
I305	17.4	162.6	3.4	95.3	0.00	Red	C
I320	-3.2	16.3	-0.6	9.6	<0.01	Red	C
Q332	4.5	29.6	0.9	17.3	0.05	Red	C
Y338	0.3	18.4	0.1	10.8	0.01	Red	C
L344	1.0	42.8	0.2	25.1	0.01	Red	C
I356	-6.4	45.8	-1.3	26.8	<0.01	Red	C
F365	-5.7	105.7	-1.1	61.9	<0.01	Red	C
A367	-5.4	23.6	-1.1	13.8	<0.01	Red	C
K373	-6.7	39.1	-1.3	22.9	<0.01	Red	C
R380	-3.5	19.2	-0.7	11.2	<0.01	Red	C
L386	-5.5	38.0	-1.1	22.2	<0.01	Red	C
L395	325.2	10.7	64.0	6.2	10.26	Blue	P

F399	506.5	14.3	99.7	8.4	11.88	Blue	P
A401	263.5	9.1	51.9	5.3	9.77	Blue	P

1. Position of the terminal amino acid of OatA followed by the reporter
2. AP and BG activities calculated with adapted Miller Units as described in Material and Methods
3. Percentage AP and BG activities relative to the maximal activity detected
4. Colony colour of expressed clone of dual-indicator media
5. Location of terminal amino acid: cytoplasm (C), transmembrane (TM), or periplasm (P)

cytoplasm, suggesting that TMS 5 is a membrane penetrating region, or a re-entrant helix, and not a transmembrane helix. The cytoplasmic loop between TMS 8 and 9 was the longest, consisting of 92 residues, and likely forms 2 cytoplasmic helices. The experimentally determined topology map differed significantly from *in silico* predictions, which predicted 11 TMS, with a large periplasmic loop between TMS 3 and 4 (Figure 4.4B).

4.3.3 Functional complementation assay

To assess the function of OatA *in vivo*, a phenotypic assay was developed that harnessed lysozyme resistance as a read-out. A marker-less deletion of *oatA* had been previously made in *S. aureus* USA300 for SCAM. *S. aureus* USA300 and *S. aureus* USA300 Δ*oatA* were grown in liquid culture in the presence of increasing concentrations of lysozyme to determine an MIC for lysozyme. Lysozyme only caused a lag in growth of *S. aureus* USA300 Δ*oatA* and did not result in complete cell death over an 18 hr growth curve (Figure 4.5A). Abolishment of both PG O-acetylation and WTA results in increased lysozyme sensitivity compared to lack of either alone (Bera et al., 2007). Tunicamycin has been shown to be a selective and potent inhibitor of TarO, the enzyme that catalyzes the first committed step in WTA synthesis, without causing other significant growth defects in *S. aureus* in rich media (Campbell et al., 2011). Lysozyme sensitivity of *S. aureus* USA300 strains was therefore tested in the presence of 0.4 µg/mL tunicamycin and an MIC of 1 mg/mL lysozyme was observed for the *S. aureus* USA300 Δ*oatA* strain, with little effect on the wild-type strain at 4 mg/mL of lysozyme (Figure 4.5B,C). Lysozyme resistance was restored to the *S. aureus* USA300 Δ*oatA* strain by complementation *in trans* with His-tagged *Sa*OatA on a constitutive expression plasmid (pACCJ3). Complementation with empty vector (pALC2073) had no effect (Figure 4.5C).

This lysozyme MIC assay was used to assess the effect of single amino acid variants of *Sa*OatA on lysozyme sensitivity of *S. aureus* USA300. A multiple sequence alignment was prepared to identify invariable or highly conserved residues among Gram-positive OatA homologues (Appendix 2). These residues were mapped onto the topology map described in section 4.3.2. Of particular interest were residues possessing charged or polar sidechains, or sidechains with functional groups. Of the 28 invariant and 46 highly conserved residues identified, several appear to be clustered in or near TMS 1 and 2, as

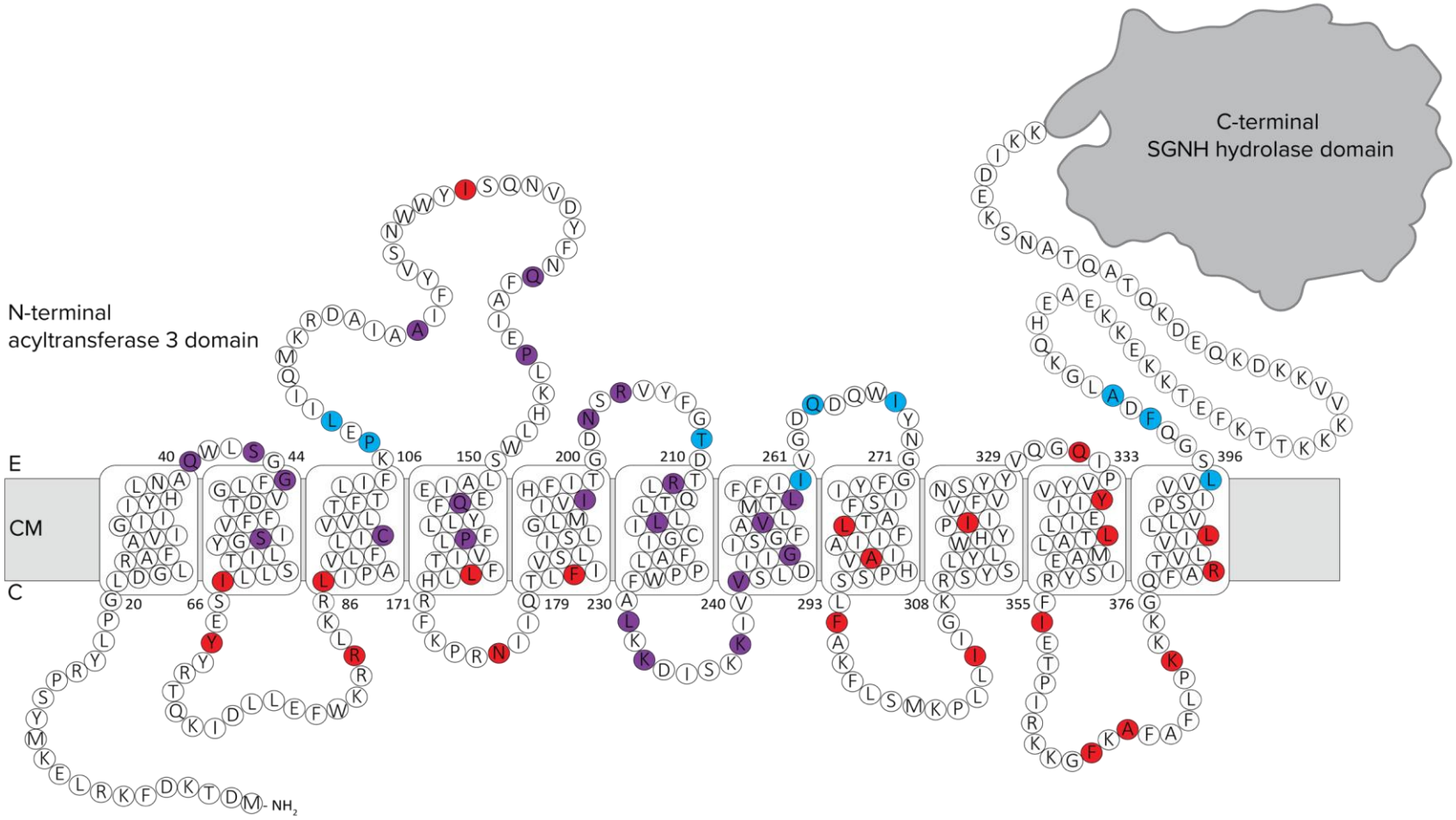

Figure 4.3 *In silico* topology map of *S. aureus* OatA with experimental data. A. The topology *phoA-lacZα* fusion data was mapped onto the consensus *in silico* topology prediction of *S. aureus* OatA. Each coloured residue represents the terminal amino acid of truncation. The colour denotes the location of the truncation as determined by colony colour on dual-indicator media and BG and AP assays: red, cytoplasm; purple, transmembrane; blue, periplasm. E, external; CM, cytoplasmic membrane; C, cytoplasm.

A.

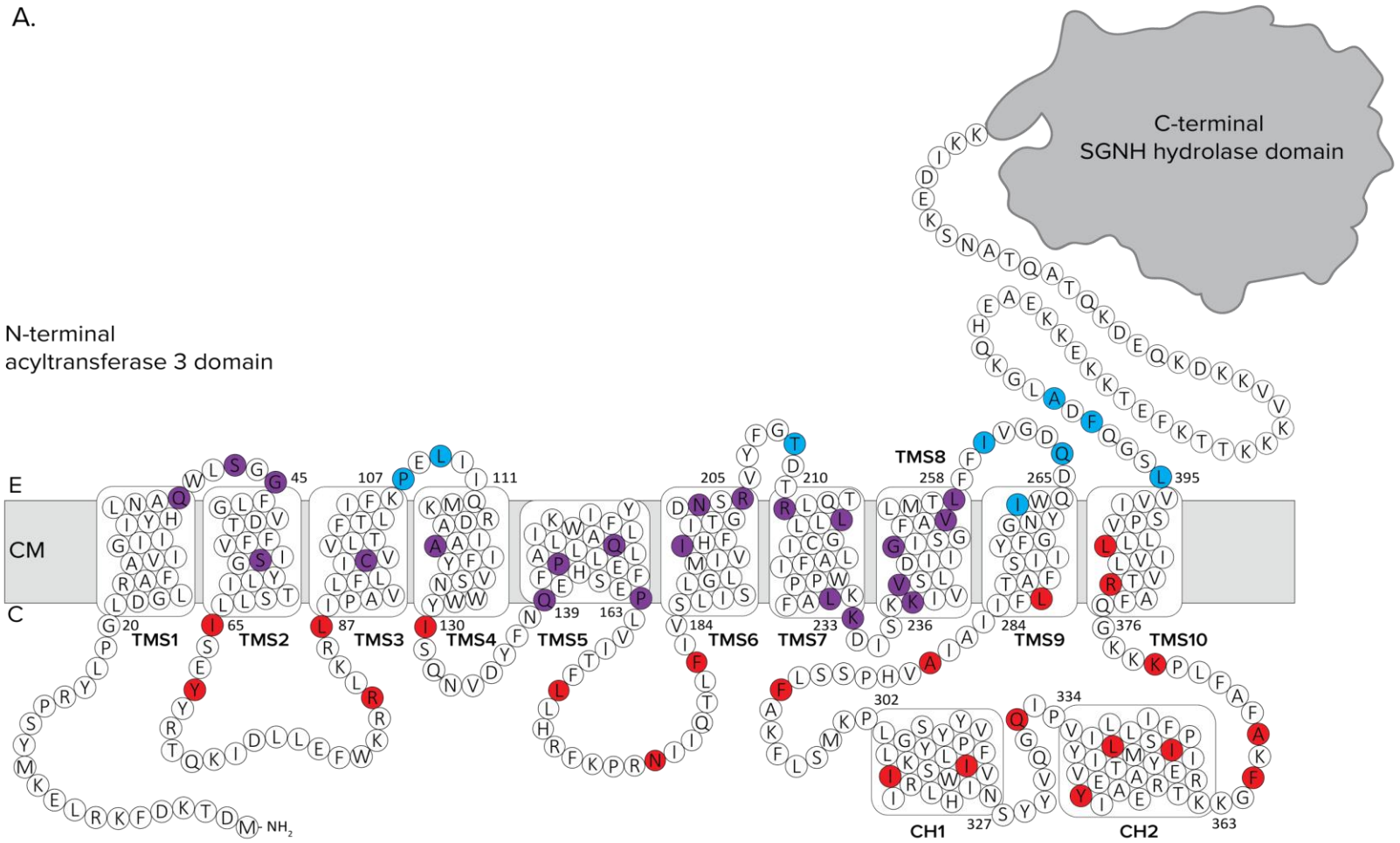
C-terminal
SGNH hydrolase domain
N-terminal
acyltransferase 3 domain
E
CM
C
TMS1
TMS2
TMS3
TMS4
TMS5
TMS6
TMS7
TMS8
TMS9
TMS10
CH1
CH2
20
45
65
87
107
111
130
139
163
184
205
210
233
236
258
265
284
302
327
334
363
376
395
- NH2

B.

TM Prediction	TMS1	TMS2	TMS3	TMS4	TMS5	TMS6	TMS7	TMS8	TMS9	TMS10	TMS11
TOPCONS	19–39	44–64	86–106	148–168	178–198	211–231	241–261	271–291	308–328	335–355	379–399
OCTOPUS	20–40	42–62	86–106	148–168	178–198	211–231	241–261	271–291	303–323	335–355	379–399
Philius	21–39	46–66	87–105	148–170	178–199	211–230	240–261	272–293	311–329	337–356	377–397
PolyPhobius	18–38	44–66	87–105	148–170	178–197	212–229	241–261	267–290	310–328	335–356	381–406
SCAMPI	19–39	45–65	87–107	151–171	178–198	209–229	242–262	267–287	311–331	336–356	381–401
SPOCTOPUS	20–40	42–62	86–106	148–168	178–198	211–231	241–261	271–291	303–323	335–355	379–399
HHMTOP	17–34	47–76	87–107	151–168	181–198	213–231	239–258	271–288	311–329	336–353	378–395

2° Structure Prediction	H1	H2	H3	H4	H5	H6	H7	H8	H9	H10	H11	H12
GOR	24–37	59–66	76–87 101–106	110–118	145–158	163–174	215–227	253–261	-----	-----	347–359	394–402
TMHMM	22–40	45–67	88–107	----	152–174	183–205	-----	243–265	278–300	315–333	340–362	382–404
HMMTOP	17–35	46–64	87–105	----	156–172	183–201	216–232	245–264	275–291	304–324	336–355	384–402
JPRED	23–36	48–69	76–105	115–130	148–197		208–226	238–259	271–287	303–327	335–363	378–397

Topology Map	TMS1	TMS2	TMS3	TMS4	TMS5	TMS6	TMS7	TMS8	TMS9	CH10	CH11	TMS12
	21–39	46–64	88–106	112–129	139–163	185–204	211–233	237–257	266–283	303–325	335–364	377–394

Figure 4.4 Topology map of *S. aureus* OatA. A. The topology of the N-terminal domain of *Sa*OatA was determined by *phoA*-*lacZα* fusion mapping. Each coloured residue represents the terminal amino acid of truncation. The colour denotes the location of the truncation as determined by colony colour on dual-indicator media and BG and AP assays: red, cytoplasm; purple, transmembrane; blue, periplasm. B. Comparison of *in silico* topology and secondary structure predictions and experimental results for the N-terminal domain of *Sa*OatA. E, external; CM, cytoplasmic membrane; C, cytoplasm; TMS, transmembrane helix; CH, cytoplasmic helix. (Drozdetskiy et al., 2015; Garnier et al., 1978; Käll et al., 2005; Krogh et al., 2001; Peters et al., 2016a; Reynolds et al., 2008; Tsirigos et al., 2015; Tusnády and Simon, 1998, 2001; Viklund et al., 2008; Viklund and Elofsson, 2008).

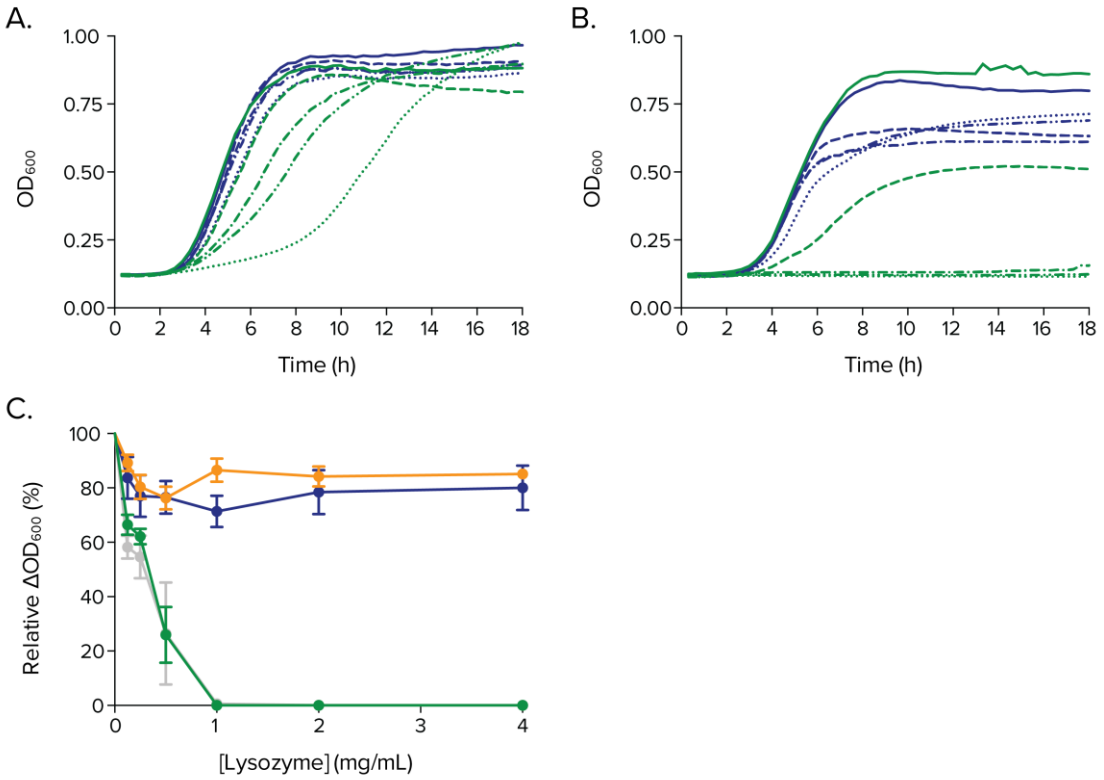

Figure 4.5 Determination of lysozyme MIC for *S. aureus* USA300 strains. A.B. Growth of *S. aureus* USA300 (blue) and *S. aureus* USA300 Δ*oatA* (green) in the presence of varying concentrations of lysozyme and (A) the absence and (B) the presence of 0.4 µg/mL tunicamycin. Solid lines, 0 mg/mL lysozyme; dotted lines, 0.5 mg/mL; dash-dot-dash, 1 mg/mL; dash-dot-dot-dash, 2 mg/mL; dotted lines, 4 mg/mL. C. Determination of lysozyme MIC 12 hr cultures of *S. aureus* USA300 (blue), *S. aureus* USA300 Δ*oatA* (green), *S. aureus* USA300 Δ*oatA* pACCJ3 (orange), and *S. aureus* USA300 pALC2073 (grey). Error bars denote standard deviation (n=3).

well as in or near TMS 5 and cytoplasmic helices 10 and 11. Candidate functional residues were replaced with Ala by site-directed mutagenesis of the *oatA* gene in the pACCJ3 plasmid. The resultant *oatA* variants were used to complement *S. aureus* USA300 Δ*oatA*. Wild-type *Sa*OatA and empty vector were used as controls. The growth of each complemented strain in the presence of 0.4 µg/mL tunicamycin and increasing concentrations of lysozyme was monitored to assess the effect of the respective amino acid replacements on lysozyme sensitivity as a measure of function. A total of 24 residues were investigated in this manner. Whereas *S. aureus* USA300 Δ*oatA* complemented with wild-type *oatA* had full lysozyme resistance at the highest concentration tested (4 mg/mL), for

10 conserved residues, single amino acid substitution caused significant lysozyme sensitivity, and for an additional 4 substitutions moderate lysozyme sensitivity was observed (Table 4.2, Figure 4.6A). To ensure that the 14 functionally impaired *Sa*OatA variants were expressed and localized correctly, the membranes from each *S. aureus* USA300 Δ*oatA* complemented strain were isolated and probed for *Sa*OatA presence by anti-His western analysis. Each *Sa*OatA variant was found in the membrane in approximately equal amounts, suggesting that the observed lack of function was not due to insufficient expression or improper membrane insertion of the OatA variants (Figure 4.6B).

S. aureus OatA has a predicted signal peptide site between the N- and C-terminal domains ($_{399}$FDA$_{401}$), and evidence suggested that the domains may be cleaved during cell growth (Schallenberger et al., 2012). Whilst there is no distinct consensus signal peptidase recognition site, an Ala-X-Ala motif commonly preceeds the cleavage site (Tuteja, 2005). Therefore, in order to render the signal peptidase site in *Sa*OatA unrecognizable, the -1 position of the signal peptidase cleavage site, A401, was replaced with Glu and Leu. Interestingly, both of the A401E and A401L variants retained lysozyme resistance, suggesting that cleavage of the domains is not essential for PG O-acetylation.

To further investigate the potential roles of the putative functional residues, certain residues were replaced with additional amino acids to assess the importance of charges or functional groups on activity (Table 4.2). Arg25 and Arg86 were replaced individually with Lys, which had no effect on lysozyme resistance, suggesting that Lys can compensate for Arg at these positions. Glu154 and Glu357 were replaced individually with Asp and Gln. Whereas neither Asp nor Gln could compensate for Glu at position 154, Asp could partially compensate for Glu at position 357. Tyr136, Tyr206, and Tyr311 were all replaced individually with Phe and Ser to determine whether the phenol ring or hydroxyl were essential for activity. Neither Tyr136 nor Tyr206 could be compensated by Phe or Ser, however, interestingly, Tyr311 could be completely compensated by Ser.

4.3.4 PG O-acetylation quantification

To verify the correlation between the lysozyme sensitivity observed in the functional complementation assay and PG O-acetylation levels, PG O-acetylation was quantified for select *S. aureus* USA300 strains. PG was isolated from *S. aureus* USA300 (WT), *S. aureus* USA300 Δ*oatA*, and *S. aureus* USA300 Δ*oatA* pACCJ3, as well as

Table 4.2 Lysozyme minimal inhibitory concentration (MIC) of *S. aureus* USA300 Δ*oatA* expressing single amino acid variants of *Sa*OatA.

Variant	MIC (mg/mL)[1]
Δ*oatA*	1
WT (pACCJ3)	> 4
R25A	0.5
R25K	> 4
Y35A	> 4
H36A	0.5
V49A	> 4
F52A	0.5
S56A	4
F79A	> 4
R83A	4
R86A	0.25
R86K	> 4
N126A	2
Y136A	0.25
Y136F	0.25
Y136S	0.25
W149A	1
E154A	0.5
E154D	0.5
E154Q	0.5
Y158A	> 4
Y206A	0.5
Y206F	1
Y206S	0.5
Y269A	> 4
H289A	> 4
S310A	> 4
Y311A	0.5
Y311F	0.5
Y311S	> 4
Y314A	4
H317A	> 4
S352A	> 4
E357A	0.5
E357D	1-2
E357Q	0.25
A401E	> 4
A401L	> 4

1. MIC with lysozyme was determined by growing *S. aureus* USA300 Δ*oatA* expressing OatA *in trans* in 0.4 μg/mL tunicamycin and increasing concentrations of lysozyme (0-4 mg/mL). Each variant was tested in technical and biological triplicates.

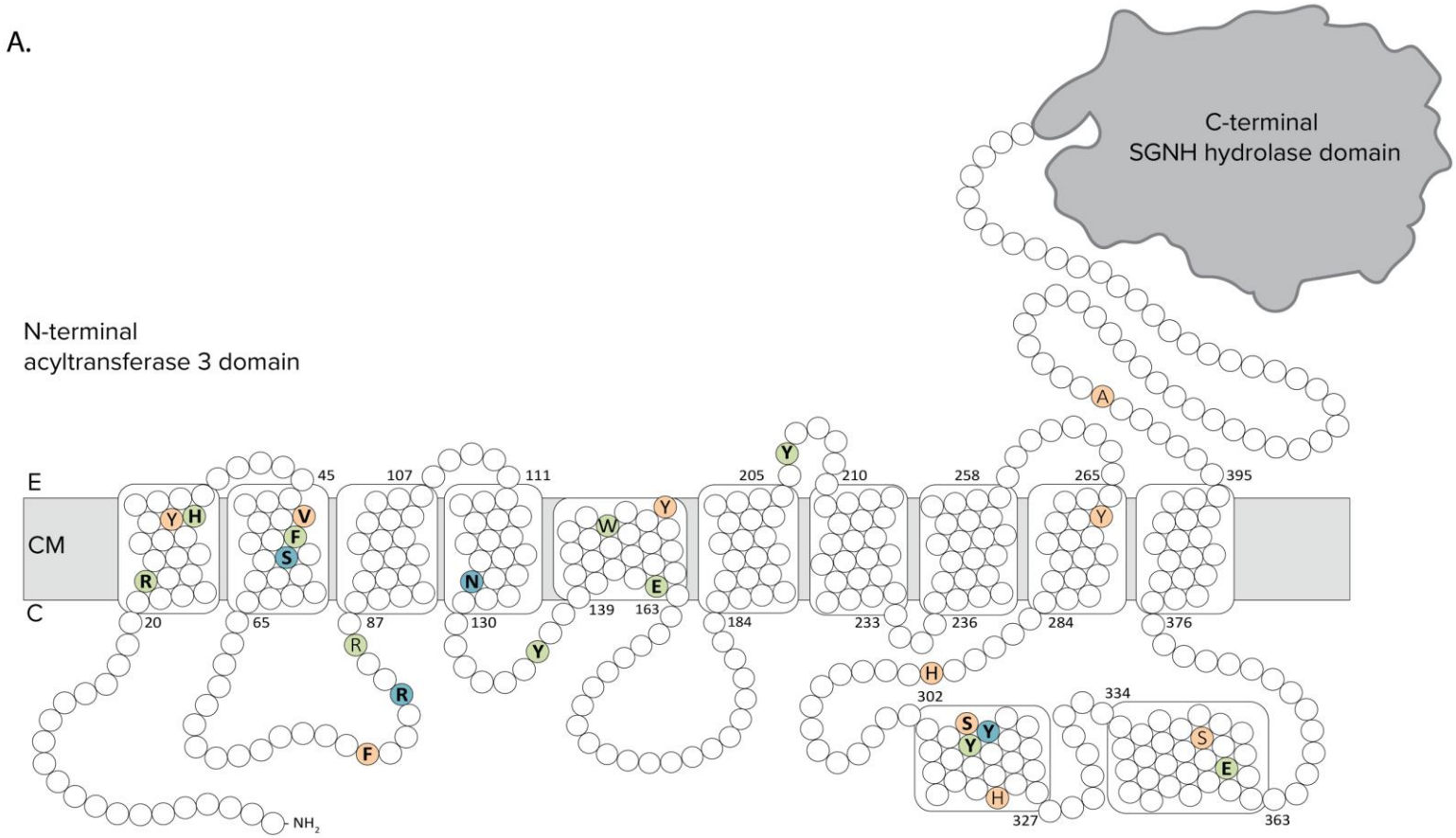
A.
C-terminal
SGNH hydrolase domain
N-terminal
acyltransferase 3 domain
E
CM
C
NH2
B.
WT
R25A
H36A
F52A
S56A
R83A
R86A
Y136A
W149A
E154A
Y206A
Y311A
Y314A
E357A
N126A
63
48

Figure 4.6 Identification of conserved and functional residues in *Sa*OatA$_N$. A. Invariable and highly conserved residues were identified by bioinformatic analysis of OatA homologues and mapped onto the topology map of *Sa*OatA$_N$. Residues with >80% conservation are labelled, and invariable residues are in bold. Selected residues were individually replaced with Ala and the resultant *Sa*OatA variants were assessed for their ability to provide lysozyme resistance in a Δ*oatA* background of *S. aureus* USA300. The amino acid colour denotes the functional complementation assay result: when replaced with Ala, the strain expressing the resulting *Sa*OatA variant was either completely lysozyme sensitive (green), partially lysozyme sensitive (blue), or completely lysozyme resistant (orange). B. The membranes from each lysozyme sensitive *S. aureus* USA300 Δ*oatA* complemented strains were isolated and probed for *Sa*OatA by anti-His western blotting to ensure proper expression and membrane localization. E, external; CM, cytoplasmic membrane; C, cytoplasm. Molecular weight markers are given in kDa.

representative OatA single amino acid variants: *S. aureus* USA300 Δ*oatA* pACCJ3 H36A, *S. aureus* USA300 Δ*oatA* pACCJ3 R83A, and *S. aureus* USA300 Δ*oatA* pACCJ3 Y206A. The purified PG was acid hydrolyzed to reduce the material into its constitutive amino sugars and amino acids, and the muramic acid content was quantified by HPAEC. A sampleof the same PG was treated with base to hydrolyze all *O*-acetyl groups and the released acetic acid was quantified using the Megazyme Acetic Acid Kit. Percentage PG O-acetylation for each strain was calculated as the amount of acetic acid relative to muramic acid content. The PG O-acetylation level of *S. aureus* USA300 (WT) was ~40%, and there was no detectable acetylation in the *S. aureus* USA300 Δ*oatA* strain (Figure 4.7). In accordance with the functional complementation assay results, *S. aureus* USA300 Δ*oatA* complemented with wild-type *Sa*OatA (pACCJ3) had ~35% PG O-acetylation, whereas the representative single amino acid variants displaying full lysozyme sensitivity, H36A and Y206A, had 0% and 1.26% PG O-acetylation, respectively. The strain expressing the R83A OatA variant that displayed only partial lysozyme sensitivity had 29% PG O-acetylation.

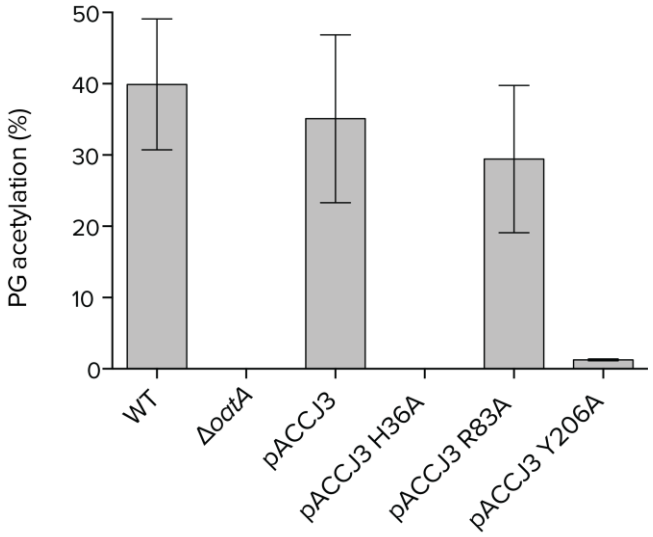

Figure 4.7 PG O-acetylation levels of *S. aureus* USA300 strains. PG was isolated from *S. aureus* USA300 (WT), *S. aureus* USA300 Δ*oatA*, and *S. aureus* USA300 expressing wild-type *Sa*OatA (pACCJ3) or an *Sa*OatA variant. The quantity of muramic acid and base-labile acetyl groups was determined by HPAEC and Megazyme acetic acid kit, respectively, to determine the relative percentage of PG O-acetylation in each strain. Error bars denote standard deviation (n=3).

4.3.5 *In vitro* esterase activity of *Sa*OatA variants

Full length *Sa*OatA was cloned with a His_{10}-tag, expressed in *E. coli* C43 DE3, and purified by immobilized metal-ion affinity chromatography to apparent homogeneity as determined by SDS PAGE analysis (Figure 4.8). Yields were approximately 3 mg protein per litre of culture. An adapted aldrithiol assay using the thiol detecting reagent 4′,4′-dithiodipyridine (DTDP) was adopted to monitor the turnover of acetyl-CoA by full length OatA (Grassetti and Murray, 1967). Given that OatA is a bimodular enzyme with proposed catalytic sites in the N- and C-terminal domains, it was important to verify that the assay was detecting N-terminal domain activity. The C-terminal domain of *S. aureus* OatA (residues 445-601; $OatA_C$) was purified and assayed and no acetyl-CoA turnover was detected using the aldrithiol assay, suggesting that the observed esterase activity was not due to the C-terminal domain. This is consistent with previous data that showed that the C-terminal domain of *Sa*OatA was unable to modify pentaacetyl-chitopentaose (G5) when acetyl-CoA was supplied as an acetyl donor (Sychantha et al., 2017).

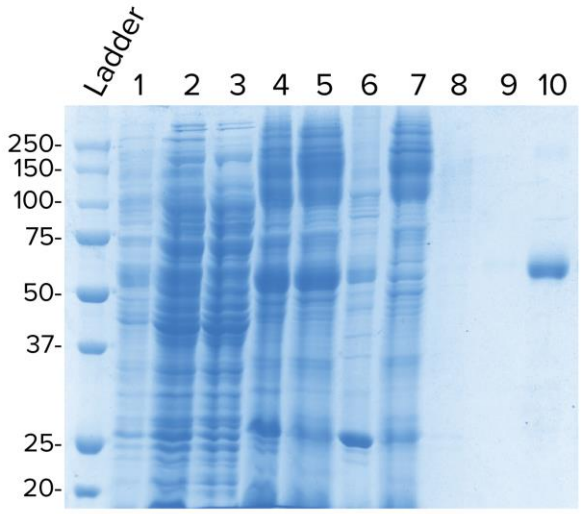

Figure 4.8 SDS-PAGE analysis of the purification of *Sa*OatA from *E. coli*. Full-length *Sa*OatA was expressed in *E. coli* C43 and purified by immobilized metal affinity chromatography. Lanes: 1, insoluble lysate; 2, clarified soluble lysate; 3, cytoplasmic fraction; 4, membrane fraction; 5, soluble fraction after treatment of membranes with 2% (w/v) DDM; 6, insoluble fraction after treatment of membranes with 2% (w/v) DDM; 7, flow through after incubation with Co^{2+} affinity (IMAC) resin; 8, IMAC wash 1; 9, IMAC wash 2 with 10 mM imidazole wash; 10, IMAC elution fraction with 250 mM imidazole. Molecular weight markers are given in kDa.

The steady state parameters were determined for full-length OatA acting as an esterase with acetyl-CoA as the substrate (Figure 4.9A,D). The determined K_M value of 15 µM is 77- and 6-fold lower than that of *Sa*OatA$_C$ with artificial substrates *p*NP-Ac and 4MU-Ac, respectively. Likewise, the overall efficiency of full length *Sa*OatA, as reflected by k_{cat}/K_M, was much higher with acetyl-CoA as substrate compared to the two pseudosubstrates (section 3.3.2). These data suggest that acetyl-CoA may be the authentic substrate of full-length OatA.

Several of the putative functional residues identified by the functional complementation assay were replaced by Ala (or Lys) and expressed, purified, and assayed with acetyl-CoA as a substrate (Table 4.3). The transferase capacity of each variant was tested by incubating the enzyme with acetyl-CoA and pentaacetyl-chitopenaose (G5) and detecting the acetylation of G5 by LC-MS (Figure 4.10). (R25A)-, (R86A)-, and (E154A)-*Sa*OatA variants retained 18.35%, 22.13%, and 4.75% esterase activity, respectively, with small amounts of acetylated G5 detected by LC-MS. (H36A)-*Sa*OatA retained only 0.64% apparent esterase activity and no transferase activity was detected. There was no detectable esterase nor transferase activity with the (Y206A)-*Sa*OatA variant. Interestingly, (Y136A)-*Sa*OatA displayed 155% esterase activity towards acetyl-CoA, however, no acetylated G5 was detected by LC-MS in the transferase assay. The (R25K)-*Sa*OatA variant also displayed increased esterase activity compared to wild-type (178%) and transferase activity was observed by LC-MS.

The steady state kinetic parameters were determined for the (Y136A)- and (R25K)-*Sa*OatA variants (Figure 4.9B,C). The K_M for (R25K)-*Sa*OatA was almost double that of wild-type OatA at 27.9 µM, however, the V_{max} was also double, such that the k_{cat}/K_M of 2940 $M^{-1}\bullet s^{-1}$ was only slightly increased compared to wild-type. Due to limitations of the assay, the reaction with (Y136A)-*Sa*OatA could not be saturated with acetyl-CoA, however, the data suggest both a significantly increased K_M of 133 µM and decreased k_{cat}/K_M of 1170 $M^{-1}\bullet s^{-1}$.

4.3.6 Interdomain acetyltransfer of *Sa*OatA

4.3.6.1 Kinetic analyses

Significant data exists to support the notion that the C-terminal domain of OatA

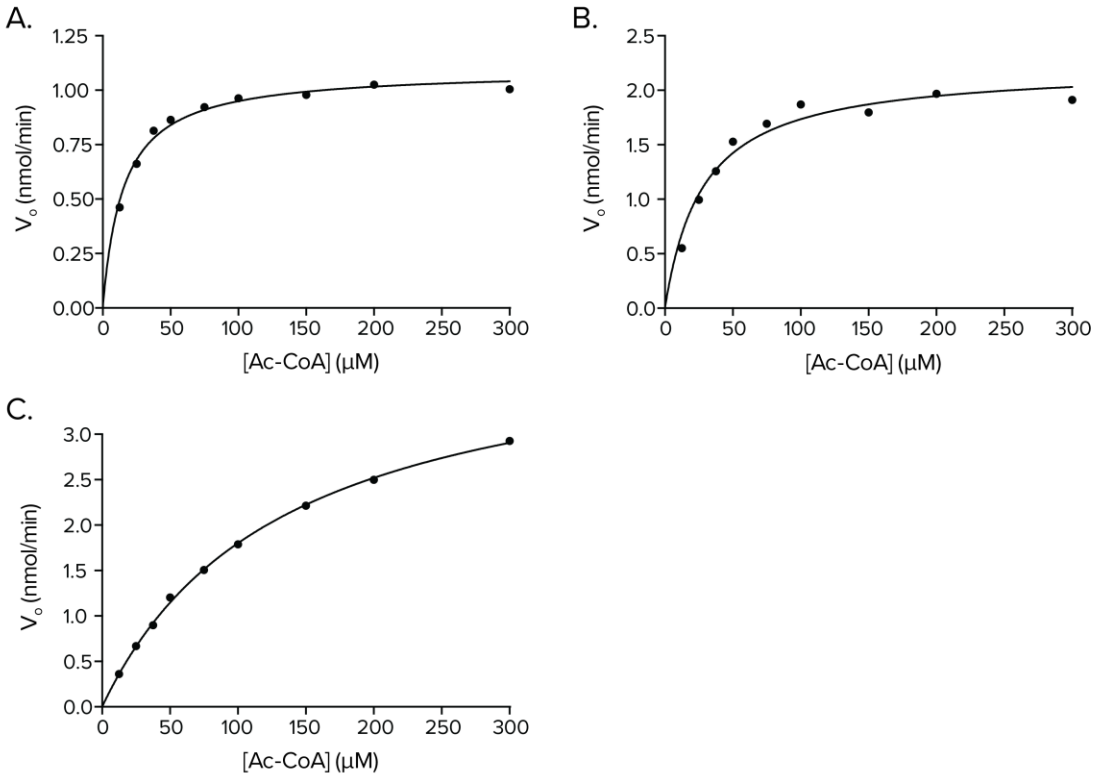

D.

Substrate	Variant	K_M (µM)	V_{max} (nmol/min)	k_{cat} (s^{-1})	k_{cat}/K_M ($M^{-1} \cdot s^{-1}$)
Acetyl-CoA	***Sa*OatA (WT)**	15.12 ± 0.708	1.09 ± 0.0104	0.0405 ± 0.000384	2680 ± 128
	(R25K)-*Sa*OatA	27.9 ± 2.33	2.22 ± 0.0495	0.0822 ± 0.000183	2940 ± 254
	(Y136A)-*Sa*OatA	133 ± 2.61	4.19 ± 0.0498	0.155 ± 0.00184	1170 ± 26.9
4MU-Ac	***Sa*OatA$_C$**[1]	112 ± 10.0	0.211 ± 0.0119	0.00469 ± 0.000265	41.8 ± 4.43

1. Described in section 3.3.2

Figure 4.9 Kinetic analysis of *Sa*OatA variants acting as an esterase with acetyl-CoA as substrate. The steady state parameters were determined for *Sa*OatA WT (A), (R25K)-*Sa*OatA (B), and (Y136A)-*Sa*OatA (C) (3µM) acting as an esterase in 50 mM sodium phosphate pH 7.0 using 12.5-300 µM acetyl-CoA as substrate. D. The Michaelis-Menten steady state parameters were determined for the experiments presented in panels A-C. Data were analyzed in GraphPad Prism. '±' denote standard deviation (n = 3); error bars are smaller than the height of the symbol.

functions to add acetyl-groups to muramoyl residues of PG (Sychantha et al., 2017). The source of these acetyl groups, however, has not been identified and it is unknown whether the N-terminal transmembrane domain and the C-terminal SGNH hydrolase domain interact directly or *via* an intermediate. Full-length *Sa*OatA showed significant esterase

Table 4.3 Esterase and transferase activities of *Sa*OatA variants with acetyl-CoA as acetyl donor

Enzyme variant	Esterase activity[1]		Transferase activity[3]
	Specific activity ($nmol \cdot min^{-1} \cdot mg^{-1}$)	**Relative activity** (%)	
***Sa*OatA (WT)**	28.8 ± 0.20	100%	yes
R25A	5.28 ± 0.07	18.4%	yes
R25K	51.3 ± 0.23	178%	yes
H36A	0.18 ± 0.05	0.64%	no
R86A	6.37 ± 0.02	22.1%	yes
Y136A	44.6 ± 0.48	155%	no
E154A	1.37 ± 0.05	4.76%	yes
Y206A	N.D.	0%	no
S453A[2]	-	5.4%	no

1. Reactions were conducted in 50 mM sodium phosphate pH 7.0, 5% (v/v) DMSO at 25 ºC with 0.1 mM acetyl-CoA and 0.2 mM DTDP. '±' denotes standard deviation; N.D. = no detectable activity.
2. The activity of this variant was tested in 5% (v/v) ethanol instead of 5% (v/v) DMSO and compared to wild-type enzyme tested under the same conditions.
3. Transferase activity determined as acetylated product formation in the transferase LC-MS assay; reactions were conducted in 50 mM sodium phosphate pH 7.0 at 25 ºC with 0.1 mM acetyl-CoA and 1 mM pentaacetyl-chitopentaose.

activity towards acetyl-CoA, whereas *Sa*OatA$_C$ was incapable of hydrolyzing acetyl-CoA. S453 was replaced with Ala in full-length *Sa*OatA to catalytically inactivate the C-terminal domain. Its esterase activity towards acetyl-CoA was then monitored. Interestingly, this variant retained only 5.4% esterase activity compared to wild-type *Sa*OatA (Table 4.3), suggesting both domains of OatA are required for efficient hydrolysis of this substrate. In order to assess transferase activity, full-length *Sa*OatA, *Sa*OatA$_C$, and (S453A)-*Sa*OatA were incubated with acetyl-CoA and muroglycan oligomers (*in vitro* polymerized Lipid II). The reaction products were digested by mutanolysin into GlcNAc-MurNAc-pentapeptide units (GM-penta) and analyzed by LC-MS as described previously (Sychantha et al., 2017). Acetylated product was only detected from the reaction with wild-type full-length *Sa*OatA and neither *Sa*OatA$_C$ nor the (S453A)-*Sa*OatA variant produced acetylated muroglycan (Figure 4.11). These data suggest that acetyltransfer to muroglycans

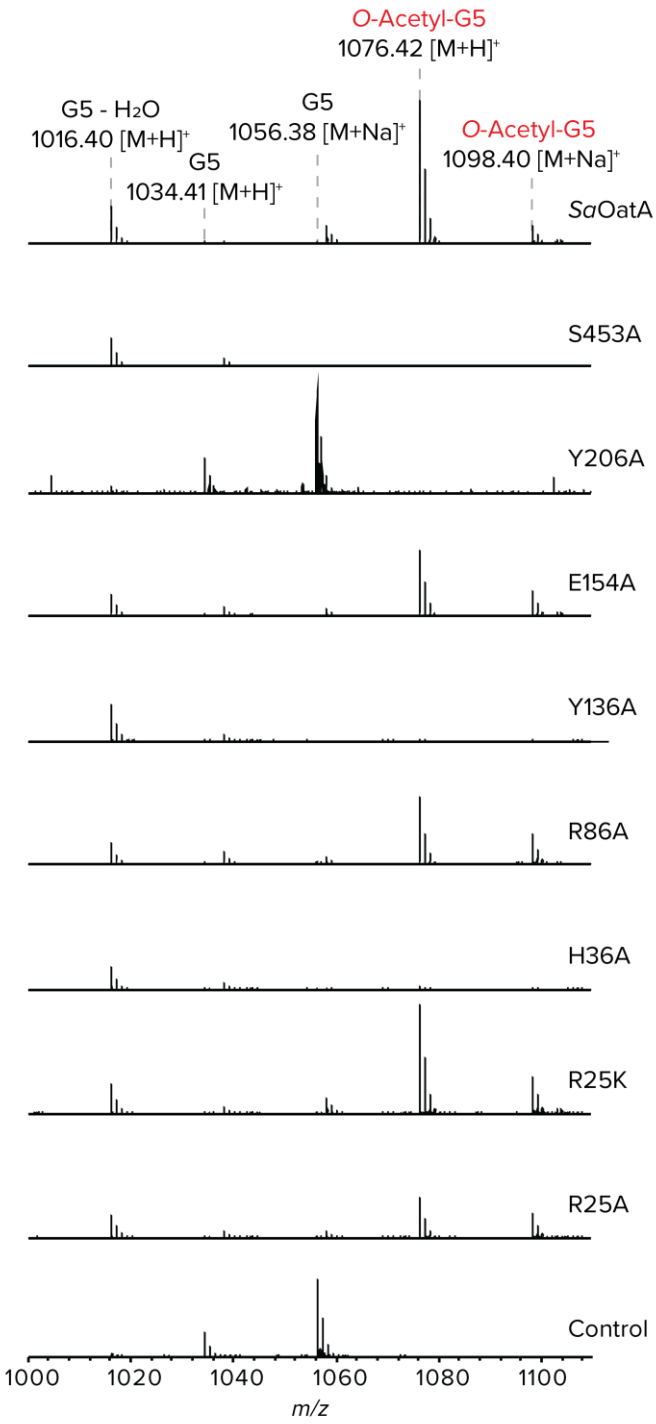

Figure 4.10 *Sa*OatA-catalyzed *O*-acetyltransferase reactions with pentaacetyl-chitopentaose as acceptor. QTOF-MS analysis of reaction products of 1 mM pentaacetyl-chitopentaose incubated in the absence (control) and presence of enzyme (5 µM) in 50 mM sodium phosphate pH 6.5 with 1 mM acetyl-CoA as acetyl donor. Single amino acid variants of *Sa*OatA are listed in figure.

requires the N-terminal domain to remove acetyl groups from acetyl-CoA, and the C-terminal domain to transfer them onto the muroglycan acceptor substrate. The 5.4% residual activity seen with the acetyl-CoA assay likely results from water occasionally entering the active site and hydrolyzing the putative acetyl-enzyme intermediate.

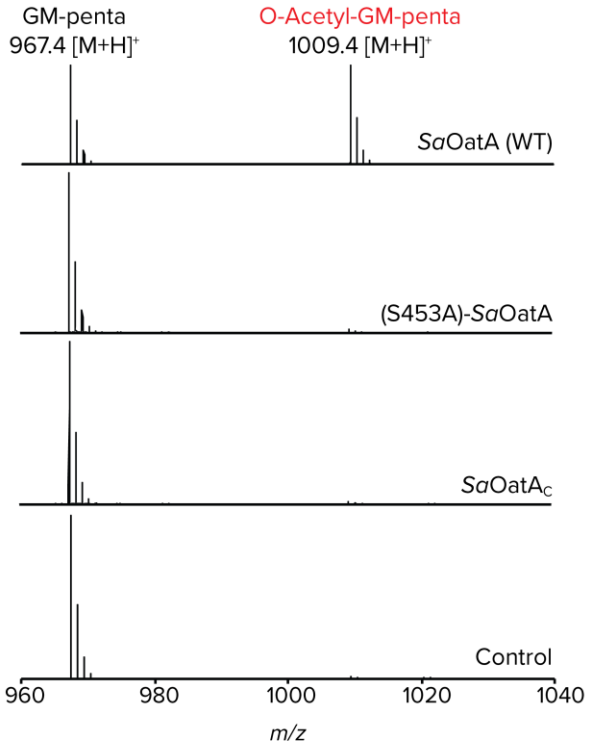

Figure 4.11 *Sa*OatA-catalyzed *O*-acetyltransferase reactions with muroglycan oligomers as acceptor. QTOF-MS analysis of mutanolysin-digested reaction products of 10 µg/mL muroglycans (GM-penta) incubated in the absence (control) and presence of enzyme (5 µM; *Sa*OatA (WT), (S453A)-*Sa*OatA, and *Sa*OatA$_C$) in 50 mM sodium phosphate pH 6.5 with 1 mM acetyl-CoA as acetyl donor.

4.3.6.2 Analysis of *S. aureus* OatA and *S. pneumoniae* OatA chimeras

To test the ability of homologous OatA to compensate for *Sa*OatA, *S. aureus* USA300 Δ*oatA* was complemented with *S. pneumoniae* OatA (*Sp*OatA) cloned into pACL2073. Growth of this strain in media containing lysozyme indicated that the complementation was unable to restore lysozyme resistance (Figure 4.12B). Chimeric proteins were constructed consisting of the N-terminal domain of *S. aureus* OatA (*Sa*OatA$_N$) and the C-terminal domain of *S. pneumoniae* OatA (*Sp*OatA$_C$) and vice versa,

joined at the signal peptidase site. Again, neither chimeric proteins were capable of restoring lysozyme resistance to *S. aureus* USA300 Δ*oatA* (Figure 4.12C,D). Proper expression and membrane insertion were confirmed by western blot (Figure 4.12E). Whilst inactivity could be related to improper localization or protein-protein interactions, these results do not support the notion of a universal intermediate and suggest activity may instead depend on co-ordinated activity and direct interaction of the two domains.

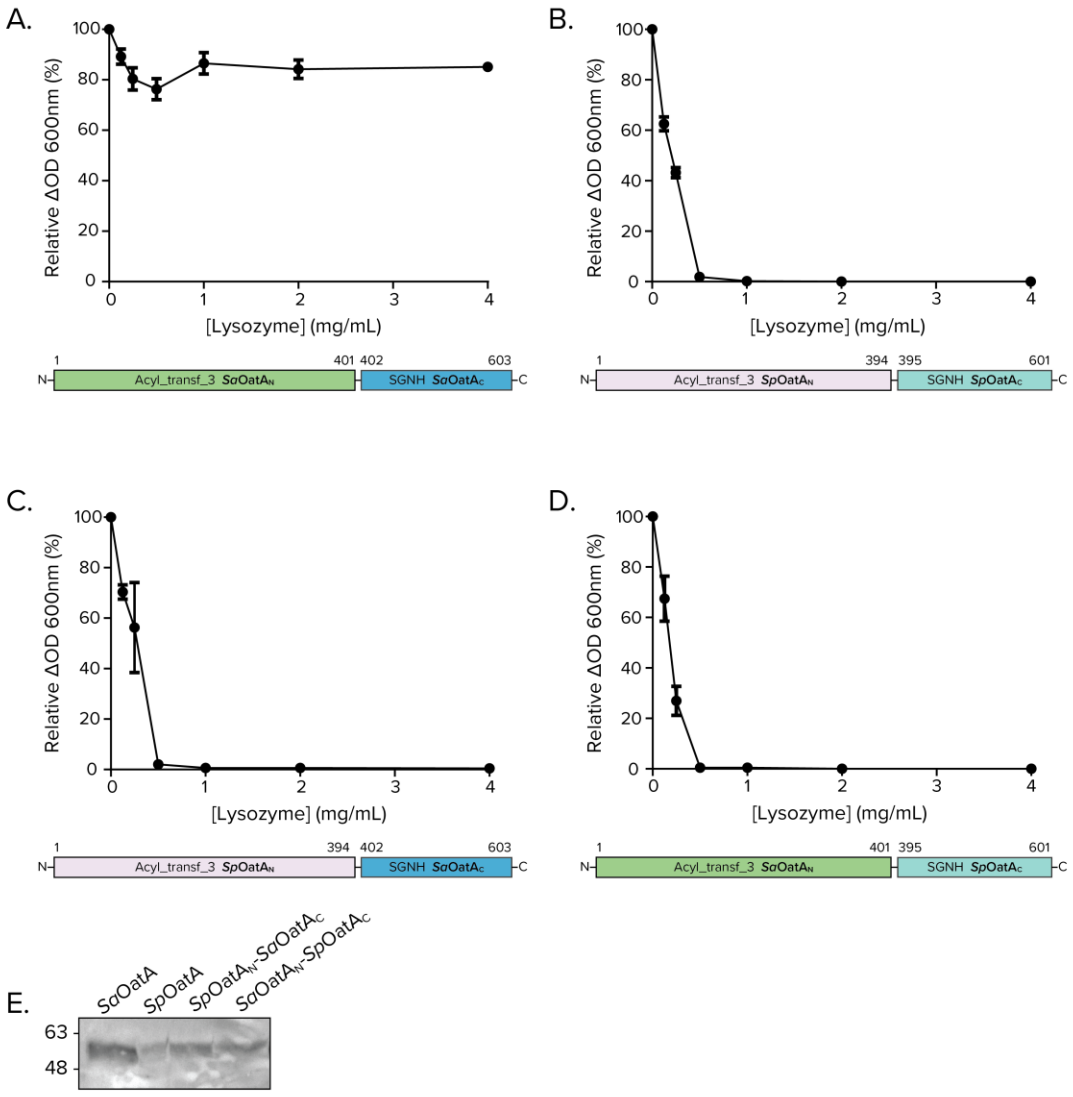

Figure 4.12 Determination of Lysozyme MIC for *S. aureus* and *S. pneumoniae* chimeras. Lysozyme MICs in the presence of 0.4 µg/mL tunicamycin of *S. aureus* USA300 Δ*oatA* complemented with *Sa*OatA (pACCJ3) (A), *Sp*OatA (pACCJ4) (B), and chimeric proteins *Sp*OatA$_N$-*Sa*OatA$_C$ (pACCJ5) (C) and *Sa*OatA$_N$-*Sp*OatA$_C$ (pACCJ6) (D). Error bars denote standard deviation (n=3). E. The membranes from each culture were isolated and probed for *Sa*OatA or *Sp*OatA by anti-His western blotting to ensure proper expression and membrane localization.

4.3.7 Activity of *Sa*OatA$_C$ towards *O*-acetyl-Tyr donor peptides

The data acquired thus far imply a direct interaction between the two catalytic domains of OatA. Since Y206 is exposed to the periplasm and is critical for function of *Sa*OatA, it was reasoned that this residue could be involved in the direct transfer of acetyl groups between the N- and C-terminal domains. To test this hypothesis, peptides based on the Y206 perisplasmic loop were purchased and synthetically acetylated at the Tyr residue and presented to SaOatA$_C$ as acetyl donors. Given the poor solubility of the acetylated peptides, assays needed to be performed in the maximal permittable DMSO concentration. The activity of *Sa*OatA$_C$ towards 4MU-Ac was tested in increasing DMSO concentrations up to 60% (v/v), with peak activity in 40% (v/v) DMSO (Figure 4.13A). Michaelis-Menten kinetics of *Sa*OatA$_C$ in 35% (v/v) DMSO showed a similar K_M to 5% DMSO but an increased V_{max} (Figure 4.13B,C). Thus, surprisingly, the overall efficiency of the enzyme was 6-fold greater when in the presence of 35% (v/v) DMSO. The peptides were therefore tested in 45% (v/v) DMSO to maximize substrate solubility whilst maintaining enzyme activity. Unfortunately, substrate availability and solubility, even in 45% (v/v) DMSO, limited the possible analyses, and it was only possible to obtain a specific activity for some peptides.

N-Acetyl-Val-(*O*-acetyl)-Tyr-Phe-Gly-amide (VYFG) and *N*-acetyl-Arg-Val-(*O*-acetyl)-Tyr-Phe-Thr-Asp-amide (RVYFGTD) represented short and long peptides, respectively, based on the Y206 extracytoplasmic loop. *N*-acetyl-Asp-(*O*-acetyl)-Tyr-Phe-amide (DYF) and *N*-acetyl-Glu-Asn-Val-Asp-(*O*-acetyl)-Tyr-Phe-Asn-Glu-amine (QNVDYFNQ) represented short and long peptides, respectively, based on the Y136 cytoplasmic loop and served as controls for these reactions along with *O*-Acetyl-Tyr-ethyl ester (Y). *N*-Acetyl-Val-(*O*-acetyl)-Tyr-Phe (VYF) was also acetylated and purified, however, its low solubility prevented activity assays. With each peptide, removal of the acetyl group from the Tyr residue of the donor peptide was detected by monitoring the increase in absorbance at 278 nm; acetylation of Tyr residues suppresses absorbance at 278 nm, and as the acetyl groups are removed, absorbance increases (Figure 4.14A). The starting concentration of *O*-acetyl Tyr in each reaction was determined by hydroxylamine treatment and the molar extinction coefficient for the conversion of *O*-acetyl-Tyr to Tyr (Riordan and Vallee, 1972), as described in section 2.4.9.2. Each peptide was tested at at

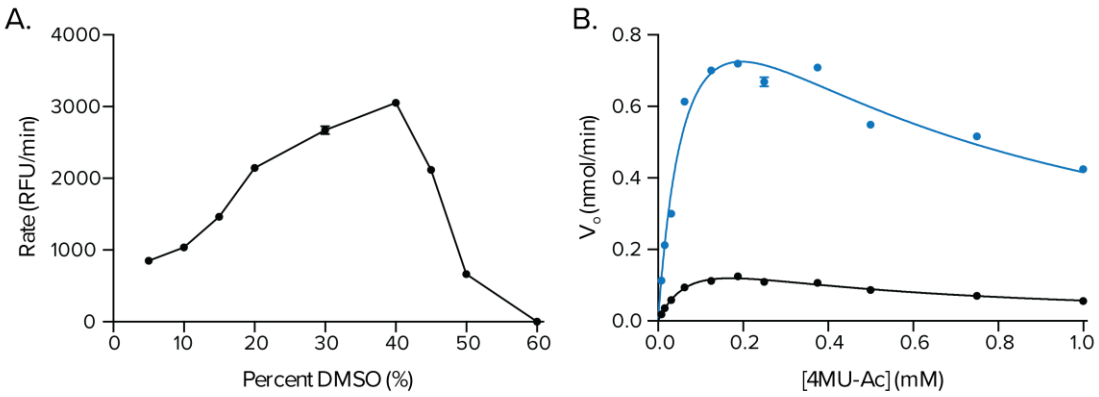

C.

DMSO (%)	K_M (mM)	V_{max} (nmol/min)	k_{cat} (s^{-1})	k_{cat}/K_M ($M^{-1} \cdot s^{-1}$)
5%	0.102 ± 0.00928	0.262 ± 0.0146	0.00583 ± 0.000324	57.0 ± 6.07
35%	0.0804 ± 0.0116	1.32 ± 0.102	0.0293 ± 0.00228	365 ± 59.8

Figure 4.13 Kinetic analysis of *Sa*OatA$_C$ esterase activity with DMSO as co-solvent. A. The rate of reaction for esterase activity of *Sa*OatA$_C$ was determined in 5–60% (v/v) DMSO, with a peak activity observed at 40% (v/v) DMSO. B. The steady state parameters were determined for *Sa*OatA$_C$ using 0.02-1 mM 4MU-Ac as substrate in 50 mM sodium phosphate pH 6.5 and 5% (v/v) DMSO (black) or 35% (v/v) DMSO (blue). C. The Michaelis-Menten steady state parameters were determined for the experiments presented in panel B. Data were analyzed in GraphPad Prism. Error bars and '±' denote standard deviation (n = 3).

least three different concentrations, in singlicate. A linear regression was performed for the range of concentrations, and a specific activity for a 1 mM concentration was interpolated using the equation of the line (Figure 4.14B). One-way ANOVA followed by Tukey's multiple comparison test was performed on the data using GraphPad Prism 6 to assess significance between Although the specific activity range was small, the specific activity of *Sa*OatA$_C$ was greatest with the longest Y206 loop-based peptide, RVYFGTD, as substrate, significantly greater than the activity towards Tyr-ethyl-ester (Y), DYF, and VYFG (Figure 4.14B). The activity of the *Sa*OatA$_C$ was greater towards the longer of each set of peptides (QNVDYFNQ vs. DYF) and (RVYFGTD vs. VYFG). The activity towards the long control peptide, QNVDYFNQ, was slightly less than that of RVYFGTD, however the difference was not significant. Michaelis-Menten parameters were determined for *O*-acetyl-Tyr-ethyl ester and RVYFGTD, although substrate availability only allowed for

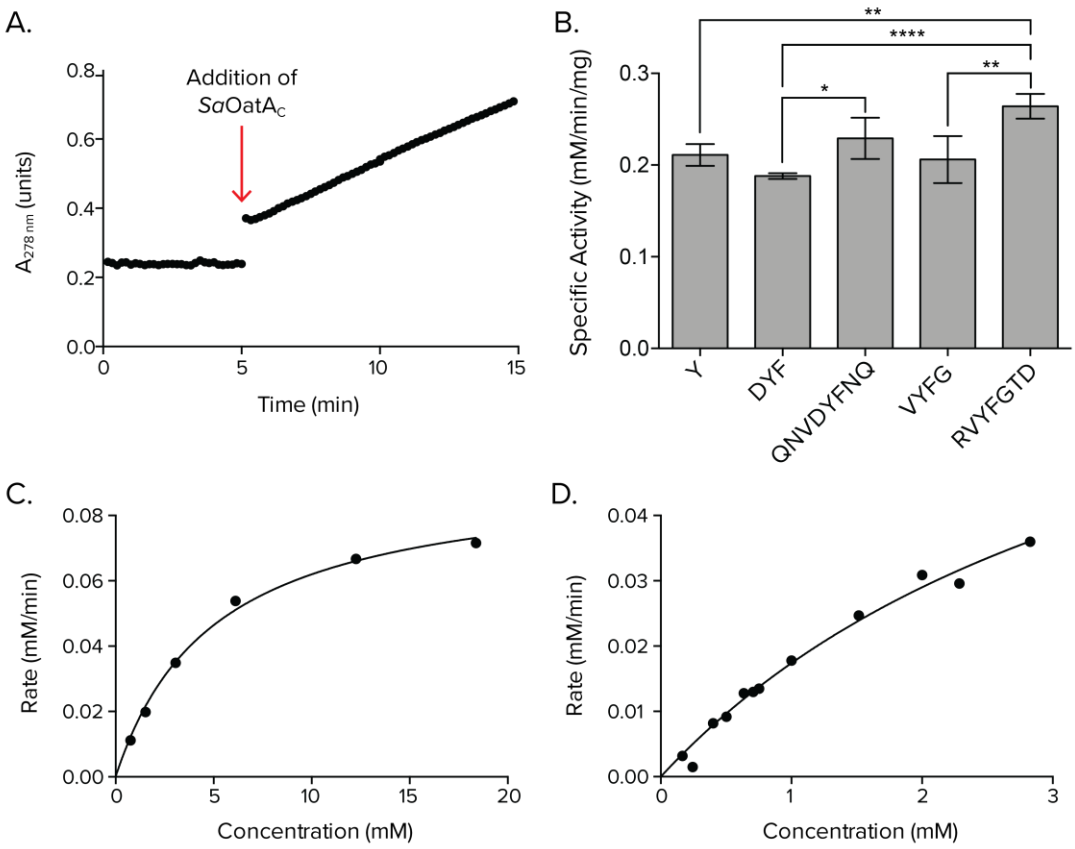

E.

Substrate	K_M (mM)	V_{max} (mM/min)	k_{cat} (s^{-1})	k_{cat}/K_M ($M^{-1} \cdot s^{-1}$)
O-Ac-Y-ethyl ester	5.05 ± 0.519	0.0932 ± 0.00363	0.311 ± 0.0121	61.6 ± 6.78
RV-(*O*-Ac)-YFGTD	4.03 ± 0.909	0.0875 ± 0.0136	0.292 ± 0.0454	72.3 ± 19.8

Figure 4.14 Kinetic analysis of *Sa*OatA$_C$ esterase activity with *O*-acetyl-Tyr peptides. A. The absorbance of acetylated peptide in 50 mM sodium phosphate pH 6.5 and DMSO was monitored at 278 nm for spontaneous hydrolysis of the acetyl group. *Sa*OatA$_C$ (5µM) was added to the reaction (indicated by red arrow) and the rate of esterase activity was monitored. B. The rate of reaction for esterase activity of *Sa*OatA$_C$ (5 µM) was determined for each acetylated peptide in 50 mM sodium phosphate pH 6.5 and 44% (v/v) DMSO. The data presented are for a 1 mM substrate concentration, determined by interpolation from a linear regression of at least 3 reactions at different concentrations. Error bars represent error of the slope of the linear regression. C,D. The steady-state parameters were determined for *Sa*OatA$_C$ (5 µM) using 0.76 – 18.4 mM *O*-Ac-Tyr-ethyl ester (C) or 0.24 – 2.8 mM Arg-Val-(*O*-Ac)-Tyr-Phe-Gly-Thr-Asp-amide (D) as substrate in 50 mM sodium phosphate pH 6.5 and 44% (v/v) DMSO. E. The Michaelis-Menten steady state parameters were determined for the reactions presented in panels C and D. Data were analyzed and a One-way ANOVA followed by Tukey's multiple comparison test was performed on the data in B using GraphPad Prism 6. *, p-value ≤ 0.05; **, p-value ≤ 0.01; ****, p-value ≤ 0.0001.

each concentration to be tested in a single reaction (Figure 4.14C-E). The K_M was lower for the enzyme with acetylated RVYFGTD, implying that *Sa*OatA$_C$ has a higher affinity for the longer peptide. The k_{cat} value was only marginally higher for the enzyme with *O*-acetyl-Tyr-ethyl ester and the k_{cat}/K_M value was lower. Together, these data imply that *Sa*OatA$_C$ has preference towards longer, more complex peptides.

4.4 Discussion

The hypothesized mechanism of action of OatA was based largely on homology-based predictions for the function of each domain of the enzyme. The C-terminal SGNH hydrolase domain of OatA has been well-characterized as a PG *O*-acetyltransferase (Sychantha and Clarke, 2018; Sychantha et al., 2017), however, the N-terminal acyltransferase 3 domain is largely uncharacterized. To date, no structure of an acyltransferase 3 family protein has been solved and very few have been studied in depth biochemically.

The topology model of *Sa*OatA revealed several unanticipated structural features (Figure 4.4). For example, the PhoA-LacZα fusion mapping data suggest that TMS 5 is a re-entrant helix, a helix that penetrates, but does not cross, the membrane. A typical transmembrane helix is between 15 and 30 amino acids long, with an average of 25 residues (Saidijam et al., 2018), and as both I130 and L168 were localized to the cytoplasm, it seems unlikely that the intervening 38 amino acids are sufficient to form two transmembrane helices that fully cross the membrane, as both the helices and the intervening loops would have to be quite short. Furthermore, helix prediction software predicts one helix in this region encompassing residues 145 to 171, depending on the prediction software. As residues Q139 and P163 in *Sa*OatA were localized to the membrane, the bounds of the helix were set as those residues, however, it is not possible to ascertain whether TMS 5 is one long or two short helices based solely on the data obtained. Whilst re-entrant helices are not seen in any of the *in silico* transmembrane predictions, re-entrant helices are encountered in transmembrane proteins with solved structures. For example, undecaprenyl pyrophosphate phosphatase (UppP) from *E. coli* possesses two short adjacent re-entrant helices (El Ghachi et al., 2018; Workman et al., 2018). Similarly, the ClC chloride channel from *E. coli* was found to have 6 re-entrant regions (Dutzler et al., 2003). CNIH3, a

mammalian cornichon family AMPA receptor auxiliary protein possessed two adjacent re-entrant helices (Nakagawa, 2019).

The region between TMS 9 and 12 was localized to the cytoplasm by 11 truncations (Table 4.1; Figure 4.4). Analysis of the hydrophobicity of the helices using HeliQuest (Gautier et al., 2008) revealed that one of the two cytoplasmic helices is amphipathic, suggesting peripheral association with the membrane. Despite not appearing in *in silico* predictions, peripherally associated helices are a common occurrence in membrane proteins. The structure of *Streptococcus thermophilus* DltB, a membrane-bound *O*-acyltransferase family involved in D-alanylation of wall teichoic acids, was recently solved by X-ray crystallography (Ma et al., 2018). Whilst several of the TMS aligned with the *in silico* predictions for this enzyme, of note were several short peripheral membrane helices on the inner and outer faces of the membrane that contain two important functional residues and were not predicted (Ma et al., 2018) (Appendix 3). These examples demonstrate the limitations of *in silico* tools and highlight the value of experimental approaches to determining the structure and topology of membrane proteins.

Oac is an acyltransferase 3 family protein involved in O-acetylation of O-antigen in *Shigella flexneri* by the temperate bacteriophage Sf6. The topology of Oac was investigated using PhoA-LacZα fusion tagging, which generated a model similar to the *in silico* predicted model for *Sa*OatA but differed from the experimental model (Thanweer et al., 2008) (Figure 4.15). However, as only 16 truncations of Oac were assayed, certain regions of the protein were not mapped, which may account for discrepancies between the Oac and *Sa*OatA experimental models.

The acyltransferase 3 protein family (IPR002656) has over 114,000 members, most of which result from automatic annotation. Despite the abundance of proteins, there is a great lack of functional data for this protein family. Functional residues are generally highly conserved amongst homologues, therefore, in order to identify candidate functional residues in *Sa*OatA, a multiple sequence alignment was generated for OatA homologues (Appendix 2). Given that acyltransferase 3 family enzymes are found in both prokaryotes and eukaryotes and act on wide array of substrates, sequences were only taken if they possessed the correct acyltransferase 3-SGNH hydrolase domain architecture and were from bacteria for which there was experimental evidence of PG O-acetylation. This was

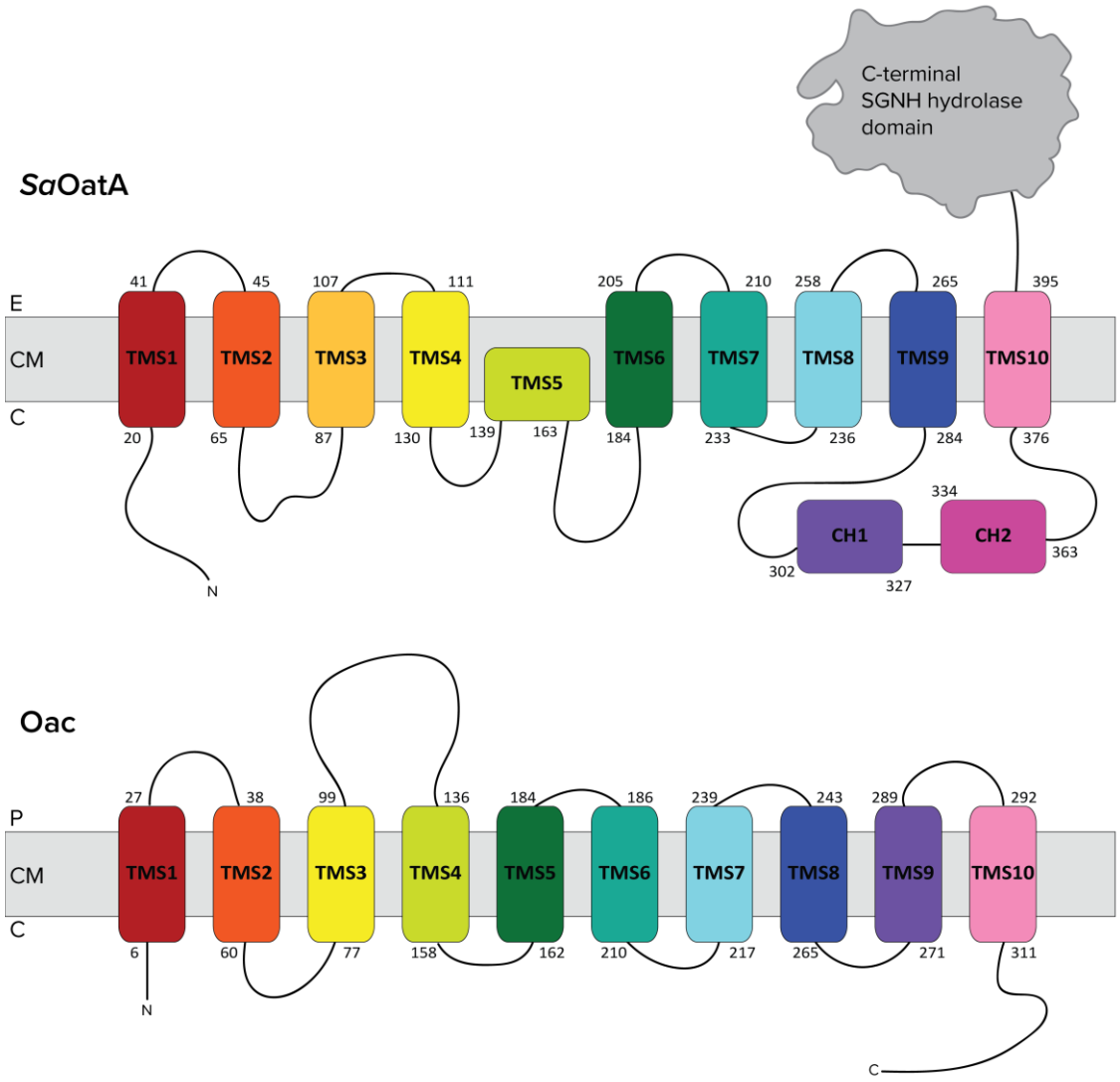

Figure 4.15 Comparison of the experimental topology maps for *S. aureus* OatA and *S. flexneri* bacteriophage Sf6 O-antigen *O*-acetyltransferase. The topology maps for *S. aureus* OatA (*Sa*OatA; upper) and *S. flexneri* bacteriophage Sf6 O-antigen *O*-acetyltransferase (Oac; lower) were both solved by PhoA-LacZα fusion mapping (Thanweer et al., 2008). E, external; P, periplasm; CM, cytoplasmic membrane; C, cytoplasm; TMS, transmembrane helix; CH, cytoplasmic helix.

done in order to increase the chances of finding residues specific for function as a PG *O*-acetyltransferase.

Candidate functional residues were investigated by a functional complementation assay. Four invariable residues, Val49, Phe52, Ser56, and Gly57 were found in a putative conserved motif (V-x-x-F-F-x-I/V/L-S-G-F/W/Y) that was first identified in several

O-antigen *O*-acetyltransferases (Lück et al., 2001; Thanweer et al., 2008). A non-functional isogenic mutant of Lag-1 in *Legionella pneumophila* carried a single point mutation that resulted in a change from a Ser to Leu in the motif (Lück et al., 2001). Thanweer *et al.* found that in Oac, the bacteriophage *O*-acetyltransferase that O-acetylates O-antigen in *Shigella flexneri*, the adjacent Ser-Gly in the motif were critical to assembly (Thanweer and Verma, 2012). In *Sa*OatA, the motif is found as $_{49}$V-D-T-F-F-V-I-S-G-Y$_{58}$. Replacement of Val49 with Ala had no effect on the lysozyme resistance of *S. aureus* expressing the *Sa*OatA variant (Table 4.2). Replacement of Phe52 with Ala, however, rendered the bacteria completely lysozyme sensitive. Replacement of Ser56 with Ala caused a reduction in lysozyme resistance, but not enough to suggest a crucial role in *Sa*OatA function.

Three Arg residues, Arg25, Arg83, and Arg86 were all found to be highly conserved and important for *Sa*OatA function (Table 4.2). In the functional complementation assay, replacement of Arg25 and Arg86 with Ala resulted in a complete loss of lysozyme resistance, whilst replacement of Arg83 with Ala resulted in partial loss of lysozyme resistance. In contrast, replacement of Arg25 and Arg86 with Lys had no effect on lysozyme resistance. Although it lacks the guanidino group, Lys maintains the positive charge of Arg and is a similar size. Indeed, Lys is often found at the equivalent position 86 in OatA homologues instead of Arg. All three Arg residues mapped to the cytoplasmic face of the membrane in the topology model, consistent with the rule that positive amino acids are usually found in cytoplasmic loops of transmembrane proteins. Furthermore, Arg residues have been found to be involved in binding to the phosphate groups of Coenzyme A (Choosangtong et al., 2015; Iyer and Ferry, 2001). Whilst the identity of the acetyl donor for *Sa*OatA$_N$ remains unknown, purified *Sa*OatA had a K_M of 15 µM for acetyl-CoA, which, in addition to the identification of the Arg residues, supports the idea that acetyl-CoA is the natural substrate. (R25A)- and (R86A)-*Sa*OatA were assayed with acetyl-CoA, retaining 18% and 22% activity, respectively (Table 4.3). Given that there are three potential residues involved in acetyl-CoA binding, it is not surprising that single Arg replacements still retain detectable activity *in vitro*, however, such reduced activity is likely not sufficient to maintain adequate levels of PG O-acetylation in the cell. Interestingly, (R25K)-*Sa*OatA was more active than wild-type enzyme, however, the

higher K_M suggests lower affinity for the substrate (Figure 4.9). These data are supported by the finding that Arg73 and Arg75-Arg76 in Oac (equivalent to Arg83 and Lys85-Arg86 in *Sa*OatA) are important for function (Thanweer et al., 2008). Although Thanweer *et al*. suggest that Arg75-Arg76 in Oac are critical to assembly (Thanweer and Verma, 2012), no differences were found in the *in vivo* expression or localization of the (R25A)- and (R86A)-*Sa*OatA variants in western blotting analysis (Figure 4.2B). These data support the proposition that the primary role of Arg25, Arg83, and Arg86 in *Sa*OatA is the binding and orientation of acetyl-CoA.

In search of putative catalytic residues, attention was focused on the invariable amino acids that were critical for lysozyme resistance in the functional complementation assay. This included one histidine, His36, three tyrosines, Tyr136, Tyr206, and Tyr311, and two glutamates, Glu154 and Glu357. Whilst both invariable glutamates were identified as important for function, Glu357 could be partially compensated by Asp, whereas Glu154 could not (Table 4.2). Tyr311 could be completely compensated by serine, suggesting that the hydroxyl group is important in this position (Table 4.2). Thanweer *et al*. suggest that the equivalent Tyr311 residue motif in Oac (Ser274-Tyr275-Gly276) is critical to assembly, which may support a model wherein a hydroxyl at position 311 is important to protein stability. Purified (Y206A)- and (H36A)-*Sa*OatA had minimal or no detectable esterase and transferase activity with acetyl-CoA, suggesting a critical role in catalysis (Table 4.3, Figure 4.10). (E154A)-*Sa*OatA retained only 5% esterase activity and minimal transferase activity. Unexpectedly, purified (Y136A)-*Sa*OatA had increased esterase activity, however, no transferase activity was detected. Overall, these data suggest that the most likely catalytic residues are Glu154, His36, and Tyr206. Precedence for these amino acids as catalytic residues exists among acetyltransferases, particularly for histidine. Before identification of the enzyme involved in sialic acid acetylation of glycoproteins in the Golgi, early experiments identified acetyl-CoA as the acetyl donor and suggested the involvement of one or more histidine residues (Higa et al., 1989). The authors proposed a two-step transmembrane reaction with an acetyl-enzyme intermediate and histidine(s) involved in both steps of the reactions. The enzyme responsible, CASD1, has since been identified as a bidomain enzyme with a GDSL/SGNH hydrolase domain and a transmembrane CAS1 acyltransferase domain (Baumann et al., 2015). The GDSL/SGNH

hydrolase domain accounts for the role of a histidine in the second half of the reaction, but leaves open the possibility of a catalytic His in the early steps of the reaction. Indeed, an unrelated membrane acetyltransferase, lysosomal heparan sulphate acetyl-CoA:α-glucosaminide *N*-acetyltransferase, was experimentally shown to form an acetyl-intermediate on a histidine (Bames and Rome, 1986; Durand et al., 2010). Although both His36 and Tyr206 are theoretically capable of being covalently modified with an acetyl group, given the current data, it is not possible to determine which residue(s) are modified in *Sa*OatA. Trapping of the acetyl-intermediate by MS may provide further insight.

Many of the enzymes in the acyltransferase 3 family are monofunctional with a single acyltransferase 3 domain, which likely acylates the target directly. WecH from *E. coli*, for example, is an acetyltransferase with a single acyltransferase 3 domain predicted to acetylate enterobacterial common antigen (Kajimura et al., 2006). In contrast, OatA is two domain enzyme with an extracytoplasmic SGNH hydrolase domain in addition to the acyltransferase 3 domain. OatA possesses a non-canonical signal peptidase site between the N-terminal acyltransferase 3 domain and C-terminal SGNH hydrolase domain. In a study from 2012, the C-terminal extracytoplasmic domain of OatA was detected in the media of a culture of *S. aureus* in proportion to signal peptidase inhibition, suggesting that cleavage of the enzyme into its two respective domains may be important for function (Schallenberger et al., 2012). To test this hypothesis, the -1 position of the signal peptidase cleavage site, Ala401, was replaced with Glu and Leu to inactivate the signal peptidase site, however, neither replacement had any effect on the lysozyme resistance of *S. aureus* (Table 4.2). Therefore, it does not appear that signal peptidase processing is necessary for function of OatA. It is possible that cleavage by signal peptidases may be important in the regulation of OatA by removing the catalytic module to prevent PG O-acetylation, however this was not investigated further.

Although OatA likely remains intact as a single polypeptide, the idea arose that a diffusable intermediate might exist to carry the acetyl group between the two domains. Such an idea was supported by the discovery that in the analogous Gram-negative system, PatB could acetylate PG using an unknown substrate generated by WecH in *E. coli* (Moynihan and Clarke, 2010). To investigate this hypothesis, the ability of *Sa*OatA to acetylate a PG mimic acceptor substrate was tested with variants possessing a functional

and non-functional C-terminal SGNH hydrolase domain (Figure 4.11). The data suggest direct transfer between the N- and C-terminal domains of *Sa*OatA. Supporting this was the discovery that *S. aureus*-*S. pneumoniae* chimeric OatA variants were nonfunctional in *S. aureus* USA300 Δ*oatA* (Figure 4.12). Although the lack of function of the chimeras could be due to various reasons, the results do not contradict the notion of direct transfer. Theoretically, if a universal intermediate existed to shuttle acetyl groups between the two domains, the N-terminal domain of *S. pneumoniae* might be able to compensate for the N-terminal domain of *S. aureus*. Given that the domains likely need to be able to directly interact, the chimeras may not have been able to coordinate their activities due to incompatible structures and sequences that precluded proper interactions.

Given the proposed location of Tyr206 in a short extracytoplasmic loop and the evidence of direct transfer, I hypothesize that acetylated Tyr206 serves as the acetyl donor for *Sa*OatA$_C$. This was tested using short acetylated peptides based on the Tyr206-loop between TMS 6 and 7 (Figure 4.14). *Sa*OatA$_C$ was capable of using both *O*-acetyl-Tyr and short peptides with *O*-acetyl-Tyr as acetyl donors. The specific activity of the enzyme using these acetyl donors increased with increasing peptide length. Furthermore, *Sa*OatA$_C$ was most active with the acetylated peptide with the sequence matching that found in the Tyr206 loop. This suggests that *Sa*OatA$_C$ has specificity for the acetylated peptide donor and the Tyr206 loop may be preferred, supporting the hypothesis. The sequence of the analogous loop from *S. pneumoniae* OatA may not be recognized by the C-terminal domain of *S. aureus* OatA, which may explain the inactivity of the *Sp*OatA$_N$-*Sa*OatA$_C$ chimera.

The data presented here support a model in which Arg25, Arg83, and Arg86 at the cytoplasmic face of the membrane bind and orient the acetyl group of acetyl-CoA, the presumed donor, toward the catalytic centre. The helices of *Sa*OatA$_N$ likely form a tunnel into which the pantothenate group is inserted. I hypothesize that the acetyl group is removed from acetyl-CoA by either a catalytic triad or a catalytic diad. In the catalytic triad model, I propose Glu154 and His36 would activate Tyr206 on the short external loop that links TMS6 and TMS7 through acid/base chemistry allowing Tyr206 to attack acetyl-CoA and form a covalent acetyl-Tyr intermediate (Figure 4.16A). Given the location of Tyr206 in an external loop, such a reaction would require some flexibility in Tyr206 to be able to interact with acetyl-CoA on one side and then be exposed externally to the C-terminal

domain. Alternatively, Glu154 and His36, which are both transmembrane, may form a catalytic diad wherein an acetyl-intermediate is formed on His36 (Figure 4.16B). The acetyl group may then migrate from His36 to Tyr206. Spontaneous migration of acetyl groups between hydroxyl groups of sialic acids is known to occur (Kamerling et al., 1987) and may occur here. In both cases, I propose *Sa*OatA$_C$ removes the acetyl group from Tyr206 and transfers it onto PG. Several other residues identified as important for function, including Phe52, Ser56, Asn126, Tyr136, Trp149, Tyr311, Tyr314, and Glu357, may play peripheral roles in substrate binding, and/or protein stability.

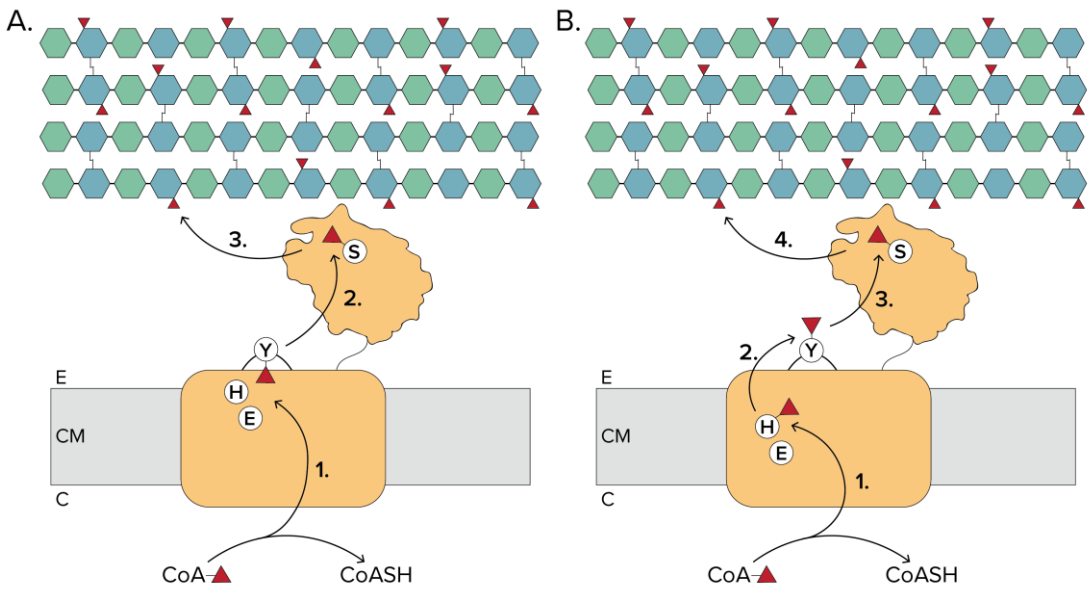

Figure 4.16 Proposed catalytic mechanism of the N-terminal domain of *S. aureus* OatA. Given the experimental data, two models are proposed for the transfer of acetyl groups from the cytoplasm to PG. In the first model (A), the N-terminal domain employs a catalytic triad of Glu154, His36, and Tyr206, with an acetyl-intermediate forming on Tyr206 in an exposed loop (1). *Sa*OatA$_C$ then removes the acetyl group from Tyr206, forming an acetyl-intermediate on Ser453 (2), and transferring the acetyl group onto PG (3). In the second model (B) the N-terminal domain employs a catalytic diad of Glu154 and His36 with an acetyl-intermediate forming of His36 (1). The acetyl group then migrates, spontaneously or with assistance, to Tyr206 (2), where it is presented to *Sa*OatA$_C$ for removal, forming an acetyl-intermediate on Ser453 (3). *Sa*OatA$_C$ then completes the transfer onto PG (4). E, external; CM, cytoplasmic membrane; C, cytoplasm.

This study presents some of the first biochemical data for an acyltransferase 3 family enzyme. Whilst the mechanism of action is still theoretical, these findings can form the basis for studies of acyltransferase 3 enzymes with a large array of roles. Furthermore,

the interaction between the two domains of *Sa*OatA was elucidated, which may have implications in the selection and designing of inhibitors to block PG O-acetylation.

Chapter 5: Structural basis for the function of the extracytoplasmic domain of OatA from *S. aureus* as an *O*-acetyltransferase

5.1 Statement of contributions

Dr. Anthony J. Clarke and I conceived the study. I performed all the experiments, with the assistance of Dr. David Sychantha for screening crystals of *Sa*OatA$_C$ for X-ray diffraction and the analysis and interpretation of X-ray data. Mass-spectrometry and DNA sequencing was performed by the Advanced Analysis Centre at the University of Guelph. Technical assistance was provided by Bryan Fraser. A.J.C., D.S., and I analyzed and interpreted the data.

5.2 Overview

The purpose of this study was to investigate the structure and function of the C-terminal domain of *S. aureus* OatA (*Sa*OatA$_C$). Although the structure of the C-terminal domain of *S. pneumoniae* OatA has been solved by X-ray crystallography, *S. aureus* and *S. pneumoniae* OatA only share 27% sequence identity. Furthermore, these homologues display differences in substrate specificity (Sychantha et al., 2017) and indeed may be phylogenetically distinct (Bernard et al., 2011). This underscores the importance of investigating both *S. aureus* and *S. pneumoniae* OatA, particularly in the context of designing inhibitors for *Sa*OatA to tackle MRSA infections. However, previous efforts to crystallize the engineered extra-cytoplasmic domain of *S. aureus* OatA (residues 445 to 601) were unsuccessful. In this study, surface entropy reduction was employed to produce crystals of *Sa*OatA$_C$ and the structure was solved by X-ray crystallography. The active site was investigated, and a model is presented for the function of *Sa*OatA$_C$ as a transferase. A structure of *Sa*OatA$_C$ and an understanding of the catalytic mechanism will be invaluable for structure aided drug-design of lead compounds for novel antimicrobials. In addition, this study provides insight into the mechanistic differences between SGNH esterases and transferases.

5.3 Results

5.3.1 Crystallization and structure determination of *Sa*OatA$_C$

Efforts to crystallize the engineered extra-cytoplasmic domain of *S. aureus* OatA, encompassing residues 445 to 601 (*Sa*OatA$_C$), were unsuccessful, despite the removal of potentially disordered regions that could hinder crystallization. This included significant

truncation of the N-terminal interdomain-linker regions and two C-terminal lysine residues. To find additional areas of disorder, we analyzed the amino acid sequence of *Sa*OatA$_C$ and found that it was enriched with residues of high conformational freedom (9.6% Lys and 5.1% Glu). Therefore, we used surface entropy reduction (SER) (Goldschmidt et al., 2007) in an effort to reduce surface disorder and promote crystallization of the domain. Three clusters of predicted high entropy surface residues, Lys464 and Lys465, Lys495 and Lys496, and Glu551 and Lys552, were identified using the SERp server (Goldschmidt et al., 2007). Each residue in these cluster pairs was replaced with alanine residues to produce three new constructs for crystallization. The specific activities of the resultant *Sa*OatA$_C$ variants were similar to wild-type enzyme (Table 5.1) and all three variants crystallized.

(E551A/K552A)-*Sa*OatA$_C$ crystallized only in the presence of zinc salts, so it was suspected that Zn^{2+} ions were bound to the protein and well ordered. Indeed, an anomalous signal was detected from protein-bound zinc and this signal was sufficient for phase determination. Consequently, the structure was solved using zinc single-wavelength anomalous dispersion (Zn-SAD) (Table 5.2). (E551A/K552A)-*Sa*OatA$_C$ crystallized as a dimer in the asymmetric unit and contained three Zn^{2+}ions coordinated by the putative catalytic His and Asp residues at the dimer interface. We presume that these protein-bound Zn^{2+} ions are not biochemically relevant as they appear to distort the active site. This is supported by the observation that zinc, amongst other first-row transition metal cations, inhibits *Sa*OatA catalysis *in vitro* (Kell, 2015). Diffraction data were therefore collected for a crystal of (K495A/K496A)-*Sa*OatA$_C$ that grew in the absence of zinc, and the structure was solved by molecular replacement using the (E551A/K552A)-*Sa*OatA$_C$ structure as a search model. This structure was determined to 1.71 Å resolution and refined to R_{work}/R_{free} values of 16.6%/19.6% (Table 5.2).

The overall structure of *Sa*OatA$_C$ adopts an atypical α/β-hydrolase fold with five parallel β-strands sandwiched between 7 α-helices (Figure 5.1). The asymmetric unit contains two molecules of the protein, however size-exclusion chromatography revealed that *Sa*OatA$_C$ is monomeric and thus the dimeric configuration and interface seen in the crystal is likely not physiologically relevant. A sodium ion was seen in the bend of α-helix 4 and β-strand 5, coordinated by three water molecules and the backbone carbonyl oxygens

Table 5.1 Specific activities of *Sa*OatA$_C$ variants

Enzyme variant	Esterase activity[1]		Transferase activity[2]		MIC with lysozyme[3] (mg/mL)	Tm[4] (°C)
	Specific activity (nmol•min^{-1}•mg^{-1})	Relative activity (%)	Specific activity (nmol•min^{-1}•mg^{-1})	Relative activity (%)		
WT	6.78 ± 0.13	100%	-	-	-	-
K464A/K465A	7.18 ± 0.090	106%	-	-	-	-
K495A/K496A	7.70 ± 0.042	114%	-	-	-	57.35 ± 0.163
E551A/K552A	7.83 ± 0.057	115%	-	-	-	-
WT	4.88 ± 0.15	100%	0.49 ± 0.19	100%	>4	59.49 ± 0.025
S453A	N.D.	0%	-	-	0.5	54.83 ± 0.233
H578A	0.12 ± 0.0034	2.08%	-	-	0.5	56.96 ± 0.086
D575A	0.06 ± 0.0033	1.06%	-	-	0.5	51.30 ± 0.234
N507A	N.D.	0%	-	-	0.5	51.26 ± 0.053
V475G	N.D.	0%	-	-	2	51.32 ± 0.057
D457A	18.5 ± 0.20	392%	4.25 ± 0.73	866%	>4	57.77 ± 0.310
D457N	18.1 ± 0.18	385%	3.25 ± 0.80	662%	>4	57.59 ± 0.376

1. Tested *in vitro* with purified *Sa*OatA$_C$. Reactions were conducted at 25ºC with 0.1 mM 4MU-Ac as substrate in 50 mM sodium phosphate pH 7.0 for upper block, and pH 6.5 for lower block.
2. Tested *in vitro* with purified *Sa*OatA$_C$. Reactions were conducted in 50 mM sodium phosphate pH 7.0 at 37 ºC with 0.1 mM 4MU-Ac and 2 mM pentaacetyl-chitopentaose
3. Tested *in vivo* with full length *Sa*OatA expressed in *S. aureus* USA300 Δ*oatA*.
4. Tm values were determined for purified *Sa*OatA$_C$ using the thermal shift assay with SYPRO Orange.
'±' denotes standard deviation (n=3); N.D. = no detectable activity; '-' not tested

Table 5.2 Summary of data collection and refinement statistics

	(K495A/K496A)-*Sa*OatA$_C$	(E551A/K552A)-*Sa*OatA$_C$
Data collection		
Beamline	NSLS-II 17-ID2	CLS 08B1-1
Wavelength (Å)	0.99961	1.28167
Space group	*P* 2_1	*P* 2_1 2_1 2_1
Unit cell parameters (Å)	*a* = 42.35	*a* = 39.51
	b = 61.30	*b* = 78.86
	c = 67.69	*c* = 106.59
	$\alpha = \gamma = 90.00^o$	$\alpha = \gamma = \beta = 90.00^o$
	$\beta = 100.90^o$	
Resolution range (last shell) (Å)	28.78 – 1.71 (1.77 – 1.71)	44.16 – 1.55 (1.61-1.55)
Total no. reflections (last shell)	71747 (6748)	574457 (19959)
No. unique reflections (last shell)	36587 (3545)	46179 (2983)
Redundancy (last shell)	1.96 (1.90)	12.43 (6.69
Completeness (last shell) (%)	99.36 (96.12)	93.85 (68.8)
Average $I/\sigma I$ (last shell)	17.32 (1.97)	17.53 (4.11)
R_{merge} (last shell) (%)[1]	0.02392 (0.4006)	0.09615 (0.3412)
$CC_{1/2}$ (last shell)[2]	0.999 (0.633)	0.997 (0.97)
Refinement		
R_{work}/R_{free}[3]	0.166 / 0.196	0.1720 / 0.1923
No. atoms	2693	2840
Protein	2423	2450
Water	268	389
Ligand	2	3
Average *B*-factor (Å)	31.84	24.82
Protein	30.74	23.41
Water	41.88	33.73
Ligand	26.85	18.46
RMS Bond lengths (Å)	0.007	0.005
RMS Bond Angles (°)	0.82	0.73
Ramachandran total favoured (%)	99.01	98.04
Ramachandran total allowed (%)	0.99	1.96
PDB entry	6VJP	6WN9

1. $R_{merge} = \Sigma_{hkl} \Sigma_i |(I_i(hkl) - \langle I(hkl)\rangle|/\Sigma_{hkl} \Sigma_i I_i(hkl)$ where I is the intensity of the reflection hkl, Σ_{hkl} is the sum over all reflections and Σ_i is the sum over i measurements of reflection hkl. $\langle I(hkl)\rangle$ is the mean value of $I(hkl)$.

2. $CC_{1/2}$ is the Pearson correlation coefficient calculated between two random half data sets. $CC = \Sigma(x - \langle x\rangle)(y - \langle y\rangle)/[\Sigma(x - \langle x\rangle)^2\Sigma(y - \langle y\rangle)^2]^{1/2}$

3. $R_{work} = \Sigma_{hkl} |F_{obs} - F_{calc}|/\Sigma_{hkl} |F_{obs}|$ where F_{obs} and F_{calc} are the observed and calculated structure factors, respectively. R_{free} was calculated identically except that all reflections belonged to a test set consisting of only 5% of the data, chosen at random.

of Ala550, Arg553, and Val556. The putative catalytic triad Ser-His-Asp residues align within a shallow active site on the surface of the protein. In chain B, the catalytic His578 is found in two conformations, facing both towards and away from the active site (occupancies of 0.54 and 0.46, respectively), suggesting that His578 is inherently flexible (Figure 5.2A).

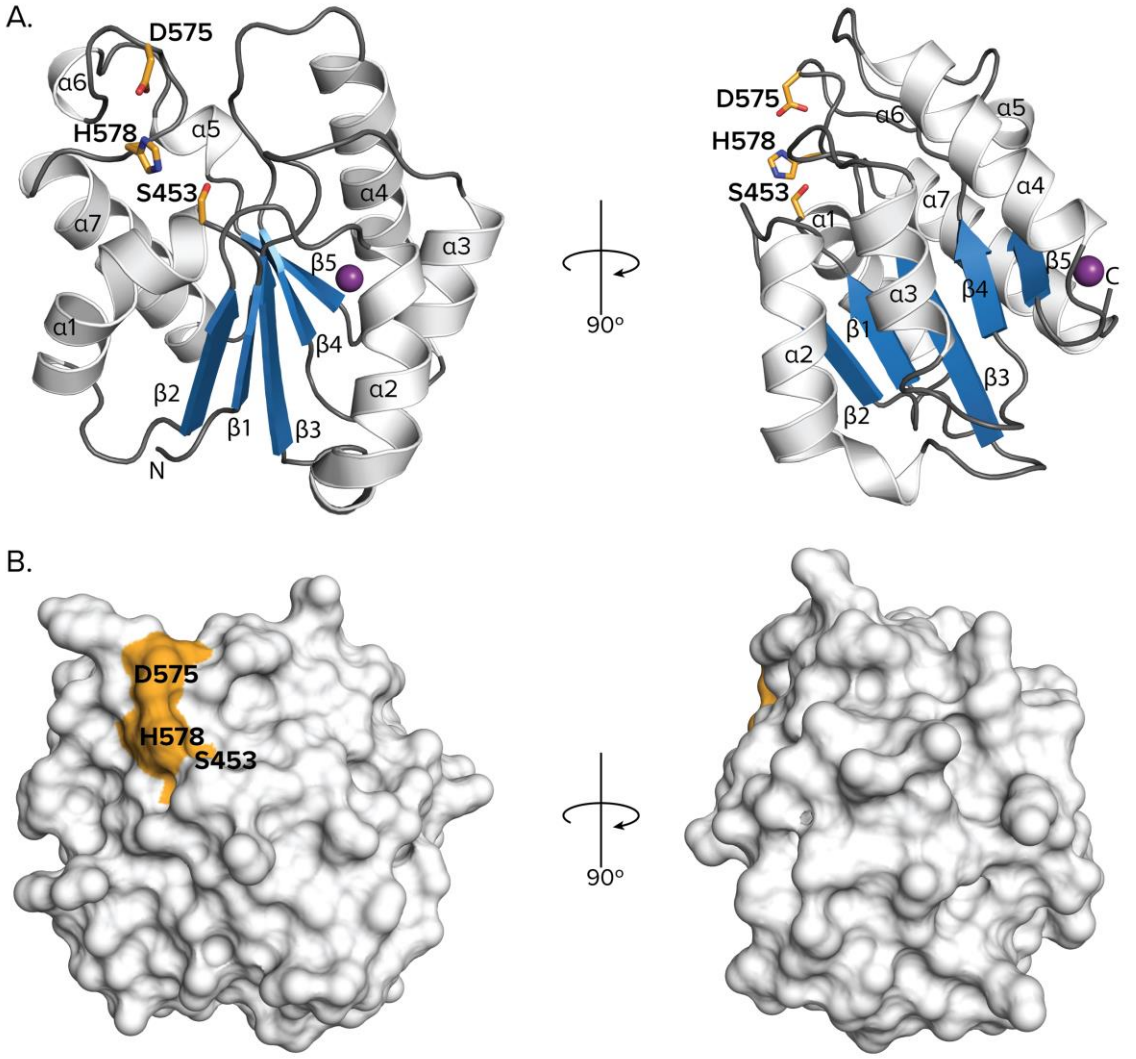

Figure 5.1 Structure of *Sa*OatA$_C$. A. Cartoon representation of *Sa*OatA$_C$ showing 7 α-helices (white) and 5 β-sheets (blue) arranged in an α/β-hydrolase fold. The putative catalytic triad residues are illustrated in orange sticks. The sodium atom located between α-helix 4 and β-sheet 5 is indicated by a purple sphere. B. Surface representation of *Sa*OatA$_C$ showing the putative catalytic triad residues in orange in a shallow active site pocket.

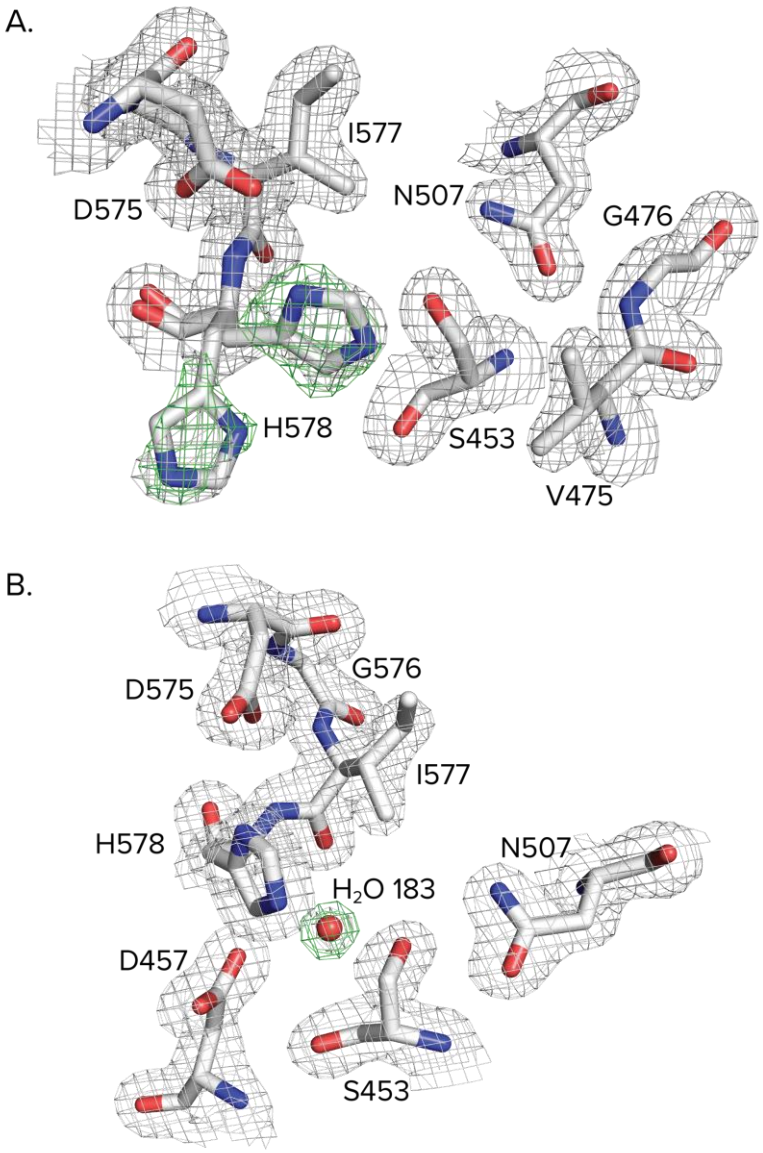

Figure 5.2 Electron density maps of *Sa*OatA$_C$ active site. A. The catalytic His578 adopts two conformations in chain B of the structure, both facing the active site and facing away. The 2mF_o-DF_c map of the active site of *Sa*OatA$_C$ chain B (gray) is contoured at 1.0 σ. The mF_o-DF_c omit map of His578 (green) is contoured at 3.0 σ. B. A water molecule (H_2O 183) was seen in the active site of *Sa*OatA$_C$ in both chains A and B. The 2mF_o-DF_c map of the active site of *Sa*OatA$_C$ chain A (gray) is contoured at 1.0 σ. The mF_o-DF_c omit map of H_2O 183 (green) is contoured at 3.0 σ.

Searching for structural homologues with DALI revealed, that *Sa*OatA$_C$ most closely resembles the C-terminal domain of OatA from *S. pneumoniae* (*Sp*OatA$_C$) (PDB ID: 5UFY, RMSD: 1.8 Å over 179 equivalent Cα's, z-score: 19.9, 27% sequence identity) (Figure 5.3A). The *Sa*OatA$_C$ structure is also homologous to numerous uncharacterized

proteins proposed to belong to the SGNH/GDSL hydrolase family. Of the characterized proteins in the PDB database, aside from *Sp*OatA$_C$, *Sa*OatA$_C$ most closely resembles Axe2, an acetylxylan esterase from *Geobacillus stearothermophilus* (PDB ID: 4JHL, RMSD: 2.2 Å over 146 equivalent Cα's, z-score: 16.5, 18% sequence identity), a family 3 carbohydrate esterase from *Clostridium thermocellum* (PDB ID: 2VPT, RMSD: 2.2 Å over 147 equivalent Cα's, z-score: 16.7, 14% sequence identity), and a family 3 carbohydrate esterase from *Talaromyces cellulolyticus* (PDB ID: 5B5S, RMSD: 2.2 Å over 149 equivalent Cα's, z-score: 16.4, 17% sequence identity) (Figure 5.3A).

5.3.2 *Sa*OatA$_C$ uses a Ser-His-Asp catalytic triad

SGNH hydrolases are characterized by four consensus sequence blocks (I, II, III, and V) containing conserved residues, Ser, Gly, Asn, and His, that give this family of enzymes their name (Akoh et al., 2004). Most SGNH hydrolases possess a catalytic triad consisting of a Ser from block I, and both an Asp and His from block V. In *Sa*OatA$_C$, the putative catalytic triad residues, Ser453, His578, and Asp575, were previously replaced with Ala in a longer construct of the enzyme (*Sa*OatA$_{435\text{-}603}$) and assayed for activity using *p*-nitrophenyl-acetate (*p*NP-Ac) (Sychantha et al., 2017). These experiments were repeated using the new construct with 4-methylumbelliferyl-acetate (4MU-Ac) as substrate. The (S453A)-*Sa*OatA$_C$ variant had no detectable activity, whereas the (H578A)- and (D575A)-variants had 2.08% and 1.02% residual esterase activity, respectively (Table 5.1). The stability of all *Sa*OatA$_C$ variants was verified by a thermal shift assay after purification.

As seen previously, wild-type *Sa*OatA$_C$ displays very limited transferase activity towards chito-oligosaccharides as acceptors (Sychantha et al., 2017) and, as such, it was not possible to determine rates of transfer for *Sa*OatA$_C$ variants. A qualitative analysis of any reaction products by liquid chromatography-mass spectrometry (LC-MS) demonstrated that the truncated wild-type *Sa*OatA$_C$ retained transferase activity (Figure 5.4), however, the sensitivity of the assay is not sufficient to discriminate between no transfer and limited transfer that may be seen with weakly active *Sa*OatA$_C$ variants. In order to indirectly assess transferase ability, the functional complementation assay was used, as described previously (section 4.3.3). Each single amino acid replacement was generated in the full length *Sa*OatA construct, expressed in *S. aureus* USA300 Δ*oatA* and

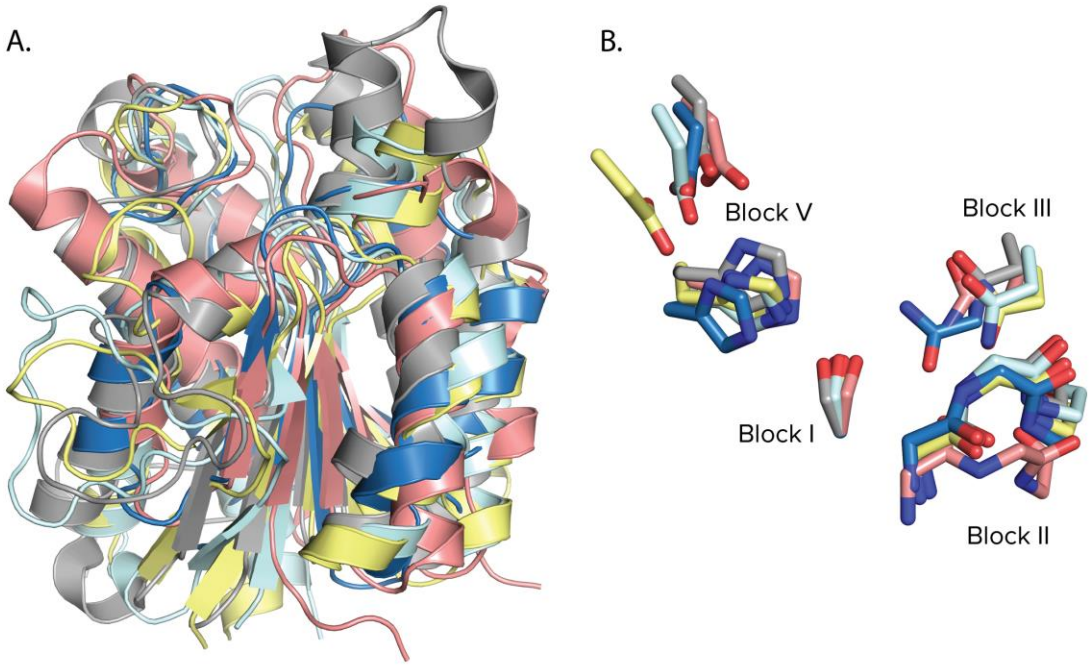

C.

	Block I	Block II	Block III	Block V
*Sa*OatA	LIGDSVMVD	KVGRQL	LGTNG	AYDGIHLE
*Sp*OatA	LIGDSVALR	QVSVTT	TGVND	GTDQVHFG
*Gs*Axe2	FIGDSITDC	ISGNTV	IGIND	AWDRVHPS
*Ct*Ces3	PVGDSCTEG	HSGWTI	IGGND	SWDGLHLS
*Tc*Ces3	LLGDSITEI	HSGWQA	LGTND	RDDGVHPN

Figure 5.3 Structural comparison of *Sa*OatA$_C$ to SGNH/GDSL hydrolase structural homologues. A. Cartoon representation of *Sa*OatA$_C$ (dark blue; PDB ID: 6VJP) overlayed with *Sp*OatA$_C$ (pink; PDB ID: 5UFY), Axe2 from *Geobacillus stearothermophilus* (*Gs*Axe2; gray; PDB ID: 4JHL), family 3 carbohydrate esterase from *Clostridium thermocellum* (*Ct*Ces3; yellow; PDB ID: 2VPT), family 3 carbohydrate esterase from *Talaromyces cellulolyticus* (*Tc*Ces3; pale blue; PDB ID: 5B5S). B. Alignment of the conserved SGNH hydrolase block residues from the aforementioned structural homologues. C. Block alignments comparing *Sa*OatA, *Sp*OatA and SGNH hydrolase structural homologs. Catalytic triad and oxyanion hole residues are in red and blue, respectively, while the highly conserved Asp present in most OatA sequences except those of the streptococci node is in green.

the MIC with lysozyme was determined in the presence of 0.4 µg/mL tunicamycin. *S. aureus* USA300 Δ*oatA* expressing (S453A)-, (H578A)-, and (D575A)-*Sa*OatA had MICs of 0.5 mg/mL with lysozyme, as seen with the *oatA* knockout strain, demonstrating insufficient PG O-acetylation for lysozyme resistance.

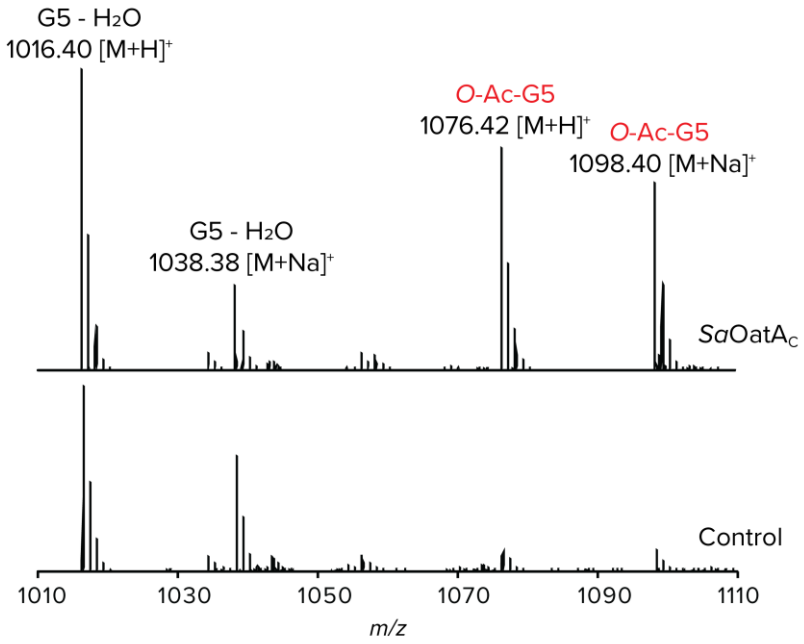

Figure 5.4. *Sa*OatA$_C$-catalyzed *O*-acetyltransferase reactions with pentaacetyl-chitopentaose acceptor. QTOF-MS analysis of reaction products of 1 mM pentaacetyl-chitopentaose (G5) in 50 mM sodium phosphate pH 6.5 incubated at 37 ºC for 18 hr with 0.1 mM 4MU-Ac in the absence (control) and presence of 5 µM *Sa*OatA$_C$.

The most prominent difference between *Sa*OatA$_C$ and its structural homologues is the geometry of the putative catalytic triad. The distances between the Nδ1 of His578 and the Oδ2 of Asp575, and the Nε2 of His578 and the Oγ of Ser453 are 3.2 Å and 4.5 Å, respectively, which are significantly longer than in homologues (Figure 5.3B). However, in the absence of a bound ligand, the crystal structure of *Sa*OatA$_C$ could represent the resting state of the enzyme and not the active conformation. Indeed, the dual conformations of His578 seen in chain B of the crystal structure, suggests that His578 is flexible, and the active site may undergo conformational changes during catalysis (Figure 5.2A). Such conformational changes have been reported previously for *Sp*OatA$_C$ and the PG esterase Ape1 (Sychantha et al., 2017; Williams et al., 2014).

Most SGNH hydrolases employ a double-displacement reaction mechanism involving a covalent acyl-enzyme intermediate at the catalytic serine residue. Indeed, this reaction mechanism was recently confirmed for *Sp*OatA$_C$ (Sychantha and Clarke, 2018). A similar strategy was employed to unambiguously assign the role of the putative catalytic Ser453. An accumulation of acetyl-*Sa*OatA$_C$ intermediate was observed by real-time

analysis of a reaction with *p*NP-Ac as acetyl donor using LC-MS (Figure 5.5A). *Sa*OatA$_C$ had a resting *m/z* value of 17562. After incubation with *p*NP-Ac for 15 min, the appearance of a new ion was observed with an *m/z* value of 17604, an *m/z* difference of 42, consistent with the addition of an acetyl group. To identify the acetylated amino acid, an identical reaction mixture was quenched with acetone after 30 min incubation and the recovered enzyme was digested with trypsin. The resulting peptides were separated by LC-MS/MS. A pair of peptides was observed with *m/z* values of 1117.59 and 1138.59, a *m/z* difference of 42. The mass and fragmentation patterns of these parent ions correspond well with the native and acetylated forms, respectively, of the peptide ^{442}AASSPLIGD**S**VMVDIGNVFTK^{464} (Ser453 underlined) (Figure 5.5B). Based on the MS/MS fragmentation pattern of the *m/z* 1138.59 parent ion, the acetyl modification was mapped to Ser453. This *m/z* 1138.59 ion was not detected amongst the digestion products of the no-substrate control reaction.

5.3.3 *Sa*OatA$_C$ possesses a typical three-component oxyanion hole

In most SGNH hydrolases, the oxyanion hole is typically formed by three conserved hydrogen-bond donors: the backbone amide of the catalytic Ser of the block I consensus sequence, the backbone amide of Gly from block II, and the sidechain amide of Asn from block III. In *Sp*OatA$_C$, the block II Gly is replaced by a Ser and the loop adopts a type I β-turn. In contrast, *Sa*OatA$_C$ retains the Gly and the loop adopts the typical type II β-turn seen in homologous SGNH esterases. The backbone amide of Gly476 faces the active site and thus likely participates in stabilizing the transition state (Figure 5.6). Interestingly, the Nδ2 of block III Asn507 is only 2.9 Å away from the Oγ of Ser453, significantly closer than typically seen in other SGNH hydrolases. The importance of Asn507 in catalysis was tested by its replacement with Ala. The (N507A)-*Sa*OatA$_C$ variant had no detectable esterase activity towards 4MU-Ac, suggesting an important role in the catalytic mechanism (Table 5.1). As with the catalytic triad residues, *S. aureus* USA300 Δ*oatA* expressing (N507A)-*Sa*OatA had an MIC of 0.5 mg/mL with lysozyme.

Sychantha *et al*. (2017) also proposed the importance of a (V/I)(G/S)(R/V) motif in the block II loop. In the resting-state structure of *Sp*OatA$_C$, a water molecule was observed coordinated by the backbone carbonyl of Val460 and the backbone carbonyl of Val462 (equivalent residues Val475 and Arg477 in *Sa*OatA$_C$). In contrast, due to the opposite turn

A.

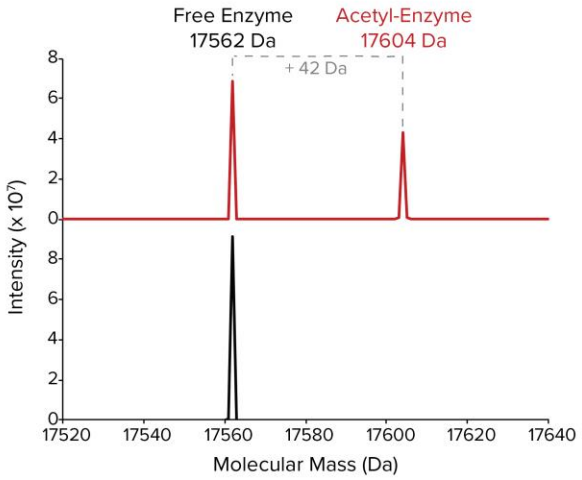

B.

Residue		[M+H]⁺		[M+H]⁺
A	b1	72.044	y22	2276.17
A	b2	143.08	y21	2205.14
S	b3	230.11	y20	2134.10
S	b4	317.14	y19	2047.07
P	b5	414.20	y18	1960.04
L	b6	527.28	y17	1862.98
L	b7	640.37	y16	1749.90
I	b8	753.45	y15	1636.81
G	b9	810.47	y14	1523.73
D	b10	925.50	y13	1466.71
S	b11	1054.53	y12	1351.68
V	b12	1153.60	y11	1222.65
M	b13	1284.64	y10	1123.58
V	b14	1383.71	y9	992.54
D	b15	1498.74	y8	893.47
I	b16	1611.82	y7	778.44
G	b17	1668.84	y6	665.36
N	b18	1782.88	y5	608.34
V	b19	1881.95	y4	494.30
F	b20	2029.02	y3	395.23
T	b21	2130.07	y2	248.16
K	b22	2258.16	y1	147.11

Figure 5.5 Direct observation of the acetyl-*Sa*OatA$_C$ intermediate. A. *Sa*OatA$_C$ was incubated with 1 mM *p*NP-Ac (red) or no substrate (black) and separated via reverse-phase LC-MS. The resulting mass spectra show the appearance of a peak with a mass increase of 42 Da after incubation with *p*NP-Ac, consistent with the formation of a covalent acetyl-enzyme intermediate. B. Table showing the expected and observed ions for the fragmentation of an ion from a trypsin-digested reaction of *Sa*OatA$_C$ with *p*NP-Ac. A reaction of *Sa*OatA$_C$ with 1 mM *p*NP-Ac was quenched by the addition of cold acetone. The recovered protein was digested with trypsin and the resultant peptides were separated by LC-MS/MS. The parent ion had an *m/z* of 1138.7, corresponding to the amino acid sequence shown. The fragmentation pattern was consistent with the acetylation of Ser 453 (shown in red). Observed ions are noted in green or blue.

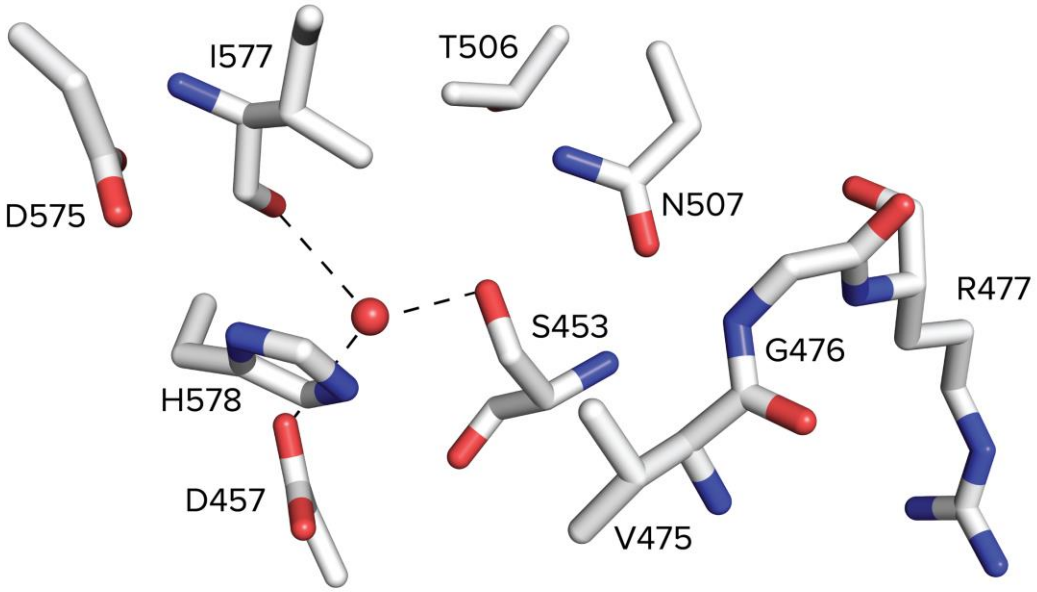

Figure 5.6 The active site of *Sa*OatA$_C$. A water molecule (red sphere) can be seen coordinated by the Oδ1 of Asp457, the backbone carbonyl of Ile577, and the Oγ of the catalytic Ser453

of the block II loop in *Sa*OatA$_C$, the carbonyl of Val475 does not face the active site and no water molecule is seen coordinated at the active site in this position (Figure 5.6). Nonetheless, Val475 is highly conserved amongst OatA homologues and in accordance, Val475 was replaced with Gly and complete abolishment of esterase activity was observed (Table 5.1). Interestingly, *S. aureus* USA300 Δ*oatA* expressing (V475G)-*Sa*OatA had an MIC of 2 mg/mL with lysozyme. This suggests moderate PG O-acetylation was occurring and that despite a complete loss of esterase activity, replacement of Val475 with Gly still permits transfer to PG.

5.3.4 Conserved Asp457 limits esterase activity

A water molecule was observed in the active site of *Sa*OatA$_C$ (H_2O 183; occupancy: 1.00; b-factor: 35.59) (Figure 5.2B). This water molecule was coordinated by the Oδ1 of Asp457, the backbone carbonyl of Ile577, and the Oγ of the catalytic Ser453 and was not present in any of the structural esterase homologues, or *Sp*OatA$_C$ (Figure 5.6). To investigate the role of the water molecule, Asp457 was substituted with Ala, and Asn. Surprisingly, the D457A and D457N variants of *Sa*OatA$_C$ displayed a 4-fold increase in esterase activity, but still maintained the ability to transfer to chito-oligosaccharides

(Table 5.1). Similarly, *S. aureus* USA300 Δ*oatA* expressing (D457A)- and (D457N)-*Sa*OatA had no measurable MIC with lysozyme, as seen with wild-type enzyme. To investigate the prevalence of an Asp at this position in SGNH hydrolases/transferases, sequences were analyzed from 200 known and hypothetical OatA homologues from Gram-positive bacteria and characterized esterases from the SGNH hydrolase family. Asp at equivalent position 457 (catalytic Ser +4) is highly conserved in OatA homologues from the *Staphyloccocus*, *Bacillus*, *Listeria*, and *Lactobacillus* genera, among others (Figure 5.7). In contrast, an Asp residue was not found at this position in any of the characterized SGNH hydrolases that act as esterases (Figure 5.3C). In most OatA homologues from *Streptococcus* species, an Arg residue is found (Figure 5.7). We propose that Asp457 is a conserved feature in many SGNH family transferases and serves to limit esterase activity through the coordination of a water molecule. This coordinated water may guard against water entering the active site to hydrolyze the acetyl-enzyme, thereby minimizing loss of acetyl groups to the environment.

5.4 Discussion

OatA belongs to the SGNH hydrolase family of enzymes along with numerous esterases with a wide range of substrate specificities. The mechanism by which OatA acts as a transferase was widely unknown until recently. The structure of *Sp*OatA$_C$ elucidated structural features that distinguished it from SGNH hydrolase family esterases, including an inverted turn of the block II loop, a conserved valine in block II, a hydrophobic active site wall, and an atypical two-residue oxyanion hole. Interestingly, the active site of *Sa*OatA$_C$ more closely resembles that of structurally homologous esterases than that of *Sp*OatA$_C$ (Figure 5.3B). *Sa*OatA$_C$ has the conserved Gly in block II and the loop adopts the typical type II β-turn seen in the homologous esterases. As a consequence, the water molecule that is coordinated by the backbone of Val460 in the block II sequence of *Sp*OatA$_C$ in the resting state is not seen in the structure of *Sa*OatA$_C$. Furthermore, replacement of Val460 of *Sp*OatA$_C$ with Gly increases esterase activity whilst resulting in loss of transferase activity. In contrast, a comparative replacement of homologous Val475 in *Sa*OatA$_C$ resulted in complete loss of esterase activity but transfer was still observed (Table 5.1). Given that the esterase assay is performed on isolated C-terminal domain, it is possible that replacement of Val475 with Gly compromised the stability or proper folding

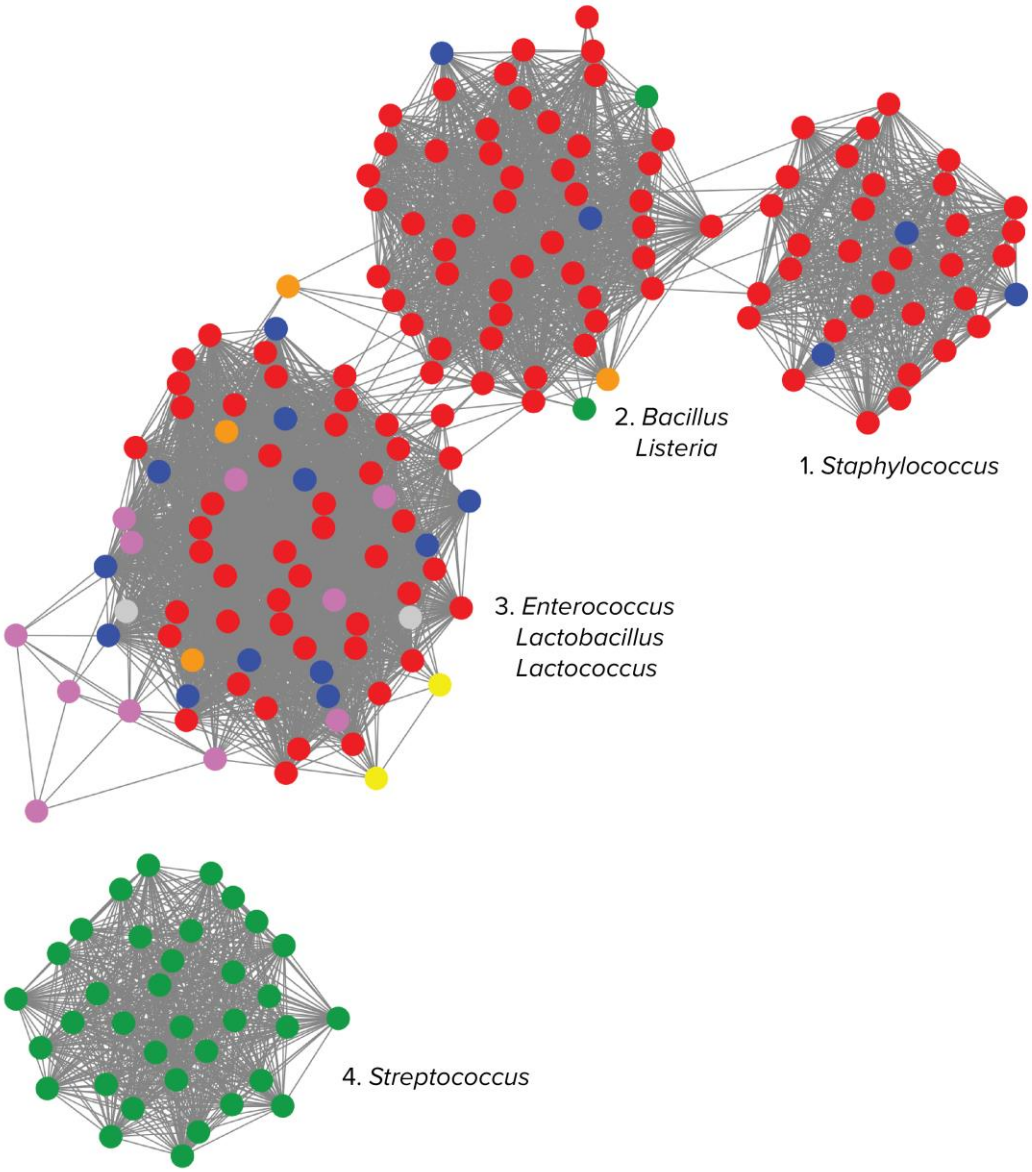

Figure 5.7 Sequence similarity network of OatA homologues. A sequence similarity network was generated for 200 OatA sequences from Gram-positive bacteria using the EFI Enzyme Similarity Tool (Gerlt et al., 2015). Each node represents a single protein connected by edges representing an alignment score of at least 128. Nodes are coloured by the identity of the amino acid found 4 residues following the catalytic Ser in block I, equivalent to position 457 in *Sa*OatA. Red, Asp; blue, Gly; green, Arg; orange, Ser; pink, Ala; grey, Asn; yellow, Met. The predominant genera found in each cluster is listed. The SSN was visualized using Cytoscape 3.6.1. Species names and accession numbers for included sequences are given in Appendix 4.

of the enzyme and that such a replacement in the context of the cell, where OatA interacts with other proteins, may be less critical. Hence, the isolated C-terminal domain with Val475 replaced with Gly was unable to turnover substrate, however, the full-length protein with the same replacement was still capable of maintaining some levels of activity. In the thermal shift assay, (V475G)-*Sa*OatA$_C$ had a Tm of ~8ºC lower than that of wild-type enzyme. Whilst, a Tm above 50ºC shows the enzyme is still folded under assay conditions, the decrease from wild-type enzyme does suggest that structural stability may have been reduced.

A thorough kinetic analysis of *Sp*OatA$_C$ confirmed that the enzyme employs a double-displacement reaction mechanism (Sychantha and Clarke, 2018). Accordingly, we propose that *Sa*OatA$_C$ follows a similar reaction mechanism, wherein the carboxyl group Asp575 forms a salt bridge with a nitrogen atom in the imidazole ring of His578, enabling His578 to deprotonate Ser453. Nucleophilic Ser453 attacks the carbonyl carbon of the acetyl donor, generating a tetrahedral transition state. Residues at the active centre of the enzyme form an oxyanion hole that stabilizes the transition state, which then collapses into a covalently-bound acetyl-enzyme intermediate. In this study, Ser453 of *Sa*OatA$_C$ was unequivocally identified as the site of acetylation (Figure 5.5). The acetyl donor is released upon acquisition of a proton from His578. The glycan accepter, a MurNAc residue of the PG backbone, can then bind the active site cleft. Through acid/base catalysis, His578 abstracts a proton from the C6-OH of MurNAc, rendering the carbon atom nucleophilic and resulting in its attack on the carbonyl centre of the acetyl-Ser453 intermediate. This leads to the formation of a second tetrahedral transition state, collapse of which results in the release of the O-acetylated product and free enzyme.

I propose that the putative transition state generated during the enzyme's reaction mechanism is stabilized by the backbone amide of Ser453 in block I, the sidechain amide of Asn507 in block III, and the backbone amide of Gly476 in block II. The three-residue oxyanion hole is typical of SGNH hydrolases, but distinguishes *Sa*OatA$_C$ from *Sp*OatA$_C$, which appears to employ an oxyanion hole formed of only two residues (Sychantha and Clarke, 2018). Replacement of the *Sp*OatA$_C$ block III Asn491 with Ala gave 58% residual esterase activity (Sychantha et al., 2017). Further kinetic analysis suggested that Asn491 may play a larger role in substrate binding than in stabilization of the first transition state

(Sychantha and Clarke, 2018). In contrast, replacement of Asn507 of *Sa*OatA$_C$ with Ala resulted in a complete loss of activity, suggesting this residue may play a more critical role in *Sa*OatA$_C$ (Table 5.1). Absolute identification of oxyanion hole H-donors would require analysis of a ligand-bound structure, ideally with a covalently bound transition-state mimic. Such a structure was achieved for *Sp*OatA$_C$ using the mechanistic inhibitor methanesulfonyl fluoride (MSF), forming a methylsulfonyl-adduct structure (PDB ID: 5UG1) (Sychantha et al., 2017). Unfortunately, MSF and related analogs do not significantly inhibit *Sa*OatA$_C$, thus a different transition state mimic will need to be found.

Bioinformatic analysis shows that OatA homologues form two distinct clades, wherein the *Streptococcus* genus forms a phylogenetically separate clade to *Staphylococcus*, *Bacillus* and other genera (Figure 5.7). The differences that were observed between the structures of *S. pneumoniae* and *S. aureus* OatA suggest that the enzymes from these clades use discrete means to preclude water from serving as the acetyl acceptor during their respective double-displacement reaction mechanisms. Sychantha *et al*. noted the occurrence of a conserved Val/Ile adjacent to the oxyanion hole block III Asn in *Streptococcus* OatA homologues, proposing that this hydrophobic residue may stabilize carbohydrate acceptor substrates (Sychantha et al., 2017). In contrast, in *Staphylococcus* and species from the same clade, this position is most commonly occupied by a Thr or Ser residue, which would not engage in the same hydrophobic interactions. I identified a water molecule coordinated by Asp457 in the structure of *Sa*OatA$_C$ and determined that this residue played an important role in limiting the esterase activity of the enzyme, whilst maintaining transferase activity (Figure 5.2B and 5.6). This suggests that the two distinct clades of OatA homologues utilize different mechanisms to preclude water from their active site in order to catalyze efficient and non-wasteful transfer of acetyl groups to peptidoglycan only. The data suggest that the coordination of a water molecule in the active site by Asp457 may be the method by which *Sa*OatA$_C$ and the majority of OatA homologues belonging to the same phylogenetic clade favour transferase activity. Unfortunately, the absence of other OatA structures prevents us from verifying whether or not these structural features are conserved amongst homologues within the same clade. The reason for these differences also remains unknown. Perhaps the selective pressure for divergence into two clades was substrate specificity recognizing that the staphylococcal

OatA O-acetylates MurNAc residues with pentapeptide stems while the streptococcal enzyme has specificity for residues with tetrapeptide stems (Sychantha et al., 2017).

Peptidoglycan *O*-acetylation is a common modification employed by pathogenic Gram-positive bacteria as a means to evade the host innate immune system. Despite knowledge of the modification for decades, OatA from *S. pneumoniae* was the only PG *O*-acetylating enzyme from a Gram-positive bacterium characterized before this study. The current data reinforces the mechanism of action proposed for both *S. pneumoniae* $OatA_C$ and *N. gonorrhoeae* peptidoglycan *O*-acetyltransferase B (PatB) (Moynihan and Clarke, 2014b; Sychantha and Clarke, 2018). *Sa*$OatA_C$, as well as *N. gonorrhoeae* PatB, have been validated as antibiotic targets with a high throughput small-molecule screen (Brott et al., 2019). The structure of *Sa*$OatA_C$ will assist in the design of anti-virulence drugs against OatA. Furthermore, my discovery of the differences between the active sites of *S. pneumoniae* and *S. aureus* $OatA_C$ is an important consideration in developing narrow or broad spectrum OatA inhibitors for the treatment of important human pathogens for which current antibacterial therapies are being threatened by multi-drug resistance.

Chapter 6: Conclusions and future directions

The research described in this thesis offers insight into the structure and mechanism of both OatA domains involved in PG O-acetylation in *S. aureus*. The structure of the C-terminal SGNH hydrolase domain of *Sa*OatA was solved by X-ray crystallography. Based on analysis of the structure and biochemical experiments, a new transferase mechanism is proposed for *Staphylococci* and closely related OatA homologues. An experimental topology map of the N-terminal acyltransferase 3 domain was presented alongside putative catalytic and binding residues. Furthermore, a direct interaction between the domains was demonstrated, suggesting an unprecedented mechanism for PG O-acetylation. Finally, a preliminary study of the inhibition of the C-terminal domain of *Sa*OatA validated the enzyme as a target for novel antimicrobials and highlighted future avenues of research.

6.1 SGNH/GDSL hydrolase family transferases

Prior to this study, the only structure of a PG *O*-acetyltransferase available was that of OatA from *S. pneumoniae* (Sychantha et al., 2017). Whilst the *Sp*OatA$_C$ had many similarities to SGNH/GDSL hydrolase family esterases, it possessed an atypical oxyanion hole and hydrophobic active site wall that were proposed to distinguish the enzyme as a transferase (Sychantha and Clarke, 2018; Sychantha et al., 2017). As the second solved structure of a PG *O*-acetyltransferase, it was expected that *Sa*OatA$_C$ would possess similar structural features to *Sp*OatA$_C$. Surprisingly, *Sa*OatA$_C$, whilst structurally very similar to *Sp*OatA$_C$ (RMSD 1.8 Å), did not appear to have these features. In fact, the active site of *Sa*OatA$_C$ was remarkably like that of other SGNH hydrolase family esterases (Figure 5.3B), however, one key active site feature appeared to differentiate OatA as a transferase. An Asp residue, Asp457, at the base of the active site was seen to coordinate a water molecule (Figure 5.2B and 5.6). Replacement of this residue with either Ala or Asn results in a large increase in esterase activity (Table 5.1), leading to the conclusion that the coordinated water in the active site might as a guard against an incoming water molecule, thereby preventing hydrolysis of the acetyl-enzyme intermediate. An Asp residue was found in this position in the majority of OatA homologues, with the exception of *Streptococci* (Figure 5.7). These findings suggest that the conserved Asp residue and coordinated water may be an important feature in this clade of OatA enzymes that enables them to preferentially act as transferases. In contrast, *Streptococci* OatA homologues may

all possess the same features as *Sp*OatA$_C$, enabling them to act as transferases. However, in order to confirm this, additional structures of homologues from both clades would need to be solved.

A previous study revealed that *Sa*OatA$_C$ and *Sp*OatA$_C$ had different PG substrate specificities, where *Sa*OatA$_C$ preferred PG with a pentapeptide stem and *Sp*OatA$_C$ preferred PG with a tetrapeptide stem (Sychantha et al., 2017). The biochemical basis for this specificity, however, remains unknown. Given that the specificity is for the terminal Ala of the peptide stem of PG, the residues involved in promoting or hindering interactions with this residue would be quite remote from the active site. It would be interesting to identify such residues and attempt to alter substrate specificity by genetic engineering. Conserved residues can be identified by a multiple sequence alignment of OatA homologues, however, in order to identify residues involved in binding the peptide stem, the sequences would need to be separated by substrate specificity. This would require a large-scale investigation into the substrate specificity of OatA homologues. It would be interesting to see if substrate specificity was also distinct in each of the phylogenetic clades of OatA, with the *Streptococci* OatA possessing one specificity and the *Staphylococci* and related OatA enzymes possessing another specificity. An alternative approach would be to dock the peptide stem onto the 3D structures of both *Sa*OatA$_C$ and *Sp*OatA$_C$ and look for putative interacting residues. As the exact orientation of PG in the active site is not known, this strategy may not be precise and obtaining a crystal structure of the peptide stem in complex with OatA would be the ideal way to determine how OatA interacts with its substrate.

6.2 Peptidoglycan O-acetylation in Gram-positive bacteria

Membrane proteins are notoriously difficult to study due to their poor solubility and low stability *in vitro*. As such, structural and biochemical information for many membrane enzymes is very limited. In particular, the N-terminal domain of OatA and its cognate in the Gram-negative PG O-acetylation system, PatA, have been understudied and their function and role in PG O-acetylation were largely unknown. As a result, an overall understanding of the process of PG O-acetylation from cytoplasmic donor to acetylated PG has not been possible. In this study, the topology and function of the N-terminal domain of *Sa*OatA were investigated, providing the first insights into the membrane component of

any PG O-acetylation system and allowing for a model to be proposed for PG O-acetylation in Gram-positive bacteria.

The topology map of *Sa*OatA$_N$ generated experimentally by PhoA-LacZα fusion mapping enabled a 2D model to be generated for the structure of the N-terminal domain (Figure 4.4). Whilst experimental methods are preferable in many regards to *in silico* prediction, the PhoA-LacZα fusion mapping method has several inherent limitations. As the method relies on locating the terminal residue of a truncated form of the protein, there is no guarantee that the rest of the protein remains properly folded. Truncations that are unable to insert into the membrane and remain in the cytoplasm may display β-galactosidase activity regardless of the natural localization of the truncation site. Furthermore, the assumption is that truncations at residues normally localized within the membrane display a "frustrated" topology wherein a certain proportion display the fusion protein in the periplasm and a certain proportion in the cytoplasm. The truncation thus possesses both alkaline phosphatase and β-galactosidase activity. However, such dual activity may also arise from a periplasmic truncation with folding or membrane insertion problems. Despite these limitations, experimental mapping methods have their advantage over *in silico* predictions, which have rigid criteria. *In silico* predictions assume each TMS crosses the membrane and do not account for certain structural features commonly found in integral membrane proteins such as peripheral membrane or partial helices. Given that *Sa*OatA can be produced in *E. coli* to relatively high yields, a high-resolution structure of the full-length enzyme may be possible. X-ray crystallography is one approach, however, as the linker between the N- and C-terminal domains is likely flexible, this may impede crystallization. Truncating the enzyme to exclude the C-terminal domain and linker might solve this problem, however, the structure would be less comprehensive. A more interesting approach would be cryo-EM of the full-length protein. Not only would this provide structural information for the N-terminal domain, it may also provide clues for the orientation of and interaction between the N- and C-terminal domains.

In this study, invariable and highly conserved residues in *Sa*OatA$_N$ were investigated for their potential role in PG O-acetylation using a phenotypic functional complementation assay. Since the readout of the functional complementation assay is simply lysozyme resistance, it is not possible to attribute a specific role to each residue

investigated. Although a western blot was performed to ensure proper expression and localization of each non-functional *Sa*OatA variant, the replaced residue may still play a structural, as opposed to catalytic, role. Replacement of a residue with Ala may produce a structurally sound enzyme, however, critical catalytic or binding residues may not be oriented correctly and thus the enzyme may be non-functional. Despite this limitation, the functional complementation assay was advantageous as it was high throughput and allowed assessment of overall system function, which is not always possible in an *in vitro* assay. For example, a residue that is critical for enzyme localization or protein-protein interactions *in vivo*, when replaced, may have no impact on activity *in vitro*. On the basis of residue localization and identity, putative catalytic and binding residues were suggested. This included three Arg residues, Arg25, Arg83, and Arg86, proposed to be involved in binding to Coenzyme A, and a putative catalytic triad or diad composed of Tyr206, His36, and Glu154 (Figure 4.16). Absolute identification of the catalytic residue would require trapping of the acetyl-enzyme intermediate and digestion of the protein to identify the modified peptide in a similar experiment to how Ser453 was identified as the catalytic residue for *Sa*OatA$_C$ and *Sp*OatA$_C$ (Sychantha and Clarke, 2018).

Unequivocal identification of the cytoplasmic acetyl donor presents a larger challenge. The *in vitro* K_M of *Sa*OatA with acetyl-CoA was very low, suggesting the enzyme has a high affinity for acetyl-CoA (Figure 5.2B and 5.6). Furthermore, the identification of essential cytoplasmic facing Arg residues presented a putative binding site for CoA, however, the identity of the donor has not been confirmed *in vivo*. One strategy would be a pulse-chase experiment with ^{14}C-labelled acetyl-CoA. A similar experiment was used to identify acetyl-CoA as the substrate for TmaT from *Corynebacterium glutamicum*, which acetylates trehalose corynomycolates for periplasmic export (Yamaryo-Botte et al., 2015). In this experiment, a wild-type strain of the bacterium and a ΔTmaT strain were treated with ^{14}C-labeled acetyl-CoA and radio-labeled acetylated trehalose corynomycolates were analyzed by high-performance thin layer chromatography (Yamaryo-Botte et al., 2015). The main challenge with this approach is that acetyl-CoA is used by many enzymes and in many processes and therefore scintillation counting of whole cells would not be informative. It would be preferable to isolate the PG and assess radioactivity in the cell wall fraction alone, however, given that the source of the *N*-acetyl

group on GlcNAc is acetyl-CoA (Mengin-Lecreulx et al., 1996), presence of radioactivity would not just indicate incorporation of ^{14}C from OatA, making data interpretation more challenging.

OatA and several O-antigen *O*-acetyltransferases, including OafA from *Salmonella typhimurium* (Slauch et al., 1996) and Oac from *Pseudomonas aeruginosa* (Newton et al., 2001), are bimodular enzymes with an N-terminal acyltransferase 3 domain and a C-terminal SGNH hydrolase domain. In contrast, other acyltransferase 3 enzymes have only the one domain. This includes Oac from the temperate bacteriophage Sf6 that acetylates the O-antigen of *Shigella flexneri* (Thanweer et al., 2008), WecH, the enterobacterial common antigen acetyltransferase from *E. coli* (Kajimura et al., 2006), NolL, a Nod factor acetyltransferase from *Sinorhizobium fredii* (Bras et al., 2000), MdoC, a succinyltransferase that succinylates osmoregulated periplasmic glucans in *E. coli* (Lacroix et al., 1999), and Lag-1, an O-antigen acetyltransferase from *Legionella pneumophila* (Lück et al., 2001). If these enzymes do possess separate partner SGNH hydrolase domain, they have not been identified. In this study, preliminary data consistent with direct transfer between the two domains of OatA was obtained (Figure 4.11) and we propose that the SGNH hydrolase domain removes acetyl groups directly from the catalytic/relay tyrosine. It is the SGNH hydrolase domain that is responsible for acetylation of the carbohydrate. In contrast, in the single domain acyltransferases, these enzymes likely directly acylate their target carbohydrates. These enzymes must therefore possess a different mechanism that enables direct acylation of the substrate, and this may require two catalytic centres – one for removal of the acyl group from the donor, and another for transfer onto the carbohydrate acceptor (assuming the two half reactions are separated by the cytoplasmic membrane). Tyr206 was conserved amongst PG *O*-acetyltransferases however it did not appear to be conserved amongst other acyltransferase 3 enzymes. This might suggest that the mechanism of direct transfer from the Tyr206 extracytoplasmic loop is unique to OatA.

Several strategies had been proposed previously for the transfer of acetyl groups to the C-terminal SGNH hydrolase domain of OatA. Evidence from the analogous PatA/PatB PG O-acetylation system in Gram-negative bacteria suggested the existence of a diffusible intermediate, however it was unknown as to whether this occurred in the Gram-positive system (Moynihan and Clarke, 2010). In this study, direct transfer of the acetyl group from

the N-terminal acyltransferase 3 domain to the C-terminal SGNH hydrolase domain is demonstrated for *Sa*OatA. An extracytoplasmic loop containing the catalytic Tyr206 is proposed as the donor for the C-terminal domain. As the SGNH hydrolase domain in Gram-positive bacteria is attached to the membrane acyltransferase, it seems logical that direct transfer would occur, however there was no precedence for the acyltransferase 3 domain to act as a channel for acetyl groups. Indeed, this was a very interesting finding as it suggests a role for an acyltransferase enzyme whereby the enzyme simply removes the acyl group from a donor and does not actually transfer it onto anything, acting instead as an acyl donor for another enzyme. Moreover, acetylated peptides are not typical substrates for SGNH hydrolases. Whilst more experimentation is needed to confirm this interaction, if it proves true, this mechanism of transfer would be rather unique.

The finding that *S. aureus* can only O-acetylate muroglycans with pentapeptide stems has implications for the timing of PG O-acetylation (Sychantha et al., 2017). Up to 80% of *S. aureus* stem peptides are cross-linked and pentapeptide stems are rarely seen in the mature PG sacculus (Snowden and Perkins, 1990). Furthermore, PG O-acetylation is a post-biosynthetic modification occurring after PG is incorporated into existing sacculus – no O-acetylated lipid II is ever detected (Snowden et al., 1989). Therefore, in *S. aureus*, PG O-acetylation must occur after the transglycosylation reaction, but before transpeptidation. We therefore present a model in which the N-terminal acyltransferase 3 domain of *Sa*OatA interacts closely with PBPs and other PG biosynthetic machinery, acting swiftly after MurJ flips lipid II and PG transglycosylases link the glycan backbone (Figure 6.1). A PG transpeptidase would then cross-link the peptide stems. Direct transfer between the N- and C-terminal domains would enable this process to be rapid, as the PG *O*-acetyltransferase domain would be presented directly with the acetyl group. Such an association is supported by the observation that the chimeric forms of OatA involving domain swapping between the *S. aureus* and *S. pneumoniae* enzymes do not restore PG O-acetylation to *S. aureus* Δ*oatA*. With *S. pneumoniae*, PG O-acetylation appears to follow transpeptidation (Sychantha et al. 2019), thus not necessarily requiring direct interactions between OatA and the PG transglycosylase(s). This close association with other PG biosynthetic enzymes, whilst strongly implied by existing data, has not been proven. Pull-

down studies with *Sa*OatA as bait and *S. aureus* lysate as prey may reveal interaction partners for the enzyme.

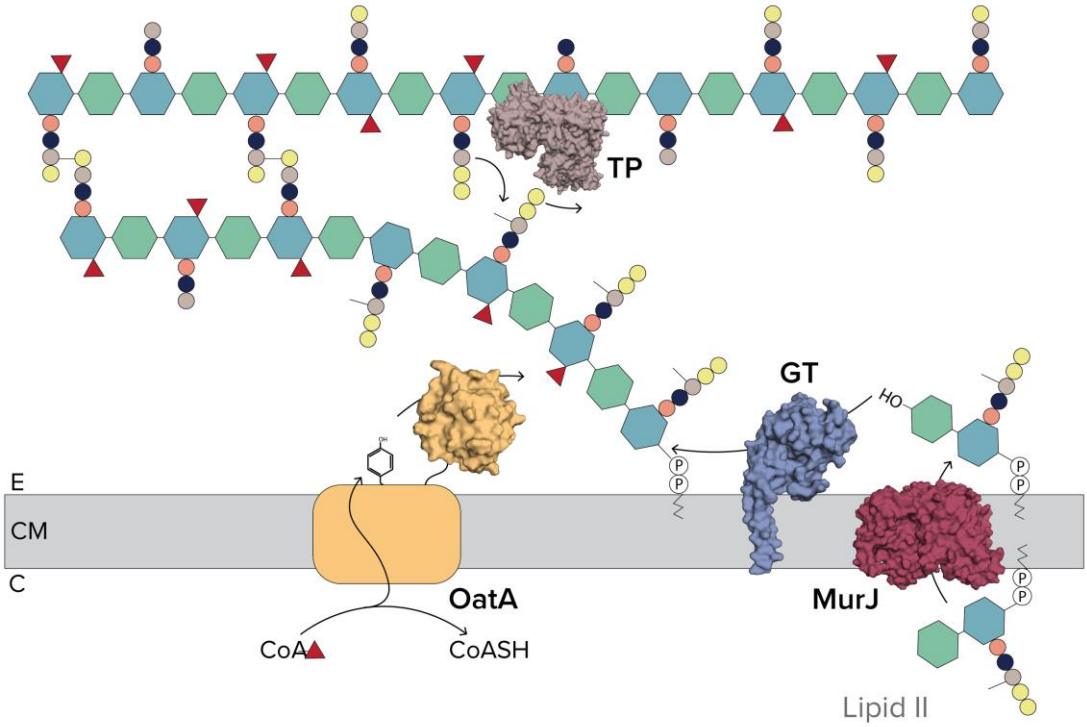

Figure 6.1 Proposed model for PG O-acetylation in *S. aureus*. MurJ flips lipid II across the cytoplasmic membrane where either a monofunctional glycosyltransferase (shown here; GT), or a bifunctional PBP, ligates lipid II to a pre-existing strand of PG. Concurrently, the N-terminal domain of OatA removes acetyl groups from acetyl-CoA and covalently modifies itself on a Tyr residue in an exposed extracytoplasmic loop. The C-terminal domain of OatA removes the acetyl group from the Tyr residue of the N-terminal domain and transfers it onto MurNAc residues of PG. The transpeptidase domain of PBP then cross-links the peptide stems of acetylated glycan strands. PDB IDs: 6VJP (OatA), 5TRO (TP), 5T77 (MurJ), 3VMQ (GT). E, external; CM, cytoplasmic membrane; C, cytoplasm.

6.3 Strategies for inhibition of PG O-acetylation

The role of PG O-acetylation in immune evasion during bacterial infections highlighted the enzymes involved as potential targets for the development of novel antimicrobials. Given that, in this context, PG O-acetylation is only essential in Gram-positive bacteria to protect from the presence of lysozyme, compounds targeting PG *O*-acetyltransferases would likely not be bactericidal or bacteriostatic outside the host. A drug

inhibiting PG O-acetylation would thus work more like an anti-virulence drug; by blocking PG O-acetylation, the ability of pathogens to establish an infection in the body would be limited. Such a drug may thus be most effective when administered prophylactically. However, there has been significant research surrounding the role of PG O-acetylation downstream in infections, such as in contributing to arthritis (Baranwal et al., 2017; Fleming et al., 1986), conferring resistance to other antimicrobials (Aubry et al., 2011; Crisostomo et al., 2006), and limiting the immune response (Sanchez et al., 2017). Therefore, a drug inhibiting PG O-acetylation also may help prevent downstream complications from bacterial infections when administered alongside a classic antimicrobial.

In this study, the C-terminal domain of *Sa*OatA was screened against a library of greater than 66,000 compounds in the effort to identify inhibitors of the enzyme. The hit rate from the initial high throughput screen was quite high (7.5%), however, none of the selected six lead compounds proved particularly successful. Two of the compounds successfully inhibited *Sa*OatA$_C$ *in vitro*, however neither affected the growth of *S. aureus* cells to a significant degree (Figure 3.5 and 3.9). Both compounds gave relatively high IC_{50} values, suggesting they were not very potent inhibitors, however, modification to the core structure may improve specificity and potency. Indeed, one of these compounds, compound HSC-0059363 shared a similar 1-(4-nitrophenyl)piperazine core structure with several other hits. It would therefore be interesting to assess potency and specificity of structural analogs of this compound. HSC-0094998 was the only compound that displayed increased killing towards *S. aureus* cells as the concentration of lysozyme increased, suggesting it may be inhibiting OatA *in vivo* (Figure 3.5). Although it was not possible to confirm the inhibitory effect of HSC-0094998 towards *Sa*OatA$_C$ *in vitro* (Figure 3.9), and the compound displayed some general toxicity, it would be interesting to test analogs of the compound as it may be possible to improve specificity and solubility.

Several of the issues faced by this screen included fluorescence-quenching and off-target effects. The problems seen with this screen raises several concerns with target-based biochemical assay HTS. The isolated environment of a biochemical assay does not enable considerations to be made for the accessibility of the target *in vivo*; a good *in vitro* inhibitor may not be able to enter the cell or access the target enzyme active site in a growing cell.

Conversely, whilst a compound might be an excellent inhibitor *in vitro*, there is no way to assess its specificity in a single-enzyme assay system. Indeed, a review in 2013 found phenotypic screening approaches to be more successful than target-based drug discovery (Swinney, 2013). A whole-cell phenotypic screen with *S. aureus* would circumvent issues of permeability or target accessibility and, with the incorporation of a counter-screen of *S. aureus* Δ*oatA*, the compound specificity could be addressed early on. Using this approach, lead compounds would be those that cause cell death of the *S. aureus* wild-type strain in the presence of lysozyme but have no effect on the growth of the *S. aureus* Δ*oatA* strain. This type of screen could potentially identify inhibitors of either the N- or C-terminal domain of OatA. This is particularly useful as screening against the full-length enzyme *in vitro* might present challenges of poor solubility, low quantity of enzyme, and high cost. Furthermore, the two domains likely have different accessibility and would be inhibited by different compounds. Additionally, whilst inhibitors of the C-terminal domain could broadly inhibit other SGNH hydrolases, inhibitors of the N-terminal domain may broadly inhibit acyltransferase 3 family enzymes. However, given the proposed unique interaction between the two domains, a compound that specifically interferes with this interaction would be a good lead compound if a narrow-spectrum antibiotic was desired.

In silico or virtual high throughput screening (vHTS) for protein inhibitors is becoming increasing popular in the world of drug-discovery. It is often being used over or in conjunction with traditional screening methods to reduce costs and accelerate drug discovery when possible. There are two approaches for vHTS: ligand-based vHTS, and structure-based vHTS. Ligand-based vHTS utilizes known substrates or inhibitors for a receptor in order to propose promising candidates from a library of molecules. This strategy may be successful for *Sa*OatA$_C$ by using the proposed donor, a short Tyr-containing peptide from *Sa*OatA$_N$ as the query ligand. Structure-based vHTS is the more popular method and consists of using *in silico* molecular docking to determine the binding of a library of compounds in the 3D structure of the target protein. The structure of *Sa*OatA$_C$ solved in this study would enable such a screen to be undertaken for *S. aureus* OatA. *In silico* screening may not directly suggest compounds with high affinity for the enzyme, however, it can provide information of the enzyme-ligand interactions and may enable focusing of a follow-up *in vitro* screen on molecules more likely to bind the target enzyme

(Zoete et al., 2009). *In silico* approaches can also be undertaken later in the screening process. For example, structure-based drug design is a strategy that may be employed after identification of lead compounds by traditional screening methods. Improvements to the lead compound can be suggested based on the proposed interaction between the protein target and the ligand, using the 3D protein structure. This strategy could be utilized for compounds HSC-0059363 or HSC-0018420 (which both displayed inhibition *in vitro* but limited effect *in vivo*) by docking the compound into the 3D structure of *Sa*OatA$_C$ to identify sites on the molecule where substitutions could improve binding and thus perhaps specificity and potency. An even better manner to assess binding of inhibitors to *Sa*OatA$_C$ would be to solve the structure protein-ligand complexes. Not only would this aid in the search for inhibitors of OatA, it would also improve our understanding of the mechanism of the enzyme. It would also be interesting to utilize the known 3D structures of PG *O*-acetyltransferases to attempt to design an inhibitor with narrow-specificity for only one of the enzymes.

Drug discovery is a long and expensive process. This study validated *Sa*OatA as a target and provided tools to study the mechanism of OatA *in vitro*, however, significantly more work is required to identify a potent and selective drug-candidate. PG *O*-acetyltransferases are still interesting targets for anti-virulence drug discovery and the additional information garnered from this thesis study would enable different screening approaches that may prove more fruitful in the search for novel inhibitors to combat antimicrobial resistance.

6.4 Concluding remarks

The major findings of this thesis have contributed substantially to understanding the process of PG O-acetylation. By solving the X-ray crystal structure of *Sa*OatA$_C$, I was able to investigate OatA substrate preference, and develop a hypothetical mechanism rationalizing non-wasteful acetyl transfer to PG (instead of water) for *Staphylococci*. Notably, this model deviated from the previously described *Streptococci* OatA model (Sychantha et al., 2017), demonstrating the importance of solving enzyme structures from homologues and the limitations of sequence analysis alone. Owing to the difficulties of studying membrane proteins, models for their function often rely on *in silico* predictions and analyses, as was the case for OatA. By determining the topology of the N-terminal

domain of OatA and identifing putative catalytic residues, a model for acetyl transfer by OatA from a cytoplasmic acetyl-CoA donor to PG was proposed. Such a mechanism is unprecedented in the literature and may inform studies of similar systems, such as O-antigen acetyltransferases. Furthermore, although none of the compounds selected from the HTS demonstrated a specific ability to sensitize *S. aureus* to lysozyme, the work described here provides several avenues forward for the continued search for inhibitors of PG O-acetylation.

References

Abanes-De Mello, A., Sun, Y.L., Aung, S., and Pogliano, K. (2002). A cytoskeleton-like role for the bacterial cell wall during engulfment of the *Bacillus subtilis* forespore. Genes Dev. *16*, 3253–3264.

Adams, P.D., Afonine, P. V, Bunkóczi, G., Chen, V.B., Echols, N., Headd, J.J., Hung, L.-W., Jain, S., Kapral, G.J., Grosse Kunstleve, R.W., et al. (2011). The Phenix software for automated determination of macromolecular structures. Methods *55*, 94–106.

Akoh, C.C., Lee, G.C., Liaw, Y.C., Huang, T.H., and Shaw, J.F. (2004). GDSL family of serine esterases/lipases. Prog. Lipid Res. *43*, 534–552.

Alexeyev, M.F., and Winkler, H.H. (1999). Membrane topology of the *Rickettsia prowazekii* ATP/ADP translocase revealed by novel dual *pho-lac* reporters. J. Mol. Biol. *285*, 1503–1513.

Anderson, E.M., Sychantha, D., Brewer, D., Clarke, A.J., Geddes-McAlister, J., and Khursigara, C.M. (2020). Peptidoglycomics reveals compositional changes in peptidoglycan between biofilm- and planktonic-derived *Pseudomonas aeruginosa*. J. Biol. Chem. *295*, 504–516.

Archibald, A.R. (1976). Cell wall assembly in Bacillus subtilis: Development of bacteriophage binding properties as a result of the pulsed incorporation of teichoic acid. J. Bacteriol. *127*, 956–960.

Atrih, A., Zöllner, P., Allmaierr, G., and Foster, S.J. (1996). Structural analysis of *Bacillus subtilis* 168 endospore peptidoglycan and its role during differentiation. J. Bacteriol. *178*, 6173–6183.

Aubry, C., Goulard, C., Nahori, M.A., Cayet, N., Decalf, J., Sachse, M., Boneca, I.G., Cossart, P., and Dussurget, O. (2011). OatA, a peptidoglycan *O*-acetyltransferase involved in *Listeria monocytogenes* immune escape, is critical for virulence. J. Infect. Dis. *204*, 731–740.

Azuma, I., Thomas, D., Adam, A., Ghuysen, J., Bonaly, R., Petit, J., and Lederer, E. (1970). Occurence of *N*-glucosylmuramic acid in bacterial cell walls. Biochim. Biophys. Acta *208*, 444–451.

Baba, T., and Schneewind, O. (1998). Targeting of muralytic enzymes to the cell division site of Gram-positive bacteria: Repeat domains direct autolysin to the equatorial surface ring of *Staphylococcus aureus*. EMBO J. *17*, 4639–4646.

Badet, B., Patricia Vermoote, Q., Haumont, P.-Y., Lederer, F., and Le Goffict, F. (1987). Glucosamine synthetase from *Escherichia coli*: purification, properties, and glutamine-utilizing site location. Biochemistry *26*, 1940–1948.

Bae, T., and Schneewind, O. (2006). Allelic replacement in *Staphylococcus aureus* with inducible counter-selection. Plasmid *55*, 58–63.

Baell, J.B., and Holloway, G.A. (2010). New substructure filters for removal of pan assay interference compounds (PAINS) from screening libraries and for their exclusion in bioassays. J. Med. Chem. *53*, 2719–2740.

Balomenou, S., Fouet, A., Tzanodaskalaki, M., Couture-Tosi, E., Bouriotis, V., and Boneca, I.G. (2013). Distinct functions of polysaccharide deacetylases in cell shape, neutral polysaccharide synthesis and virulence of *Bacillus anthracis*. Mol. Microbiol. *87*, 867–883.

Bames, K.J., and Rome, L.H. (1986). Acetyl-coenzyme A:α-glucosaminide N-acetyltransferase. J. Biol. Chem. *261*, 10127–10132.

Baranwal, G., Mohammad, M., Jarneborn, A., Reddy, B.R., Golla, A., Chakravarty, S., Biswas, L., Götz, F., Shankarappa, S., Jin, T., et al. (2017). Impact of cell wall peptidoglycan O-acetylation on the pathogenesis of *Staphylococcus aureus* in septic arthritis. Int. J. Med. Microbiol. *307*, 388–397.

Bateman, B.T., Donegan, N.P., Jarry, T.M., Palma, M., and Cheung, a L. (2001). Evaluation of a tetracycline-inducible promoter in *Staphylococcus aureus* in vitro and in vivo and its application in demonstrating the role of *sigB* in microcolony formation. Infect. Immun. *69*, 7851–7857.

Baumann, A.M.T., Bakkers, M.J.G., Buettner, F.F.R., Hartmann, M., Grove, M., Langereis, M.A., De Groot, R.J., and Muhlenhoff, M. (2015). 9-O-Acetylation of sialic acids is catalysed by CASD1 via a covalent acetyl-enzyme intermediate. Nat. Commun. *6*, 7673.

Bera, A., Herbert, S., Jakob, A., Vollmer, W., and Götz, F. (2005). Why are pathogenic staphylococci so lysozyme resistant? The peptidoglycan *O*-acetyltransferase OatA is the major determinant for lysozyme resistance of *Staphylococcus aureus*. Mol. Microbiol. *55*, 778–787.

Bera, A., Biswas, R., Herbert, S., and Götz, F. (2006). The presence of peptidoglycan *O*-acetyltransferase in various staphylococcal species correlates with lysozyme resistance and pathogenicity. Infect. Immun. *74*, 4598–4604.

Bera, A., Biswas, R., Herbert, S., Kulauzovic, E., Weidenmaier, C., Peschel, A., and Götz, F. (2007). Influence of wall teichoic acid on lysozyme resistance in *Staphylococcus aureus*. J. Bacteriol. *189*, 280–283.

Bernard, E., Rolain, T., Courtin, P., Guillot, A., Langella, P., Hols, P., and Chapot-Chartier, M.-P. (2011). Characterization of *O*-acetylation of *N*-acetylglucosamine: A novel structural variation of bacterial peptidoglycan. J. Biol. Chem. *286*, 23950–23958.

Bernard, E., Rolain, T., David, B., André, G., Dupres, V., Dufrêne, Y.F., Hallet, B., Chapot-Chartier, M.P., and Hols, P. (2012). Dual role for the *O*-acetyltransferase OatA in peptidoglycan modification and control of cell septation in *Lactobacillus plantarum*. PLOS One *7*, e47893.

Biswas, R., Voggu, L., Simon, U.K., Hentschel, P., Thumm, G., and Götz, F. (2006). Activity of the major staphylococcal autolysin Atl. FEMS Microbiol. Lett. *259*, 260–268.

Blackburn, N.T., and Clarke, A.J. (2002). Characterization of soluble and membrane-bound family 3 lytic transglycosylases from *Pseudomonas aeruginosa*. Biochemistry *41*, 1001–1013.

Blundell, J.K., Smith, G.J., and Perkins, H.R. (1980). The peptidoglycan of *Neisseria*

gonorrhoeae: *O*-acetyl groups and lysozyme sensitivity. FEMS Microbiol. Lett. *9*, 259–261.

Bogdanov, M., Zhang, W., Xie, J., and Dowhan, W. (2005). Transmembrane protein topology mapping by the substituted cysteine accessibility method (SCAM^{TM}): Application to lipid-specific membrane protein topogenesis. Methods *36*, 148–171.

Bolla, J.R., Sauer, J.B., Wu, D., Mehmood, S., Allison, T.M., and Robinson, C. V (2018). Direct observation of the influence of cardiolipin and antibiotics on lipid II binding to MurJ. Nat. Chem. *10*, 363–371.

Boneca, I.G., Dussurget, O., Cabanes, D., Nahori, M.-A., Sousa, S., Lecuit, M., Psylinakis, E., Bouriotis, V., Hugot, J.-P., Giovannini, M., et al. (2007). A critical role for peptidoglycan N-deacetylation in *Listeria* evasion from the host innate immune system. Proc. Natl. Acad. Sci. *204*, 997–1002.

Borisova, M., Gisin, J., and Mayer, C. (2014). Blocking peptidoglycan recycling in *Pseudomonas aeruginosa* attenuates intrinsic resistance to fosfomycin. Microb. Drug Resist. *20*, 231–237.

Borisova, M., Gaupp, R., Duckworth, A., Schneider, A., Dalügge, D., Mühleck, M., Deubel, D., Unsleber, S., Yu, W., Muth, G., et al. (2016). Peptidoglycan recycling in Gram-positive bacteria is crucial for survival in stationary phase. MBio *7*, e00923-16.

Borisova, M., Gisin, J., and Mayer, C. (2017). The *N*-acetylmuramic acid 6-phosphate phosphatase MupP completes the *Pseudomonas* peptidoglycan recycling pathway leading to intrinsic fosfomycin resistance. MBio *8*, e00092-17.

Born, P., Breukink, E., and Vollmer, W. (2006). *In vitro* synthesis of cross-linked murein and its attachment to sacculi by PBP1A from *Escherichia coli*. J. Biol. Chem. *281*, 26985–26993.

Bras, C.P., Jordá, M.A., Wijfjes, A.H.M., Harteveld, M., Stuurman, N., Thomas-Oates, J.E., and Spaink, H.P. (2000). A *Lotus japonicus* nodulation system based on heterologous expression of the fucosyl transferase NodZ and the acetyl transferase NolL in *Rhizobium leguminosarum*. Mol. Plant-Microbe Interact. *13*, 475–479.

Brönneke, V., and Fiedler, F. (1994). Production of bacteriolytic enzymes by *Streptomyces globisporus* regulated by exogenous bacterial cell walls. Appl. Environ. Microbiol. *60*, 785–791.

Brott, A.S., Jones, C.S., and Clarke, A.J. (2019). Development of a high throughput screen for the identification of inhibitors of peptidoglycan *O*-acetyltransferases, new potential antibacterial targets. Antibiotics *8*, 65.

Brown, S., Santa, J.P., Jr, M., and Walker, S. (2013). Wall teichoic acids of Gram-positive bacteria. Annu. Rev. Microbiol. *67*, 313–336.

Brumfitt, W. (1959). The mechanism of development of resistance to lysozyme by some Gram-positive bacteria and its results. Br. J. Exp. Pathol. *40*, 441–451.

Bugg, T.D.H., Wright, G.D., Dutka-Malen, S., Arthur, M., Courvalin, P., and Walsh, C.T. (1991). Molecular basis for vancomycin resistance in *Enterococcus faecium* BM4 147: Biosynthesis of a depsipeptide peptidoglycan precursor by vancomycin resistance proteins

VanH and VanA. Biochemistry *30*, 10408–10415.

Butler, E.K., Davis, R.M., Bari, V., Nicholson, P.A., and Ruiz, N. (2013). Structure-function analysis of MurJ reveals a solvent-exposed cavity containing residues essential for peptidoglycan biogenesis in *Escherichia coli*. J. Bacteriol. *195*, 4639–4649.

Campbell, J., Singh, A.K., Santa Maria Jr, J.P., Kim, Y., Brown, S., Swoboda, J.G., Mylonakis, E., Wilkinson, B.J., and Walker, S. (2011). Synthetic lethal compound combinations reveal a fundamental connection between wall teichoic acid and peptidoglycan biosyntheses in *Staphylococcus aureus*. ACS Chem. Biol. *6*, 106–116.

Centers for Disease Control and Prevention (2002). Staphylococcus aureus resistant to vancomycin - United States, 2002. Morb. Mortal. Weekley *51*, 565–567.

Centers for Disease Control and Prevention (2013). Antibiotic resistance threats in the United States, 2013.

Chastanet, A., and Losick, R. (2007). Engulfment during sporulation in *Bacillus subtilis* is governed by a multi-protein complex containing tandemly acting autolysins. Mol. Microbiol. *64*, 139–152.

Cheng, Q., Li, H., Merdek, K., and Park, J.T. (2000). Molecular characterization of the β-*N*-acetylglucosaminidase of *Escherichia coli* and its role in cell wall recycling. J. Bacteriol. *182*, 4836–4840.

Cho, H., Wivagg, C.N., Kapoor, M., Barry, Z., Rohs, P. DA, Suh, H., Marto, J.A., Garner, E.C., and Bernhardt, T.G. (2017). Bacterial cell wall biogenesis is mediated by SEDS and PBP polymerase families functioning semi-autonomously. Nat. Microbiol. *1*, 16172.

Choosangtong, K., Sirithanakorn, C., Adina-Zada, A., Wallace, J.C., Jitrapakdee, S., and Attwood, P. V. (2015). Residues in the acetyl CoA binding site of pyruvate carboxylase involved in allosteric regulation. FEBS Lett. *589*, 2073–2079.

Christianson, S., Golding, G.R., Campbell, J., Mulvey, M.R., Boyd, D., Bryce, E., Conly, J., Dow, G., Embil, J., Embree, J., et al. (2007). Comparative genomics of Canadian epidemic lineages of methicillin-resistant *Staphylococcus aureus*. J. Clin. Microbiol. *45*, 1904–1911.

Clarke, A.J. (1993a). Extent of peptidoglycan O acetylation in the tribe *Proteeae*. J. Bacteriol. *175*, 4550–4553.

Clarke, A.J. (1993b). Compositional analysis of peptidoglycan by high-performance anion-exchange chromatography. Anal. Biochem. *212*, 344–350.

Clarke, A.J., and Dupont, C. (1992). *O*-Acetylated peptidoglycan: its occurrence, pathobiological significance, and biosynthesis. Can. J. Microbiol. *38*, 85–91.

Cohen-Gonsaud, M., Barthe, P., Bagnéris, C., Henderson, B., Ward, J., Roumestand, C., and Keep, N.H. (2005). The structure of a resuscitation-promoting factor domain from *Mycobacterium tuberculosis* shows homology to lysozymes. Nat. Struct. Mol. Biol. *12*, 270–273.

Coulombe, F., Divangahi, M., Veyrier, F., de Léséleuc, L., Gleason, J.L., Yang, Y., Kelliher, M.A., Pandey, A.K., Sassetti, C.M., Reed, M.B., et al. (2009). Increased NOD2-

mediated recognition of *N*-glycolyl muramyl dipeptide. J. Exp. Med. *206*, 1709–1716.

Crisostomo, M.I., Vollmer, W., Kharat, A.S., Inhulsen, S., Gehre, F., Buckenmaier, S., and Tomasz, A. (2006). Attenuation of penicillin resistance in a peptidoglycan *O*-acetyl transferase mutant of *Streptococcus pneumoniae*. Mol. Microbiol. *61*, 1497–1509.

Daft, M.J., Burnham, J.C., and Yamamoto, Y. (1985). Lysis of *Phormidium luridum* by *Myxococcus fulvus* in continuous flow cultures. J. Appl. Bacteriol. *59*, 73–80.

van Dam, V., Sijbrandi, R., Kol, M., Swiezewska, E., De Kruijff, B., and Breukink, E. (2007). Transmembrane transport of peptidoglycan precursors across model and bacterial membranes. Mol. Microbiol. *64*, 1105–1114.

Denome, S.A., Elf, P.K., Henderson, T.A., Nelson, D.E., and Young, K.D. (1999). *Escherichia coli* mutants lacking all possible combinations of eight penicillin binding proteins: Viability, characteristics, and implications for peptidoglycan synthesis. J. Bacteriol. *181*, 3981–3993.

Dong, T.G., Ho, B.T., Yoder-Himes, D.R., and Mekalanos, J.J. (2013). Identification of T6SS-dependent effector and immunity proteins by Tn-seq in *Vibrio cholerae*. P. Natl. Acad. Sci. USA *110*, 2623–2628.

Dougherty, T.J. (1985). Involvement of a change in penicillin target and peptidoglycan structure in low-level resistance to β-lactam antibiotics in *Neisseria gonorrhoeae*. Antimicrob. Agents Chemother. *28*, 90–95.

Dover, R.S., Bitler, A., Shimoni, E., Trieu-Cuot, P., and Shai, Y. (2015). Multiparametric AFM reveals turgor-responsive net-like peptidoglycan architecture in live streptococci. Nat. Commun. *6*, 7193.

Drozdetskiy, A., Cole, C., Procter, J., and Barton, G.J. (2015). JPred4: a protein secondary structure prediction server. Nucleic Acids Res. *43*, W389–W394.

Du, W., Brown, J.R., Sylvester, D.R., Huang, J., Chalker, A.F., So, C.Y., Holmes, D.J., Payne, D.J., and Wallis, N.G. (2000). Two active forms of UDP-*N*-acetylglucosamine enolpyruvyl transferase in Gram-positive bacteria. J. Bacteriol. *182*, 4146–4152.

Duncan, K., van Heijenoort, J., and Walsh, C.T. (1990). Purification and characterization of the D-alanyl-D-alanine-adding enzyme from *Escherichia coli*. Biochemistry *29*, 2379–2386.

Durand, S., Feldhammer, M., Bonneil, É., Thibault, P., and Pshezhetsky, A. V. (2010). Analysis of the biogenesis of heparan sulfate acetyl-CoA:α- glucosaminide *N*-acetyltransferase provides insights into the mechanism underlying its complete deficiency in mucopolysaccharidosis IIIC. J. Biol. Chem. *285*, 31233–31242.

Dutzler, R., Campbell, E.B., and MacKinnon, R. (2003). Gating the selectivity filter in ClC chloride channels. Science *300*, 108–112.

Emirian, A., Fromentin, S., Eckert, C., Chau, F., Dubost, L., Delepierre, M., Gutmann, L., Arthur, M., and Mesnage, S. (2009). Impact of peptidoglycan *O*-acetylation on autolytic activities of the *Enterococcus faecalis N*-acetylglucosaminidase AtlA and *N*-acetylmuramidase AtlB. FEBS Lett. *583*, 3033–3038.

Emsley, P., and Cowtan, K. (2004). *Coot*: Model-building tools for molecular graphics. Acta Crystallogr. Sect. D *60*, 2126–2132.

Farha, M.A., Leung, A., Sewell, E.W., D'Elia, M.A., Allison, S.E., Ejim, L., Pereira, P.M., Pinho, M.G., Wright, G.D., and Brown, E.D. (2013). Inhibition of WTA synthesis blocks the cooperative action of pbps and sensitizes MRSA to β-lactams. ACS Chem. Biol. *8*, 226–233.

Fernández-Tornero, C., López, R., García, E., Giménez-Gallego, G., and Romero, A. (2001). A novel solenoid fold in the cell wall anchoring domain of the pneumococcal virulence factor LytA. Nat. Struct. Biol. *8*, 1020–1024.

Fiser, A., Filipe, S.R., and Tomasz, A. (2003). Cell wall branches, penicillin resistance and the secrets of the MurM protein. Trends Microbiol. *11*, 547–553.

Fleming, T.J., Wallsmith, D.E., and Rosenthal, R.S. (1986). Arthropathic properties of gonococcal peptidoglycan fragments: implications for the pathogenesis of disseminated gonococcal disease. Infect. Immun. *52*, 600–608.

Fox, K.L., Yildirim, H.H., Deadman, M.E., Schweda, E.K.H., Moxon, E.R., and Hood, D.W. (2005). Novel lipopolysaccharide biosynthetic genes containing tetranucleotide repeats in *Haemophilus influenzae*, identification of a gene for adding *O*-acetyl groups. Mol. Microbiol. *58*, 207–216.

Fukushima, T., Yamamoto, H., Atrih, A., Foster, S.J., and Sekiguchi, J. (2002). A polysaccharide deacetylase gene (*pdaA*) is required for germination and for production of muramic δ-lactam residues in the spore cortex of *Bacillus subtilis*. J. Bacteriol. *184*, 6007–6015.

Fumeaux, C., and Bernhardt, T.G. (2017). Identification of MupP as a new peptidoglycan recycling factor and antibiotic resistance determinant in *Pseudomonas aeruginosa*. MBio *8*, e00102-17.

Furlong, S.E., Ford, A., Albarnez-Rodriguez, L., and Valvano, M.A. (2015). Topological analysis of the *Escherichia coli* WcaJ protein reveals a new conserved configuration for the polyisoprenyl-phosphate hexose-1-phosphate transferase family. Sci. Rep. *5*, 9178.

Garcia-Bustos, J.F., Chait, B.T., and Tomasz, A. (1987). Structure of the peptide network of pneumococcal peptidoglycan. J. Biol. Chem. *262*, 15400–15405.

Garnier, J., Osguthorpe, D.J., and Robson, B. (1978). Analysis of the accuracy and implications of simple methods for predicting the secondary structure of globular proteins. J. Mol. Biol. *120*, 97–120.

Gautier, R., Douguet, D., Antonny, B., and Drin, G. (2008). HELIQUEST: A web server to screen sequences with specific α-helical properties. Bioinformatics *24*, 2101–2102.

Gerlt, J.A., Bouvier, J.T., Davidson, D.B., Imker, H.J., Sadkhin, B., Slater, D.R., and Whalen, K.L. (2015). Enzyme function initiative-enzyme similarity tool (EFI-EST): A web tool for generating protein sequence similarity networks. Biochim. Biophys. Acta *1854*, 1019–1037.

El Ghachi, M., Howe, N., Huang, C.Y., Olieric, V., Warshamanage, R., Touzé, T., Weichert, D., Stansfeld, P.J., Wang, M., Kerff, F., et al. (2018). Crystal structure of

undecaprenyl-pyrophosphate phosphatase and its role in peptidoglycan biosynthesis. Nat. Commun. *9*, 1078.

Ghosh, A.S., Chowdhury, C., and Nelson, D.E. (2008). Physiological functions of D-alanine carboxypeptidases in *Escherichia coli*. Cell *16*, 309–317.

Ghuysen, J.M., Tipper, D.J., Birge, C.H., and Strominger, J.L. (1965). Structure of the cell wall of *Staphylococcus aureus* strain Copenhagen. VI. The soluble glycopeptide and its sequential degradation by peptidases. Biochemistry *4*, 2245–2254.

Gilmore, M.E., Bandyopadhyay, D., Dean, A.M., Linnstaedt, S.D., and Popham, D.L. (2004). Production of muramic δ-lactam in *Bacillus subtilis* spore peptidoglycan. J. Bacteriol. *186*, 80–89.

Gisin, J., Schneider, A., Nägele, B., Borisova, M., and Mayer, C. (2013). A cell wall recycling shortcut that bypasses peptidoglycan *de novo* biosynthesis. Nat. Chem. Biol. *9*, 491–493.

Gmeiner, J., and Kroll, H.-P. (1981). Murein biosynthesis and *O*-acetylation of *N*-acetylmuramic acid during the cell-division cycle of *Proteus mirabilis*. Eur. J. Biochem. *117*, 171–177.

Gmeiner, J., and Sarnow, E. (1987). Murein biosynthesis in synchronized cells of *Proteus mirabilis*. Quantitative analysis of *O*-acetylated murein subunits and of chain terminators incorporated into the sacculus during the cell cycle. Eur. J. Biochem. *163*, 389–395.

Goldschmidt, L., Cooper, D.R., Derewenda, Z.S., and Eisenberg, D. (2007). Toward rational protein crystallization: A Web server for the design of crystallizable protein variants. Protein Sci. *16*, 1569–1576.

Goodell, E.W. (1985). Recycling of murein by *Escherichia coli*. J. Bacteriol. *163*, 305–310.

Gordon, E., Flouret, B., Chantalat, L., Van Heijenoort, J., Mengin-Lecreulx, D., and Dideberg, O. (2001). Crystal structure of UDP-*N*-acetylmuramoyl-L-alanyl-D-glutamate: *meso*-diaminopimelate ligase from *Escherichia coli*. J. Biol. Chem. *276*, 10999–11006.

Grassetti, D.R., and Murray, J.F. (1967). Determination of sulfhydryl groups with 2,2′- or 4,4′-dithiodipyridine. Arch. Biochem. Biophys. *119*, 41–49.

Guiral, S., Mitchell, T.J., Martin, B., and Claverys, J.-P. (2005). Competence-programmed predation of noncompetent cells in the human pathogen *Streptococcus pneumoniae*: Genetic requirements. P. Natl. Acad. Sci. USA *102*, 8710–8715.

Hayashi, H., Araki, Y., and Ito, E. (1973). Occurrence of glucosamine residues with free amino groups in cell wall peptidoglycan from Bacilli as a factor responsible for resistance to lysozyme. J. Bacteriol. *113*, 592–598.

Hébert, L., Courtin, P., Torelli, R., Sanguinetti, M., Chapot-Chartier, M.-P., Auffray, Y., and Benachour, A. (2007). *Enterococcus faecalis* constitutes an unusual bacterial model in lysozyme resistance. Infect. Immun. *75*, 5390–5398.

Heidrich, C., Templin, M.F., Ursinus, A., Merdanovic, M., Berger, J., Schwarz, H., De Pedro, M.A., and Höltje, J.V. (2001). Involvement of *N*-acetylmuramyl-L-alanine

amidases in cell separation and antibiotic-induced autolysis of *Escherichia coli*. Mol. Microbiol. *41*, 167–178.

Heidrich, C., Ursinus, A., Berger, J., Schwarz, H., and Höltje, J.V. (2002). Effects of multiple deletions of murein hydrolases on viability, septum cleavage, and sensitivity to large toxic molecules in *Escherichia coli*. J. Bacteriol. *184*, 6093–6099.

Heilmann, C., Hussain, M., Peters, G., and Götz, F. (1997). Evidence for autolysin-mediated primary attachment of *Staphylococcus epidermidis* to a polystyrene surface. Mol. Microbiol. *24*, 1013–1024.

Herlihey, F.A., and Clarke, A.J. (2017). Controlling autolysis during flagella insertion in Gram-negative bacteria. Adv. Exp. Med. Biol. - Protein Rev. *925*, 41–56.

Herlihey, F.A., Moynihan, P.J., and Clarke, A.J. (2014). The essential protein for bacterial flagella formation FlgJ functions as a β-*N*-acetylglucosaminidase. J. Biol. Chem. *289*, 31029–31042.

Higa, H.H., Butor, C., Diaz, S., and Varki, A. (1989). *O*-Acetylation and de-*O*-acetylation of sialic acids. J. Biol. Chem. *264*, 19427–19434.

Höltje, J.-V. (1996). A hypothetical holoenzyme involved in the replication of the murein sacculus of *Escherichia coli*. Microbiology *142*, 1911–1918.

Höltje, J.-V. (1998). Growth of the stress-bearing and shape-maintaining murein sacculus of *Escherichia coli*. Microbiol. Mol. Biol. Rev. *62*, 181–203.

Höltje, J.-V., Mirelman, D., Sharon, N., and Schwarz, U. (1975). Novel type of murein transglycosylase in *Escherichia coli*. J. Bacteriol. *124*, 1067–1076.

Hoover, D.G., and Gray, R.J. (1977). Function of cell wall teichoic acid in thermally injured *Staphylococcus aureus*. J. Bacteriol. *131*, 477–485.

Horsburgh, G.J., Atrih, A., and Foster, S.J. (2003). Characterization of LytH, a differentiation-associated peptidoglycan hydrolase of *Bacillus subtilis* involved in endospore cortex maturation. J. Bacteriol. *185*, 3813–3820.

Hoskins, J.A., Matsushima, P., Mullen, D.L., Tang, J., Zhao, G., Meier, T.I., Nicas, T.I., and Jaskunas, S.R. (1999). Gene disruption studies of penicillin-binding proteins 1a, 1b, and 2a in *Streptococcus pneumoniae*. J. Bacteriol. *181*, 6552–6555.

Hottmann, I., Mayer, V.M.T., Tomek, M.B., Friedrich, V., Calvert, M.B., Titz, A., Schäffer, C., and Mayer, C. (2018). *N*-Acetylmuramic acid (MurNAc) auxotrophy of the oral pathogen *Tannerella forsythia*: Characterization of a MurNAc kinase and analysis of its role in cell wall metabolism. Front. Microbiol. *9*, 19.

Hoyle, B.D., and Beveridge, T.J. (1984). Metal binding by the peptidoglycan sacculus of *Escherichia coli* K-12. Can. J. Microbiol. *30*, 204–211.

Huynh, K., and Partch, C.L. (2015). Analysis of protein stability and ligand interactions by thermal shift assay. Curr. Protoc. Protein Sci. *79*, 28.9.1-28.9.14.

Ikeda, M., Wachi, M., Jung, H.K., Ishino, F., and Matsuhashi, M. (1991). The *Escherichia coli mraY* gene encoding UDP-*N*-acetylmuramoyl- pentapeptide:undecaprenyl-phosphate phospho-*N*-acetylmuramoyl-pentapeptide transferase. J. Bacteriol. *173*, 1021–1026.

Inoue, A., Murata, Y., Takahashi, H., Tsuji, N., Fujisaki, S., and Kato, J.-I. (2008). Involvement of an essential gene, *mviN*, in murein synthesis in *Escherichia coli*. J. Bacteriol. *190*, 7298–7301.

Islam, S.T., Taylor, V.L., Qi, M., and Lam, J.S. (2010). Membrane topology mapping of the O-antigen flippase (Wzx), polymerase (Wzy), and ligase (WaaL) from *Pseudomonas aeruginosa* PAO1 reveals novel domain architectures. MBio *1*, e00189-10.

Ito, E., and Strominger, J.L. (1973). Enzymatic synthesis of the peptide in bacterial uridine nucleotides. VII. Comparative biochemistry. J. Biol. Chem. *248*, 3131–3136.

Iyer, P.P., and Ferry, J.G. (2001). Role of arginines in coenzyme A binding and catalysis by the phosphotransacetylase from *Methanosarcina thermophila*. J. Bacteriol. *183*, 4244–4250.

Jacobs, C., Huang, L.-J., Bartowsky, E., Normark, S., and Park, J.T. (1994). Bacterial cell wall recycling provides cytosolic muropeptides as effectors for β-lactamase induction. EMBO J. *13*, 4684–4694.

Jacobs, C., Joris, B., Jamin, M., Klarsov, K., van Beeumen, J., Mengin-Lecreulx, D., van Heijenoort, J., Park, J.T., Normark, S., and Frère, J.-M. (1995). AmpD, essential for both β-lactamase regulation and cell wall recycling, is a novel cytosolic N-acetylmuramyl-L-alanine amidase. Mol. Microbiol. *15*, 553–559.

Jaeger, T., Arsic, M., and Mayer, C. (2005). Scission of the lactyl ether bond of N-acetylmuramic acid by *Escherichia coli* "etherase." J. Biol. Chem. *280*, 30100–30106.

Jiang, Y., Morley, K.L., Schrag, J.D., and Kazlauskas, R.J. (2011). Different active-site loop orientation in serine hydrolases versus acyltransferases. ChemBioChem *12*, 768–776.

Johannsen, L., Labischinski, H., Reinicke, B., and Giesbrecht, P. (1983). Changes in the chemical structure of walls of *Staphylococcus aureus* grown in the presence of chloramphenicol. FEMS Microbiol. Lett. *16*, 313–316.

Joris, B., Englebert, S., Chu, C.-P., Kariyama, R., Daneo-Moore, L., Shockman, G.D., and Ghuysen, J.-M. (1992). Modular design of the *Enterococcus hirae* muramidase-2 and *Streptococcus faecalis* autolysin. FEMS Microbiol. Lett. *91*, 257–264.

Kajimura, J., Rahman, A., Hsu, J., Evans, M.R., Gardner, K.H., and Rick, P.D. (2006). O Acetylation of the enterobacterial common antigen polysaccharide is catalyzed by the product of the *yiaH* gene of *Escherichia coli* K-12. J. Bacteriol. *188*, 7542–7550.

Käll, L., Krogh, A., and Sonnhammer, E.L.L. (2005). An HMM posterior decoder for sequence feature prediction that includes homology information. Bioinformatics *21*, i251–i257.

Kamerling, J.P., Schauer, R., Shukla, A.K., Stoll, S., Halbeek, H. van, and Vliegenthart, J.F.G. (1987). Migration of *O*-acetyl groups in *N*,*O*-acetylneuraminic acids. Eur. J. Biochem. *162*, 601–607.

Kamio, Y., and Nikaido, H. (1976). Outer membrane of *Salmonella typhimurium*: Accessibility of phospholipid head groups to phospholipase C and cyanogen bromide activated dextran in external medium. Biochemistry *15*, 2561–2570.

Keck, W., and Schwarz, U. (1979). *Escherichia coli* murein-DD-endopeptidase insensitive to β-lactam antibiotics. J. Bacteriol. *139*, 770–774.

Keck, W., Van Leeuwen, A.M., Huber, M., and Goodell, E.W. (1990). Cloning and characterization of *mepA*, the structural gene of the penicillin-insensitive murein endopeptidase from *Escherichia coli*. Mol. Microbiol. *4*, 209–219.

Keep, N.H., Ward, J.M., Cohen-Gonsaud, M., and Henderson, B. (2006). Wake up! Peptidoglycan lysis and bacterial non-growth states. Trends Microbiol. *14*, 271–276.

Kell, L.F. (2015). Investigation of novel inhibitory compounds of *O*-acetyltransferase A (OatA) from *Staphylococcus aureus*. University of Guelph.

Kluj, R.M., Ebner, P., Adamek, M., Ziemert, N., Mayer, C., and Borisova, M. (2018). Recovery of the peptidoglycan turnover product released by the autolysin Atl in *Staphylococcus aureus* involves the phosphotransferase system transporter MurP and the novel 6-phospho-*N*-acetylmuramidase MupG. Front. Microbiol. *9*, 2725.

Koch, A.L., and Doyle, R.J. (1985). Inside-to-outside growth and turnover of the wall of Gram-positive rods. J. Theor. Biol. *117*, 137–157.

Koraimann, G. (2003). Lytic transglycosylases in macromolecular transport systems of Gram-negative bacteria. CMLS-Cell. Mol. Life Sci. *60*, 2371–2388.

Korsak, D., Vollmer, W., and Markiewicz, Z. (2005). *Listeria monocytogenes* EGD lacking penicillin-binding protein 5 (PBP5) produces a thicker cell wall. FEMS Microbiol. Lett. *251*, 281–288.

Kranz, J.K., and Schalk-Hihi, C. (2011). Protein Thermal Shifts to Identify Low Molecular Weight Fragments. In Methods in Enzymology, p.

Kreiswirth, B.N., Löfdahl, S., Betley, M.J., O'reilly, M., Schlievert, P.M., Bergdoll, M.S., and Novick, R.P. (1983). The toxic shock syndrome exotoxin structural gene is not detectably transmitted by a prophage. Nature *305*, 709–712.

Krogh, A., Larsson, B., Von Heijne, G., and Sonnhammer, E.L.L. (2001). Predicting transmembrane protein topology with a hidden Markov model: Application to complete genomes. J. Mol. Biol. *305*, 567–580.

Kuk, A.C.Y., Mashalidis, E.H., and Lee, S.-Y. (2017). Crystal structure of the MOP flippase MurJ in an inward-facing conformation. Nat. Struct. Mol. Biol. *24*, 171–176.

Kuk, A.C.Y., Hao, A., Guan, Z., and Lee, S.-Y. (2019). Visualizing conformation transitions of the Lipid II flippase MurJ. Nat. Commun. *10*, 1736.

Laaberki, M.-H., Pfeffer, J., Clarke, A.J., and Dworkin, J. (2010). *O*-Acetylation of peptidoglycan is required for proper cell separation and S-layer anchoring in *Bacillus anthracis*. J. Biol. Chem. *286*, 5278–5288.

Lacroix, J.-M., Lanfroy, E., Cogez, V., Lequette, Y., Bohin, A., and Bohin, J.-P. (1999). The *mdoC* gene of *Escherichia coli* encodes a membrane protein that is required for succinylation of osmoregulated periplasmic glucans. J. Bacteriol. *181*, 3626–3631.

Laemmli, U.K. (1970). Cleavage of structural proteins during the assembly of the head of Bacteriophage T4. Nature *227*, 680–685.

Lara, B., and Ayala, J.A. (2002). Topological characterization of the essential *Escherichia coli* cell division protein FtsW. FEMS Microbiol. Lett. *216*, 23–32.

Lear, A.L., and Perkins, H.R. (1986). *O*-Acetylation of peptidoglycan in *Neisseria gonorrhoeae*. Investigation of lipid-linked intermediates and glycan chains newly incorporated into the cell wall. J. Gen. Microbiol. *132*, 2413–2420.

Lejon, S., Ellis, J., and Valegård, K. (2008). The last step in cephalosporin C formation revealed: Crystal structures of deacetylcephalosporin C acetyltransferase from *Acremonium chrysogenum* in complexes with reaction intermediates. J. Mol. Biol. *377*, 935–944.

Liger, D., Masson, A., Blanot, D., Van Heijenoort, J., and Parquet, C. (1995). Over-production, purification and properties of the uridine-diphosphate-*N*-acetylmuramate: L-alanine ligase from *Escherichia coli*. Eur. J. Biochem. *230*, 80–87.

Lück, P.C., Freier, T., Steudel, C., Knirel, Y.A., Lüneberg, E., Zähringer, U., and Helbig, J.H. (2001). A point mutation in the active site of *Legionella pneumophila O*-acetyltransferase results in modified lipopolysaccharide but does not influence virulence. Int. J. Med. Microbiol. *291*, 345–352.

Ma, D., Wang, Z., Merrikh, C.N., Lang, K.S., Lu, P., Li, X., Merrikh, H., Rao, Z., and Xu, W. (2018). Crystal structure of a membrane-bound *O*-acyltransferase. Nature *562*, 286–290.

Mahendrarajah, K., Dalby, P.A., Wilkinson, B., Jackson, S.E., and Main, E.R.G. (2011). A high-throughput fluorescence chemical denaturation assay as a general screen for protein-ligand binding. Anal. Biochem. *411*, 155–157.

Manoil, C., and Alan, M.T. (1991). Analysis of membrane protein topology using alkaline phosphatase and β-galactosidase gene fusions. In Methods in Cell Biology, (San Diego, CA: Academic Press), pp. 61–75.

Marquardt, J.L., Siegele, D.A., Kolter, R., and Walsh, C.T. (1992). Cloning and sequencing of *Escherichia coli murZ* and purification of its product, a UDP-*N*-acetylglucosamine enolpyruvyl transferase. J. Bacteriol. *174*, 5748–5752.

Marquis, R.E., Mayzel, K., and Carstensen, E.L. (1976). Cation exchange in cell walls of Gram positive bacteria. Can. J. Microbiol. *22*, 975–982.

Matias, V.R.F., and Beveridge, T.J. (2005). Cryo-electron microscopy reveals native polymeric cell wall structure in *Bacillus subtilis* 168 and the existence of a periplasmic space. Mol. Microbiol. *56*, 240–251.

Matias, V.R.F., and Beveridge, T.J. (2006). Native cell wall organization shown by cryo-electron microscopy confirms the existence of a periplasmic space in *Staphylococcus aureus*. J. Bacteriol. *188*, 1011–1021.

Mayer, C., Kluj, R.M., Mühleck, M., Walter, A., Unsleber, S., Hottmann, I., and Borisova, M. (2019). Bacteria's different ways to recycle their own cell wall. Int. J. Med. Microbiol. *309*, 151326.

McDonough, M.A., Anderson, J.W., Silvaggi, N.R., Pratt, R.F., Knox, J.R., and Kelly, J.A. (2002). Structures of two kinetic intermediates reveal species specificity of penicillin-

binding proteins. J. Mol. Biol. *322*, 111–122.

McPherson, D.C., and Popham, D.L. (2003). Peptidoglycan synthesis in the absence of class A penicillin-binding proteins in *Bacillus subtilis*. J. Bacteriol. *185*, 1423–1431.

Meeske, A.J., Sham, L.-T., Kimsey, H., Koo, B.-M., Gross, C.A., Bernhardt, T.G., and Rudner, D.Z. (2015). MurJ and a novel lipid II flippase are required for cell wall biogenesis in *Bacillus subtilis*. Proc. Natl. Acad. Sci. *112*, 6437–6442.

Mengin-Lecreulx, D., and Heijenoort, J. Van (1993). Identification of the *glmU* gene encoding *N*-acetylglucosamine-1-phosphate uridyltransferase in *Escherichia coli*. J. Bacteriol. *175*, 6150–6157.

Mengin-Lecreulx, D., and Van Heijenoort, J. (1994). Copurification of glucosamine-1-phosphate acetyltransferase and *N*-acetylglucosamine-1-phosphate uridyltransferase activities of *Escherichia coli*. J. Bacteriol. *176*, 5788–5795.

Mengin-Lecreulx, D., and Van Heijenoort, J. (1996). Characterization of the essential gene *glmM* encoding phosphoglucosamine mutase in *Escherichia coli*. J. Biol. Chem. *271*, 32–39.

Mengin-Lecreulx, D., Texier, L., Rousseau, M., and Van Heijenoort, J. (1991). The *murG* gene of *Escherichia coli* codes for the UDP-*N*-acetylglucosamine:*N*-acetylmuramyl-(pentapeptide) pyrophosphoryl-undecaprenol *N*-acetylglucosamine transferase involved in the membrane steps of peptidoglycan synthesis. J. Bacteriol. *173*, 4625–4636.

Mengin-Lecreulx, D., van Heijenoort, J., and Park, J.T. (1996). Identification of the *mpl* gene encoding UDP-*N*-acetylmuramate: L-alanyl-γ-D-glutamyl-*meso*-diaminopimelate ligase in *Escherichia coli* and its role in recycling of cell wall peptidoglycan. J. Bacteriol. *178*, 5347–5352.

Michaud, C., Mengin-Lecreulx, D., van Heijenoort, J., and Blanot, D. (1990). Over-production, purification and properties of the uridine-diphosphate-*N*-acetylmuramoyl-alanyl-glutamate: *meso*-2,6-diaminopimelate ligase from *Escherichia coli*. Eur. J. Biochem. *194*, 853–861.

Miroux, B., and Walker, J.E. (1996). Over-production of proteins in *Escherichia coli*: Mutant hosts that allow synthesis of some membrane proteins and globular proteins at high levels. J. Mol. Biol. *260*, 289–298.

Mohammadi, T., van Dam, V., Sijbrandi, R., Vernet, T., Zapun, A., Bouhss, A., Diepeveen-de Bruin, M., Nguyen-Distè che, M., de Kruijff, B., and Breukink, E. (2011). Identification of FtsW as a transporter of lipid-linked cell wall precursors across the membrane. EMBO J. *30*, 1425–1432.

Mohammadi, T., Sijbrandi, R., Lutters, M., Verheul, J., Martin, N.I., Den Blaauwen, T., De Kruijff, B., and Breukink, E. (2014). Specificity of the transport of lipid II by FtsW in *Escherichia coli*. J. Biol. Chem. *289*, 14707–14718.

Monteiro, J.M., Pereira, A.R., Reichmann, N.T., Saraiva, B.M., Fernandes, P.B., Veiga, H., Tavares, A.C., Santos, M., Ferreira, M.T., Macário, V., et al. (2018). Peptidoglycan synthesis drives FtsZ treadmilling-independent step of cytokinesis. Nature *554*, 528–532.

Moynihan, P.J., and Clarke, A.J. (2010). O-Acetylation of peptidoglycan in Gram-negative

bacteria: Identification and characterization of peptidoglycan *O*-acetyltransferase in *Neisseria gonorrhoeae*. J. Biol. Chem. *285*, 13264–13273.

Moynihan, P.J., and Clarke, A.J. (2011). *O*-Acetylated peptidoglycan: Controlling the activity of bacterial autolysins and lytic enzymes of innate immune systems. Int. J. Biochem. Cell Biol. *43*, 1655–1659.

Moynihan, P.J., and Clarke, A.J. (2014a). Substrate specificity and kinetic characterization of peptidoglycan *O*-acetyltransferase B from *Neisseria gonorrhoeae*. J. Biol. Chem. *289*, 16748–16760.

Moynihan, P.J., and Clarke, A.J. (2014b). Mechanism of action of peptidoglycan *O*-acetyltransferase B involves a Ser-His-Asp catalytic triad. Biochemistry *53*, 6243–6251.

Moynihan, P.J., Sychantha, D., and Clarke, A.J. (2014). Chemical biology of peptidoglycan acetylation and deacetylation. Bioorg. Chem. *54*, 44–50.

Mukamolova, G. V., Murzin, A.G., Salina, E.G., Demina, G.R., Kell, D.B., Kaprelyants, A.S., and Young, M. (2006). Muralytic activity of *Micrococcus luteus* Rpf and its relationship to physiological activity in promoting bacterial growth and resuscitation. Mol. Microbiol. *59*, 84–98.

Mukamolova, G. V, Kaprelyants, A.S., Young, D.I., Young, M., and Kell, D.B. (1998). A bacterial cytokine. P. Natl. Acad. Sci. USA *95*, 8916–8921.

Mullineaux, C.W., Nenninger, A., Ray, N., and Robinson, C. (2006). Diffusion of green fluorescent protein in three cell environments in *Escherichia coli*. J. Bacteriol. *188*, 3442–3448.

Münch, D., Roemer, T., Lee, S.H., Engeser, M., Sahl, H.G., and Schneider, T. (2012). Identification and *in vitro* analysis of the GatD/MurT enzyme-complex catalyzing lipid II amidation in *Staphylococcus aureus*. PLOS Pathog. *8*.

Nair, D., Memmi, G., Hernandez, D., Bard, J., Beaume, M., Gill, S., Francois, P., and Cheung, A.L. (2011). Whole-genome sequencing of *Staphylococcus aureus* strain RN4220, a key laboratory strain used in virulence research, identifies mutations that affect not only virulence factors but also the fitness of the strain. J. Bacteriol. *193*, 2332–2335.

Nakagawa, T. (2019). Structures of the AMPA receptor in complex with its auxiliary subunit cornichon. Science *366*, 1259–1263.

Nelson, D.E., and Young, K.D. (2001). Contributions of PBP 5 and DD-carboxypeptidase penicillin binding proteins to maintenance of cell shape in *Escherichia coli*. J. Bacteriol. *183*, 3055–3064.

Neuhaus, F.C. (1962). The enzymatic synthesis of D-alanyl-D-alanine. I. Purification and properties of D-alanyl-d-alanine synthetase. J. Biol. Chem. *237*, 778–786.

Neuhaus, F.C., and Struve, W.G. (1965). Enzymatic synthesis of analogs of the cell-wall precursor. I. Kinetics and specificity of uridine diphospho-*N*-acetylmuramyl-L-alanyl-D-glutamyl-L-lysine:D-Alanyl-D-alanine ligase (adenosine diphosphate) from *Streptococcus faecalis* R. Biochemistry *4*, 120–131.

Newton, G.J., Daniels, C., Burrows, L.L., Kropinski, A.M., Clarke, A.J., and Lam, J.S.

(2001). Three-component-mediated serotype conversion in *Pseudomonas aeruginosa* by bacteriophage D3. Mol. Microbiol. *39*, 1237–1247.

Oliver, J.D. (2005). The viable but nonculturable state in bacteria. J. Microbiol. *43*, 93–100.

Oshida, T., Sugai, M., Komatsuzawa, H., Hong, Y.M., Suginaka, H., and Tomasz, A. (1995). A *Staphylococcus aureus* autolysin that has an *N*-acetylmuramoyl-L-alanine amidase domain and an endo-β-*N*-acetylglucosaminidase domain: Cloning, sequence analysis, and characterization. P. Natl. Acad. Sci. USA *92*, 285–289.

Østdal, H., and Andersen, H.J.J. (1996). Non-enzymic protein induced hydrolysis of *p*-nitrophenyl acyl esters in relation to lipase/esterase assays. Food Chem. *55*, 55–61.

Otwinowski, Z., and Minor, W. (1997). Processing of X-ray diffraction data collected in oscillation mode. Methods Enzymol. *276*, 307–326.

Pantoliano, M.W., Petrella, E.C., Kwasnoski, J.D., Lobanov, V.S., Myslik, J., Edward, G., Carver, T., Asel, E., Springer, B.A., Lane, P., et al. (2001). High-density miniaturized thermal shift assays as a general strategy for drug discovery. J. Biomol. Screen. *6*, 429–440.

Pape, T., and Schneider, T.R. (2004). HKL2MAP : a graphical user interface for macromolecular phasing with SHELX programs . J. Appl. Crystallogr. *37*, 843–844.

Park, J.T., and Strominger, J.L. (1957). Mode of action of penicillin. Biochemical basis for the mechanism of action of penicillin and for its selective toxicity. Science *125*, 99–101.

Pazos, M., Peters, K., and Vollmer, W. (2017). Robust peptidoglycan growth by dynamic and variable multi-protein complexes. Curr. Opin. Microbiol. *36*, 55–61.

Peri, K.G., Goldie, H., and Waygood, E.B. (1990). Cloning and characterization of the *N*-acetylglucosamine operon of *Escherichia coli*. Biochem. Cell Biol. *68*, 123–137.

Peschel, A., Otto, M., Jack, R.W., Kalbacher, H., nther Jung, G., and Götz, F. (1999). Inactivation of the dlt operon in Staphylococcus aureus confers sensitivity to defensins, protegrins, and other antimicrobial peptides. J. Biol. Chem. *274*, 8405–8410.

Peschel, A., Vuong, C., Otto, M., and Götz, F. (2000). The D-alanine residues of *Staphylococcus aureus* teichoic acids alter the susceptibility to vancomycin and the activity of autolytic enzymes. Antimicrob. Agents Chemother. *44*, 2845–2847.

Peters, C., Tsirigos, K.D., Shu, N., and Elofsson, A. (2016a). Improved topology prediction using the terminal hydrophobic helices rule. Bioinformatics *32*, 1158–1162.

Peters, K., Kannan, S., Rao, V.A., Biboy, J., Vollmer, D., Erickson, S.W., Lewis, R.J., Young, K.D., and Vollmer, W., K. (2016b). The redundancy of peptidoglycan carboxypeptidases ensures robust cell shape maintenance in *Escherichia coli*. MBio *7*, e00819-16.

Pfeffer, J.M., Strating, H., Weadge, J.T., and Clarke, A.J. (2006). Peptidoglycan O acetylation and autolysin profile of *Enterococcus faecalis* in the viable but nonculturable state. J. Bacteriol. *188*, 902–908.

Phillips, D.C. (1967). The hen egg-white lysozyme molecule. Proc. Natl. Acad. Sci. *57*,

483–495.

Pittet, D., and Wenzel, R.P. (1995). Nosocomial bloodstream infections. Arch. Intern. Med. *155*, 1177–1184.

Popham, D.L. (2002). Specialized peptidoglycan of the bacterial endospore: The inner wall of the lockbox. Cell. Mol. Life Sci. *59*, 426–433.

Popham, D.L., Helin, J., Costello, C.E., and Setlow, P. (1996). Muramic lactam in peptidoglycan of *Bacillus subtilis* spores is required for spore outgrowth but not for spore dehydration or heat resistance. P. Natl. Acad. Sci. USA *93*, 15405–15410.

Pratviel-Sosa, F., Mengin-Lecreulx, D., and van Heijenoort, J. (1991). Over-production, purification and properties of the uridine diphosphate *N*-acetylmuramoyl-L-alanine:D-glutamate ligase from *Escherichia coli*. Eur. J. Biochem. *202*, 1169–1176.

Pucci, M.J., Discotto, L.F., and Dougherty, T.J. (1992). Cloning and identification of the *Escherichia coli murB* DNA sequence, which encodes UDP-*N*-acetylenolpyruvoylglucosamine reductase. J. Bacteriol. *174*, 1690–1693.

Pushkaran, A.C., Nataraj, N., Nair, N., Götz, F., Biswas, R., Mohan, C.G., Götz, F., Biswas, R., and Mohan, C.G. (2015). Understanding the structure-function relationship of lysozyme resistance in *Staphylococcus aureus* by peptidoglycan O-acetylation using molecular docking, dynamics, and lysis assay. J. Chem. Inf. Model. *55*, 760–770.

Raetz, C.R.H., and Whitfield, C. (2002). Lipopolysaccharide endotoxins. Annu. Rev. Biochem. *71*, 635–700.

Rasko, D.A., Ravel, J., Økstad, O.A., Helgason, E., Cer, R.Z., Jiang, L., Shores, K.A., Fouts, D.E., Tourasse, N.J., Angiuoli, S. V, et al. (2004). The genome sequence of *Bacillus cereus* ATCC 10987 reveals metabolic adaptations and a large plasmid related to *Bacillus anthracis* pXO1. Nucleic Acids Res. *32*, 977–988.

Rauwerdink, A., and Kazlauskas, R.J. (2015). How the same core catalytic machinery catalyzes 17 different reactions: The serine-histidine-aspartate catalytic triad of α/β-hydrolase fold enzymes. ACS Catal. *5*, 6153–6176.

Raymond, J.B., Mahapatra, S., Crick, D.C., and Pavelka, M.S. (2005). Identification of the *namH* gene, encoding the hydroxylase responsible for the *N*-glycolylation of the mycobacterial peptidoglycan. J. Biol. Chem. *280*, 326–333.

Reichmann, N.T., and Gründling, A. (2011). Location, synthesis and function of glycolipids and polyglycerolphosphate lipoteichoic acid in Gram-positive bacteria of the phylum Firmicutes. FEMS Microbiol. Lett. *319*, 97–105.

Reichmann, N.T., Tavares, A.C., Saraiva, B.M., Jousselin, A., Reed, P., Pereira, A.R., Monteiro, J.M., Sobral, R.G., VanNieuwenhze, M.S., Fernandes, F., et al. (2019). SEDS–bPBP pairs direct lateral and septal peptidoglycan synthesis in *Staphylococcus aureus*. Nat. Microbiol. *4*, 1368–1377.

Renner-Schneck, M., Hinderberger, I., Gisin, J., Exner, T., Mayer, C., and Stehle, T. (2015). Crystal structure of the *N*-acetylmuramic acid α-1-phosphate (MurNAc-α1-P) uridylyltransferase MurU, a minimal sugar nucleotidyltransferase and potential drug target enzyme in Gram-negative pathogens. J. Biol. Chem. *290*, 10804–10813.

Rex, J.H., Lynch, H.F., Cohen, I.G., Darrow, J.J., and Outterson, K. (2019). Non-traditional antibacterial agents. Nat. Commun. *10*, 3416.

Reynolds, P.E., Snaith, H.A., Maguire, A.J., Dutka-Malen, S., and Courvalin, P. (1994). Analysis of peptidoglycan precursors in vancomycin-resistant *Enterococcus gallinarum* BM4174. Biochem. J. *301*, 5–8.

Reynolds, S.M., Käll, L., Riffle, M.E., Bilmes, J.A., and Noble, W.S. (2008). Transmembrane topology and signal peptide prediction using dynamic Bayesian networks. PLoS Comput. Biol. *4*, e1000213.

Rice, L.B., Carias, L.L., Rudin, S., Hutton, R., Marshall, S., Hassan, M., Josseaume, N., Dubost, L., Marie, A., and Arthur, M. (2009). Role of class A penicillin-binding proteins in the expression of β-lactam resistance in *Enterococcus faecium*. J. Bacteriol. *191*, 3649–3656.

Riordan, J.F., and Vallee, B.L. (1972). *O*-Acetyltyrosine. In Methods in Enzymology, pp. 500–506.

Rohrer, S., Ehlert, K., Tschierske, M., Labischinski, H., and Berger-Bachi, B. (1999). The essential *Staphylococcus aureus* gene *fmhB* is involved in the first step of peptidoglycan pentaglycine interpeptide formation. P. Natl. Acad. Sci. USA *96*, 9351–9356.

Roseman, S. (1957). Glucosamine metabolism, I. *N*-acetylglucosamine deacetylate. J. Biol. Chem. *226*, 115–124.

Ruscitto, A., Hottmann, I., Stafford, G.P., Schäffer, C., Mayer, C., and Sharma, A. (2016). Identification of a novel *N*-acetylmuramic acid transporter in *Tannerella forsythia*. J. Bacteriol. *198*, 3119–3125.

Rusconi, F., Valton, É., Nguyen, R., and Dufourc, E. (2001). Quantification of sodium dodecyl sulfate in microliter-volume biochemical samples by visible light spectroscopy. Anal. Biochem. *295*, 31–37.

Russell, A.B., Hood, R.D., Bui, N.K., Leroux, M., Vollmer, W., and Mougous, J.D. (2011). Type VI secretion delivers bacteriolytic effectors to target cells. Nature *475*, 343–349.

Saidijam, M., Azizpour, S., and Patching, S.G. (2018). Comprehensive analysis of the numbers, lengths and amino acid compositions of transmembrane helices in prokaryotic, eukaryotic and viral integral membrane proteins of high-resolution structure. J. Biomol. Struct. Dyn. *36*, 443–464.

Sanchez-Puelles, J.M., Ronda, C., Garcia, J.L., Garcia, P., Lopez, R., and Garcia, E. (1986). Searching for autolysin functions: Characterization of a pneumococcal mutant deleted in the *lytA* gene. Eur. J. Biochem. *158*, 289–293.

Sanchez, M., Kolar, S.L., Müller, S., Reyes, C.N., Wolf, A.J., Ogawa, C., Singhania, R., De Carvalho, D.D., Arditi, M., Underhill, D.M., et al. (2017). O-Acetylation of peptidoglycan limits helper T cell priming and permits *Staphylococcus aureus* reinfection. Cell Host Microbe *22*, 1–9.

Sauvage, E., Kerff, F.E.E., Terrak, M., Ayala, J.A., Charlier, P., Fr´, F., Fréd´, F., Kerff, F.E.E., Terrak, M., Ayala, J.A., et al. (2008). The penicillin-binding proteins: structure and role in peptidoglycan biosynthesis. FEMS Microbiol. Rev. *32*, 234–258.

Schäffer, C., and Messner, P. (2005). The structure of secondary cell wall polymers: How Gram-positive bacteria stick their cell walls together. Microbiology *151*, 643–651.

Schallenberger, M.A., Niessen, S., Shao, C., Fowler, B.J., and Romesberg, F.E. (2012). Type I signal peptidase and protein secretion in *Staphylococcus aureus*. J. Bacteriol. *194*, 2677–2686.

Schleifer, K.H., and Kandler, O. (1972). Peptidoglycan types of bacterial cell walls and their taxonomic implications. Bacteriol. Rev. *36*, 407–477.

Schuster, C., Dobrinski, B., and Hakenbeck, R. (1990). Unusual septum formation in *Streptococcus pneumoniae* mutants with an alteration in the D,D-carboxypeptidase penicillin-binding protein 3. J. Bacteriol. *172*, 6499–6505.

Sham, L.-T., Butler, E.K., Lebar, M.D., Kahne, D., Bernhardt, T.G., and Ruiz, N. (2014). MurJ is the flippase of lipid-linked precursors for peptidoglycan biogenesis. Science *345*, 220–222.

Shibata, Y., Kawada, M., Nakano, Y., Toyoshima, K., and Yamashita, Y. (2005). Identification and characterization of an autolysin-encoding gene of *Streptococcus mutans*. Infect. Immun. *73*, 3512–3520.

Silhavy, T.J., Kahne, D., and Walker, S. (2010). The bacterial cell envelope. Cold Spring Harb. Perspect. Biol. *2*, a000414.

Slauch, J.M., Lee, A.A., Mahan, M.J., and Mekalanos, J.J. (1996). Molecular characterization of the *oafA* locus responsible for acetylation of *Salmonella typhimurium* O-antigen: OafA is a member of a family of integral membrane trans-acylases. J. Bacteriol. *178*, 5904–5909.

Smith, T.J., and Foster, S.J. (1995). Characterization of the involvement of two compensatory autolysins in mother cell lysis during sporulation of *Bacillus subtilis* 168. J. Bacteriol. *177*, 3855–3862.

Snowden, M.A., and Perkins, H.R. (1990). Peptidoglycan cross-linking in *Staphylococcus aureus*: An apparent random polymerisation process. Eur. J. Biochem. *191*, 373–377.

Snowden, M.A., Perkins, H.R., Wyke, A.W., Hayes, M. V, and Ward, J.B. (1989). Cross-linking and *O*-acetylation of newly synthesized peptidoglycan in *Staphylococcus aureus* H. J. Gen. Microbiol. *135*, 3015–3022.

Song, H., Inaka, K., Maenaka, K., and Matsushima, M. (1994). Structural changes of active site cleft and different saccharide binding modes in human lysozyme co-crystallized with hexa-*N*-acetyl-chitohexaose at pH 4.0. J. Mol. Biol. *244*, 522–540.

Steen, A., Buist, G., Horsburgh, G.J., Venema, G., Kuipers, O.P., Foster, S.J., and Kok, J. (2005). AcmA of *Lactococcus lactis* is an *N*-acetylglucosaminidase with an optimal number of LysM domains for proper functioning. FEBS J. *272*, 2854–2868.

Steinmoen, H., Teigen, A., and Håvarstein, L.S. (2003). Competence-induced cells of *Streptococcus pneumoniae* lyse competence-deficient cells of the same strain during cocultivation. J. Bacteriol. *185*, 7176–7183.

Strandén, A.M., Ehlert, K., Labischinski, H., and Berger-Bächi, B. (1997). Cell wall

monoglycine cross-bridges and methicillin hypersusceptibility in a *femAB* null mutant of methicillin-resistant *Staphylococcus aureus*. J. Bacteriol. *179*, 9–16.

Strating, H., and Clarke, A.J. (2001). Differentiation of bacterial autolysins by zymogram analysis. Anal. Biochem. *291*, 149–154.

Swim, S.C., Gfell, M.A., Wilde, C.E., and Rosenthal, R.S. (1983). Strain distribution in extents of lysozyme resistance and O-acetylation of gonococcal peptidoglycan determined by high-performance liquid chromatography. Infect. Immun. *42*, 446–452.

Swinney, D.C. (2013). Phenotypic vs. target-based drug discovery for first-in-class medicines. Clin. Pharmacol. Ther. *93*, 299–301.

Sychantha, D., and Clarke, A.J. (2018). Peptidoglycan modification by the catalytic domain of *Streptococcus pneumoniae* OatA follows a ping-pong bi-bi mechanism of action. Biochemistry *57*, 2394–2401.

Sychantha, D., Jones, C.S., Little, D.J., Moynihan, P.J., Robinson, H., Galley, N.F., Roper, D.I., Dowson, C.G., Howell, P.L., and Clarke, A.J. (2017). *In vitro* characterization of the antivirulence target of Gram-positive pathogens, peptidoglycan *O*-acetyltransferase A (OatA). PLOS Pathog. *13*, e1006667.

Sychantha, D., Little, D.J., Chapman, R.N., Boons, G.J., Robinson, H., Howell, P.L., and Clarke, A.J. (2018). PatB1 is an *O*-acetyltransferase that decorates secondary cell wall polysaccharides. Nat. Chem. Biol. *14*, 79–85.

Taguchi, A., Welsh, M.A., Marmont, L.S., Lee, W., Sjodt, M., Kruse, A.C., Kahne, D., Bernhardt, T.G., and Walker, S. (2019). FtsW is a peptidoglycan polymerase that is functional only in complex with its cognate penicillin-binding protein. Nat. Microbiol. *4*, 587–594.

Takahashi, J., Komatsuzawa, H., Yamada, S., Nishida, T., Labischinski, H., Fujiwara, T., Ohara, M., Yamagishi, J. ichi, and Sugai, M. (2002). Molecular characterization of an atl null mutant of *Staphylococcus aureus*. Microbiol. Immunol. *46*, 601–612.

Templin, M.F., Ursinus, A., and Höltje, J.-V. (1999). A defect in cell wall recycling triggers autolysis during the stationary growth phase of *Escherichia coli*. EMBO J. *18*, 4108–4117.

Terrak, M., Ghosh, T.K., van Heijenoort, J., Van Beeumen, J., Lampilas, M., Aszodi, J., Ayala, J.A., Ghuysen, J.-M., and Nguyen-Distèche, M. (1999). The catalytic, glycosyl transferase and acyl transferase modules of the cell wall peptidoglycan-polymerizing penicillin-binding protein 1b of *Escherichia coli*. Mol. Microbiol. *34*, 350–364.

Terwilliger, T.C. (2003). Automated main-chain model building by template matching and iterative fragment extension. Acta Crystallogr. Sect. D *59*, 38–44.

Terwilliger, T.C., Grosse-Kunstleve, R.W., Afonine, P. V., Moriarty, N.W., Zwart, P.H., Hung, L.W., Read, R.J., and Adams, P.D. (2007). Iterative model building, structure refinement and density modification with the *PHENIX AutoBuild* wizard. Acta Crystallogr. Sect. D *64*, 61–69.

Thanweer, F., and Verma, N.K. (2012). Identification of critical residues of the serotype modifying *O*-acetyltransferase of *Shigella flexneri*. BMC Biochem. *13*, 13.

Thanweer, F., Tahiliani, V., Korres, H., and Verma, N.K. (2008). Topology and identification of critical residues of the *O*-acetyltransferase of serotype-converting bacteriophage, SF6, of *Shigella flexneri*. Biochem. Biophys. Res. Commun. *375*, 581–585.

The World Health Organization (2017). Global priority list of antibiotic-resistant bacteria to guide research, discovery, and development of new antibiotics.

Tong, S.Y.C., Davis, J.S., Eichenberger, E., Holland, T.L., and Fowler, V.G. (2015). *Staphylococcus aureus* infections: Epidemiology, pathophysiology, clinical manifestations, and management. Clin. Microbiol. Rev. *28*, 603–661.

Tsirigos, K.D., Peters, C., Shu, N., Käll, L., and Elofsson, A. (2015). The TOPCONS web server for consensus prediction of membrane protein topology and signal peptides. Nucleic Acids Res. *43*, W401–W407.

Turner, R.D., Vollmer, W., and Foster, S.J. (2014). Different walls for rods and balls: The diversity of peptidoglycan. Mol. Microbiol. *91*, 862–874.

Tusnády, G., and Simon, I. (1998). Principles governing amino acid composition of integral membrane proteins: Application to topology prediction. J. Mol. Biol. *283*, 489–506.

Tusnády, G.E., and Simon, I. (2001). The HMMTOP transmembrane topology prediction server. Bioinformatics *17*, 849–850.

Tuteja, R. (2005). Type I signal peptidase: An overview. Arch. Biochem. Biophys. *441*, 107–111.

Typas, A., Banzhaf, M., Gross, C.A., and Vollmer, W. (2012). From the regulation of peptidoglycan synthesis to bacterial growth and morphology. Nat. Rev. Microbiol. *10*, 123–136.

Uehara, T., and Park, J.T. (2004). The *N*-acetyl-D-glucosamine kinase of *Escherichia coli* and its role in murein recycling. J. Bacteriol. *186*, 7273–7279.

Uehara, T., Suefuji, K., Valbuena, N., Meehan, B., Donegan, M., and Park, J.T. (2005). Recycling of the anhydro-*N*-acetylmuramic acid derived from cell wall murein involves a two-step conversion to *N*-acetylglucosamine-phosphate. J. Bacteriol. *187*, 3643–3649.

Uehara, T., Suefuji, K., Jaeger, T., Mayer, C., and Park, J.T. (2006). MurQ etherase Is required by *Escherichia coli* in order to metabolize anhydro-*N*-acetylmuramic acid obtained either from the environment or from its own cell wall. J. Bacteriol. *188*, 1660–1662.

Vázquez-Laslop, N., Lee, H., Hu, R., and Neyfakh, A.A. (2001). Molecular sieve mechanism of selective release of cytoplasmic proteins by osmotically shocked *Escherichia coli*. J. Bacteriol. *183*, 2399–2404.

Veiga, P., Bulbarela-Sampieri, C., Furlan, S., Maisons, A., Chapot-Chartier, M.-P., Erkelenz, M., Mervelet, P., Noirot, P., Frees, D., Kuipers, O.P., et al. (2007). SpxB regulates *O*-acetylation-dependent resistance of *Lactococcus lactis* peptidoglycan to hydrolysis. J. Biol. Chem. *282*, 19342–19354.

Veyrier, F.J., Williams, A.H., Mesnage, S., Schmitt, C., Taha, M.K., and Boneca, I.G.

(2013). De-*O*-acetylation of peptidoglycan regulates glycan chain extension and affects *in vivo* survival of *Neisseria meningitidis*. Mol. Microbiol. *87*, 1100–1112.

Viklund, H., and Elofsson, A. (2008). OCTOPUS: Improving topology prediction by two-track ANN-based preference scores and an extended topological grammar. Bioinformatics *24*, 1662–1668.

Viklund, H., Bernsel, A., Skwark, M., and Elofsson, A. (2008). SPOCTOPUS: A combined predictor of signal peptides and membrane protein topology. Bioinformatics *24*, 2928–2929.

Vollmer, W., and Seligman, S.J. (2010). Architecture of peptidoglycan: more data and more models. Trends Microbiol. *18*, 59–66.

Vollmer, W., and Tomasz, A. (2000). The *pgdA* gene encodes for a peptidoglycan *N*-acetylglucosamine deacetylase in *Streptococcus pneumoniae*. J. Biol. Chem. *275*, 20496–20501.

Vollmer, W., Blanot, D., and De Pedro, M.A. (2008a). Peptidoglycan structure and architecture. FEMS Microbiol. Rev. *32*, 149–167.

Vollmer, W., Joris, B., Charlier, P., and Foster, S. (2008b). Bacterial peptidoglycan (murein) hydrolases. FEMS Microbiol. Rev. *32*, 259–286.

Wang, G., Olczak, A., Forsberg, L.S., and Maier, R.J. (2009). Oxidative stress-induced peptidoglycan deacetylase in *Helicobacter pylori*. J. Biol. Chem. *284*, 6790–6800.

Wang, G., Lo, L.F., Forsberg, L.S., and Maier, R.J. (2012). *Helicobacter pylori* peptidoglycan modifications confer lysozyme resistance and contribute to survival in the host. MBio *3*, e00409-12.

Wang, L., Khattar, M.K., Donachie, W.D., and Lutkenhaus, J. (1998). FtsI and FtsW are localized to the septum in *Escherichia coli*. J. Bacteriol. *180*, 2810–2816.

Warth, A.D., and Strominger, J.L. (1969). Structure of the peptidoglycan of bacterial spores: occurrence of the lactam of muramic acid. P. Natl. Acad. Sci. USA *64*, 528–535.

Warth, A.D., and Strominger, J.L. (1972). Structure of the peptidoglycan from spores of *Bacillus subtilis*. Biochemistry *11*, 1389–1396.

Weadge, J.T., and Clarke, A.J. (2006). Identification and characterization of *O*-acetylpeptidoglycan esterase: A novel enzyme discovered in *Neisseria gonorrhoeae*. Biochemistry *45*, 839–851.

Weadge, J.T., and Clarke, A.J. (2007). *Neisseria gonorrheae O*-acetylpeptidoglycan esterase, a serine esterase with a Ser-His-Asp catalytic triad. Biochemistry *46*, 4932–4941.

Weadge, J.T., Pfeffer, J.M., and Clarke, A.J. (2005). Identification of a new family of enzymes with potential *O*-acetylpeptidoglycan esterase activity in both Gram-positive and Gram-negative bacteria. BMC Microbiol. *5*, 49.

Weidenmaier, C., and Peschel, A. (2008). Teichoic acids and related cell-wall glycopolymers in Gram-positive physiology and host interactions. Nat. Rev. Microbiol. *6*, 276–287.

Williams, A.H., Veyrier, F.J., Bonis, M., Michaud, Y., Raynal, B., Taha, M.-K., White,

S.W., Haouz, A., and Boneca, I.G. (2014). Visualization of a substrate-induced productive conformation of the catalytic triad of the *Neisseria meningitidis* peptidoglycan *O*-acetylesterase reveals mechanistic conservation in SGNH esterase family members. Acta Crystallogr. Sect. D *70*, 2631–2639.

Workman, S.D., Worrall, L.J., and Strynadka, N.C.J. (2018). Crystal structure of an intramembranal phosphatase central to bacterial cell-wall peptidoglycan biosynthesis and lipid recycling. Nat. Commun. *9*, 1159.

Wyss, C. (1989). Dependence of proliferation of *Bacteroides forsythus* on exogenous *N*-acetylmuramic acid. Infect. Immun. *57*, 1757–1759.

Yamaryo-Botte, Y., Rainczuk, A.K., Lea-Smith, D.J., Brammananth, R., van der Peet, P.L., Meikle, P., Ralton, J.E., Rupasinghe, T.W.T., Williams, S.J., Coppel, R.L., et al. (2015). Acetylation of trehalose mycolates is required for efficient MmpL-mediated membrane transport in Corynebacterineae. ACS Chem. Biol. *10*, 734–746.

Yao, X., Jericho, M., Pink, D., and Beveridge, T. (1999). Thickness and elasticity of Gram-negative murein sacculi measured by atomic force microscopy. J. Bacteriol. *181*, 6865–6875.

Yousif, S.Y., Broome-Smith, J.K., and Spratt, B.G. (2009). Lysis of *Escherichia coli* by β-Lactam antibiotics: Deletion analysis of the role of penicillin-binding proteins 1A and 1B. Microbiology *131*, 2839–2845.

Zhang, J.-H., Chung, T.D.Y., and Oldenburg, K.R. (1999). A simple statistical parameter for use in evaluation and validation of high throughput screening assays. J. Biomol. Screen. *4*, 67–73.

Zipperle, G.F., Ezzell, J.W., and Doyle, R.J. (1984). Glucosamine substitution and muramidase susceptibility in *Bacillus anthracis*. Can. J. Microbiol. *30*, 553–559.

Zoete, V., Grosdidier, A., and Michielin, O. (2009). Docking, virtual high throughput screening and in silico fragment-based drug design. J. Cell. Mol. Med. *13*, 238–248.

Appendix 1

IC50 values for the dose response assay completed at the SPARC BioCentre (Sick Kids Hospital, Toronto).

Molecule Name	IC50 (µM)
HSC-0128739	16.6
HSC-0128790	24.8
HSC-0113332	31.8
HSC-0094998	40.5
HSC-0114311	41.2
HSC-0059363	44.9
HSC-0127193	47.6
HSC-0117668	56.8
HSC-0037577	56.9
HSC-0101346	71.8
HSC-0128223	76.4
HSC-0018420	86.6
HSC-0114908	91.4
HSC-0101351	97.2
HSC-0117073	146
HSC-0115423	> 159
HSC-0100859	> 159
HSC-0101370	> 159
HSC-0114201	> 159
HSC-0106496	> 159
HSC-0099609	> 159

Appendix 2

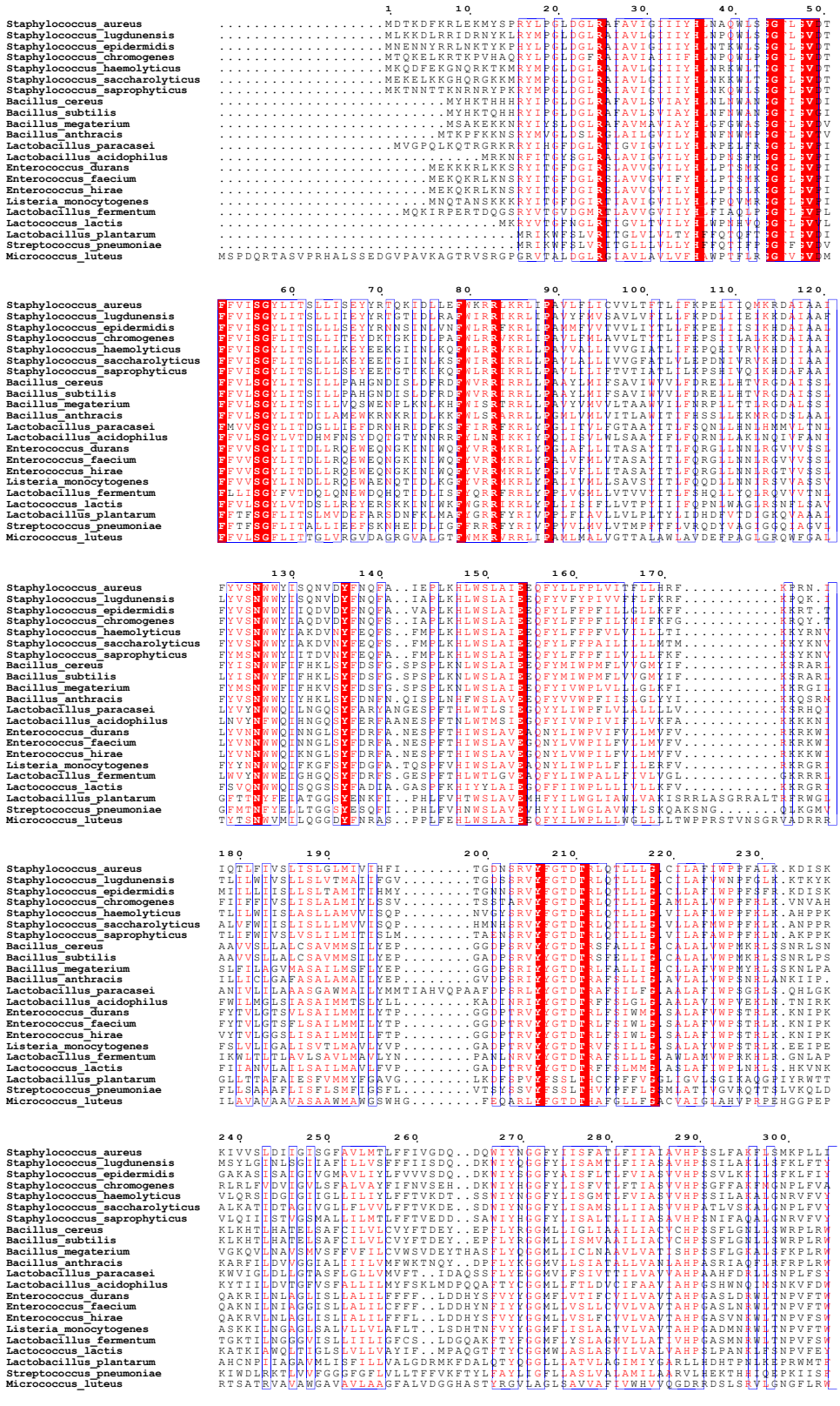
Staphylococcus_aureus
Staphylococcus_lugdunensis
Staphylococcus_epidermidis
Staphylococcus_chromogenes
Staphylococcus_haemolyticus
Staphylococcus_saccharolyticus
Staphylococcus_saprophyticus
Bacillus_cereus
Bacillus_subtilis
Bacillus_megaterium
Bacillus_anthracis
Lactobacillus_paracasei
Lactobacillus_acidophilus
Enterococcus_durans
Enterococcus_faecium
Enterococcus_hirae
Listeria_monocytogenes
Lactobacillus_fermentum
Lactococcus_lactis
Lactobacillus_plantarum
Streptococcus_pneumoniae
Micrococcus_luteus

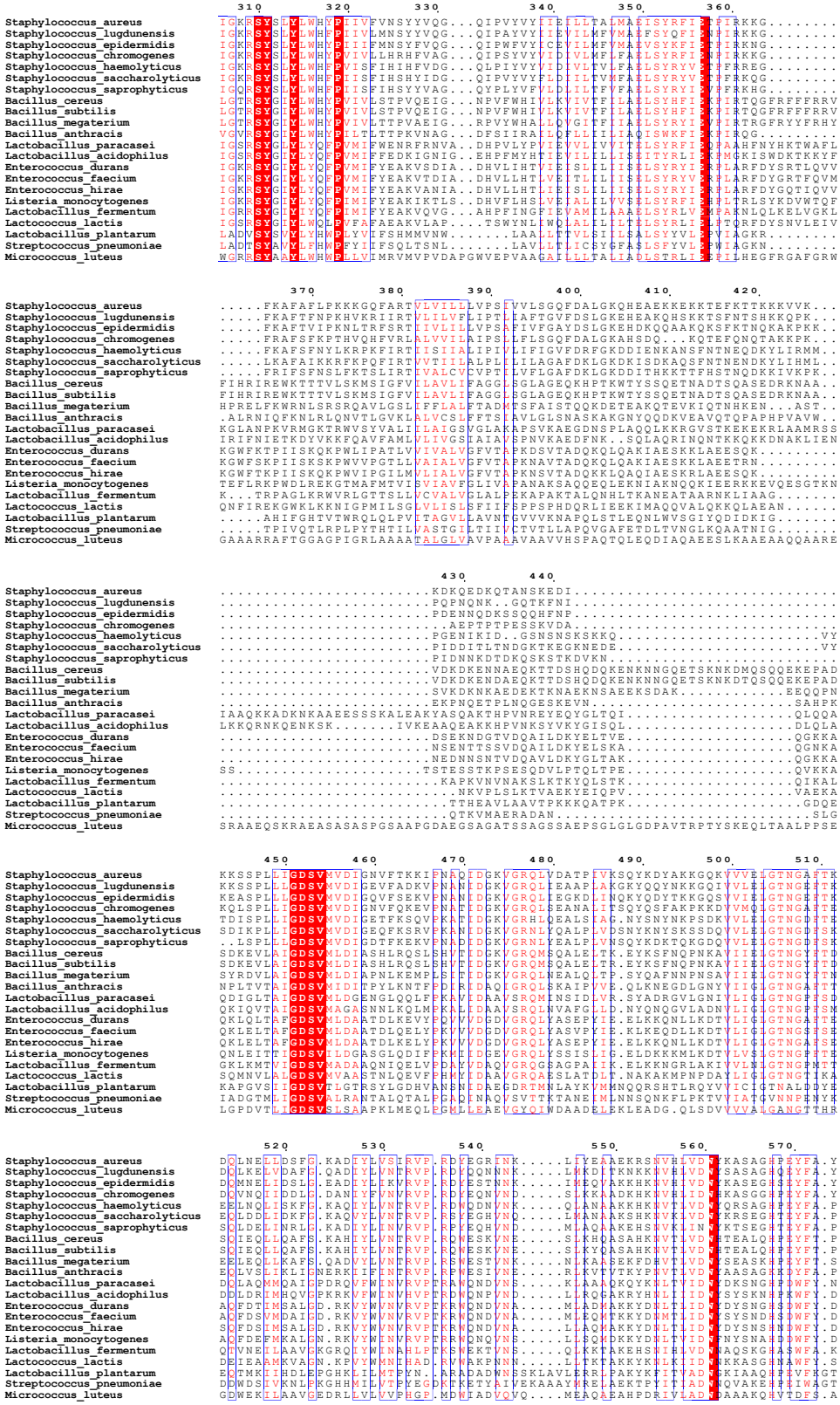
Staphylococcus_aureus
Staphylococcus_lugdunensis
Staphylococcus_epidermidis
Staphylococcus_chromogenes
Staphylococcus_haemolyticus
Staphylococcus_saccharolyticus
Staphylococcus_saprophyticus
Bacillus_cereus
Bacillus_subtilis
Bacillus_megaterium
Bacillus_anthracis
Lactobacillus_paracasei
Lactobacillus_acidophilus
Enterococcus_durans
Enterococcus_faecium
Enterococcus_hirae
Listeria_monocytogenes
Lactobacillus_fermentum
Lactococcus_lactis
Lactobacillus_plantarum
Streptococcus_pneumoniae
Micrococcus_luteus

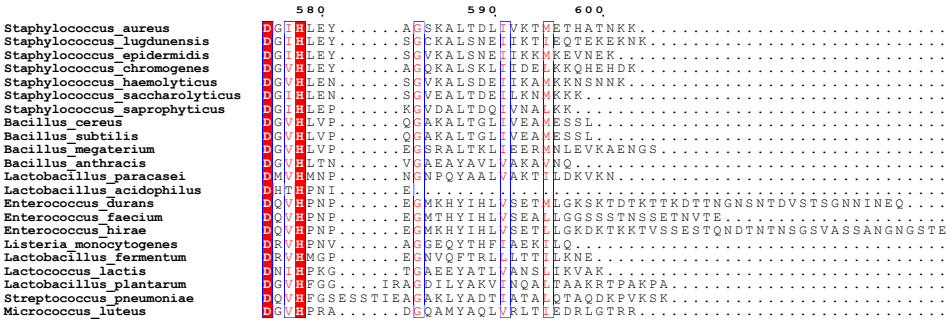

Multiple sequence alignment of Gram-positive OatA homologues. Selected sequences possesses the acyltransferase 3 – SGNH hydrolase domain architechture and were from Gram-positive species that had been experimentally shown to have acetylated PG. NCBI or Uniprot accession for included sequences: *Staphylococcus aureus* (Q2FV54), *Staphylococcus lugdunensis* (WP_084951408.1), *Staphylococcus epidermidis* (WP_002467975.1), *Staphylococcus chromogenes* (WP_037576177.1), *Staphylococcus haemolyticus* (WP_053029744.1), *Staphylococcous saccharolyticus* (WP_002441817.1), *Staphylococcus saprophyticus* (WP_048792699.1), *Bacillus cereus* (A0A0K6JLK2), *Bacillus subtilis* (G4NXW6), *Bacillus megaterium* (A0A0H4R9D2), *Bacillus anthracis* (WP_071729126.1), *Lactobacillus paracasei* (Q039J2), *Lactobacillus acidophilus* (WP_021874357.1), *Enterococcus durans* (WP_081134900.1), *Enterococcus faecium* (A0A133CQE1), *Enterococcus hirae* (WP_010737092.1), *Listeria monocytogenes* (A0A0Y71HE8), *Lactobacillus fermentum* (WP_057194879.1), *Lactococcus lactis* (WP_046124352.1), *Lactobacillus plantarum* (A0A1A0DGM4), *Streptococcus pneumoniae* (WP_016399047.1), *Micrococcus luteus* (KWW38872.1).

Appendix 3

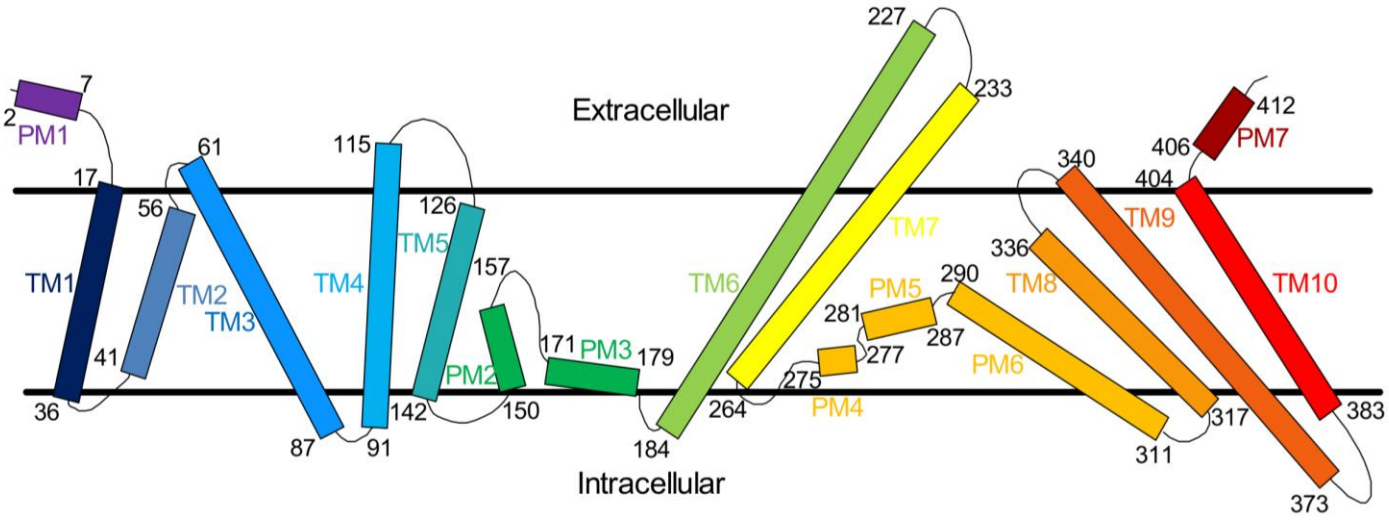

Crystal Structure	PM1 2-7	TM1 17-36	TM2 41-56	TM3 61-87	TM4 91-115	TM5 126-142	PM2 150-157	PM3 171-179	TM6 184-227	TM7 233-264	PM4 275-277	PM5 281-287	PM6 290-311	TM8 317-336	TM9 340-373	TM10 383-404
TM Predictions																
TOPCONS		15-35	42-62	64-84	92-112		150-170		194-214	242-262				318-338	340-360	386-406
OCTOPUS		15-35	47-77		90-110	116-136	152-172		191-211	232-262				323-337	339-353	386-406
Philius		18-36	40-61	64-81	92-110	119-136			197-220	241-266			288-307		338-360	383-407
PolyPhobius		16-35	42-58	64-82	92-113	120-138	150-168		194-217	237-265			287-306	318-336	342-359	385-407
SCAMPI		15-35	42-62	64-84	92-112		148-168		198-218	246-266				318-338	340-360	383-403
SPOCTOPUS		15-35	47-77		90-110	116-136	152-172		191-211	232-262				323-337	339-353	386-406

DltB experimental topology vs. *in silico* predictions. The structure of the MBOAT protein DltB was solved by X-ray crystallography (Ma et al., 2018), revealing a different topology than those predicted *in silico* by various transmembrane protein structure prediction software. Figure courtesy of Anthony J. Clarke.

Appendix 4

Species names and accession numbers for included sequences of the SSN shown in Figure 5.7

Cluster 1 - *Staphylococcus hyicus* (WP_119635835.1), *Staphylococcus agnetis* (WP_107396800.1), *Staphylococcus gallinarum* (WP_119484550.1), *Staphylococcus felis* (WP_116253576.1), *Staphylococcus argensis* (WP_103371601.1), *Staphylococcus cohnii* (WP_107359981.1), *Staphylococcus xylosus* (WP_107545640.1), *Staphylococcus auricularis* (WP_107398150.1), *Staphylococcus simulans* (WP_107604516.1), *Staphylococcus edaphicus* (WP_099090106.1), *Staphylococcus succinus* (WP_101117530.1), *Staphylococcus schleiferi* (WP_082704419.1), *Staphylococcus warneri* (WP_107532087.1), *Staphylococcus capitis* (WP_064262550.1), *Staphylococcus pseudintermedius* (WP_099994912.1), *Staphylococcus petrasii* (WP_103297609.1), *Staphylococcus lugdunensis* (WP_084951408.1), *Staphylococcus hominis* (WP_103288106.1), *Staphylococcus chromogenes* (WP_037576177.1), *Staphylococcus caprae* (WP_126501990.1), *Staphylococcus pasteuri* (WP_108016848.1), *Staphylococcus devriesei* (WP_107507457.1), *Staphylococcus muscae* (WP_095118115.1), *Staphylococcus vitulinus* (WP_107592782.1), *Staphylococcus stepanovicii* (WP_095085490.1), *Staphylococcus rostri* (WP_103358717.1), *Staphylococcus microti* (WP_044361338.1), *Staphylococcus fleurettii* (WP_126496560.1), *Staphylococcus aureus* (Q2FV54), *Staphylococcus saprophyticus* (WP_048792699.1), *Staphylococcus haemolyticus* (WP_053029744.1), *Staphylococcus epidermidis* (WP_002467975.1), *Mycobacteroides abscessus subsp. Abscessus* (SKT67628.1), *Micrococcus lylae* (STY74625.1), *Bacillus amyloliquefaciens* (POO70182.1); cluster 2 - *Bacillus indicus* (WP_029566187.1), *Bacillus nakamurai* (WP_061528359.1), *Bacillus filamentosus* (WP_046218022.1), *Bacillus endophyticus* (WP_113714815.1), *Bacillus glycinifermentans* (WP_048355719.1), *Bacillus swezeyi* (WP_076761302.1), *Bacillus mycoides* (WP_059038237.1), *Bacillus bingmayongensis* (WP_017153741.1), *Bacillus halotolerans* (WP_127696713.1), *Bacillus aryabhattai* (WP_048020582.1), *Bacillus intestinalis* (WP_061186647.1), *Bacillus badius* (WP_063383984.1), *Bacillus firmus* (WP_113881376.1), *Bacillus kochii* (WP_095370194.1), *Bacillus koreensis* (WP_053403215.1), *Bacillus safensis* (WP_075623609.1), *Bacillus thuringiensis* (WP_098562715.1), *Bacillus pumilus* (WP_034660506.1), *Bacillus toyonensis* (WP_098820676.1), *Bacillus massilioanorexius* (WP_019243741.1), *Bacillus circulans* (WP_095258160.1), *Bacillus anthracis* (WP_071729126.1), *Bacillus cereus* (A0A0K6JLK2), *Bacillus subtilis subsp. spizizenii* (G4NXW6), *Bacillus megaterium* (A0A0H4R9D2), *Fictibacillus phosphorivorans* (WP_082820816.1), *Fictibacillus aquaticus* (WP_094253633.1), *Fictibacillus gelatini* (WP_026678670.1), *Listeria fleischmannii* (WP_007548165.1), *Listeria goaensis* (WP_088825257.1), *Listeria kieliensis* (WP_115752320.1), *Listeria welshimeri* (WP_011702113.1), *Listeria thailandensis* (WP_122865461.1), *Listeria newyorkensis* (WP_036093866.1), *Listeria ivanovii* (WP_014092689.1), *Listeria innocua* (WP_033838131.1), *Listeria booriae* (WP_036085509.1), *Listeria grayi* (WP_036106524.1), *Brochothrix thermosphacta* (WP_069136743.1), *Brachybacterium faecium* (SLN02199.1), *Lysinibacillus xylanilyticus* (WP_068983674.1), *Lysinibacillus fusiformis* (WP_025114335.1), *Lysinibacillus parviboronicapiens* (WP_107924758.1), *Exiguobacterium enclense* (WP_058265505.1), *Exiguobacterium acetylicum* (WP_029343251.1), *Sporosarcina globispora*

(WP_053435521.1), *Clostridium luticellarii* (WP_106008643.1), *Massilibacterium senegalense* (WP_062197353.1), *Cohnella lupini* (WP_115994599.1), *Eggerthella lenta* (WP_114538407.1), *Gemella haemolysans* (WP_003145891.1), *Paenibacillus wulumuqiensis* (WP_046214122.1), *Vagococcus humatus* (WP_125942361.1), *Kurthia gibsonii* (WP_121178303.1); cluster 3 - *Listeria monocytogenes* (A0A0Y7IHE8), *Carnobacterium divergens* (WP_119907939.1), *Carnobacterium maltaromaticum* (WP_035063770.1), *Lactococcus fujiensis* (WP_096817386.1), *Lactococcus termiticola* (WP_109245463.1), *Lactococcus garvieae* (WP_081165630.1), *Lactococcus lactis* (WP_046124352.1), *Lactococcus petauri* (WP_117516819.1), *Enterococcus pallens* (WP_010759682.1), *Enterococcus mundtii* (WP_104775750.1), *Enterococcus malodoratus* (WP_010739863.1), *Enterococcus casseliflavus* (WP_128487608.1), *Enterococcus avium* (WP_049218997.1), *Enterococcus faecalis* (WP_127688510.1), *Enterococcus wangshanyuanii* (WP_088268240.1), *Enterococcus rivorum* (WP_069697682.1), *Enterococcus termitis* (WP_086345219.1), *Enterococcus phoeniculicola* (WP_010768236.1), *Enterococcus hermanniensis* (OJG45979.1), *Enterococcus devriesei* (WP_071863176.1), *Enterococcus pseudoavium* (WP_067626321.1), *Enterococcus asini* (WP_118339913.1), *Enterococcus villorum* (WP_081182932.1), *Enterococcus aquimarinus* (WP_071873897.1), *Enterococcus moraviensis* (WP_010765624.1), *Enterococcus cecorum* (WP_047339318.1), *Enterococcus durans* (WP_081134900.1), *Enterococcus faecium* (A0A133CQE1), *Enterococcus hirae* (WP_010737092.1), *Lactobacillus salivarius* (WP_081561525.1), *Lactobacillus ceti* (WP_027106955.1), *Lactobacillus vini* (WP_010580776.1), *Lactobacillus cacaonum* (WP_057828868.1), *Lactobacillus saerimneri* (WP_009554789.1), *Lactobacillus algidus* (WP_112250026.1), *Lactobacillus oryzae* (WP_034529363.1), *Lactobacillus hordei* (AUJ30112.1), *Lactobacillus hayakitensis* (WP_025021881.1), *Lactobacillus nagelii* (WP_057886865.1), *Lactobacillus pentosus* (WP_122211011.1), *Lactobacillus satsumensis* (WP_056959914.1), *Lactobacillus paracollinoides* (WP_056987878.1), *Lactobacillus murinus* (WP_076149417.1), *Lactobacillus backii* (WP_068224702.1), *Lactobacillus silage* (WP_089137058.1), *Lactobacillus kimchicus* (WP_082593541.1), *Lactobacillus senmaizukei* (WP_061777100.1), *Lactobacillus capillatus* (WP_057742191.1), *Lactobacillus manihotivorans* (WP_056964054.1), *Lactobacillus hominis* (WP_008470326.1), *Lactobacillus fabifermentans* (WP_024626104.1), *Lactobacillus johnsonii* (WP_117285366.1), *Lactobacillus taiwanensis* (WP_094523305.1), *Lactobacillus lindneri* (WP_065866166.1), *Lactobacillus kefiri* (WP_056982209.1), *Lactobacillus curvatus* (WP_056966498.1), *Lactobacillus parakefiri* (WP_057961345.1), *Lactobacillus ruminis* (WP_003693813.1), *Lactobacillus parabuchneri* (WP_084972755.1), *Lactobacillus rodentium* (WP_117118350.1), *Lactobacillus nasuensis* (WP_056950488.1), *Lactobacillus futsaii* (WP_057814769.1), *Lactobacillus metriopterae* (WP_129044884.1), *Lactobacillus apis* (WP_082089550.1), *Lactobacillus amylovorus* (WP_082588989.1), *Lactobacillus kitasatonis* (WP_025015105.1), *Lactobacillus oris* (AMS08593.1), *Lactobacillus plantarum WCFS1* (CCC78307.1), *Lactobacillus paracasei* (Q039J2), *Lactobacillus fermentum* (WP_057194879.1), *Lactobacillus acidophilus* (WP_021874357.1), *Tetragenococcus solitarius* (WP_068707380.1), *Tetragenococcus osmophilus* (WP_123934689.1), *Tetragenococcus halophilus* (WP_103103628.1), *Melissococcus plutonius* (WP_015695200.1), *Weissella oryzae* (WP_027699234.1),

Weissella koreensis (WP_013989448.1), *Weissella cibaria* (WP_106444593.1), *Pediococcus acidilactici* (WP_070366449.1), *Pediococcus cellicola* (WP_083490453.1), *Pediococcus ethanolidurans* (WP_057806861.1), *Pediococcus parvulus* (OAD64515.1), *Pediococcus pentosaceus* (WP_060743542.1), *Gardnerella vaginalis* (WP_102169170.1), *Leuconostoc carnosum* (WP_014974670.1), *Streptococcus downei* (WP_044123767.1), *Streptococcus sobrinus* (WP_019790787.1); cluster 4 - *Streptococcus mitis* (WP_001220863.1), *Streptococcus pseudopneumoniae* (WP_023940835.1), *Streptococcus oralis* (WP_084881227.1), *Streptococcus milleri* (WP_115263542.1), *Streptococcus intermedius* (WP_003071340.1), *Streptococcus gordonii* (WP_061594208.1), *Streptococcus cristatus* (WP_048779176.1), *Streptococcus anginosus* (WP_117645147.1), *Streptococcus constellatus* (WP_039677545.1), *Streptococcus viridans* (WP_126403590.1), *Streptococcus equinus* (WP_107372410.1), *Streptococcus sanguinis* (WP_125338089.1), *Streptococcus thermophilus* (WP_011227608.1), *Chlamydia trachomatis* (CRH90979.1), *Streptococcus pneumoniae* (WP_016399047.1), *Streptococcus parasanguinis* (WP_049498137.1), *Streptococcus vestibularis* (WP_003091969.1), *Streptococcus porci* (WP_027973554.1), *Streptococcus suis* (WP_105111935.1), *Streptococcus agalactiae* (WP_001220903.1), *Streptococcus agalactiae* (WP_047205431.1), *Streptococcus cuniculi* (WP_075104524.1), *Streptococcus azizii* (WP_076995396.1), *Streptococcus canis* (WP_125074309.1), *Streptococcus pyogenes* (WP_111680963.1), *Streptococcus pantholopis* (WP_067064786.1), *Streptococcus didelphis* (WP_018367209.1), *Streptococcus varani* (WP_093651275.1), *Streptococcus parauberis* (WP_003103149.1), *Streptococcus plurextorum* (WP_027972087.1), *Streptococcus dysgalactiae* (WP_003049091.1), *Streptococcus thoraltensis* (WP_018380206.1), *Streptococcus acidominimus* (WP_095121260.1), *Streptococcus ictaluri* (WP_008090122.1), *Streptococcus marimammalium* (WP_018370137.1), *Atopobacter phocae* (WP_025729486.1).